A Closer Look at Water/Oil Emulsions in Energy and Environment: Modeling Strategy

By

Fatemeh Goodarzi

Submitted the School of Graduate Studies in partial

Fulfillment of the requirement

For the degree of

Masters of Engineering

Memorial University of Newfoundland

May 2019

St. John’s Newfoundland and Labrador

ABSTRACT

The formation and presence of water/oil emulsion is an important phenomena in the oil and gas sector, drug delivery systems and food emulsion industry. In this work, mesoscale simulation is employed to investigate the structural and interfacial behaviour of the system. Both aliphatic and cyclic structures of the oil molecules were considered. A non-ionic surfactant was introduced to the system and the interfacial tension at the interface was measured at varying surfactant concentration. The effect of brine is also investigated on its ability to modify the electrostatic forces between the particles in the system. Flory-Huggins chi parameter were measured using molecular dynamics simulation and Monte Carlo method and implemented as an input in dissipative particle dynamics simulation. This parameter acted as a bridge between microscale and mesoscale simulation. The effect of temperature is studied on the solubility parameter and energy of mixing which are the parameters used to calculate the chi parameter. Water/oil ratio turned out to be an influencing factor in determining the type of emulsion formed in the system. According to the results of the MD simulations, the presence of salt improves the interfacial efficiency of the surfactant by decreasing the interfacial tension, which is in a good agreement with the literature data. . Comparing the snapshots taken at different simulation time steps, concertation profiles and radius of gyration values, it was observed that in the case of aliphatic hydrocarbons, surfactant molecules will stretch more due to the linear structure of oil molecules, however, for cyclic hydrocarbons, radius of gyration values reported to be smaller since less space is available for the interaction of surfactant tail groups with oil molecules — however, interfacial tension obtained to be a function of molecular weight of hydrocarbon, as it calculated to be the highest for Dodecane(43.62mN/m) and smallest for Benzene(29.68mN/m), regardless of their structure and polarity of the molecule. Based on the parameter considered to affect the properties of the system, an ideal case was introduced to have the lowest interfacial tension.

Keywords: Emulsion; Interfacial behaviors; Surfactant; Salinity; Dissipative particle dynamics; Molecular dynamic simulations

ACKNOWLEDGMENTS

Firstly, I would like to express my sincere gratitude to my advisor Dr. Zendehboudi for the continuous support of my MEng. study and related research, for his patience, motivation, and immense knowledge. His guidance helped me in all the time of research and writing of this thesis. I could not have imagined having a better advisor and mentor for my MEng. study.

Besides my advisor, I would like to thank the rest of my thesis committee: Dr. John Shirokoff, and Dr. Amer Aborig, for serving on my thesis committee and their helpful and valuable comments.

I thank all my groupmates from RAEEG's research group for their support in my MEng research.
Financial support from Equinor (formerly Statoil) Canada, InnovateNL, Memorial University, and NSERC is highly acknowledged.
At the End, I would like to express my gratitude and deepest appreciation to family and friends, for support and encouragement during my studies.
Without supports and encouragements from them, I could not have finished this work.

TABLE OF CONTENTS

LIST OF FIGURES

LIST OF TABLES

INTRODUCTION

Emulsion refers to an immiscible mixture of oil and water in the presence of an emulsifying agent. Emulsion is made of a disperse phase in the form of droplets in a continuous flow of the other phase present in the system. Emulsion may form and employ during various chemical processes such as water flooding of heavy oil reservoirs, food emulsions or drug delivery systems. Stability of water/oil systems is a very important feature of emulsion to be considered in various situations. One of the factors influencing the emulsion stability is the interfacial tension. Interfacial tension is an important characteristics of emulsion to be considered in liquid-liquid mixtures studies. In thermodynamics perspective, interfacial tension represents the free energy for the formation of an interface between oil and water phase. The addition of surfactant can significantly change the interfacial tension of the system. Surfactant molecules are composed of hydrophilic polar segment called surfactant head and a linear hydrophobic chain of hydrocarbons called the tail. Due to the nature of the segments, the head is attracted to the water phase and the surfactant tail will penetrate into the oil phase and reduce the interfacial tension between the two immiscible phases. Due to the difficulty in predicting the forces and interactions at the interface, prediction of interfacial tension is a challenging area in emulsion studies. A comprehensive description of fundamental forces such as electrostatic, van-der-Waals and hydrogen bonding among the molecules are required to accurately determine the interfacial tension values. Hence, in addition to experimental approaches, the application of computational methods with the ability to model the particles and molecules individually is essential. Experimental measurements can provide us with in-depth description regarding the interfacial characteristic of the system, however, due to the complexity of the multicomponent mixtures and the limitations of experimental approaches to model such complexity, an accurate prediction of the particles behaviour in the system is still missing. Hence, employing new molecular simulation methods are required. Configuration and dynamics of the molecules at the oil/water interface is important toward a better description of the system and dissipative particle dynamics (DPD) is a strong tool to model such complicated coarse-grained systems. DPD is a mesoscopic numerical technique developed to model complex systems.

The main objectives of this work is to study the behaviour of brine/surfactant/oil molecule at different conditions. This thesis is composed of three individual chapters with references at the end of each chapter. The first paper summarizes the current and past discussions on different aspects of emulsion stability. This document gathers useful and practical information regarding emulsion formations and its stability. Basic emulsion definitions, stability mechanisms, governing equations to model the flow of emulsion is discussed in this chapter. Different experimental and measuring techniques to characterize emulsion droplet is also covered in this chapter. The effect of operational condition, fluid and reservoir properties is discussed and advantages and disadvantages of the proposed methods in literature is also reviewed. Next chapter, highlights the importance of oil molecule structures on the characteristics of the system. Samples of aliphatic and cyclic hydrocarbon molecules were considered and using molecular dynamics simulation and Monte Carlo method, the input variable for dissipative particle dynamics is calculated. The effect

of temperature, surfactant concentration and water cut is monitored through plots of relative concertation, radius of gyration and interfacial tension value.

The third chapter, considers a more complicated system of water/surfactant/oil. Two types of salt are being introduced to the system and the effect of the dissociated ions on the electrostatic interactions between the surfactant head and tail group with water and oil phase is studied. Through snapshots taken at different simulation time steps, the evolution of the system is monitored. Solubility parameter and energy of mixing calculation were performed to obtain the chi parameter values requited to estimate the conservative force parameter in DPD simulation.

The last chapter summarized the main findings of this work and recommend future applications of this work to further expand water/surfactant/oil simulation studies.

1 A Comprehensive Review on Emulsions and Emulsion Stability in Chemical and Energy Industries

Fatemeh Goodarzi, Sohrab Zendehboudi

Faculty of Engineering and Applied Science, Memorial University, St. John's, NL, Canada

ABSTRACT

Emulsion refers to a mixture that includes two or more liquid phases. The uses of emulsions are found in several chemical, energy, and environmental industries such as food, health care, chemical synthesis, and firefighting sectors. Water in oil emulsions is formed spontaneously during oil production when oil and water are mixed together and in the presence of asphaltene as a naturally occurring surfactant. For operational and economic reasons, oil emulsions need to be treated to recover both oil and water phases. To develop more efficient emulsion treatments, it is essential to have a better understanding of the factors that affect emulsion formation and stability. The droplet size variation is an important parameter that influences the stability and rheological characteristics of the emulsions. In addition, the available interfacial area for any possible chemical reactions might affect the behaviour and properties of the emulsions in various transport phenomena systems. The adequate knowledge of the factors and mechanisms affecting the droplet size and emulsion stability still needs further engineering and research activities. This study is aimed to provide a comprehensive literature review on the formation of water/oil emulsion and its stability in various physical systems (e.g., pipeline and porous media). In this review, fundamental aspects of emulsions, emulsion formation mechanisms, analytical models, and numerical solutions for description and characterization of the behaviour of emulsions in porous media or/and separators are discussed. The effects of different fluid properties, physical model characteristics, and operational conditions on emulsion behaviours are also studied. This paper also summarizes the experimental and modeling studies and methodologies with focus on reliable laboratory equipment/tools and simulation and modeling packages/strategies for investigation of emulsion stability and droplet size distribution where a systematic parametric sensitivity analysis to study various effects of important thermodynamic, process, and medium properties on the targeted variables is conducted. This review manuscript will provide useful guidelines to characterize and model emulsions and their behaviours in different industrial sectors, which considerably help to conduct better design and optimal operation of corresponding equipment.

Keywords: Emulsion; Emulsion Stability; Droplet Size; Characterization; Modeling and Experimental; Energy and Environment

1.1 INTRODUCTION

Systems of at least two immiscible phases are called dispersion. A disperse system is made of a dispersed phase in a continuous flow. There are three major types of dispersions based on the physics of dispersed phase namely: foams of a gas in liquid mixture, suspensions of a solid in liquid blend, and emulsion of a liquid in liquid system. [1] Emulsion is a mixture of two immiscible liquids, which generally forms during various chemical processes such as water flooding of heavy oil reservoirs, water treatment membranes, and packed bed separators. [2] For instance, emulsion can be categorized as water-in-oil emulsion (with water droplets as a dispersed phase in the flow of oil as the continuous phase), oil-in-water emulsion (with oil droplets in the flow of water) and more complex configuration of emulsion such as water-in-oil-in-water emulsion. [3] Crude oil is a blend of hydrocarbons with different sizes that can have various applications in chemical and energy industries. The type and composition of crude oils (as vital factors) play important roles in the development of emulsions. Water-in-crude oil emulsions are stable dispersions of water droplets in a continuous flow of oil, stabilized by heavy particles/components (naturally occurring emulsifiers) present in the oil. Emulsion formation is a recurring issue which is undesirable in the oil industry as it might cause flow blockage, inefficient separation, operational problems, corrosion, and consequently adding high costs to the transportation, processing, and separation units. [4] For instance, the dispersed water droplets occupy a considerable volume of the processing facilities and pipelines, leading to appreciable variations in normal operating conditions and an increase in the operational expenses. Furthermore, the physical properties of oil are significantly altered owing to the presence of emulsions. [5] The criteria/conditions for formation and stability of the emulsions are practically the same in various processes and industries. There are a number of studies on emulsion characteristics and factors contributing to its stability. However, there are still several unsolved technical and practical issues such as finding a proper measurement technique to monitor emulsion stability or deriving a correlation to account the effect of various parameters influencing emulsion stability and droplet size variation (or/and distribution). These challenges call for extensive research investigations on the flow of liquid-liquid suspensions in complex physical systems such as porous media where the droplet size and pore sizes may be comparable. A systematic theoretical and experimental research work was conducted on the rheological properties of emulsions and their impacts on droplet size distribution. [6, 7] The proposed correlations were planned to account all the factors, influencing viscosity based on the experimental data and correlations in the literature. In offshore oil production, emulsions are observed at various steps of the transportation and production operations. A variety of process equipment (separators and coalesces) and measurement tools are required to design a platform for destabilization of the produced emulsions. [8] Souza *et al*. [9] suggested a variety of techniques to be involved in treatment and transportation of crude oil. The emulsion droplet size distribution is an important feature affecting the stability of emulsion. The size of droplets dispersed in the emulsion is a vital characteristic as it can modify the rheological behaviour and stability of emulsions. This property is used to calculate the surface area required for gas hydrate formation, since the area/interface controls the mass and heat transfer rate. [10] There are numerous techniques in the

literature to determine emulsion stability and size distribution [1, 2] such as Nuclear Magnetic Resonance (NMR), Near Infrared Spectroscopy (NIR), acoustics and electroacoustics or optical microscopy method. However, each technique has its own pros and cons. For example, NIR requires calibration and cannot report droplet size distribution directly. NMR has some biased distributions functions and fit the data based on them. Electroacoustic and acoustic may result in inaccurate measurements due to the effect of solid particles [3]. Since water-in-oil emulsions and their stability have been challenges to the oil industry, it is crucial to have an adequate understanding of the factors influencing the emulsion stability so that effective treatment techniques are proposed to solve this matter.

In general, the heterogeneous dispersion of liquid/ liquid systems can be classified into two categories [4]; including, a) Emulsions with droplet size of microns which are thermodynamically unstable, and b) Microemulsions with a droplet size in the nanometer scale, which are considered as stable emulsions thermodynamically. A transition from emulsion to microemulsion occurs when there is a considerable change in the droplet size. It is clear that microemulsions can be converted into emulsions, and vice versa under particular thermodynamic and process conditions. For instance, López-Montilla et al. [5] reported that a simple temperature shift causes emulsion–microemulsion transition. Two approaches are mainly applied to understand the stability behaviour of emulsions; namely, (a) zeta potential measurements for the surface of the particles to predict the emulsion stability [6] and (b) ageing tests which represent the study of the emulsion properties changes with time. Two common destabilization processes that influence the uniformity of dispersions are migration of the particles and droplet size variation or accumulation. It is crucial to examine how the operational conditions such as water content of the water/ oil (W/O) emulsions and temperature affect the stability to make logical recommendations for improvement of the industrial processes while dealing with the emulsion issue.

There are some research studies with focus on application of new modeling and connectionist tools to model emulsion behaviours and stability. For instance, Yetilmezsoy et al.[7] employed the fuzzy logic to estimate water in oil emulsion stability where the input parameters were density, viscosity, saturates, asphaltenes, aromatics, and resins. In another research investigation, Fingas[8] obtained a class index to identify stable, meso-stable, entrained, and unstable emulsions through employing a Gaussian-style regression expansion technique, where various variables such as asphaltene and resin contents, viscosity, and density were considered as the inputs.

During production, transportation, and processing stages in petroleum industry, the crude oil viscosity is one of the fundamental characteristics that influence the transport phenomena, interactions between phases, and flow properties of the dispersions. Water is frequently produced from oil reservoirs or is injected in the form of steam and liquid into the reserves to enhance oil production [7, 8] . Water and crude oil mix while passing through the well and the valves. The mixture flow will produce stable water-in-crude oil emulsions. Stable emulsions consist of 60% to 85 % water [9]. The stable emulsions are normally found in crude oils with higher viscosity [7]. The

presence of natural surfactants (e.g., asphaltene and resin) in crude oil causes the formation and stabilization of emulsions where the presence of these heavy particles/parts of crude oil strongly affect the oil viscosity. For instance, crude oil viscosity increases when the amount of heavy suspended particles increases [7, 10]. Resins and Asphaltenes are two soluble groups of crude oils which are identified as important factors affecting the emulsion stability. The formation of an elastic layer at the oil/water interface is due to the interactions between the asphaltene and resin [11]. Emulsion formation in oil production is a challenge due to causing an unexpected behaviour from production fluid. There are a very few research works in the literature which extensively review important concepts regarding emulsion and emulsion stability. The main objective of this review manuscript is to summarize the current and previous discussions on emulsion stability and various methods to determine droplet size distribution. This document provides practising engineers useful information and guidelines about emulsions, emulsion formation, and emulsion characteristics. This review paper is made of different sections. Section 1 provides an introduction on emulsion and its stability. Section 2 describes the water-in-oil emulsions phenomena. First, the basic emulsion definitions, properties of emulsions, and stabilization mechanisms are discussed in this section. Second, the importance of heavy oil particles and solids in emulsion stability is highlighted. The role of asphaltene in emulsion formation is also emphasized. Section 3 outlines the models and governing equations used to describe the flow of emulsions, limitations, and assumptions. A brief on methodologies and correlations is also discussed. Section 4 summarizes the previous experimental works, measurements technologies, and theoretical techniques implemented to characterize the size, shape, and stability of emulsions. Effects of process/operational conditions; namely, temperature, flow rate, and water/oil ratio on the emulsions and emulsion stability are briefly described. The main findings are also discussed for further understanding. Section 5 describes the influences of fluid properties on the emulsions and emulsion stability. The compositional and structural properties of injected fluids and crude oil are studied. This review highlights how important characteristics such as interfacial tension and salinity of the water affect the droplet size variation. The modeling studies and previous correlations are also covered in this section. Section 6 evaluates the effects of reservoir properties (e.g., porosity and permeability) on emulsions and emulsion stability. The flow of emulsion through porous media is elucidated. The previous studies based on deep bed filtration model are covered in this section. The snap off phenomenon as an important factor in droplet size distribution and emulsion stability is also discussed. Section 7 covers the simulation and optimization tools/packages for modeling of emulsions and emulsion stability. The experimental techniques used for analysis and accuracy examination of models developed for water-in-oil emulsions are discussed where the advantages and drawbacks of the models are summarized. Section 8 explains the strategies for control of emulsion stability. The theoretical and practical challenges in emulsions and emulsion stability are also discussed in this section. Section 9 summarizes the main conclusions and suggests recommendations for further research.

1.2 THEORETICAL ASPECTS OF EMULSIONS

1.2.1 Description of oil emulsions.

An emulsion is defined as the dispersion (droplets) of a liquid in an immiscible liquid. The phase, which is suspended, is called the external or continuous phase. The phase, which appears in the form of droplets, is the internal or dispersed phase. In the case of oil emulsions, one of the liquid phases is crude oil and the other liquid is aqueous or water. The percentage of water, which emulsifies the crude oil, broadly differs so that it can be greater than 70% and even less than 2% in a few cases. In 1973, McAuliffe[12] conducted experiments on crude oil-water emulsions injection as a plugging agent to improve the recovery of a water-flood test. The researcher reported that a key characteristic for emulsions in a flooding test is the presence of droplets with diameters slightly bigger than the pore-throat in the porous system. Bragg[13] also developed a method to extract hydrocarbons through injecting a mixture, containing oil and water, into the formation to improve the oil recovery. Austad and Strand [14] concluded that a reduced interfacial tension might be attained through employing micro-emulsions. The micro-emulsions flow easily through the porous media, resulting in an improvement in oil recovery. Khmbharatana et al. [15] highlighted the physical characteristics of a stable emulsion flow in Ottawa sand pack systems and Berea sandstone where the pore size and droplet diameter are comparable. Based on Zeidani et al. [16], it was found that oil-in-water emulsion is an effective mixture in sealing unconsolidated samples for long periods of time. The success of their recommended method was directly related to a proper experimental design which depends on the sand pack and emulsion preparation and an appropriate injection scheme of a surface-active agent. Constructing a model which describes the favourable conditions is time consuming and requires high accuracy. Furthermore, the experimental errors while determining different properties are inevitable. A number of researchers have provided adequate discussions on the flow mechanics of emulsions in porous media to develop analytical models to better characterize water/oil emulsions and their behaviours [17, 18].

1.2.2 Formation of emulsions

The adequate mixing and presence of a surface-active agent are two vital factors that lead to emulsion formation where oil and water phases are brought together. During production of crude oils, there are a variety of mixing sources that result in creating the shear. Generally, the bigger the amount of shear, the smaller the droplet size of dispersed phase and the tighter the emulsion[19]. The second most important factor in emulsion formation is the presence of an emulsifying agent. The composition and amount of the emulsifier considerably dictate the type and tightness of the emulsion. The natural emulsifiers in a heavy oil are the resident particles in the crude. Less stable emulsions are formed from heavy oil with a smaller extent of heavy fractions which tend to separate more easily. Other samples with the adequate amount and different types of emulsifier might produce stable and tight emulsions. **Figure 1** shows a typical water-asphaltene-oil emulsion where asphaltene molecules (with three different components) consist of aromatic rings. The aliphatic and heteroatom parts are at equilibrium with the oil phase and water droplets and form emulsions[20]

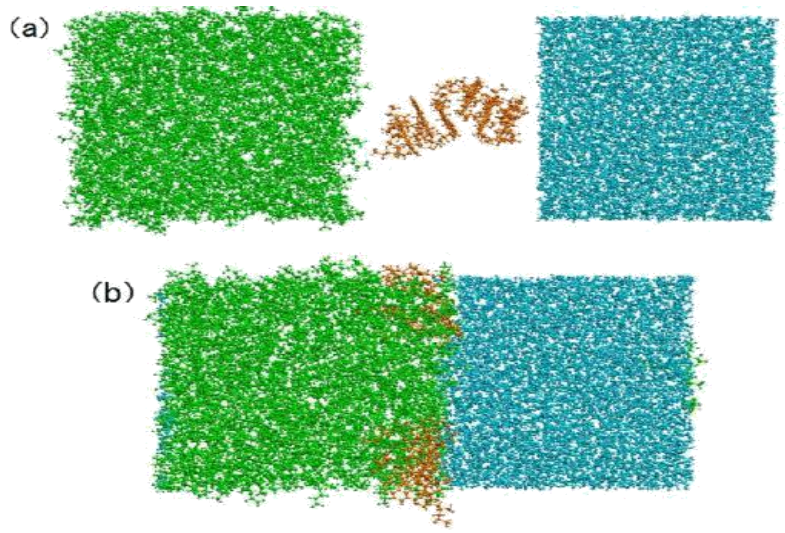

Figure 1-1: Interface system (oil-asphaltene-water): a) first configuration and b) last configuration. Green molecules (left) show heptane, and blue molecules (right) show water[20].

1.2.3 Types of emulsions

Produced emulsions in the oil fields can be categorized into three classes: water-in-oil, oil-in-water, and multiple or complex emulsions. Water-in-oil emulsions comprise of water droplets in an oil-continuous phase, and oil-in-water emulsions are attributed to droplets of the oil phase in a continuous flow of water[21]. Multiple emulsions are more complicated and made of tiny droplets in larger droplets which are suspended in a continuous phase. For example, an oil-in-water-oil emulsion consists of oil droplets suspended in bigger water droplets that are suspended in a continuous flow of oil phase. In the case of oilfield emulsions, the most common emulsions are in the category of water/oil as they are produced the most. "Reverse" emulsions are sometimes referred to the oil-in-water emulsions [27]. The type of the formed emulsions depends on a variety of factors such as water/oil ratio, temperature. As a rule of thumb, a phase is recognized as the dispersed phase if the volume fraction of the phase is smaller, compared to the other phase, and the other phase is tagged as the continuous phase. When there is an equal ratio of both present phases, other controlling factors including temperature or interfacial properties of the phases would specify the type of emulsion [27].

Emulsions can be categorized according to the size of droplets in the continuous phase flow [22]. Emulsion is known as a macro-emulsion if the dispersed droplets are bigger than 0.1 μm. This category of emulsions is generally thermodynamically unstable as the two phases tend to coalesce and separate due to the reduction in interfacial energies over time. However, the stabilization mechanisms are able to eliminate the rate of droplet coalescence[23]. A majority of the produced emulsions belong to this category. There is a second group of emulsions, in contrast to macro-emulsions, labelled as micro-emulsions. This class of emulsions is formed when two immiscible

fluids exist and emulsions are created due to their severe low-interfacial energy. The size of droplets in micro-emulsions is less than 10 nm, which are considered thermodynamically stable mixtures. Micro-emulsions are generally different from macro-emulsions in terms of stability and formation[24].

Winsor[24] presented a well-known categorisation for micro-emulsions in terms of phase equilibria as described in **Table 1**.

Table 1-1: Various categories of micro-emulsions to illustrate thermodynamic equilibrium [30].

Micro-emulsions Type	**Phase equilibria**	**Description**
Type I	Oil-in-water (o/w)	In this type, the surfactant is usually soluble in water (Winsor I). A small concentration of soluble surfactant exists in water in the form of monomers.
Type II	Water-in-oil (w/o)	In this class, the surfactant is preferentially soluble in oil phase. The aqueous phase is present along with an oil phase rich in surfactant (Winsor II).
Type III	Three-phase system	Excess water and oil phase coexist with a middle phase of rich surfactant in this category (Winsor III or middle-phase micro-emulsions).
Type IV	Micellar solution	In this class, an isotropic single-phase micellar solution forms by adding a sufficient quantity of surfactant with alcohol.

1.2.4 Emulsion characteristics.

To prepare a stable emulsion, the interfacial behavior should be altered by surfactants or/and heavy oil solid particles to preclude its driving force which is responsible for coalescence[25]. Another criterion for stable emulsion formation is that the droplet size is small enough so that the thermal collisions forces acting on the continuous phase molecules produce the Brownian motion which prevents settling[26]. The characteristics of an emulsion constantly vary from the moment of formation to the time of total phase inversion. Accordingly, fresh emulsions can demonstrate a different characteristic, compared to aged samples. This is attributed to the variation in the oil type due to the presence of absorbable components, differences in emulsifier adsorption rate, and its ability in producing a film at the interface. When the mixture is subjected to a considerable change

in the temperature or pressure, the emulsion characteristics such as viscosity or droplet size can alter significantly[21]

1.2.4.1 Emulsifying agents.

In oil fields, the produced water-in-oil emulsions contain oil, water, and an emulsifier. The emulsifying agents are developed to stabilize emulsions. They are classified into two types; namely, finely divided solids and surface-active agents[27].

Fine solids generally stabilize an emulsion mechanically. These materials, which are wetted by both water and oil, should be smaller than emulsion droplets and should accumulate at the water/oil interface .The effectiveness of these particles in stabilizing emulsions are strongly dependent on various factors such as inter-particle interactions, particle size, and wettability of the material [28]. Fine solid materials existing in the produced oil include clay particles, sand, asphaltene/ wax, silt, and mineral scales deposited on the water/oil interface [29, 30].

Surface-active agents or surfactants are the particles which are soluble in both oil and water phases. They have a hydrophilic branch, which has tendency to interact with oil and there is a hydrophobic branch that has an affinity towards water. Due to their special chemical structure, surfactants tend to create an interfacial film at the oil-water interface [31]. This phenomenon generally leads to a reduction in the interfacial tension (IFT) and consequently enhances droplets dispersion and emulsification. Naturally acting surfactants such as asphaltenes and resins in the heavy oil have high boiling-temperature fractions. These materials appear to be the main components of intervening films that form between the water and oil droplets in the field emulsions. Other emulsifying agents might come from the injected chemicals including asphaltene control agents, wax, stimulation chemicals, corrosion inhibitors, scale inhibitors, and drilling fluids to the wellbores or formation [32].

1.2.4.2 Stability of oil emulsions

From a thermodynamic perspective, an emulsion is an unstable system due to its natural tendency for a liquid/liquid mixture to minimize its interfacial interactions (or/and interfacial energies)[33].However, most emulsions demonstrate a kinetic stability after a period of time. Oil-field emulsions are usually categorized based on their degree of kinetic stability. The interactions between the surface-active agents and water/oil interfaces are primarily responsible for emulsion stability. During emulsification, emulsifying agents are adsorbed to the freshly formed interfacial film, which weakens the interfacial forces and allows the immiscible phases to be partially mixed. Following the first drop formation, the former emulsion begins to be altered because of different time-dependent processes, which are Ostwald ripening, coalescence, flocculation, sedimentation, and creaming as the most controversial processes[34]. Providing more details on stabilizing mechanisms, water/oil emulsions are assumed to be liquid/liquid colloidal dispersions. Their kinetic stability is a result of droplets with a small size and formation of an interfacial layer between water and oil droplet. **Table.2** provides a descprtion of different demuslsifcation processes. **Figure.2** also represents a cartoon of the emulsion breakup steps that illustrate a typical

approach towards oil demulsification; including, (1) sedimentation or creaming which corresponds to the density difference between the dispersed and continuous phases; (2) flocculation; (3) coalescence; and (4) phase separation. Before any phase separation happens through coalescence, emulsions should lose a considerable degree/level of the structural integrity.

Table 1-2: Demulsification mechanisms observed in water/oil and oil/water emulsions (from [33] [33] [33])

Demulsification process	Definition	Details
Sedimentation	Water droplets falling from an emulsion, which normally occurs due to the difference in water and oil density[35]	-It is a function of chemical structure and surfactant adsorption - Due to the difference in oil and water density
Creaming	Not an actual breaking, but the separation of emulsion into the denser part (cream) and the other parts.	-It is a function of chemical structure and surfactant adsorption - Due to the difference in oil and water density
Flocculation	It exhibits grouping of individual suspended droplets together, while each droplet keeps its identity	-It depends on surfactant structure - First step towards further emulsion ageing and coalescence. - More frequent mechanisms in oil/water emulsions
Coalescence	It represents the mechanism by which two or more separate groups of miscible particles are active as they pull each other to reach the slightest contact	-It is affected by interfacial film viscosity, surfactant film elasticity, and the dynamics of thin liquid film drainage
Aggregation	It corresponds to formation of accumulated droplets in a suspension	- It is the most common process, resulting in destabilization of colloidal systems
Ostwald ripening	It represents the diffusion of droplets into the continuous phase to describe the inhomogeneous structure modification such as re-deposition of surfactant particles into larger particles over time	- Generally experienced in water/oil emulsions - It is observed in liquid droplets or solid solutions
Phase separation	It is defined as complete separation of oil and water into two distinct phases.	-It is a function of time and emulsifier type

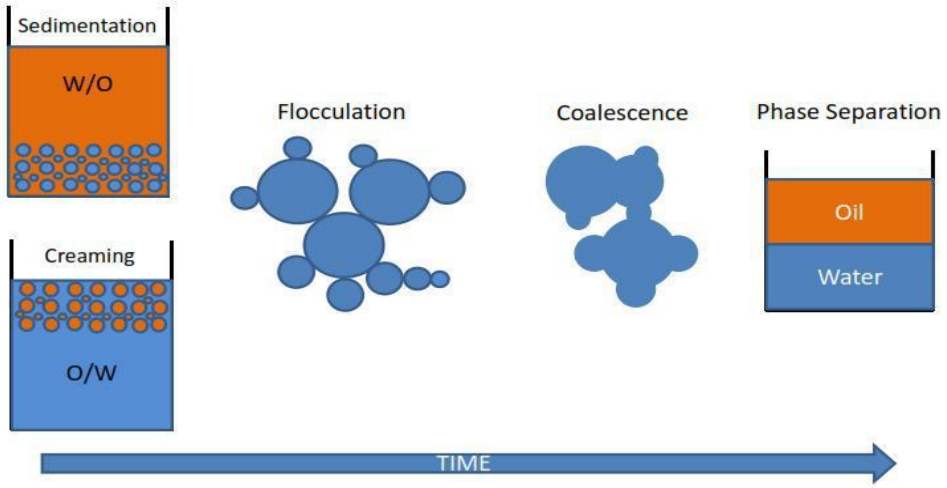

Figure 1-3 Demulsification and phase separation in oil/water emulsions [35]

Controlling agents are generally against emulsion destabilization in most cases. Emulsion stabilization is improved by surfactant injection as a consequence of electrostatic and steric forces. Interfacial interactions play a significant role in enhanced oil recovery (EOR) processes. One of the essential goals in EOR at the microscopic scale is to minimize the interfacial tension at the water/oil interfaces to mobilize the trapped oil by means of surface active agents (or surfactants). Considering the impact of surfactants in EOR design by affecting water/oil interfacial energies, the final recovery can be improved significantly.

Stabilization of water/oil emulsions produced from the oil fields occurs by formation of a thin film at the interface of the suspended droplets in the continuous phase. These layers are a consequence of polar high-molecular-weight molecules that behave as a surfactant which are interfacially active. These films increase the emulsion stability through increasing the viscosity of the interfacial film. The viscous interfacial films reduce the drainage rate of the film during water droplets coalescence by creating a repulsive barrier, which consequently lowers the emulsion break-down rate [36]. **Figure.3** depicts the presence of a film in a water/oil emulsion. The contribution of solids particles can also enhance the formation of the interfacial film, resulting in further emulsion stabilization.

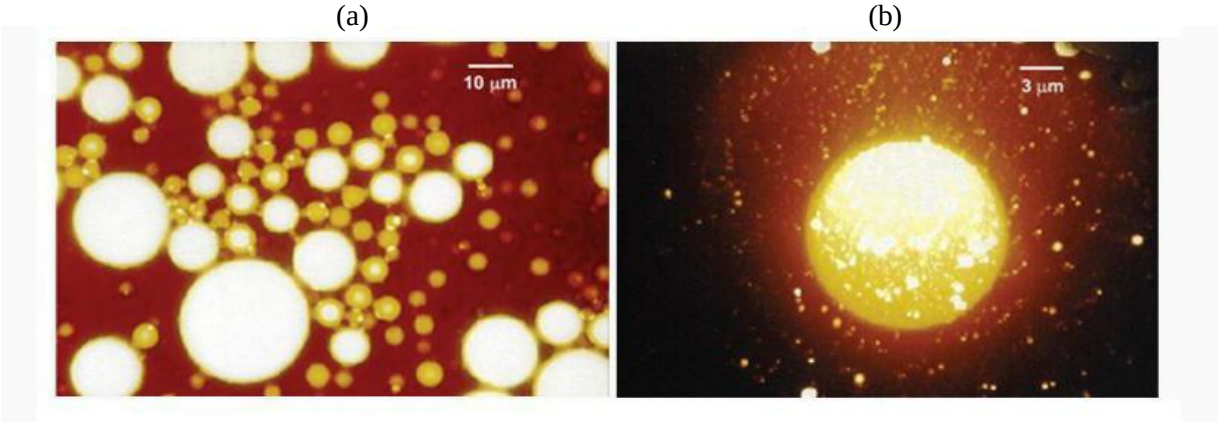

Figure 1-4: Schematic of emulsions, a) Photomicrograph of the interfacial films, and b) Magnified photomicrograph of emulsion interfacial films [37].

The properties of interfacial films depend on a number of factors such as polar molecules concentration in the heavy oil, crude oil type (asphaltic and paraffinic), aging time, temperature, and pH and composition of the water phase [37, 38].

Emulsion stability is correlated to the mobility of the interfacial films [34]. Since the interfacial layers are mostly responsible for stability of emulsions, it is of great importance to understand essential elements including presence of a surface-active agent or temperature which influence the interfacial films [40]. The effectiveness of important factors such as organic (e.g., asphaltene) and inorganic (e.g., clays) solid materials, polar heavy fractions of crude oil, droplet size, size distribution, brine composition and pH, and temperature in the emulsion stability in terms of interfacial film and interfacial tension (IFT) behaviours will be discussed in next sections.

1.3 CHARACTERIZATION TOOLS/METHODS

Separation of two-phase flow, including continuous and dispersed phases, is a common challenge for industrial and research sectors. Liquid and liquid suspensions demand the utilization of multiple equipment when the droplet size is small, typically in the range of 1-50 µm [39]. Thus, it is essential to recognize the effective methods and technologies to treat the produced oil and demulsify the emulsions present in the flow systems. To attain the ultimate separation goal, one should comprehensively understand the factors influencing the droplet size and therefore stability of emulsion. Researchers and engineers used (are using) different experimental set-ups/technologies to characterize the emulsions and to figure out important aspects (e.g., evolution of droplets, shape change, equilibrium conditions, and emulsion stability)[27].

1.3.1 Droplet size distribution techniques

Droplet size distribution is one of the most important characteristics of the emulsions since it determines the potential demulsification processes [40] .Thus, it can be used as a stability proxy. Zhou and Kresta [41] conducted an extensive review on the correlations and measurement techniques (light transmission, image analysis, and coulter counter) employed for determination of droplet size in the oil/water emulsions [42-44]. In the case of oil/ water emulsions, the inertial effects dominate the viscous energies as the continuous phase has a low viscosity than the suspended phase[45]. If the water drops exist in the oil emulsion phase, the viscus forces override the inertial forces in this type of emulsion. Although there are methods such as Nuclear magnetic resonance (NMR), and video enhanced microscopy to measure the droplet size distribution in water/oil emulsions[46, 47]; sampling is generally required before conducting measurements. Among the measurement tools, particle video microscope(PVM) and focused beam reflectance measurement (FBRM) particle size analysis probes offer an in-situ droplet size measurement [32].
In a research study, Sprow [44] concluded that there is a proportionality between the mean droplet diameter and the maximum measured value for droplet size of the aqueous fluid as the continuous phase. This finding has been confirmed by several researchers [48-50]. Boxall et al. [51] also obtained a relationship between the mean and maximum droplet size for a water droplet in oil emulsions. Droplet measurements are usually carried out in a mixing cell with a six-blade turbine impeller. Two droplet size analysis probes are normally installed at 45^{o} in the cell, oriented in front of each other; namely, a focused beam reflectance measurement (FBRM) probe and a particle video microscope (PVM) probe. They are placed at an equal level to the top of impeller to facilitate measurements and make the most of the flow passing the window. The turbine blade mixes all the materials to produce steady droplet size which can be achieved when there is a minor variation in FBRM distribution [49]. An optical rotating lens, which is placed at the top of the probe and is responsible for deflecting the laser, will reflect a laser beam, when the probe is inserted into an emulsion system. This occurs only when the beam scans the surface of a particle. The probe is responsible to determine the reflection time and to measure the chord length which is time multiplying by the speed of laser scan [51].
Particle video microscope (PVM) is a complementary droplet size analysis tool. The PVM contains six lasers to illuminate the probe front face [52] as it is depicted in **Figure 4**. The probe takes images of the lightened area and identifies droplets. Particles smaller than 20 µm cannot be identified by the PVM probe as individual droplets[51]. Once a steady-state distribution is reached, the PVM probe takes random images for different distributions and the droplets are counted to calculate the droplet size distribution. Supplementary information on the PVM and FBRM can be found in the literature [53] [52, 54]. Nuclear magnetic resonance (NMR) is one of the reliable and popular methods to measure the droplet size distribution (DSD) in both water/oil and oil/water emulsions so that a simple sample preparation is needed and an acceptable accuracy is attained. Emulsion stability analysis by the NMR method is based on the signal attenuation which is a result of random movements of droplets when the sample is imposed to two magnetic fields, since the intensity of NMR signal is related to the number of nuclei which are produced [35]. The technique is relatively

fast and is not limited to concentrated emulsions. Hollingsworth et al. [55] proposed a new method to calculate DSD by NMR which significantly reduced the experiment time. Van der Tuuk et al. [56] then combined the previous approaches and introduced a fast strategy. Amani et al. [57] used the Van der Tuuk model to obtain the droplet variation. Depending on the size range of droplets, two different methods were employed to determine DSD. A Fourier-Transform NMR Spectroscopy ordered from Bruker Company was used for DSD measurements [58]. The samples are placed inside the machine right after preparation for conducting spectroscopy measurements. The experimental design and interpreting the results can be made using Taguchi method. Droplet size variation plots are generated based on the measured data/values.

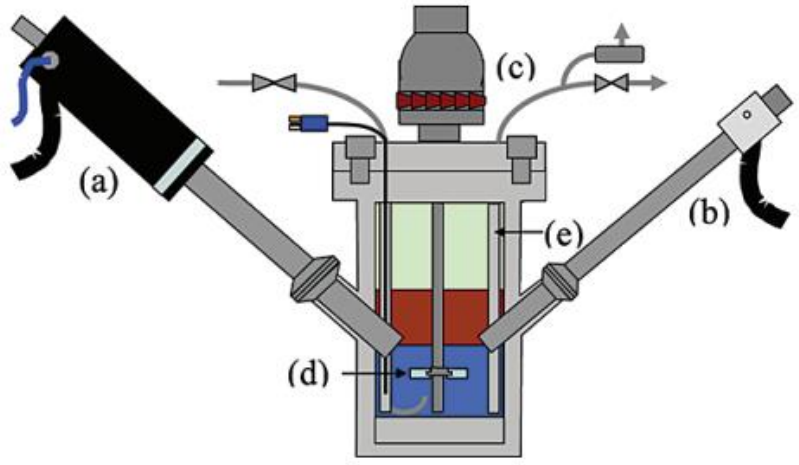

Figure 1-5: A simple schematic of DSD measurement tool made of (a) PVM probe, (b) FBRM probe, (c) magnetic agitator, (d) impeller, and (e) baffles (taken from [51]).

Another approach to calculate/ determine the droplet size distribution is through the combination of a microscopic equipment, a digital image processing software, and a statistical tool [18, 59]. ZEISS Particle Analysis systems provide extensive information on the particle droplet analysis. Through employing a proper microscope, one can obtain important information including particle length to detect the smallest particles from a targeted image. The various modules of the software deliver image analysis in multiple dimensions for various time steps. Microscope cameras, in contrast to the classical digital cameras, offer the maximum light sensitivity required for research activities. AxioVision is one of the light microscopes used for analysis and measurement of shape, size, and orientation of the materials in single or multiphase samples. Souza et al.[59]used the combined tools to investigate the effect of process conditions on the settling velocities of emulsions. Digital pictures were taken by a charged-coupled device (CCD) from an optical microscope as shown in **Figure.5**. The droplet size distribution was determined by the AxioVision software. Different modules of this software enable us to perform systematic analysis on the phase distribution of the samples. The module can classify the particles by area or diameter. The research outputs included the droplet diameters and number of particles for each sample. The researchers took several pictures and scrutinized them to obtain $d_{4,3}$ diameter. The *d*32 or Sauter

diameter is the volumetric average diameter of a spherical droplet similar to the mean diameter of particle system[59] .Laser diffraction is another widely used technique to obtain the particle size distribution [31]. Malvern diffractometer is one of the experimental apparatuses to determine the particle diameter, based on the optical properties of light. When a laser beam passes through a droplet, the sensors detect the angular variation in the scattered light intensity. Small particles scatter the light at big angles, whereas small deviations were reported for large particles. The angular deviation intensity of the scattered light is then studied to estimate the particle size where the Mie theory to analyse the scattered light is utilized[31]. The finding includes the droplet diameter of an equivalent sphere. Laser diffraction techniques cover a wide range of materials in terms of size from nanometers to millimetre droplet size. The assembly is able to continuously monitor and control the droplet behavior and to provide instant feedbacks[31].

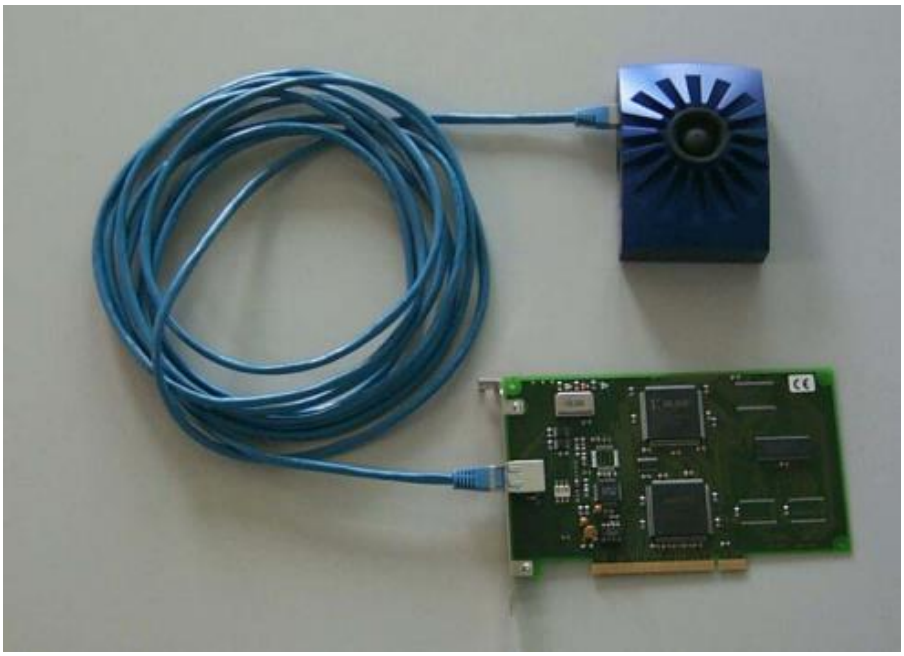

Figure 1-6: AxioCam Camera, PCI interface board, and data cable for transferring data from camera to motherboard (taken from[60]).

1.3.2 Stability determination methods.

One of the widely used methods for determining the emulsion stability is bottle test [32]. This method relies on the water resolution so that the procedure involves diluting emulsion with a solvent, adding emulsifier, shaking, and monitoring phase separation by time. The test is normally conducted at a specific temperature and may be performed using a centrifuge to accelerate the separation process. Different approaches were introduced in the literature [32, 61]. ASTM (American Society for Testing and Materials) method is a broadly accepted strategy to specify the sediment and emulsion stability. This method is also applicable to examine the effect of different emulsifiers on emulsion stability. Turbiscan™ LAB is an appropriate equipment to fully characterise different types of dispersions such as emulsions or suspensions in terms of properties, type, and stability[62]. It is used to perform the aging tests to provide adequate information on destabilisation mechanisms (e.g., sedimentation, coalescence,

flocculation, and creaming). Turbiscan Lab Expert offers more useful information, compared to the typical experimental approaches. For instance, it is possible to determine the stability of both concentrated and opaque colloidal dispersions with a single equipment[62]. The instability phenomena are also observed much quicker and simpler through using this tool, compared to the classical techniques [63, 64]. Xu et al. [65] performed electrical Microscope Analysis to investigate the stability of water/oil emulsions. The emulsion behaviours were monitored by an electrical microscope to take the amplified images of microscopic configuration and to determine the type of created emulsions. A proper statistical software was employed to obtain the average droplet size. Measurements through Turbiscan Lab Expert Stability Analysis were conducted by a pulsed near infrared LED. Two separate optical sensors captured and detected the light transmitted and backscattered by the samples. For water/oil emulsions, only the backscattering (BS) light was investigated since this type of dispersion was opaque and the transmission light was weak or/and almost negligible [58]. The stability analysis is performed via interpreting the variation in backscattering (ΔBS) profiles, according to the following formula [65]:

$$BS \approx \frac{1}{\sqrt{\lambda^*}} \quad (1)$$

in which, λ^* stands for the photon transport mean free path. To conduct the dispersion analysis, one needs to know the value of $\lambda^*(\Phi, d)$ which can be calculated by a relationship as follows [65]:

$$\lambda^*(\Phi, d) = \frac{2d}{3\Phi(1-g)Q_s} \quad (2)$$

In Equation (2), Φ represents the particle volume fraction, d is the droplet mean diameter, and $g(d)$ and Q_S introduce the optical parameters. The backscattering data are used to generate ΔBS profiles by means of Turbiscan EasySoft Converter. Turbiscan Stability Index (TSI) parameter is utilized to assess the stability of emulsion as given below[65]:

$$TSI = \sqrt{\frac{\sum_{i=1}^{n}(x_i - x_{BS})^2}{n-1}} \quad (3)$$

where x_i denotes the average BS, x_{BS} represents the average x_i , and n indicates the number of scans. Large values of TSI correspond to unstable emulsions.

Turbidity measurement is another effective method to determine the stability of emulsions. Turbidity is a direct function of droplet size and concentration[66]. This optical density measurement method relies on magnitudes of the wavelengths in a dispersing medium. Turbidity is due to the presence of particles with various sizes. Adsorbed or scattered light represents the emulsion fluctuation. This causes the value of turbidity to change. In a turbidity versus time plot, the small slop values demonstrate a stable emulsion. Turbidity meter devices work with both infrared and white light sources. A simple schematic of this apparatus is depicted in **Figure.6**.

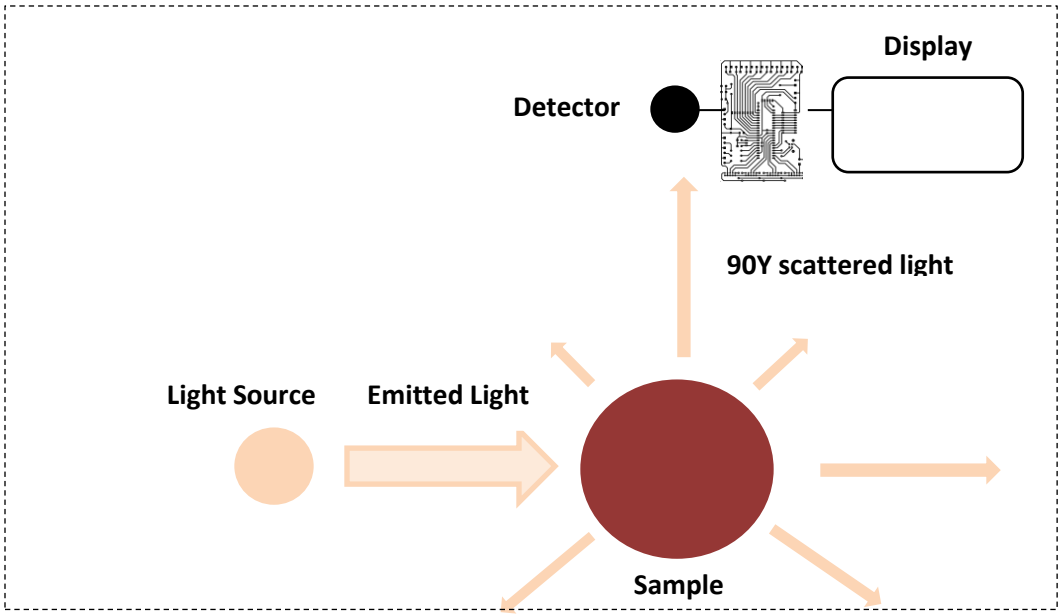

Figure 1-7: Schematic of a turbidity measurement device (modified after [67]).

Dukhin and Goetz[4] applied the electrostatic and conductivity measurements to monitor the emulsion evolution and transition from the emulsion to micro emulsion. They compared their results with the optical microscopic imaging information. It was found that their proposed approach has some advantages over the optical method, since this method is based on the weight of the particles and the samples are polydisperse systems. This method can also provide information about properties of the electric surface; while other optical techniques are not able to offer such information [4]. To screen droplets at micro and nanoscales at the same time, this is the only strategy that provides reliable results. The electrical conductivity methods are another fast technique to analyze the Electrical field stability by determining the critical electric field (CEF). This methodology is based on polarizing the water droplets and formation of aggregates. According to Aske et al. [68], a high amount of CEF shows high emulsion stability.

A summary of the stability proxy methods and their pros and cons are given in **Table.3**.

Table 1-3: A list of characterization tools to determine emulsion properties

Method	Previous works	Device	Disadvantages	Advantages
NMR (nuclear magnetic resonance)	Amani et al.[4]	Fourier-Transform NMR Spectroscopy	▪ biased DSD assumption for all types of emulsions ▪ requires preparation steps ▪ an outside force is needed for stiff emulsions	▪ provides various information regarding size and shape of molecules ▪ applicable for complex mixtures
NIR (near infrared spectroscopy)	Kallevik et al.[69]	NIR Spectrometer and Analyser	▪ DSD cannot be quantified directly ▪ needs calibration, ▪ time and energy consuming technique	▪ simple to operate ▪ multiplicity of analysis ▪ provides both physical and chemical characteristics of sample
Optical microscopy	Boxall et al. [51] Moradi et al. [35]	PVM, FBRM Olympus BX51 transmitted-light microscope	▪ sensitive to sampling procedure ▪ requires calibration and proper focusing	▪ direct measurement of the shape and size of droplet ▪ It is possible to estimate phase concentration
TEM (transmission electron microscopy) and SEM (scanning electron microscopy)	Binks et al. [70]	Oxford instrument of Jeol 5600 Scanning Electron Microscope	▪ requires sample coating for taking image ▪ can only work at high pressure chambers. ▪ the electron can change sample properties	▪ high resolution due to the use of electron beam ▪ can be used for the study of small structures
Zeta potential measurement	Hannisdal et al. [7]	Malvern 3000HS Zetasizer	▪ requires correlation and cannot be measured directly ▪ Small variation causes significant changes in results.	▪ multi-measurement capability ▪ short analysis time ▪ excludes the effect of electrode polarization

Acoustics and electroacoustic	Dukhin and Goetz [4]	-DT-1200 dispersion technology for DST -Scientifica conductivity meter -Zeta potential probe DT-300 for electroacoustic measurements	▪ Effect of solid particle is neglected ▪ needs calibration ▪ requires data for phase concertation	▪ no sample preparation ▪ effective for concentrated emulsion ▪ continuously characterizes emulsion evolution ▪ is not restricted to aqueous phase and provides data for non-polar solutions
Bottle test	Kokal [32]	ASTM	▪ not a direct stability proxy ▪ needs large equipment ▪ Often inaccurate	▪ simple to perform based on defined standard methods
Light scattering and diffraction	Bink et al.[31]	Malvern diffractometer	▪ Not reliable results for large droplets and w/o emulsion. ▪ requires external forces	▪ simple and fast method ▪ small sample volume
Electrical conductivity	Almeida et al.[71]	Gehaka conductivimeter CG2000 coupled with Sensoglass conductivity cell SCC04	▪ requires information to compare the results	▪ small sample volume ▪ fast generation of reliable information
Turbidity measurements	Kundu et al.[72]	Aqualytic turbidity meter	▪ Sample has to be diluted	▪ fast and inexpensive

1.4 MODELING APPROACHES/STUDIES

Deep bed filtration theory was developed to describe the governing mechanisms in liquid-liquid suspensions[73]. Like solid - particle dispersion[74], the emulsion droplets can stick on the wall of pore throats by straining capture, or they may be retained at the porous medium surface due to several forces such as capillary or/and shear forces (interception capture) [75]. When the emulsion droplet size is larger than the pore size diameter, the droplets will be trapped in the pores and block the fluid flow. This phenomenon is known as straining capture. A schematic of these two phenomena is illustrated in **Figure.7**.

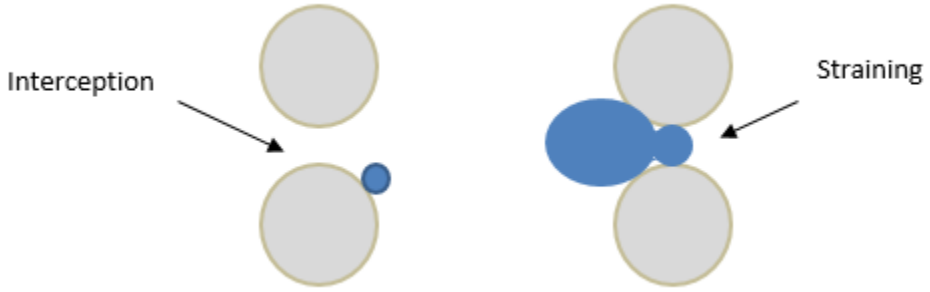

Figure 1-8: Pore blocking mechanism by interception and straining (modified after Rezaei & Firoozabadi, [75]).

In dilute suspensions, velocity controls the flow where drops enter the pores in a consecutive way [18]. Droplet re-entrainment occurs either when high-pressure force squeezes the drops through pore constriction or captured drops break-up. Droplet squeezing happens when the drops clog small pores. As the pressure increases, they are forced to enter a smaller pore until the velocity reaches high enough to re-entrain the droplets [75]. Based on Laplace equation, the capillary pressure is proportional to the interfacial forces and difference between the mean drop curvatures of downstream and upstream [18]. Filtration theory is required to predict the effect of velocity on squeezing phenomena. When the viscous forces exceed the interfacial forces, the captured drops may break up. Snap off or viscous fingering may cause this break up. Snap off takes place in a long neck pore constriction, when the wetting phase bypasses a nonwetting drop in a particular geometrical configuration. At high capillary pressures, it was observed that the drop squeezes through pore constriction without snapping off, when the drop size to pore throat size ratio is approximately equal to one [75]. The second mechanism for strained drop break-up is the hydrodynamical instabilities. When a less viscous phase penetrates through a trapped droplet with a higher viscosity, a droplet break-up may occur by fingering. The interception capture process occurs when the drops are trapped on the sand grain surface or in the recirculation eddies. When there is a possibility of re-entrainment such as straining capture, velocity plays an important role [76].

Clogging rate is affected by the fluid velocity in the interception regime. Captured drops may be torn from the surface of the sand grains once the hydrodynamic force exceeds the colloidal attraction forces between the droplet and sand grains. Flow interruption can also cause re-entering of captured drops in recirculation eddies to the flow stream. Furthermore, high velocity and low interfacial tension can contribute to the interception capture phenomenon[54] .For example, in a system with high ionic strength or low zeta potential, van der Waals attraction forces are greater than the double layer repulsion. Hence, the retained particles strongly stick to the grain surface and a large portion of hydrodynamic forces should be applied to dislodge the drop. This normally happens under turbulent flow condition for solid particles. For liquid suspensions, even bigger hydrodynamic forces are required to rip the droplet off in the laminar flow regime [77]. It is found that an increase in the velocity lessens the interaction time between the droplet and grain surface, which leads to a lower capture rate. Droplet wedging is another interception capturing mechanism.

In the droplet wedging capture, droplets can be wedged between the curved surface of sand grains, and stay there by dynamic pressure forces[77]. Most of wedging capture, occurs at the front part of the sand grains. Increasing velocity pushes the drops tighter into the crevice. As a result, no velocity effect is expected. Particles can also be captured in pockets formed by several sand grains, where either recirculation occurs, or the fluid is nearly stagnant where no velocity impact is anticipated. Droplet rupture might also be experienced in captured droplets. As mentioned earlier, viscous forces cause the droplet to shear apart, and the interfacial tension forces are responsible for holding the droplets together[54] . When the viscous forces exceed the interfacial forces, the droplet will break-up. Since, the droplet diameter is almost equal to the pore throats size in the porous medium, flow in underground porous medium would not follow the classical deep-bed filtration theory. The high droplet diameter to pore size ratio causes high droplet capture rate; a considerable change in the local permeability of the porous media; and a significant velocity increase. This velocity increase appreciably influences the rate of droplet capture. Again, if the velocity increases, captured drops by straining, may enter the flow stream due to the domination of local pressure gradient over capillary resistance of droplet [18, 78]. In the interception regime, captured drops may be ripped from the porous walls when the hydrodynamic forces dominate the attraction forces between the droplets and grain[79]. If the viscous forces exceed the interfacial forces, the drops may break up. Based on the filtration model, one would be able to describe the transient flow of emulsion through porous medium by three parameters; namely, a filter coefficient, a flow-redistribution parameter, and a flow-restriction parameter (R). The filter parameter is attributed to the emulsion front sharpness; the flow-redistribution coefficient controls the flow redistribution phenomenon and steady state retention. The influence of the captured drops in permeability reduction is explained by the flow-restriction parameter[80]. Development of comprehensive models is time consuming and requires strong knowledge and understanding of theoretical concept for attaining high accuracy. Furthermore, there are fairly high costs and errors with the common experimental procedures to determine different fluid/emulsion and physical model properties. A number of researchers focused on the transport phenomena of emulsions in porous media to develop analytical models for better characterization of water/oil emulsions[17, 59] . Characterising fluids by surface tension (σ), density (ρ), viscosity (μ), a characteristic linear dimension (L), velocity (u), and influence of gravitational force (g) field, these six variables may be expressed in the form of dimensionless numbers through employing Buckingham's Theorem. Reynolds number (*Re*) is an important dimensionless number in fluid dynamics which is the relative magnitude of the inertial forces and viscous forces [54]. Inertial forces are the forces due to the momentum of the fluid as expressed by$(\rho u)u$. Thus, the denser a fluid is, and the higher its velocity and consequently the more inertia (momentum) it has. Viscous forces are the frictional shear forces due to the relative motion of the different layers in a flowing fluid, resulting in different velocities for different layers, which are directly related to dynamic pressure and shearing stresses[81]. When a fluid is subjected to an internal movement (difference in velocity) or subjected

to a higher velocity stream of a fluid, this generates the friction, which is the onset of turbulent flow. The Reynolds number describes the ratio of these two forces as expressed below [81]:

$$\text{Re} = \frac{inertia\ forces}{viscos\ forces} = \frac{\rho u L}{\mu} \quad (4)$$

in which, ρ stands for the density of the fluid, u signifies the fluid velocity, L represents a characteristic linear dimension, and μ refers to the fluid viscosity. Based on the value of this dimensionless group, the flow regime can be identified. At low Reynolds number values, the viscous forces are greater than the inertial forces and the flow regime is laminar. When the viscous forces are dominated by the inertial forces, the turbulent flow occurs. Flow instabilities are normally observed at high magnitudes of Reynolds number [81].

Another important dimensionless group is the Weber number (*We*), which represents the ratio of inertial forces and curvature forces or surface tension within a fluid [82]. This parameter is used to describe the fluid flow with curved surfaces for multiphase flow systems. The Weber number is defined as follows[82]:

$$\text{We} = \frac{inertia\ forces}{interfacial\ \ forces} = \frac{\rho\, u^2 d}{\sigma} \quad (5)$$

where d is the droplet diameter and σ denotes the surface tension.

In the continuum mechanics, Fraude number (*Fr*) is a dimensionless number to represent the ratio of the inertial forces and external field, which is usually gravity. The general formula for this dimensionless number is given as follows [83]:

$$Fr = \frac{inertia\ forces}{gravity\ forces} = \frac{u}{\sqrt{gL}} \quad (6)$$

In Equation (6), g stands for the gravitational acceleration.

In fluid mechanics, the Bond number (*Bo*) is an indicator of the relative importance of forces induced by the gravity, compared to surface tension as shown below [84]

$$Bo = \frac{gravity\ forces}{interfacial\ forces} = \frac{\Delta\rho g L^2}{\sigma} \quad (7)$$

In Equation (7), $\Delta\rho$ represents the density difference between the two phases, L refers to the characteristic length, σ denotes the surface tension, and g is the acceleration due to the gravity. The Bond number is normally used to describe the shape of droplets in a continuous fluid while dealing with emulsions.

The capillary number (*Ca*) in the context of transport phenomena is defined as the ratio of viscous and interfacial (curvature) forces as given below [85]

$$Ca = \frac{viscous\ forces}{curvature\ forces} = \frac{\mu u}{\sigma} \quad (8)$$

As a rule of thumb, flow in porous media is controlled by the capillary forces at law capillary numbers. Whereas the capillary forces can be neglected, in comparison to the viscous forces, when the capillary number holds high values. It is worth to mention that the relative significance of surface tension and gravity (compared to other forces) increases as the fluid particles in the system become smaller. This is the main reason that the surface tension effect is dominant in the microscale analysis and the interfacial tension is one of the vital factors, contributing to the droplet size distribution [54].

Since emulsions are thermodynamically unstable dispersions, they tend to separate and settle to reduce the interfacial energy between the oil and water phases [75]. Due to the density difference in the dispersed and continuous phases, the droplets experience a gravitational force and a buoyancy force. The frictional drag force also opposes the gravitational force. The balance of the forces is formulated as the Stokes's law to determine the settling rate [86], as given by Equation (9).

$$V_{STOKES} = \frac{(\rho_d - \rho_c) g d^2}{18 \mu_c} \quad (9)$$

In the Stokes's law, V_{STOKES} signifies the sedimentation velocity (m/s); ρ_d and ρ_c represent the dispersed and continuous phase densities (kg/m^3), respectively; *d* refers to the particle diameter (m); *g* denotes the acceleration due to the gravity; and μ_c is the dynamic viscosity of the continuous phase (Pa.s). The Stokes's law has a number of limitations. For instance, the interactions between the particles are neglected. It is also assumed that the particles are spherical, which is only applicable to low-concentration emulsions with a simplified droplet size distribution [87]. Calculations and estimations related to concentrated dispersions are therefore complicated [87, 88]. The Stokes's law is the analytical solution for the Navier-Stokes's equation, where a simple flow model for the solid particles is assumed. Internal circulation inside the particle will cause a reduction in the drag force in the absence of surface active components. Hence, the viscosity term should be modified. To incorporate this modification, the correction term was introduced by Hadamard-Rybczynski equation [89]. This correction term is analytically calculated by solving the momentum transfer equations for the velocity fields in the case of isolated drop settling. The modified term for the viscosity is given by the following expression[90] :

$$V_{HR} = \frac{(\rho_d - \rho_c) g d^2}{18 \mu_c} \frac{\mu_c + \mu_d}{\frac{2}{3}\mu_c + \mu_d} \quad (10)$$

In Equation (10), V_{HR} represents the correction term for the viscosity and μ_d is the viscosity of dispersed phase.

Based on the proposed equation/model, the settling rate will approach 3/2 of the value estimated by the Stokes's law for a large difference between the viscosity of the dispersed and continuous phases[59]. Assuming the viscous droplets flow in a gas phase (e.g., the circulation is negligible), the Stokes's law is valid, while the predicted settling velocity will be 3/2 of the Stokes's velocity in a system of viscous liquid with gas bubbles due to a high degree of circulation[91]. Considering the impact of phase concentration on the settling velocities of complex dispersions, Richardson and Zaki, [92] developed an empirical correlation as given below:

$$V_{RZ} = V_{STOKES}(1 - \Phi)^n \quad (11)$$

Equation (11) can be rewritten as follows:

$$V_{RZ} = V_{STOKES}(1 - 0.01WC)^n \quad (12)$$

where ϕ refers to the volume fraction of dispersed phase (which is usually 0.01 of water content) and n is an experimental constant between 2.3 and 5[92]. Equations (9) through (12) build the fundamental basis for the droplet settling studies; however, the theoretical model is not able to adequately describe the complex interfacial characteristics such as surfactant adsorption and the interaction between heavy particles such as asphaltenes and resins. Further studies were performed by various researchers on the sedimentation and coalescence of liquid-liquid dispersions [87, 93-98].

1.5 REVIEW ON PARAMETRIC SENSITIVITY ANALYSIS

Various parameters are reported to be responsible for emulsion stability as it was mentioned in the previous parts of the manuscript. The aim of this section is to assess the effect of different operational condition, fluid and reservoir properties on the droplet size distribution and emulsion stability. The impact of each parameter is discussed though presenting some figures and tables, based on the results reported in literature.

1.5.1 Effect of Process/Operational Conditions

1.5.1.1 Water oil ratio

When the size of droplets is small, it is difficult to separate the water and oil phases [39]. Crude oil is a complex mixture of heavy particles (e.g., asphaltene and resins), solid particles, gas, and water. The first step in separation is to allow the fluid to settle in cylindrical vessels and then allow the gravity to slowly separate the phases. When the mixture is heterogenous, measuring/identifying the interface position between different phases is crucial from the economical point of view since it can improve the equipment design and eventually prevents the ecological hazards and oil

discharge over offshore processes [99]. Residual particles including: asphaltene, emulsified water, and oil cause formation of a rag layer. The formation of this layer is not desirable since it damages the separation facilities. The development of this layer is a function of settling and coalescence rate; which strongly depends on the droplet size, interfacial characteristics, viscosity, and density [100]. The fluid dynamic analysis of the immiscible liquids separation, can be performed through the sedimentation tests. Souza et al. [59] studied the gravitational settling for a diluted Brazilian crude oil. They investigated the effect of factors such as: water cut and temperature, which influence the sedimentation and coalescence phenomena, on the droplet size variation of the samples. The sedimentation velocity of a complex mixture, consisting of water in oil emulsions, were examined in an experimental study, to obtain the droplet size distribution as a function of interface position and time [59]. The researchers noticed that as time goes on, the bigger droplets move downward and water cut is reduced at the top. According to Grimes[101], the depth of the interface position can be considered zero at the separator top and can be extended positively downward. However, they observed change in the behaviour of the system so that it did not follow the pattern that they predicted. Souza et al. [59] did not find a direct relationship between the selected variables. A modified version of Richardson-Zaki correlation was developed to calculate the settling velocity where the effects of process variables (e.g., temperature, pressure, and concentration) were considered. Since the researchers did not take into account the impacts of surfactant adsorption and interactions between asphaltenes and resins, the proposed model was not the same as the original equation in terms of their constant values. This correlation was based on the dependency of droplet diameter to the water content, however, the proposed model exhibited high deviation (error) when the water content was more than 30%[59] .To access water content changes with time and position using a sedimentation profile, 3D plots were constructed. They explained about the effect of temperature on the settling velocity and how droplets behave at different positions in the vessel[59]. They observed unpredicted patterns in their experiments. In some cases, adequate explanation about the trend was not provided. For example, the researchers expected to see large droplet size in the middle of the vessel due to the coalescence at low temperatures [59]. However, the result showed a different trend so that the mean droplet size remained constant in the middle. It is noteworthy that the approach introduced in this research work was based on a simple experimental apparatus. This is the main reason that they did not consider non-diluted or opaque emulsions for the comparison purposes and model development[59]. As discussed before, water-oil ratio of water /crude oil emulsions has a great impact on the stability of the dispersions and the subsequent stabilization processes applied for treatment of the produced oil. Xu et al. [65] also performed experiments to investigate the effect of these parameters (water content and temperature) on the stability of a synthetic water/oil emulsion. Electrical microscopes and Turbiscan stability analyzer were employed as tools to create backscatter profiles to study the emulsion behaviour at various temperatures and water contents [65]. Through using homogenizer, the synthetic emulsion was prepared by adding a purified oil to the wastewater. As water has a higher specific gravity than oil, the water droplets will migrate to the bottom. They observed that

the sedimentation of water at the bottom leads to an increase in back scatter (BS) light as a result of growth in the water volume fraction[63]. They observed that a larger variation in ΔBS is experienced when the water content is higher, implying a less stable emulsion is formed. Their results confirmed that the stability of water oil emulsion decreases if the water content of emulsions increases. It is suggested that the water content should be around 30% to have a stable emulsion and consequently to prevent demulsification processes [65]. Anisa and Nour [102] reported that droplet size distribution is persuaded by the water cut. The magnitude of viscosity was determined for two different water cuts. It was found that the droplets interactions increase as the water cut increases, while the relationship between viscosity and shear rate is constant. Hence, they concluded that the viscosity variation is caused by the droplet size variation [102]. Based on Souza et al. [59], **Figure.8** demonstrates a general representative on the relation between the water oil ratio and mean droplet diameter.

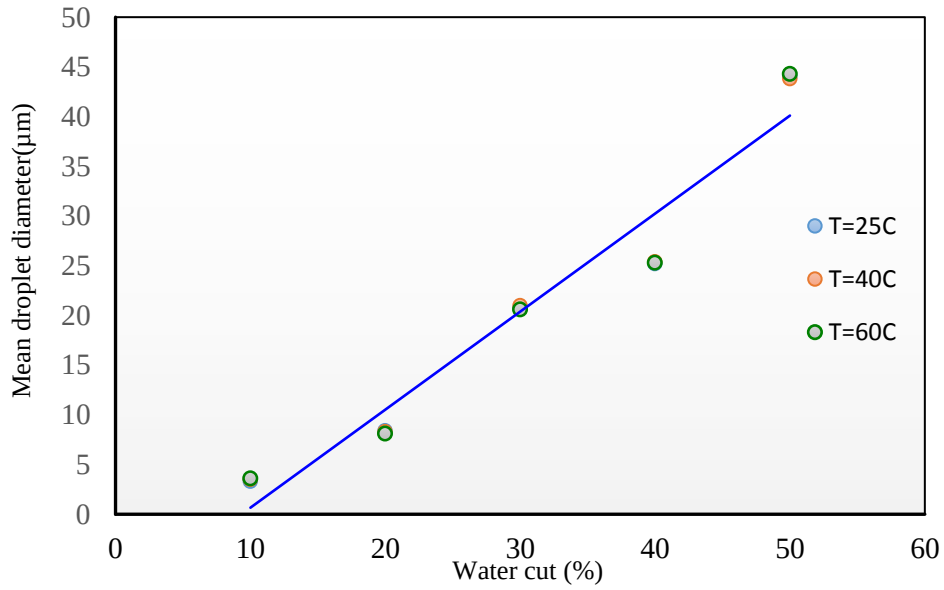

Figure 1-9: Effect of water content on mean droplet diameter at different temperatures (data from Souza et al., Anisa and Nour) [59, 102].

1.5.1.2 Temperature

Physical properties are strongly affected by temperature. For instance, the interfacial characteristics of oil and water and emulsifying agent solubility are dependent on thermodynamic conditions, particularly temperature. One of the important factor which is influenced by temperature is viscosity. Focusing on the backscattering profiles, Xu et al. [65] studied the impact of temperature on the emulsion stability. According to the Stokes's equation, an increase in the viscosity (due to the temperature reduction) leads to droplet variation, and consequently particle migration. Furthermore, high temperature can accelerate the demulsification process to increase

the water droplets collision. Based on the backscatter profiles, the Turbiscan stability index (TSI) is defined in terms of BS data and number of scans as follows:

$$TSI = \sqrt{\frac{\sum_{i=1}^{n}(x_i - x_{BS})^2}{n-1}} \quad (13)$$

where x_i is the average of BS, x_{BS} is the average of x_i, and n represents the number of scans [65]. A linear relationship between the TSI and temperature were found[65]. The novelty of their work was their lab equipment; which enabled them to determine the stability parameters easier and faster, compared to common methods. Conducting corresponding measurements at different depths of the emulsion sample, Souza et al. [59] related the coalescence and sedimentation rate to the temperature. It was concluded that, since the sedimentation is low, the droplets accumulate and the coalescence is likely to happen at low temperatures; however, droplets settle faster and coalescence rate increases at higher temperatures [59]. Binks and Rocher [103] investigated the effect of temperature on the water oil emulsion stability in the presence of wax as an emulsifier. Two different types of samples were prepared manually by hand shaking and homogenizer. It was claimed that the temperature changes, initiate variation in wax properties such that the interfacial layer behaviour of oil and water phases will progressively change; which cause subsequent coalescence and sedimentation. Wax (as a hydrophobic insoluble particle in water) can be adsorbed at the water/oil interface and creates the steric force. Due to this molecular structure, Becker[104] believed that wax is responsible for the emulsion stability. Binks and Rocher [103] subjected two sets of samples to a gradual increase in temperature from 10°C to 95°C (see **Figure 9**). The overall trend for both hand-shaken and homogenized prepared emulsions shows an increase in coalescence (f_w) and sedimentation (f_o) rate with increasing temperature. However, the initial stability of hand-shaken sample was significantly higher than that of the homogenized emulsion. It is attributed to the partial melting of wax particle in areas close to the impeller [103]. They explained that as temperature increases, the wax particles melt, leading to the interface rupture and phase separation. It was suggested by Binks and Rocher [103] that the dominant effect of temperature is on the wax particle properties, influencing the emulsion stability. The same pattern is observed in other samples in the literature [59, 102, 105], where by increasing the temperature, the average diameter of the droplets increases. The similar behaviour is experienced when the coalescence and sedimentation rate increase.

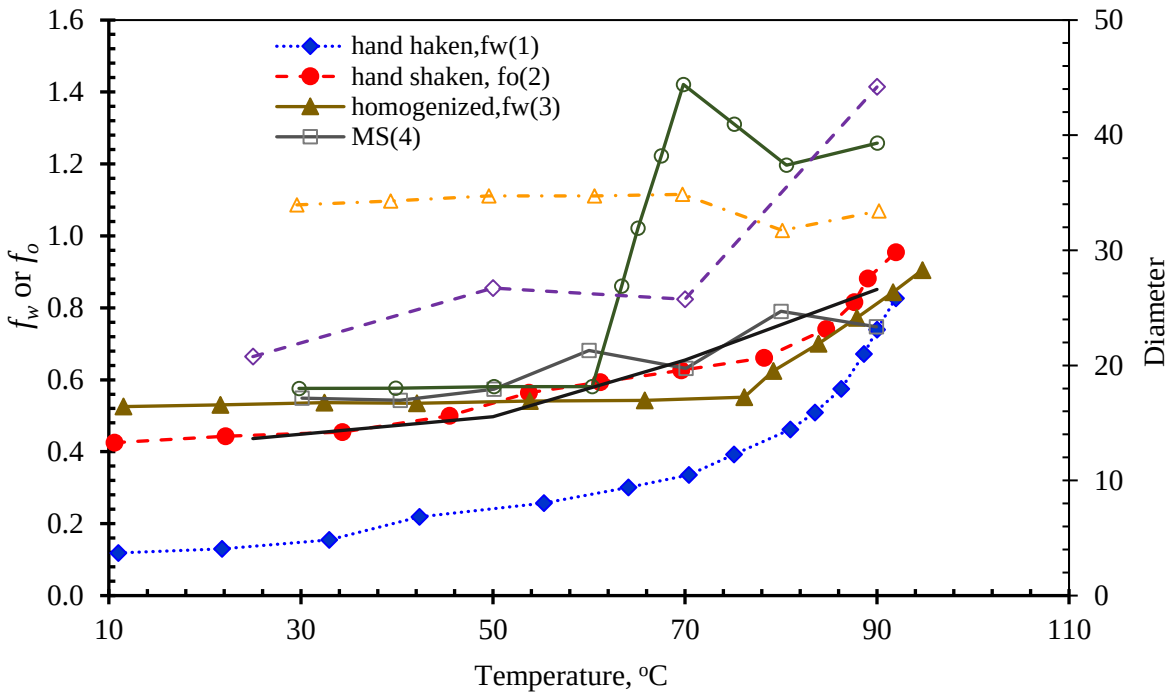

Figure 1-10: Effect of temperature on various emulsion samples in the presence of different emulsifiers: modified starch (MS), Whey Protein Isolate (WPI), Gum Arabic (GA); and hand shaken and homogenized; at two different water cut. [The first 6 samples are shown on primary y-axis and the last 2 samples are depicted on the secondary y-axis] (Data extracted from [59, 102, 103, 105])

1.5.1.3 Flow regime

Emulsion formation at turbulent flow conditions occurs in different industrial, environmental, and biological fields such as membrane processes and enhanced oil recovery [88], pharmaceutical emulsions [106], suspended polymers[107], and oil spill cleaning strategies[108-110]. The theoretical framework for the droplet size determination in a turbulent flow was first introduced by Kolmogorov [111]. In the turbulent flow, the interfacial stresses are at equilibrium with the viscous or/and inertial stresses [111].

Turbulent flow at high Reynolds number is described by Kolmogorov length. The largest stable droplet can be detected in either inertial subrange where the inertial energies/forces are dominant or they balance the interfacial tension, or they are in the viscous subrange where the interfacial forces are balanced by the viscous forces [111]. Shinnar [112] attempted to explain the relationship between the droplet size and the viscosity of the continuous phase in the viscous subrange system. This researcher theoretically described the impact of turbulence flow on the coalescence and droplet size variation. However, it was not feasible to validate the statistical/modeling results on the droplet size with the experimental values. Several experimental and theoretical studies were conducted on the droplet size prediction for the fluid flow of oil/water emulsions under turbulent regime conditions [41, 45]. For a system where the interfacial stresses are balanced by the inertia

(e.g., they are independent of the viscosity of the continuous phase), the largest stable droplet is bigger than the smallest eddies. The interfacial stress, which is the ratio of interfacial tension and droplet diameter, is equal to the turbulent inertial stress. Hence, in the low-viscosity continuous aqueous phase where the droplet breakup is controlled by the inertial forces, the following expression represents a relationship between the droplet diameter and important variables such as tank diameter and fluid density[45]:

$$d_{max} \propto \rho^{-3/5} N^{-6/5} D^{-4/5} \Gamma^{3/5} \quad (14)$$

in which, d_{max} stands for the maximum droplet size, ρ is the fluid density, Γ denotes the interfacial tension, N refers to the impreller speed, and D siginifies the diameter of the mixing tank.

In the viscous subrange, the droplets are smaller than the smallest eddies and the balance of forces is different. The viscous forces are greater than the inertial forces and the viscosity considerably influences the droplet size diameter. The researchers [54, 112] proposed the following equation to incorporate the main parameters (e.g., density and interfacial tension) in the droplet size in the viscous subrange regime:

$$d_{max} \propto \rho^{-1/2} N^{-3/2} D^{-1} \eta^{-1/2} \Gamma \quad (15)$$

Since a small variation in the viscosity was considered in the previous studies, a few research investigations focused on the droplet size behavior in the viscous subrange processes [54, 113]. For instance, Groeneweg et al.[113] performed experimental analysis of droplet size distribution for water/oil emulsions in a turbulent flow within limited ranges of shear rate. They did not discuss about the type of flow (e.g., viscous and inertial subrange). The relationship between the droplet size, viscosity, and interfacial tension or shear rate in the viscous subrange was studied by Boxall et al. [54]. The researchers performed the experiments for a wide range of viscosity which enabled them to identify the sub-regimes. They used dimensionless numbers to find a relationship between droplet size and dependent variables in the viscous subrange of a turbulent flow. For example, Weber number and Reynolds number are two key dimensionless numbers to reasonably estimate the droplet size based on viscosity, interfacial tension, and shear rate. Employing PVM and FBRM for droplet measurements, they obtained a graphical model for the droplet size in terms of Weber and Reynolds numbers [54]. The generated curve separates the inertial and viscous subrange. It showed the functionality of droplet size to the viscosity in the inertial subrange. It was also found that the droplet size is related to the inverse square root of viscosity of the continuous phase in the viscous subrange [54]. Though the droplet deformation in the turbulent flow was not studied in their research, they derived an equation to predict the droplet break-up using the Weber and

Reynolds numbers for both inertial and subrange flow conditions. **Figure.10** clearly indicates the droplet diameter versus viscosity as the flow regime changes. The model proposed by Boxall et al. [54] was used and validated by Aman et al. [114] to forecast the deep-water blowout. They claimed that the formation of oil droplet in water dispersions is an important factor that influences the oil migration during blowout. The oil droplet size distribution was monitored using a high-pressure sapphire autoclave cell. The experimental results were in a good agreement with the data available in the literature; however, the tuned inertial sub-regime is slightly different than the results obtained by Boxall et al. [54] (see **Figure.11**). The mean diameter versus Reynolds number is shown in **Figure.10** for two different regimes. They concluded that the new tuned model can fit the data better as the previous model did not take into account the characteristics of the dispersed phase. As it is clear from **Figure.11**, at low Reynolds numbers due to small dispersion of oil droplets into water, an excess shear force is created, which is required to form the droplets. [112] This phenomenon leads to the considerable deviation from the Boxall et al.'s model. Since the model used by Boxall et al. [54] was obtained for the oil-in-water emulsion systems and Aman et al. [114] performed experiments using water-in-oil emulsion based on Boxall et al.'s model, a generalized model for the inertial subrange flow condition is still missing. Furthermore, no research studies have been conducted to investigate the effect of Reynolds number (over a wide range) for turbulent or subrange flow in a cell. Thus, all calculations are based on the corresponding assumptions on flow rates, Reynolds number ranges and geometries[54].

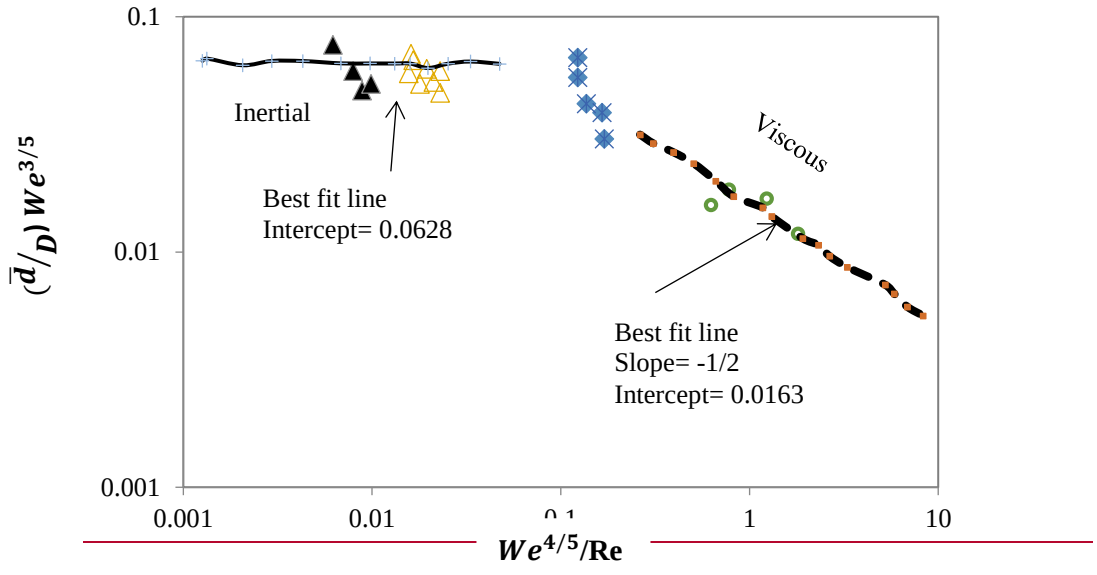

Figure 1-11: Mean droplet diameter versus the dimensionless group for different oil samples (modified after Boxall et al. [54]).

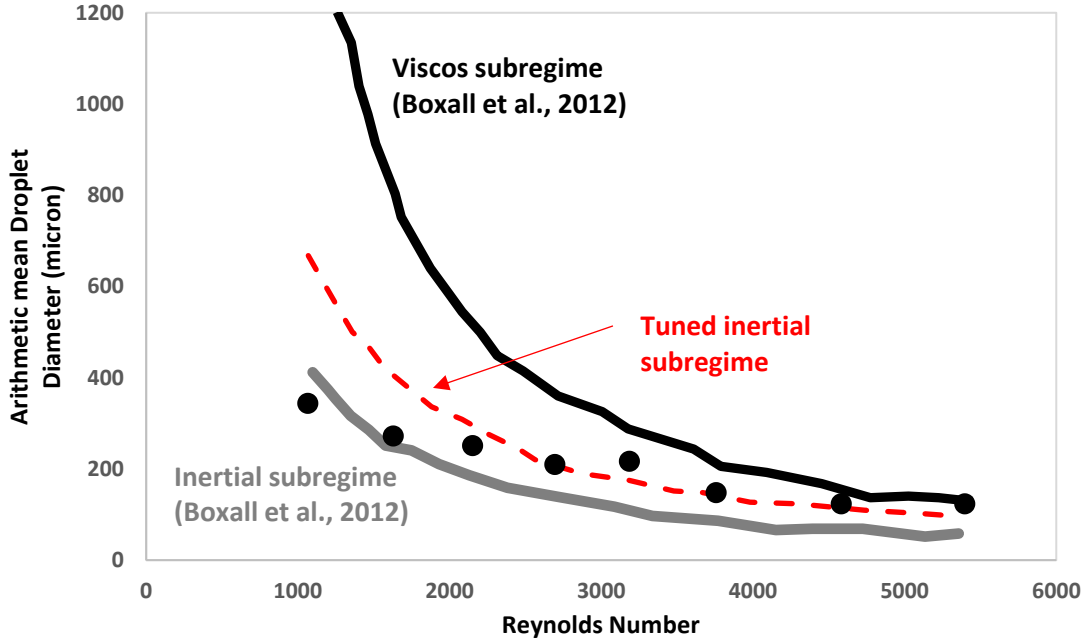

Figure 1-12: Arithmetic mean droplet diameter variation in terms of Reynolds number based on a new tuned model for the inertial subrange and the break up model presented by Boxall et al. & Aman et al. [54, 114].

1.5.2 Effect of Fluid Properties

1.5.2.1 Viscosity

Viscosity is one of the important rheological characteristics of emulsions in petroleum industry. Emulsions are generally formed in heavy oil due to the presence of asphaltenes and resins which act like natural surfactants, decrease the interfacial tension between oil and water phases, and facilitates the formation of droplets. The viscosity of oil is strongly dependent on the number of these heavy particles. Many researchers investigated the effects of different variables such as shear rate and phase concentration on the rheological properties including viscosity [115-118]. For instance, Schramm [36] concluded that the viscosity of emulsion is a function of different factors; namely: continuous and dispersed phase viscosities, concentration of dispersed phase, presence of emulsifier, droplet size distribution, temperature, and shear rate. According to the literature, water content (WC) can drastically change the viscosity of emulsions [32]. It has been reported that in low-dispersed phase concentration (WC<30 %), the system shows the Newtonian behaviour. At higher water oil ratios (30 % <WC), the emulsion behaves as a pseudo-plastic fluid and when the water content reaches to 80 % , the type of emulsion will change from water-in-oil emulsion to oil-in-water emulsion[32]. Several crude oils (as sample emulsions) with emulsifiers were selected

by Anisa and Nour [102] to monitor the droplet variation using the Axiovision software. They observed that the viscosity decreases by increasing temperature; however, when the temperature goes up as high as 90 ^{o}C, the viscosity will increase by increasing the temperature due to the phase inversion. They also concluded that when the water cut decreases, the emulsion behaves as a Newtonian fluid[116]. In this case, the droplet size distribution effect is dominant. Thus, the viscosity will increase as the temperature increases. The researchers specified the type of emulsions under study in terms of the rheological behaviours; however, they did not figure out how the fluid properties might modify the droplet size distribution for Newtonian and/or Non-Newtonian fluids[102]. Several researchers developed correlations for the oil and emulsion viscosity where various variables such as water-cut were incorporated in the model development [119-121] . Table 4 summarizes the previous correlations for determination of viscosity in terms of phase ratio and temperature. Anisa and Nour [102] also examined the impacts of temperature, water content, and stirring speed on the viscosity so that they were successful to relate the viscosity variation to the droplet size distribution. They conducted several experiments on viscosity variation and observed that the phase ratio can alter the viscosity due to the hydrogen bond increase which leads to an increase in the flow resistance. A decrease in the viscosity was noticed at high water cuts. At high phase ratio conditions, the possibility of droplet collision increases and thus coalescence occurs faster [102]. Since no changes on the relationship between the viscosities to shear rate were experienced, it was concluded that the viscosity reduction is resulted from increasing the droplet size distribution. Their outcomes were in agreement with the previous published works. According to the literature, it can be concluded that coarse emulsions have smaller apparent viscosity, compared to the fine emulsions [102, 118] since,

- Higher flocculation rate for small droplets is observed.
- Smaller droplet size causes changes in (or lowers) the droplet size distribution and fine emulsions have a smaller range of droplet diameters.
- When the size of droplets is small, the hydrodynamic interactions are less and hence the viscosity is small.

Table 1-4: A summary of proposed correlations for viscosity based on the literature.

Reference	Correlation	Variables definitions	Remark
Einstein [120, 122]	$\mu_r = 1 + 2.5V$ & $\mu_r = \frac{\mu}{\mu_C}$	•μ_C=Continuos phase viscosity •μ=Emulsion viscosity •μ_r=Relative viscosity •V= Valume fraction of dispersed phase	• Colloids model dilute systems, for dispersed phase fraction of more than 2%, the prediction results are not reliable. • It is assumed that μ_r and V are propotional linerly.
Brinkman [123]	$\mu = \mu_C(1-\emptyset)^{-2.5}$	•μ=Emulsion viscosity •μ_C=Continuos phase viscosity •$\emptyset$ = Volume fraction of dispered phase	• The equation represents the viscosity of emulsion with spherical surface droplets.
Pal and Rhodes[118]	$\mu_r = (1 - K_0 K_f(\gamma)\emptyset)^{-2.5}$	•K_o=hydration factor •Function of shear rate and volume fraction • Depends on the nature of emulsifier •K(γ) represents the flocculation •Used for non-Newtonian emulsions	• It can be used to determine the Newtonian and non-Newtonian emulsions viscosity. • It accounts for the hydration effect and dispersed droplets flocculation.
Dan and Jing[115]	$\mu_r = (1 - K_e\emptyset)^{-25}$ ϕ_{max}: $K_e(\emptyset_{max}) = \frac{K_e(\gamma,\emptyset)\|_{\emptyset=\emptyset_{max}}}{K_e(\gamma)\|_{\emptyset=\emptyset_{max}}} = 1$ ϕ_{min}: $K_e(\emptyset_{min}) = \frac{K_e(\gamma,\emptyset)\|_{\emptyset=\emptyset_{min}}}{K_e(\gamma)\|_{\emptyset=\emptyset_{max}}} = \frac{\frac{1-\mu_r^{-0.4}(\gamma,\emptyset_{min})}{\emptyset_{min}}}{\frac{1-\mu_r^{-0.4}(\gamma,\emptyset_{max})}{\emptyset_{max}}}$	•$K_e(\gamma,\emptyset) = K_e(\gamma)K_e(\emptyset)$ •Non-Newtonian factor, $K_e(\gamma)$, represents the hydration effect and floc. It is a function of shear rate and determined by experiments at the highest dispersed phase volume fraction (ϕ_{max}) •$K_e(\phi)$ represents the effect of the volume fraction of dispersed phase: $K_e(\phi)$ is a function of volume fraction of dispersed phase (ϕ).	• Improved Pal and Phondes model is not applicable for inverse point water cuts, because of collision of dispersed phase caused by high dispersed phase fraction.
Eilers [124]	$\mu_r = (1 + (\frac{1.25\emptyset}{1 - a_E\emptyset}))^2$	a_E emprical constant is between 1.28 and 1.30	• It was obtained based on the bitumen emulsions. • It is also applicable for Newtonian behavior.
Taylor [121]	$\mu = 1 + \left[2.5\left(\frac{k+0.4}{k+1}\right)\right]V$	•k is defined as follows: $k = \frac{\mu_D}{\mu_C}$	• Dispersed and continuous phase viscosities were considered. • It is valid for emulsions with small dispersed spherical drops concentration.

			• For spherical solid particles, $\frac{\mu_D}{\mu_C} \to \infty$ and the equation is equivalent to Einstein's model
Choi and Schowater [125] & Yaron and Gal-Or [126]	$\mu_r = \frac{\mu}{\mu_C} = 1 + f(V^{\frac{1}{3}})V$	• $f\left(V^{\frac{1}{3}}\right)$ is calculated by two different equations provided in the references[125] 124]	• The droplets interact with each other and deform from the original spherical shape at high concentrations of dispersed phase. • The researchers suggested a correction factors as a function of dispersed phase volume fraction to consider the deformation of droplets:
Phan-Thien and Pham [127]	$\mu_r^{\frac{2}{5}}(\frac{2\mu_r + 5k}{2 + 5k})^{3/5} = \frac{1}{1 - V}$	• V= Valume fraction of dispersed phase • $k = \frac{\mu_D}{\mu_C}$	• This equation under-predicts the relative viscosity of concentrated emulsions. • This model does not consider the surfactant presence. • This model can be utilized for concentrated emulsions using the approach of effective medium averaging. It is valid for low capillary numbers (Nc).
Pal [119]	$\mu_r = (\frac{2\mu_r + 5K}{2 + 5K})^{\frac{3}{2}} = (1 - K_0\emptyset)^{-5/2}$	• K_0 is a factor that takes into account the presence of adsorbed surfactant on the surface of the droplets.	• This equation determines the relative viscosity of concentrated emulsions.
Krieger and Dougherty [128]	μ_r=$[1 - \frac{V}{V_M}]^{-\mu V_m}$	• V_M is the maximum concentration of dispersed phase. • μ is the intrinsic viscosity, as given below: $[\mu]$=$\frac{\mu_D}{\mu c} - 1$	• It is valid for high V_m, when the viscosity of suspension becomes infinite. • V_m depends on drops size.
Pal [118]	$V_M^{\frac{1}{2}}\left(1 - \mu_r^{\frac{-1}{\mu V_m}}\right) = c_0 + c_1 \log(N_{Re,p}) + c_1 \log(N_{Re,p})^2$	• c_0, c_1, and c_2 are the constants. $N_{Re,p}$ is the Reynolds particle number, as follows: $N_{Re,p} = \frac{\rho_c \gamma r^2}{\mu_c}$ • ρ_c and μ_c are the continuous phase density and viscosity, respectively; r is the particle radius; and γ is the shear rate.	• It is valid for mono-dispersed emulsions, with low interfacial tension and comparable phase densities. • Brownian movement of droplets is neglected and the flow is assumed to be steady-state.
Richardson [129]	$\mu_r = e^{k\emptyset}$	• μ_r=Relative viscosity • $\emptyset$ = volume fraction of dispered phase • k= constant	• An exponential increase is noticed in the relative viscosity as a function of volume fraction of dispersed phase.

Ronningsen [130]	$\ln(\mu_r) = a_1 + a_2T + a_3V + a_4TV$	• a_1, a_2, a_3, and a_4 represent the shear rate-dependent coefficients of the correlation.	• The coefficients were obtained based on experimental data of viscosity at different shear rates and temperatures. • It fails for fluids which are very different from the experimental oil samples.
ASTM [61]	$z = v + 0.7 + f(v)$ $\ln(\ln(z)) = A - B\ln(T)$	• $f(v) = e^{(-1.47-1.84v-0.51v^2)}$ • A and B represent the characteristics of each product and T is the absolute temperature (K). • v stands for the kinematic viscosity • Z refers to the viscosity function	• It includes the kinematic viscosity variation with the temperature. • It is only valid for petroleum fluids and their fractions.
Farah et al.[116]	$T > WAT$: $\ln(\ln(v + 0.7)) = k_1 + k_2V + k_3\ln(T) + k_4V\ln(T)$ T>WAT: $\ln(\ln(v + 0.7)) = k_1' + k_2'V + k_3'\ln(T) + k_4'V\ln(T)$	• WAT= the wax appearance temperature. • Experimental coefficients were obtained from temperature independent parameters (A, A', B, B') versus volume fraction plot as follows: A: k_1+k_2V; B: k_3+k_4V; A': $k_1' + k_2'V$; B': $k_3' + k_4'V$	• The correlation can estimate emulsion viscosity of oil at various dispersed phase volume fractions and temperatures (below and above WAT).
Becher[131] and Schramm [36]	$\mu = \mu_c(1 + c_1\emptyset + c_2\emptyset^2 + c_3\emptyset^3)$	• c = empirical coefficient • $\emptyset^2$ and $\emptyset^3$= interactions between droplets	• It considers the droplets interactions within wide range of dispersed phase concentration.

1.5.2.2 Salinity

Demulsification can occur as a result of density difference between the continuous and dispersed phases. When the thin film between the drops approaches a critical value, the coalescence happens. The equilibrium at the interface of a water, oil, and surfactant system is known to be a vital factor to identify the emulsion type and its stability [31, 132, 133]. Despite the solid particle dispersions, which DLVO theory can fully explain their behaviours, droplets in liquid-liquid systems can deform. Because of the liquid surfaces, emulsions are much more difficult to be accurately characterized. Intermolecular interactions are appreciably influenced by these two factors (liquid surface and droplet deformation). The stability for coalescence of emulsions, is generally governed by the thinning rate of the film between the droplets and the stability against deformation [134]. Moradi et al. [3] used the droplet size evolution versus time, as a proxy for the emulsion stability. Measurements were made by employing an optical microscopy; and were confirmed with the previous data, measured by the bottle test. Using a light-transmitted microscope, several pictures were taken at different times; and salinity values. Pictures enhancement was made using an image processing software to determine the droplet size distribution[3]. The researchers mitigated the effect of overlapping droplets by diluting the samples. Log-normal, Weibull, and log-hyperbolic probability density functions generally employ the distribution models to fit DSD data. As illustrated in the **Figure.12**, the log-hyperbolic function can result in a better fit to model the experimental data[3]. By increasing the salinity, the frequency of larger droplets increases, an increase in coalescence rate is experienced, and phase separation occurs sooner, based on the observations. Their finding concerning the effect of salinity on the emulsion stability, was the same as the research outcome attained by Wang et al., [135] who performed the same experiments; using the bottle tests and an electro rheology for droplet size evaluation[135]. Maaref and Ayatollahi [136] also discussed on the influence of water salinity on the emulsion stability. They made synthesized brine according to North seawater, Red seawater, and Mediterranean and Persian Gulf seawater brine characteristics. Emulsion instability can be defined as the change in droplet size distribution. Tracking the changes in this proxy, a time log-normal pdf was found to fit the data best. The effect of different salts on the emulsion stability, was also reported. First, they prepared different samples containing different NaCl salt concentrations. They observed that by adding more salt, larger droplets were formed which made the emulsion unstable[136]. Then, they added Na_2SO_4 to the previous samples and observed a significant decrease in the number of large droplets. They concluded that the formation of a film around the droplets causes a reduction in the rate of coalescence. To investigate the influence of magnesium ions, they prepared samples by adding $MgCl_2$ to the emulsions containing NaCl and Na_2SO_4. They noticed that the frequency of larger droplets for this type of emulsion is higher than that for the samples prepared with NaCl and Na_2SO_4 , but less than that for the samples prepared only with NaCl[136].It should be noted that the effects of Na_2SO_4 and $MgCl_2$ were not separately discussed in their work where other ions were present in the samples[136]. Their observations offer useful information on the effect of brine

salinity on the emulsion stability. **Figure.13** demonstrates the effect of salt concentration on the droplet size distribution according to their results.

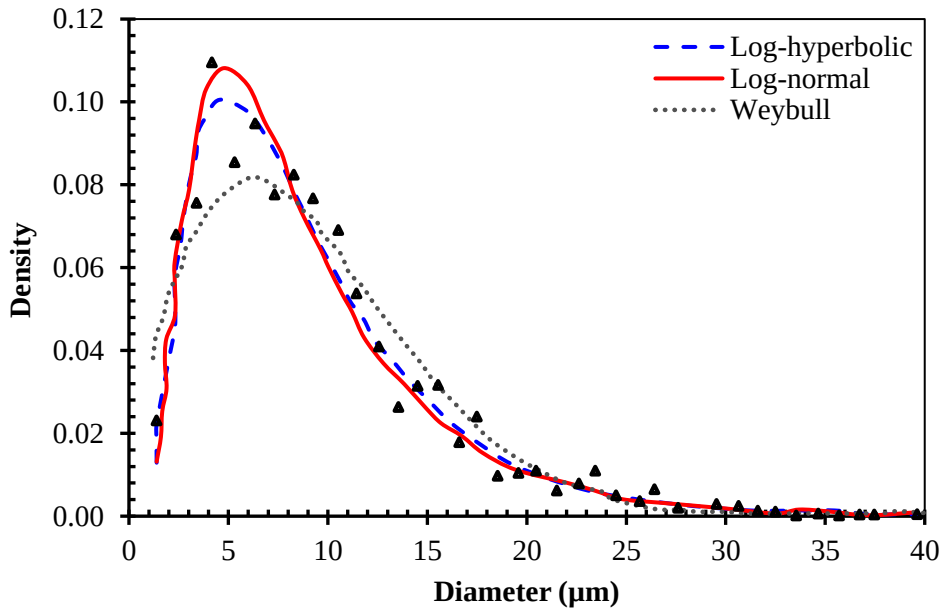

Figure 1-13: Comparison of different probability functions for droplet size diameters [3].

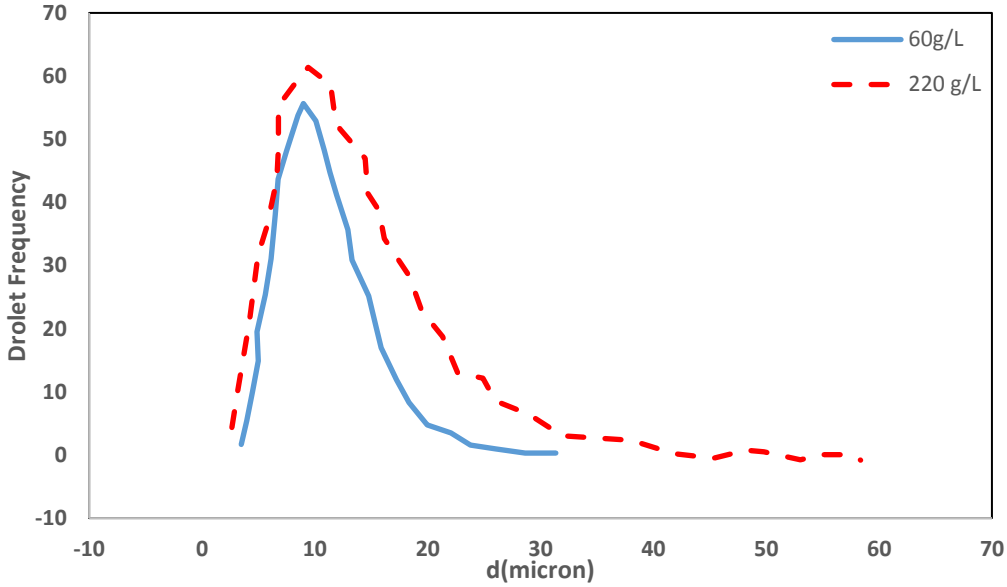

Figure 1-14: Effect of salt concentration on droplet size distribution [136].

1.5.2.3 Interfacial tension

Binks et al. [31] studied the stability of a Winsor 1 type emulsion as a function of salt concentration. An anionic surfactant stabilized the water/oil emulsion. The droplet deformation was most likely to happen since the interfacial tension between the oil and water phases reaches a very low value close to the salt concentration of the phase inversion[137]. In the literature, it was not discussed if the deformation occurs in smaller droplets. It seems that high capillary pressure in small droplets opposes the deformation. On the other hand, intensive Brownian motion provides the additional force which boosts the deformation [31]. These ideas have been confirmed by the theoretical works; and no experiments have yet been performed to validate their findings. In a research study conducted by Binks et al. [31], two different sets of samples were prepared to separately investigate the effect of droplet size and salt concentration on the emulsion stability. They highlighted that a very accurate control/procedure was implemented on the samples to achieve the desired characteristics. Measurements of droplet size distribution were performed by a Malvern diffractometer [31]. Since the conductivity of water/oil and oil/water emulsions differs significantly, it is easy to detect the type of created emulsion by a digital conductivity meter. The researchers observed that the emulsion type converted from o/w to w/o by increasing salt concentration [31]. Change in salt concentration leads to variation in the interfacial tension so that it lowers with increasing IFT and it then increases. **Figure.14** shows the relation between salt concentration, IFT and average droplet diameter. Droplet diameter also follows the same pattern. It was concluded that, the initial decrease in droplet diameter is a result of a decrease in the interfacial tension. The size increase is resulted from the coalescence which occurs due to adding salt and thus destabilizing emulsion[136]. Below 0.035 mol/L of NaCl concentration, the coalescence is negligible [31]. It has been reported in the literature[138] that an increase in the amount of ionic surfactant, causes flocculation through changing the double layer repulsion between the droplets. In other words, at high concentration of salt, the interfacial tension is significantly reduced; and the deformation of droplets occurs, which leads to the attraction between the droplets and instability. However, a decrease in the creaming rate was observed at low salt concentrations. They explained their experimental observations through a proposed physical framework [31]. Calculations of interaction energy between droplets were match with the experimental values.

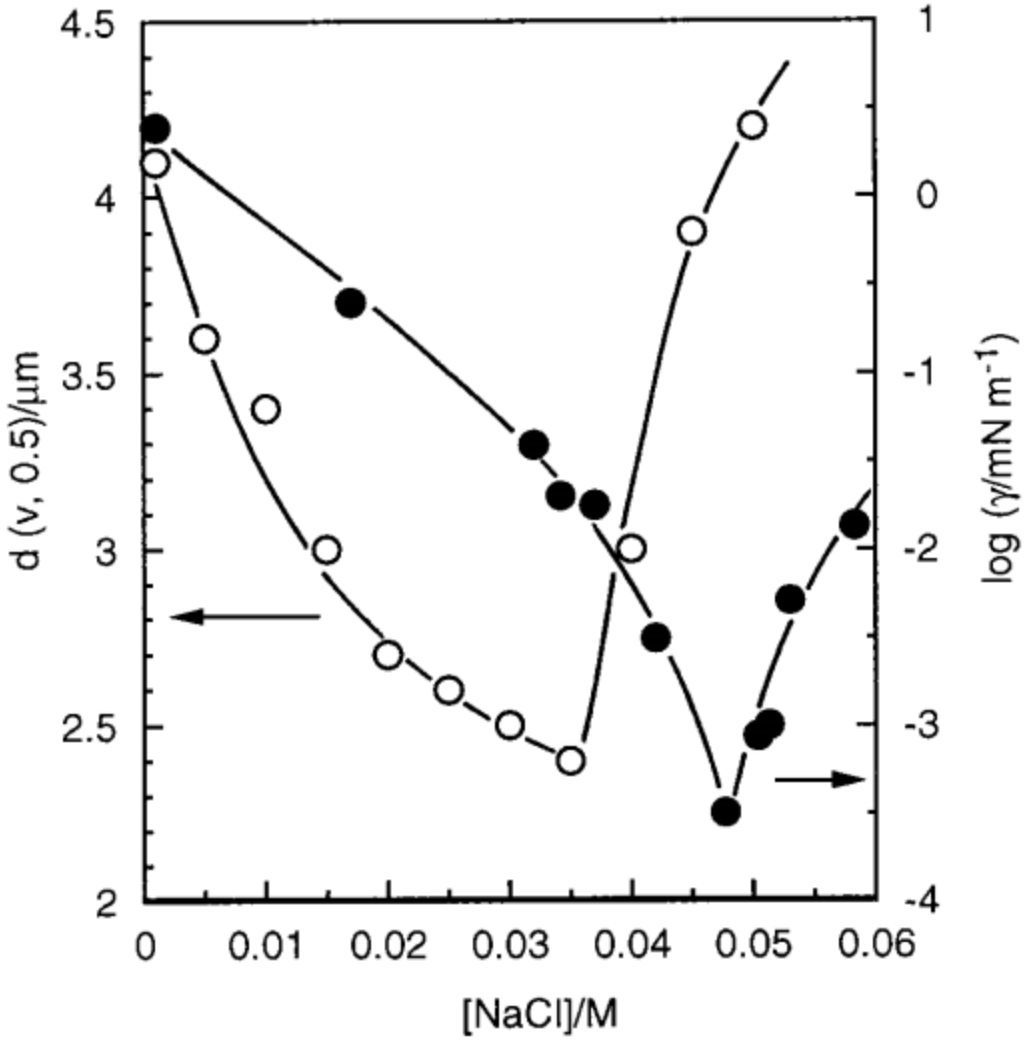

Figure 1-15: Relationship between average droplet size, IFT, and salt concentration (open circles show droplet size variation and full circles indicate IFT variation) [31].

Saito and Shinoda [139] claimed that interfacial tension is affected by the temperature as depicted in **Figure.15**. It was found that the surfactant distribution and solubility significantly change with temperature. By performing experiments on the unpurified samples, they showed that the interfacial tension of a system containing micelles (due to the presence of an emulsifier) approaches zero at high temperatures close to phase inversion temperature (PIT)[139]. They concluded that the destabilization rate increases at PIT and high temperatures. The rapid breakdown close to PIT is caused by the interactions and structure of the surfactant and emulsion, while low viscosity (at high temperatures) and fast movements of droplets result in emulsion instability [139].

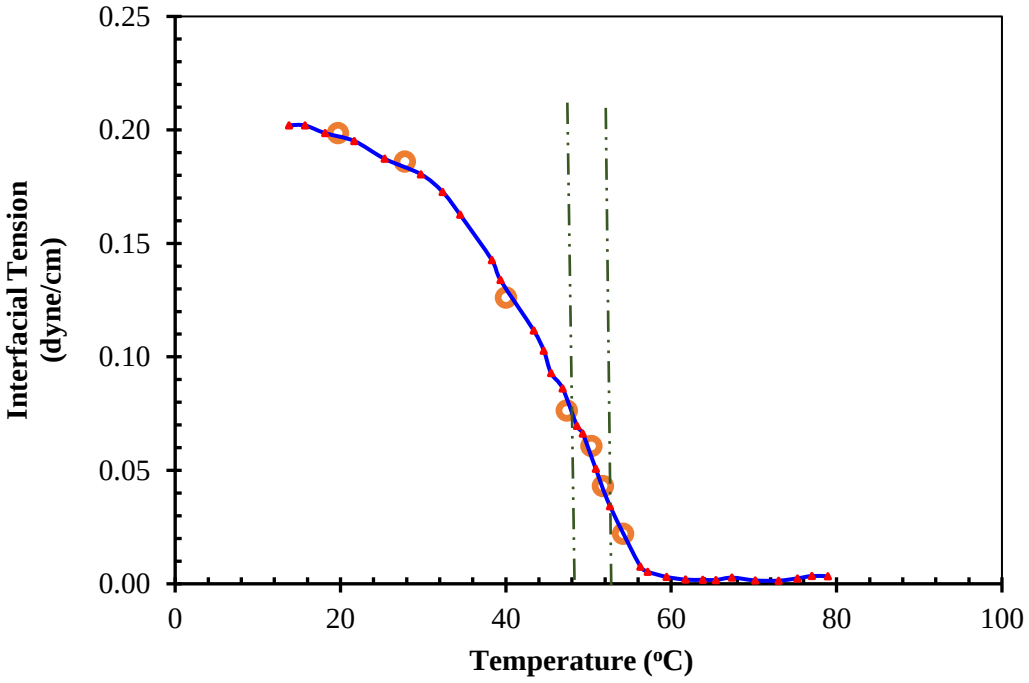

Figure 1-16: Interfacial tension versus temperature (modified after Saito and Shinoda [139]).

1.5.3 Effect of Reservoir Properties on Emulsions and Emulsion Stability

Emulsions flow in underground porous media can be found in several oil recovery techniques. Since the porous media have mainly low to moderate permeabilities, the emulsion droplet size can partly or totally block/cover the pore throats. Consequently, considerable interactions exist between the pore constrictions and emulsion droplets, leading to the redistribution of local flow. A theoretical approach is required to forecast the transportation behaviour of emulsions in porous systems that enables us to understand the emulsion droplets and porous media interactions. There are a number of factors (e.g., permeability and heterogeneity) that affect the emulsion transport in porous media.

1.5.3.1 Pore size

Formation of emulsions in porous systems has been one of the most challenging issues in oil transportation and production. Emulsion formation, plays a crucial role in the secondary oil recovery methods. Emulsion transport in pore throats is still not well understood, since the presence of emulsions in porous media drastically changes the characteristics of oil. For instance, Alkali surfactant flooding in a reservoir causes a reduction in the interfacial tension and therefore emulsions are formed[33] .The secondary recovery operation is first performed by implementation of water injection processes; which might not be useful due to water fingering and breakthrough

in some reservoirs. Then, a chemical flooding process such as alkali surfactant injection is performed which causes emulsion formation[140]. Due to the presence of emulsions, pore throats will be blocked, pressure will build up, and recovery factor will increase. The presence of emulsions in the flow, can be monitored by an increase in the pressure which is followed by a decrease in water cut[75]. The geometry and pore size of the porous medium govern the emulsion flow. Not only the larger droplets can block the flow by straining, smaller droplet can also partially block the flow by Interception [75]. Interception and Straining is a direct function of pore size distribution. As it was reported by Romero et al.[141] in a water flooding experiment, the emulsion concentration was found to be lower with smaller droplet size at the outlet, compared to the initial emulsion concertation. However, after some time, the outlet concertation reached the initial value. It can be attributed to the straining of emulsion droplets at the small pore throats. At the beginning, large droplets would clog the pore size. Thus, the concentration is lower than entrance and small droplets are present; however, by the time both reach the initial values[142]. Pore size distribution has a direct impact on this transition. As it was reported by Błaszczyk et al.,[142] in the case of a porous bed with small pore throat, the flow resistance is small and the steady state condition reaches faster. It implies that a porous medium with higher pore throats has less number of pores with a diameter smaller than droplet size. Therefore, fewer pore throats will be blocked by the emulsions. As it is clear from Figure 16, for a porous medium with high pore size fraction, the emulsion concertation reaches faster and the pressure drop is lower. The capillary number is also a vital parameter to be considered; while studying the effect of pore size on the emulsion stability, particularly when the pore throats are smaller than the emulsion droplets[141]. According to Soo and Radke[143] , at high capillary numbers, the strained droplets may break up either by snapping off or by fingering and return to the flow. If the pore size is very smaller than droplet size, snap off is a possibility where the emulsion instability initiates. If the ratio of pore throat to droplet size is the same, the droplets will pass without snapping off[143] .

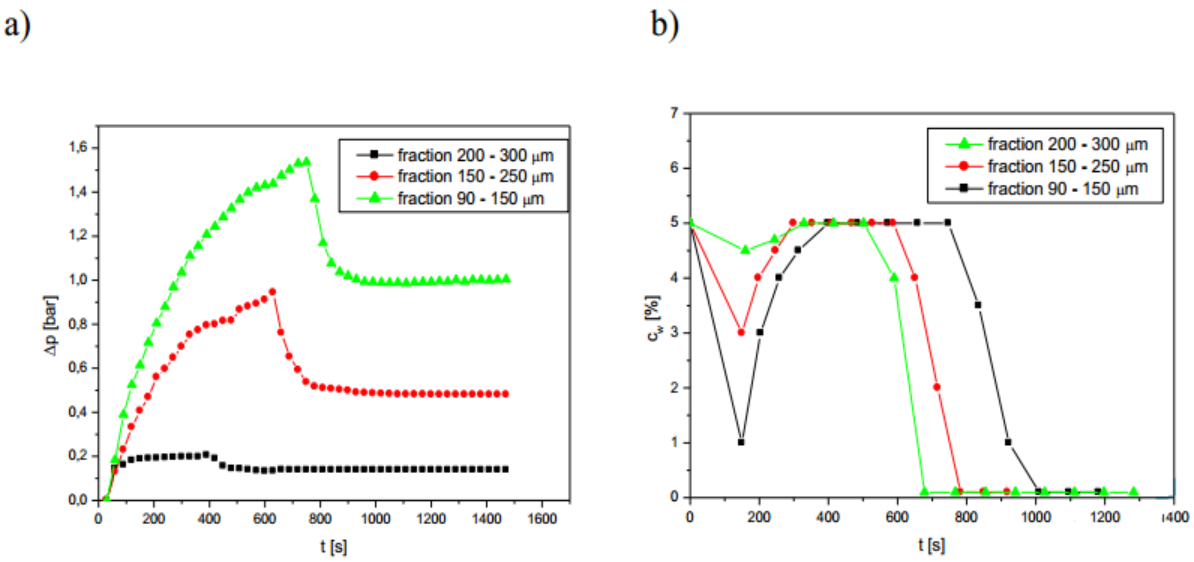

Figure 1-17: Effect of pore size distribution on; a) pressure drop and b) emulsion concentration in porous media [135].

*1.5.3.2 **Relative permeability***

To be able to model emulsion flow in porous media, a multi-phase system incorporating the flow of emulsions along other phases should be defined where various phenomena such as plugging, emulsion formation, and breakage are considered. The effect of these variables can be expressed in the form of different relative permeability correlations, which showa reduction in water relative permeability caused by water channel plugging[144]. Permeability is one of the most important characteristics of porous media to be considered while studying the the emulsion stability. As discussed earlier, the straining and interception are the two important phenomena that can happen in porous media[18]. If the pore sizes of the porous bed is small and pores are not well connected, implying a low permeable rock. In this case, most emulsion droplets may plug the pores and cause droplet rupture due to straining. If the permeability of the porous medium is high with connected large pore throats, the emulsions (if they are comparable with the pore size) may block the flow both by straining and interception phenomena. Under this condition, the emulsions will be more stable, compared to the case of a low permeability rock. This mechanism was also approved by Fu et al. [145]. They performed several core flooding in different samples with various porosity, permeability, and core length. They claimed that the emulsion breakdown is higher at high flow rates where the rock samples have lower permeability. Emulsions passing through high permeability rocks are found to be highly stable[145]. A number of researchers conducted modeling and simulation investigations of emulsions during the secondary oil recovery operations and validated their results, using the real data obtained from the core flooding tests [144, 146, 147]. They concluded that the presence of emulsions in a porous medium causes a lower water relative permeability; however, it does not change the residual oil saturation and only accelerates the oil production. In the oil displacement processes, if the injected fluid is less viscous than the oil in place, the instability occurs, known as viscous instability or viscous fingering[148]. This will lead

to a significant reduction in the oil sweep efficiency. One of the promising strategies to lower the possibility of this undesired effect, is reduction of the effective permeability of the porous medium through emulsion injection[149] .To guarantee the effectiveness of an emulsion, the oil droplets in the emulsion should be larger than the pore throat constriction. This will lead to the flow restriction by emulsions. When oil in water emulsions is injected, the emulsions start to flow to more permeable zones, which results in the flow restriction. As a result, the injected water starts to flow to zones with less permeability, leading to a greater sweep efficiency [75]. McAuliffe [148] employed stable emulsions as the mobility control agents in the enhanced oil recovery operation. Laboratory investigations were conducted, to study the transient permeability behavior and emulsions flow through porous media. Heterogenous core samples (as small-scale reservoirs) were considered as porous systems. Emulsion viscosity was assumed to be the same as the water viscosity as the emulsions tend to have the viscosity of the continuous (external) phase. He concluded that, oil in water emulsions containing more than 60% oil exhibit the pseudo non-Newtonian flow characteristics, due to the interactions between the oil droplets. He made efforts to comprehend the non-Newtonian behaviours by flooding emulsions through several cores under various pressure conditions. It means that, the viscosity of emulsion flow is dependent on the shear rate. At an oil content of 50%, the emulsions behave as Newtonian fluids[148]. Mandal and Bera[150] observed the same behaviour for the emulsion mixture. They related the rheological characteristics, to the shear rate so that the fluid is a non-Newtonian at low shear rates; while high shear rates exhibit the Newtonian behaviours. McAuliffe[12] observed that the permeability reduces at small shear rates and the fluid behaves as pseudo non-Newtonian by increasing the injection pressure; however, the emulsion shows Newtonian rheological characteristics. A justification was provided, concerning squeezing the oil droplets through constriction by overcoming the capillary forces which resulted in a higher pressure drop. This justification does not seem acceptable, since McAuliffe's results showed that the relative permeability reduction occurs even when the emulsion droplets are smaller than the pore throats. Emulsions with smaller diameters were produced by increasing the concentration of sodium hydroxide in the aqueous phase[148]. Sodium hydroxide neutralized a high number of interracially active acids in the crude oil; and produced emulsions with a smaller diameter. The variation of droplet size was also reported by changing concentration of the synthetic surfactant added to the crude oil[12].A decrease in the core permeability by the emulsion injection was also confirmed based on the experimental results. It was concluded that, emulsion with a larger average droplet size is more effective in redirecting fluid flow into less permeable zones[12].Also oil-in-water emulsions displaced the oil phase from sandstone core material more effectively than did water alone[12]. Similar results for a permeability reduction were reported by Soo and Radke[18, 76, 77, 80, 143]. As it is depicted in **Figure.17**, they observed a permeability reduction in their samples. This reduction was attributed to the pore blockage by the emulsion droplets. The corresponding emulsion concentration was also recorded. It was observed that at the beginning, the outlet concentration is less than the initial emulsion concentration, implying the clogging of emulsion droplets in the pore throats. **[76]** After a while, the concentration increased

again and reached the initial inlet concentration. At this time, the permeability reduction stopped. [18]

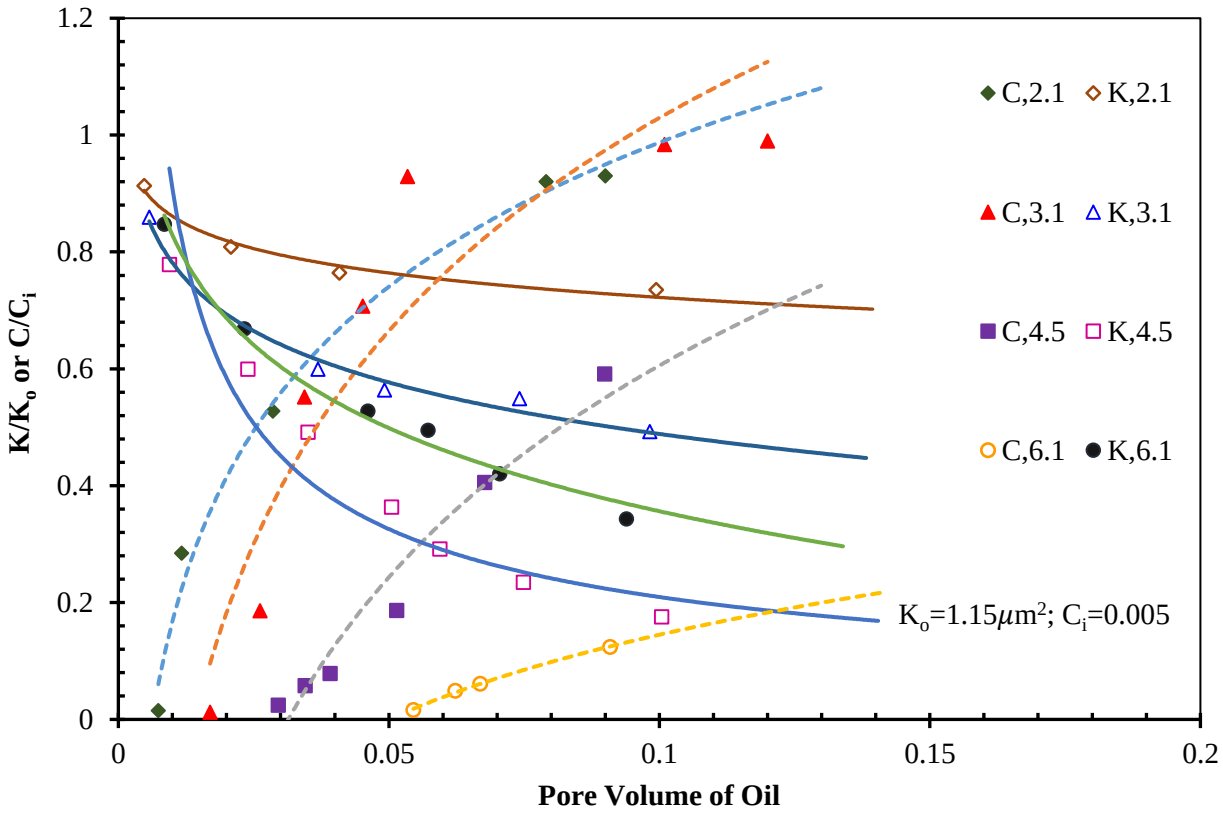

Figure 1-18: Permeability reduction and emulsion concentration in porous media during emulsion formation and flow for different droplet size diameter (μm) (modified after [76]).

1.5.3.3 Heterogeneity

Considering deep bed filtration model, Soo and Radke [18, 76, 77, 80, 143] conducted several research studies regarding the flow of emulsions in porous media to investigate the effect of reservoir heterogeneity or flow velocity on permeability reduction and droplet size distribution where different water-flooding experiments using a variety of crude oils and porous media were performed. To visualize oil-drop migration in the porous medium, permeability experiments were implemented by utilizing micro-models. Emulsion flow in the porous medium is physically analogous to a filtration process[77, 80]. When emulsions are injected into a porous medium, drops are retained in the pores and the permeability declines. Through analyzing the effluent emulsion concentration and transient behaviour of mean droplet size, the flow mechanisms and stability of emulsions in the porous medium can be comprehended [143]. The emulsions were prepared by mixing the Chevron oil with distilled water. The porous medium consisted of a fine Ottawa sand with a known grain size distribution which was assessed by the screen sieves in a stainless-steel cylinder. Drop size distribution and drop volume concentration of the emulsions were

photographically analyzed for the emulsion samples by the photomicrograph of ZIESS software. In this work, not only the transient permeability was monitored, porous medium pore size distribution and droplet concentration were also determined[143].For better understanding of the physical mechanisms of emulsion flow in porous media, a visual micromodel study was performed. The study showed that the permeability reduction during emulsion flow primarily is resulted from drops retaining in pores. This work outlined two main factors that determine the overall reduction in permeability: the volume of retained drops and how effective the drops are in restricting the flow [76]. Droplets were not only captured in the pores where are smaller than them, they are also trapped in crevices or pockets formed by the sand grains and sometimes on the surface of the sand grains[76]. The entrapment and interception will cause an intense pressure fluctuation which will be described in the next section. Their experimental data is in a good agreement with the experimental results obtained by Mandal and Bera[90]where sand packs with different sizes were employed and pressure drop curves versus flow rate were drawn. As shown in **Figure 18**, the flow path for emulsion decreases with an increase in the size of grains and higher pressure loss is attained with the same flow rate. It was found that the dilute and stable oils (as viscous continuous fluid) in water emulsions do not flow. Viscosity of the oil phase also has a minor influence on both effluent concentration and transient permeability histories. Droplets did not squeeze through pore restrictions but they captured the disperse phase which caused permeability reduction with respect to the continuous phase[42]. Using the capillary number as a bridge between the macroscopic scale and microscopic flow characteristics, Romero[151] described the transport of emulsions in pore scale using a capillary network model. The researcher performed laboratory tests to analyze the flow of emulsions through sandstones. It was observed that in a low-permeable sample at low capillary numbers (due to the high values of surface tension), an extra pressure is required for the droplets to pass through the pore throats, which causes a high apparent viscosity [151]. When the interfacial forces are higher, the partial blocking is more dominant. It was found that the partial blocking is a function of droplet diameter and pore throat diameter. For instance, if the emulsion flows through a low permeable rock with relatively small pore throats, the partial blocking is more possible, compared to a high permeable rock. The core flooding was conducted twice in a sample and a bimodal distribution for the droplet size was obtained[151]. No justification for this behaviour was provided.

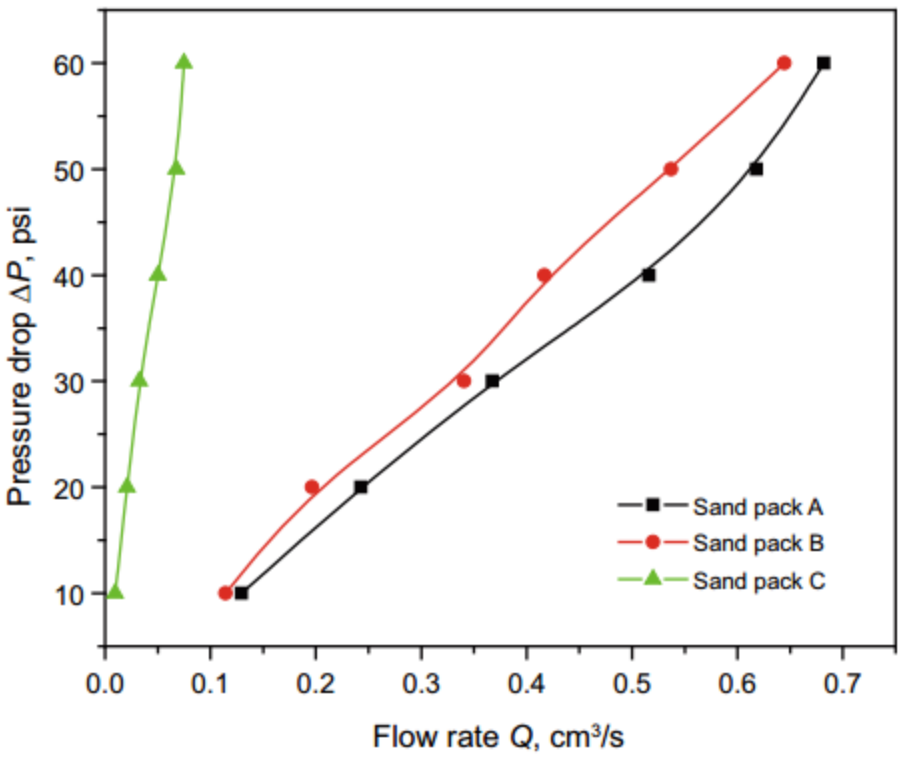

Figure 1-19: Effect of sand pack particle size on pressure drop for three different samples [mesh size sand pack A: 12-30; sand pack B: 30-60; sand pack C: 60-70] [150].

1.5.3.4 Pressure/pressure drop

In petroleum reservoirs and other types of porous systems, it is of great importance for engineers to realize how pressure drop and flow rate variations affect the emulsion flow. Rezaei and Firoozabadi[75] conducted a series of water flooding experiments to investigate the influence of injection rate on the pressure drop. As mentioned earlier, two important phenomena (straining and interception) happen in the porous medium due to the presence of emulsions. Both small and large droplets can block the pore throats and deviate the flow. This droplet capturing causes pressure fluctuations in the reservoir. They reported waterflooding results for two different samples (with and without emulsions). Some features in terms of pressure behaviour are distinguishable as demonstrated in **Figure 19**. An intense pressure fluctuation was observed in the sample containing emulsions which was caused by continuous droplet capturing and re-entrainment[75]. A pore, which is completely blocked by staining or is partially blocked due to the accumulation of small droplets, causes the flow to be considerably disturbed. Another interesting phenomenon observed in the samples containing emulsions was higher injection pressure for the lower injection rate. However, the intensity of mixing is more at high injection rates. However, at low injection rates, due to the prolonged contact time between oil and water phases, the possibility of emulsion formation increases and produced droplets block the pore throats, which results in an additional pressure drop[75]. The same findings were reported by other researchers[148, 152]. Another important aspect

which is seen in the pressure plots is an initial spike observed at the early injection stage. As it was highlighted by the researchers[75], an excess pressure is required to initiate the flow due to the high mobility ratio as a result of viscosity contrast. While finding an optimum demulsifier concentration, Sun et al. [153] also observed this pressure spike in cases where no demulsifier was added to the samples and emulsions were present. They concluded that the pressure spike and the following pressure fluctuations are minimized if an optimum concentration of demulsifier is added.

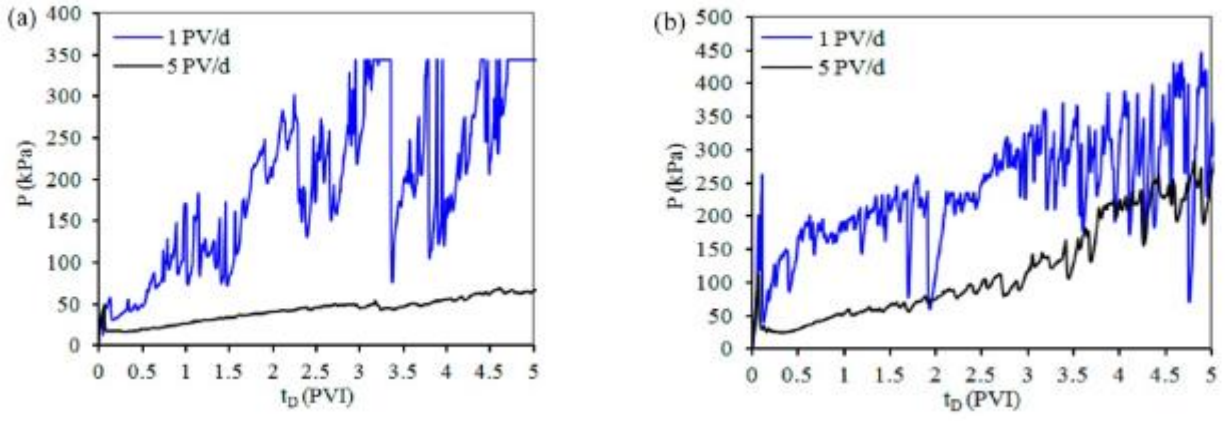

Figure 1-20: Injection pressure variation and effect of flow rate for (a) sample without emulsions and (b) sample with a significant amount of emulsions[75].

1.5.3.5 Flow rate

Shear forces can break the residual oil into drops and generate in-situ emulsions. These emulsions may flow as emulsions of two types, oil in water or water in oil emulsions. Velocity is a very important parameter in emulsion flow through porous medium as it determines the flow behavior of the droplets. McAuliffe[148] proposed a qualitative justification for his observation of permeability reduction at high pressure drops. Quantitative analysis is also found in a research study by Soo and Radke[143] to explain McAuliffe observations. This modeling and experimental work outlined the transport of dilute and stable o/w emulsions flow through porous media. This research investigation is based on the deep-bed filtration theory. Providing further information, the emulsion was injected into an unconsolidated sand pack of known grain size distribution, pore-throat-size distribution, and initial permeabilities to validate the analytical modeling results. They also investigated the possibility of the retained droplets disruption if the velocity reached high enough to overcome the hydrodynamic forces[143]. According to their theoretical results, at low velocities and particle size smaller than pore sizes, the drop capturing occurs in crevices where the flow is almost stagnant. Physical forces on the surface of the sand grains can also influence the droplet capturing. If the particle size is larger than pore throats, drops clog in the pores. When velocity approaches a critical value (corresponded to a high capillary number), the drop squeezing

and shear-thinning flow occur. This critical velocity is a strong function of surface properties such as adhesion or zeta potential value of the system and the drop size to pore size ratio[143]. It was also observed that the droplet break-up is not a function of the capture mechanisms. It only happens when the capillary number is equal or exceeds unity. They found that permeability is independent of flow rate and interfacial tension at high flow rates; however, a strong sensitivity of permeability to the velocity was noticed at high flow rates [143]. The experimental results attained in this research work follow the theory, implying that the emulsion flow is not sensitive to the velocity at low capillary numbers [143]. It does no matter that which capture mechanism is a controlling factor.

A similar research work was conducted by Yazhou et al.[154] so that the effect of emulsifier injection flow rate was investigated on droplet size distribution in the porous medium. They found out at small flow rates, the created emulsions have a smaller droplet size, compared to the pore throats. As the flow rate increases, the droplet size distribution reaches higher values and bigger than the pore throats as illustrated in **Figure 20**. They explained that at low flow rate the driving force to move the large elements of oil is not enough. Thus., the emulsion formation is mainly due to the shear forces, while at high injection rates the pressure gradient is high enough to push the oil through high permeable zones and form droplets with bigger size[154].

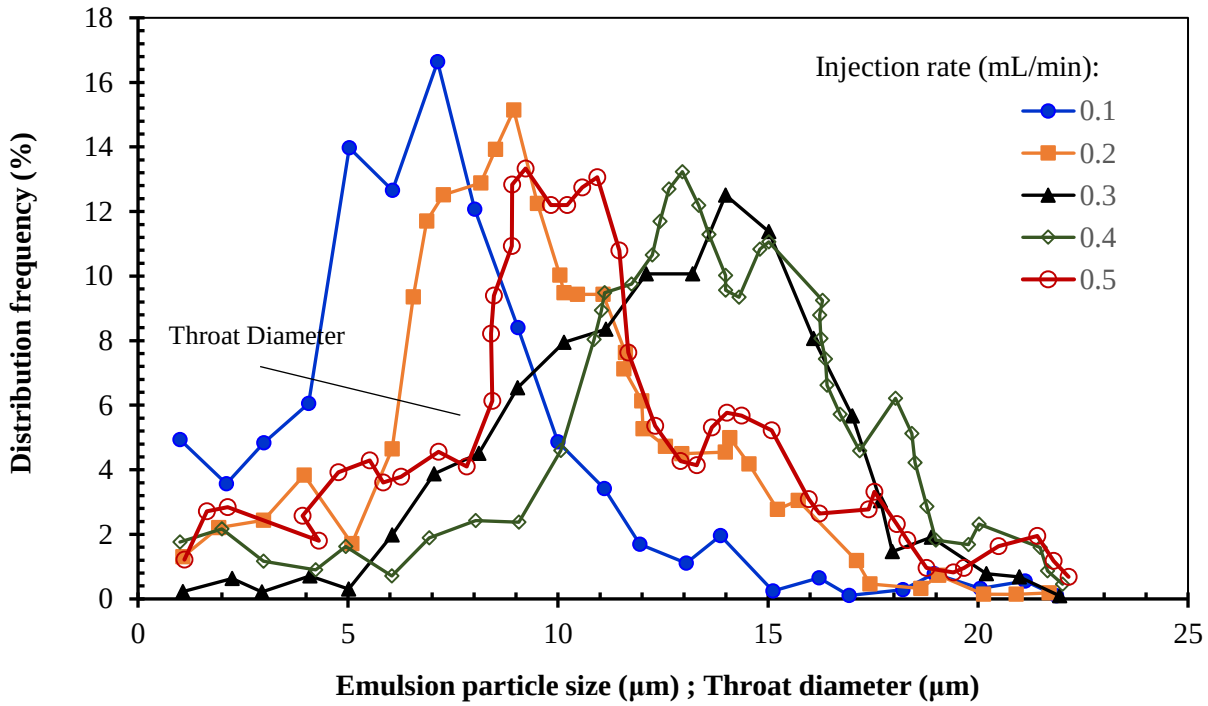

Figure 1-21: Influence of flow rate on droplet size distribution, compared to pore throat in the porous medium at different injection flow rates [154] .

1.6 SIMULATION/OPTIMIZATION PACKAGES

Emulsions are thermodynamically unstable systems with various characters at different molecular, microscopic and macroscopic levels which dictate their physical and chemical properties[155]. It is clear that a multiscale method is a suitable approach to study emulsion at the internal dynamic scale up to its characteristic as a fluid[156]. Due to the emulsion behaviours and instability, a detailed study on the rock and fluid properties, surface energies, and interactions/associations of emulsion systems are required to explore several unknown aspects of emulsion flow and conditions[157]. Experimental measurements often fail to record particular thermodynamic and process conditions of the entire system and usually provide an average value for vital factors. Hence, researchers seek computer simulation techniques to analyze the fluid behaviour under various conditions (temperature, pressure, and composition). Computer simulation methods can provide extensive information on the behaviour of emulsions in pipeline and porous media. There have been various analytical and numerical studies on liquid-liquid surface and interactions using Molecular Dynamic Simulation[43] ,Computational Fluid Dynamic (CFD)[158-160], and Monte Carlo methods[161]; however, a few technical reports/documents are available on CFD or MD investigations of the properties of emulsions and pore structure systems and their interactions. Fluid/pore surface properties such as adsorption rate can significantly influence the transport properties in oil and gas industry[162]. CFD is a numerical simulation technique to study various fluid flow and heat-transfer cases under several condition[158, 160]. By discretizing a geometric domain and applying the finite element/volume method, the conservation equations are solved numerically. CFD simulations can be performed using appropriate software packages such as CFD-ACE+ and COMSOL[158, 159].The oil/water interface movement is tracked based on the volume fraction (*F*) of fluid in each computational cell. This value can be obtained by solving the continuum equation as follows:

$$\frac{\partial F}{\partial t} + (U.\nabla)F = 0 \qquad (16)$$

in which, *U* and *t* represent the fluid velocity and time, respectively. The results can be obtained by numerically solving the mass and momentum conservation equations if the fluid is assumed to be incompressible as follows:

$$\nabla.U = 0 \qquad (17)$$

$$\frac{\partial U}{\partial t} + \nabla.(UU) = -\frac{1}{\rho}\nabla p + g + \frac{\eta}{\rho}\nabla^2 U + \frac{1}{\rho}F_{iv} \qquad (18)$$

where ρ stands for the fluid density, η refers to the viscosity, g symbolizes the gravitational acceleration, and F_{iv} denotes the volumetric interfacial tension. After entering the fluid properties such as density, viscosity, and interfacial tension of phases, a geometry system is defined to specify the computational cells. Depending on the resultant equations, the initial and boundary conditions need to be determined. The values of inlet and outlet pressures is set and for specific time steps

and iterations. The continuity equations will be then solved and the droplet formation mechanisms and drop characteristics can be analyzed and obtained by CFD-ACE+ post processing application. A simple schematic of a general algorithm for emulsion studies using CFD is depicted in **Figure 21.** There are some research works in the literature, showing that there is a good match between the experimental measurements and CFD results while working with the software for modeling of liquid/emulsion systems [158-160].

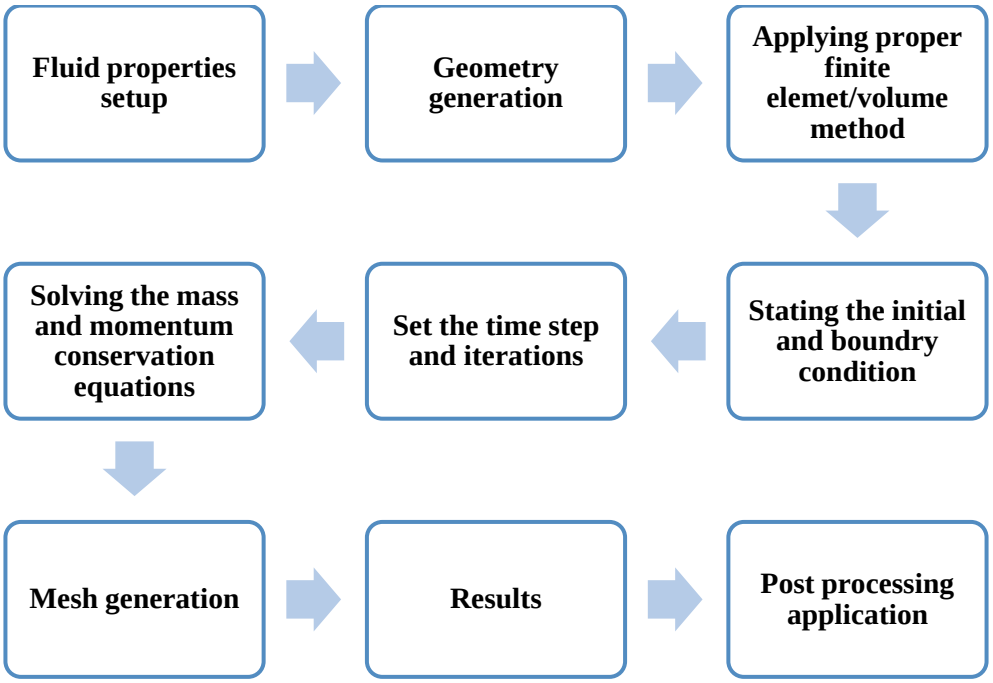

Figure 1-22: A simple algorithm using CFD to model emulsion stability

Another widely used simulation package to study the microscopic systems (including thousands of molecules) is Molecular Dynamics (MD) Simulation. This method provides a bridge between the experiment and conventional physical chemistry/thermodynamic models[163]. MD provides precise prediction of the system behaviour through accurate computation of the interactions between the molecules. This modeling technique has been recently employed due to several benefits. For instance, it appears to be an unique approach to obtain chemical, physical and thermodynamic properties of a system through fundamental and statistical thermodynamic approaches[164]. Using the statistical dynamics, all characteristics of the system such as viscosity and interfacial tension can be obtained by computing the potential energy according to the position of the atoms[162]. Another advantage of the MD strategy is attributed to the difficulty of classical modeling approaches systems such as equations of state or activity coefficient models, in the absence of experimental results. For systems containing corrosive components such as H_2S or/and the systems under high temperature or pressure conditions, implementation of corresponding experiments to obtain the real data is a difficult task. Molecular dynamic simulation is based on

solving the classical Newtonian equation of motion, considering intramolecular and intermolecular interactions as presented by the following equation[165]:

$$\overrightarrow{F_i} = m_i \frac{d^2\overrightarrow{r_i}}{dt^2} \quad (19)$$

where r_i stands for the atom position; and F_i refers to the forces on the atom from the neighbour atoms. The force vector can be calculated by deriving the potential energy function as follows[165]:

$$\overrightarrow{F_i} = \nabla(U(\mathrm{ri})) \quad (20)$$

In Equation (20), U represents the interaction energy. The energy term consists of all Non-bonded interactions and bonding potentials. To solve the equation of motion, some properties such as temperature or pressure are assumed to be constant. The statistical ensemble is a collection of all possible phases of system with sets of constraint including the imposed volume or number of molecules[165]. Based on the assumptions, thermodynamic properties such as enthalpy, fugacity, and vapor pressure can be computed. According to **Table 5**, different ensembles can be used, depending on the desired situation. Molecular dynamic simulation technique determines most of the dynamic properties (e.g., enthalpy) at equilibrium condition. Currently, there are a variety of MD simulators such as Material Studio and GROMACS [166-168] .A simple algorithm to present the utilization procedure of the molecular dynamic simulation is demonstrated in **Figure 22**.

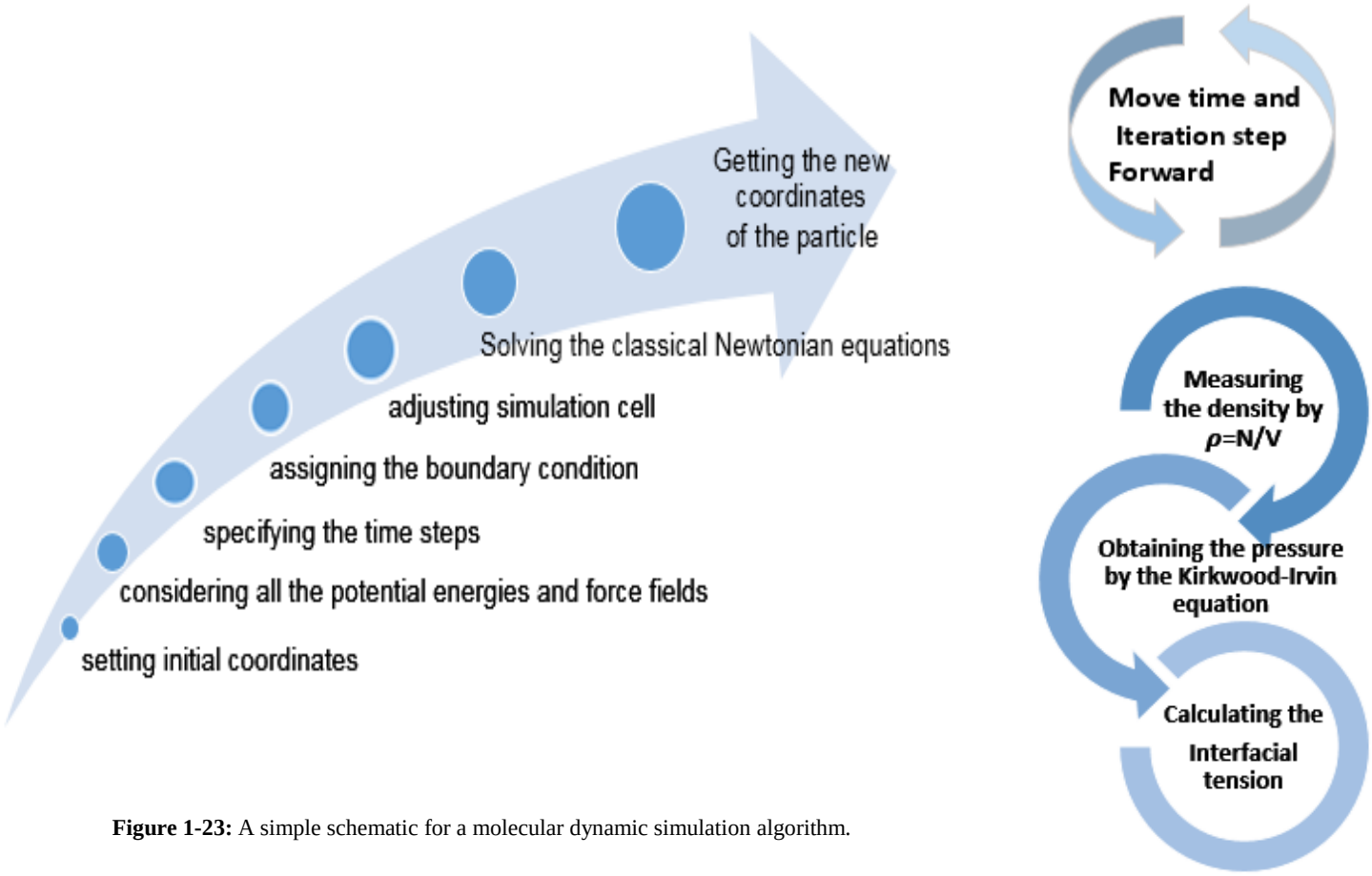

Figure 1-23: A simple schematic for a molecular dynamic simulation algorithm.

Table 1-5: Different statistical ensembles in molecular dynamics simulation and their application [165].

Statistical ensemble	Imposed variables	Definition of Variables	Applications
Canonical ensemble	N, V, T	N: number of moles V: volume T: temperature	Phase properties ($P, H, \mu_i, \dots$)
Grand canonical ensemble	μ_i, V, T	μ_i: initial concentration V: volume T: temperature	Adsorption isotherms, selectivity
Isothermal-Isobaric ensemble	N, P, T	N: number of moles P: pressure T: temperature	Phase properties ($H, C_p, \rho, \mu_i, \dots$)
Micro canonical ensemble	E, V, T	E: Energy V: volume T: temperature	Transport properties from molecular dynamics
Gibbs ensemble at imposed global volume (m phase)	$N = N_1 + \cdots N_m,$ $V = V_1 + \cdots V_{m,}$ T	N: number of moles V: volume T: temperature	Phase equilibrium of pure components and mixtures
Gibbs ensemble at imposed pressure (m phase)	$N = N_1 + \cdots N_m$ P ,T	N: number of moles P: pressure T: temperature	Phase equilibrium of mixtures

1.7 THEORETICAL AND PRACTICAL CHALLENGES

Emulsions formed in porous media can either help or hinder the optimal production. It has been reported that the presence of emulsions contributes to more efficient recovery in chemical flooding processes[149] .The improved sweep efficiency due to the presence of emulsions in injected fluid has been one of the fundamental application of emulsions in EOR processes. On the other hand, there are numerous cases where emulsion formation is undesirable due to a large pressure drop especially in Alkaline-Surfactant (AS) flooding. However, understanding of emulsion stability and demulsification processes is crucial to identify the role of emulsions in production steps. Droplet size distribution is one of the most important factors indicating the stability of emulsion, however this property is a function of various factors such as salinity, presence of emulsifying agent. However, determination and monitoring of these parameters instantaneous variations in various physical systems such as pipeline and porous media are not feasible in most cases, since these factors are functions of other properties/characteristics as well. There are a variety of research studies with focus on the influences of fluid and reservoir characteristics individually[65, 136, 151].However, no adequate systematic studies are found in the open sources to investigate the impacts of fluid and rock properties simultaneously when emulsions and porous media are in contact. There are several cases where presence of emulsion was reported as a problem owing to

the significant operational and production challenges such as pressure fluctuation or damage to surface facilities that are caused owing to the fluid viscosity increase and permeability reduction. In addition, the produced water, containing a considerable amount of oil (as droplets) needs to be treated. In this case, a demulsifier should be added to break and destabilise the emulsion which is costly.

Based on the experimental test conducted to describe emulsion stability, there are various measurement technique for determining emulsion stability. As explained earlier in this manuscript, there are some limitations (e.g., poor accuracy and complicated procedure). Thus, better procedures, empirical correlations, and statistical tools need to be developed to attain acceptable accuracy and reliability.

Modeling of emulsion flow through porous media is a difficult task because of the variation in rheological properties of the fluids with respect to time and position. Viscosity of emulsion is one of the important properties which can be strongly affected by the emulsion droplets. However, no reliable correlation is available to accurately predict the magnitude and behaviour of viscosity in porous media since the nature and structure of emulsions are not well understood, yet. The two main modeling approaches to describe the emulsion flow in porous media are the continuum theory and deep bed filtration method. The continuum theory assumes a single-phase flow with a higher viscosity, which is not always valid due to the dependency of the viscosity to the shear rate, pressure drop and several other factors such as temperature and phase concentration[75] . The filtration theory elusion transport is explained by straining and interception phenomena. A majority of researchers prefer to utilize the filtration theory; however, this method is found to be inaccurate to simulate the permeability alteration in porous systems. The simulation approaches such as MD and CFD seem to be valuable tools to investigate the stability and interfacial tension behavior of emulsions. However, there are a variety of computational restrictions in emulsion simulation using MD and CFD. First, even for the dilute mixtures, the number of molecules is very high at normal condition. Thus, it is not possible to model the movement of each molecule individually and drops [34]. Second, the simulation time steps have to be small enough to properly account the interfacial interactions in droplets. These time steps are in the range of nanoseconds which is difficult to be considered in practice. Incorporation of all the droplets interactions/movements in the equation of motion makes it very complicated to be solved. The potential of interactions alters with time because of adsorption of some components/molecules and the rapid change in emulsion interfacial area as a results of drops coalescence or/and breakage. This demands the repeated calculation of the interfacial characteristics that compute the forces between the particles with high accuracy.

1.8 CONCLUSIONS

A comprehensive review study is performed to further investigate the characteristics of emulsion and the factors affecting its stability. Effects of operational conditions, fluid properties, and reservoir characteristics on the emulsion behaviours and properties are studied in detail. Base on the previous studies on emulsions, the main findings are as follows:

- Emulsion is characterized in different classes according to the phase equilibria, droplet size, and stability.
- Stability of emulsion depends on several factors including temperature, water/oil ratio, and salinity of the water. There might be interactive forces and reactions that affect dependent and independent variables in the emulsion stability.
- Emulsion is mostly characterized by its stability. There are several methods to determine the stability. The most common technique is through measuring droplet size variation.
- Adequate description of the emulsion transport through porous media is difficult mainly due to the complex pore structure and rheological behaviours of emulsions.
- The presence of emulsions in porous media has advantages and disadvantages while conducting enhanced oil recovery technology such as water flooding. For instance, the formation of emulsions causes pressure flocculation and the presence of emulsions in the produced oil stream might damage surface facilities. On the other hand, emulsions generally lead to an increase in the viscosity of displacing fluid so that this impact has been noticed in EOR techniques by lowering the viscous fingering and improving the sweep efficiency. However, a proper understanding of the characteristics of petroleum fluids and operational conditions is required to attain an effective oil production strategy.
- The properties of porous media and resident fluids strongly affect the flow conditions and regime of emulsions in pores and different layers of the porous systems. The emulsion flow may also considerably influence important properties such as the relative permeability, viscosity, capillary pressure, and interfacial tension of the phases.
- There are no reliable (and accurate) models/correlations in the literature to appropriately relate emulsion formation mechanisms and emulsion stability to vital factors such as salinity, permeability, pore size, temperature, and water cut.
- Molecular Dynamic Simulation and Computational Fluid Dynamic are two important software packages to be employed for determination/description of thermodynamic properties and transport phenomena behaviours in porous media.
- The advanced CFD and MD modeling strategies may take from few hours to several weeks. Such a computational time is much longer, compared to the classical modeling approaches. However, the use of these new modeling/simulation techniques in a variety of chemical and energy industries is being increased to further figure out important molecular aspects (e.g., molecular forces and association terms) in terms of transport phenomena and thermodynamic concepts towards better design and optimization process.

- Utilization of modeling strategies/ software packages, which consider all the forces and interactions between oil and water phases in porous media to study the behaviour of interfacial film around the droplets, and systematic experimental works at both macro and micro scales are encouraged to further understand the governing mechanisms/behaviours.

ACKNOWLEDGEMENTS

We would like to acknowledge the financial assistance offered by Statoil Canada, Natural Sciences and Engineering Research Council of Canada (NSERC), Memorial University (NL, Canada), and InnovateNL (formerly RDC).

NOMENCLATURES

Acronyms

AS: Alkaline-Surfactant

ASTM: American Society for Testing and Materials

BS: Backscattering

CCD: Charged-Coupled Device

CEF: Critical Electric Field

CFD: Computational Fluid Dynamic

DSD: Droplet Size Distribution

EOR: Enhanced Oil Recovery

FBRM: Focused Beam Reflectance Measurement

GA: Gum Arabic

IFT: Interfacial Tension

MD: Molecular Dynamics

MS: Modified Starch

NIR: Near Infrared Spectroscopy

NMR: Nuclear Magnetic Resonance

O/W: Oil-in-water emulsion

PVM: Particle Video Microscope

TSI Turbiscan Stability Index

W/O: Water-in- oil emulsion

WAT: Wax Appearance Temperature

WPI: Whey Protein Isolate

English letters

$A,\ A', B, B'$: Temperature independent parameters

a_1, a_2, a_3, a_4 : Shear rate-dependent coefficients of the correlation.

a_E : Empirical constant

Bo: Bond number

c: Empirical coefficient

Ca : Capillary number

D: Diameter of the mixing tank or/and Droplet mean diameter

d_{max} : The maximum droplet size

F_{iv} : Volumetric interfacial tension

F_i : Forces on the atom from neighbour atoms

f_o : Sedimentation rate

Fr: Fraude number

f_w : Coalescence rate

g : Acceleration due to the gravity

g(d) : An optical parameter

$K(\gamma)$: Flocculation function for non-Newtonian emulsions

$K_e(\gamma)$:Hydration effect and floc

$K_e(\phi)$: Effect of the volume fraction of dispersed phase

K_o : Hydration factor

L : A characteristic linear dimension

n : Number of scans

N : Impeller speed

Q : Flow rate

Q_S : An optical parameters

Re : Reynolds number

r_i : Atom positionV_M : The maximum concentration of dispersed phase

T: Temperature

u : Velocity

V_{RZ} : Richardson and Zaki correction for Stokes velocity

V : Volume fraction of dispersed phase

V_{HR} : Hadamard-Rybczynski correction for Stokes velocity

V_{STOKES} : Sedimentation velocity

We : Weber number

x_{BS} : Average of x_i

x_i : Average BS

Z : Viscosity function

Greek letters

λ^* : Photon transport mean free path

μ_c : Dynamic viscosity of the continuous phase

μ_i: Initial concentration

μ_r : Relative viscosity

ρ_c : Continuous phase densities

ρ_d : Represent the dispersed phase density

$\emptyset$: Volume fraction of dispersed phase

ΔP : Pressure gradient

$\Delta\rho$: Density difference between the two phases

v : Kinematic viscosity

μ : Viscosity

ρ : Density

σ : Surface tension

Γ : Interfacial tension

REFERENCES

[1] D. B. Curtis, M. Aycibin, M. A. Young, V. H. Grassian, and P. D. Kleiber, "Simultaneous measurement of light-scattering properties and particle size distribution for aerosols: Application to ammonium sulfate and quartz aerosol particles," *Atmospheric Environment*, vol. 41, no. 22, pp. 4748-4758, 2007.

[2] S. Chodankar, V. Aswal, P. Hassan, and A. Wagh, "Structure of protein–surfactant complexes as studied by small-angle neutron scattering and dynamic light scattering," *Physica B: Condensed Matter*, vol. 398, no. 1, pp. 112-117, 2007.

[3] M. Moradi, V. Alvarado, and S. Huzurbazar, "Effect of salinity on water-in-crude oil emulsion: evaluation through drop-size distribution proxy," *Energy & fuels*, vol. 25, no. 1, pp. 260-268, 2010.

[4] A. Dukhin and P. Goetz, "Evolution of water-in-oil emulsion controlled by droplet-bulk ion exchange: acoustic, electroacoustic, conductivity and image analysis," *Colloids and Surfaces A: Physicochemical and Engineering Aspects*, vol. 253, no. 1-3, pp. 51-64, 2005.

[5] J. C. López-Montilla, P. E. Herrera-Morales, S. Pandey, and D. O. Shah, "Spontaneous emulsification: mechanisms, physicochemical aspects, modeling, and applications," *Journal of dispersion science and technology*, vol. 23, no. 1-3, pp. 219-268, 2002.

[6] O. C. Mullins, "Rebuttal to Strausz et al. regarding time-resolved fluorescence depolarization of asphaltenes," *Energy & Fuels*, vol. 23, no. 5, pp. 2845-2854, 2009.

[7] A. Hannisdal, M.-H. Ese, P. V. Hemmingsen, and J. Sjöblom, "Particle-stabilized emulsions: effect of heavy crude oil components pre-adsorbed onto stabilizing solids," *Colloids and Surfaces A: Physicochemical and Engineering Aspects*, vol. 276, no. 1-3, pp. 45-58, 2006.

[8] M. Fingas and B. Fieldhouse, "Formation of water-in-oil emulsions and application to oil spill modelling," *Journal of Hazardous Materials*, vol. 107, no. 1-2, pp. 37-50, 2004.

[9] M. J. Rosen and J. T. Kunjappu, *Surfactants and interfacial phenomena*. John Wiley & Sons, 2012.

[10] L. L. Schramm, *Emulsions, foams, and suspensions: fundamentals and applications*. John Wiley & Sons, 2006.
[11] N. v. d. T. Opedal, I. Kralova, C. Lesaint, and J. Sjöblom, "Enhanced sedimentation and coalescence by chemicals on real crude oil systems," *Energy & Fuels,* vol. 25, no. 12, pp. 5718-5728, 2011.
[12] C. D. McAuliffe, "Crude-oil-water emulsions to improve fluid flow in an oil reservoir," *Journal of Petroleum Technology,* vol. 25, no. 06, pp. 721-726, 1973.
[13] J. R. Bragg, "Oil recovery method using an emulsion," ed: Google Patents, 1999.
[14] T. Austad and S. Strand, "Chemical flooding of oil reservoirs 4. Effects of temperature and pressure on the middle phase solubilization parameters close to optimum flood conditions," *Colloids and Surfaces A: Physicochemical and Engineering Aspects,* vol. 108, no. 2-3, pp. 243-252, 1996.
[15] F. Khambharatana, S. Thomas, and S. Ali, "Macroemulsion rheology and drop capture mechanism during flow in porous media," in *SPE International Oil and Gas Conference and Exhibition in China*, 1998: Society of Petroleum Engineers.
[16] K. Zeidani, M. Polikar, H. Huang, and J. Boyd, "Heavy oil-in-water emulsion as a novel sealant in the near well bore region," in *Canadian International Petroleum Conference*, 2007: Petroleum Society of Canada.
[17] O. F. Devereux, "Emulsion flow in porous solids: I. a flow model," *The Chemical Engineering Journal,* vol. 7, no. 2, pp. 121-128, 1974.
[18] H. Soo and C. J. Radke, "Flow mechanism of dilute, stable emulsions in porous media," *Industrial & engineering chemistry fundamentals,* vol. 23, no. 3, pp. 342-347, 1984.
[19] C. Liu, M. Li, R. Han, J. Li, and C. Liu, "Rheology of Water-in-Oil Emulsions with Different Drop Sizes," *Journal of Dispersion Science and Technology,* vol. 37, no. 3, pp. 333-344, 2016.
[20] Y. Mikami, Y. Liang, T. Matsuoka, and E. S. Boek, "Molecular dynamics simulations of asphaltenes at the oil–water interface: from nanoaggregation to thin-film formation," *Energy & Fuels,* vol. 27, no. 4, pp. 1838-1845, 2013.
[21] T. F. Tadros, *Emulsion formation and stability*. John Wiley & Sons, 2013.
[22] P. Janssen, C. Noïk, and C. Dalmazzone, "Emulsion formation in a model choke-valve," in *SPE Annual Technical Conference and Exhibition*, 2001: Society of Petroleum Engineers.
[23] P. Posocco, A. Perazzo, V. Preziosi, E. Laurini, S. Pricl, and S. Guido, "Interfacial tension of oil/water emulsions with mixed non-ionic surfactants: comparison between experiments and molecular simulations," *RSC Advances,* vol. 6, no. 6, pp. 4723-4729, 2016.
[24] P. Winsor, "Hydrotropy, solubilisation and related emulsification processes," *Transactions of the Faraday Society,* vol. 44, pp. 376-398, 1948.
[25] G. Urbina-Villalba and M. García-Sucre, "Brownian dynamics simulation of emulsion stability," *Langmuir,* vol. 16, no. 21, pp. 7975-7985, 2000.
[26] J. C. Chen and A. S. Kim, "Brownian dynamics, molecular dynamics, and Monte Carlo modeling of colloidal systems," *Advances in colloid and interface science,* vol. 112, no. 1-3, pp. 159-173, 2004.
[27] Available: http://petrowiki.org/Oil_emulsions
[28] C. Dalmazzone, C. Noik, P. Glenat, and H.-M. Dang, "Development of a methodology for the optimization of dehydration of extraheavy-oil emulsions," *SPE Journal,* vol. 15, no. 03, pp. 726-736, 2010.
[29] S. Kokal and J. Al-Juraid, "Reducing emulsion problems by controlling asphaltene solubility and precipitation," in *SPE Annual Technical Conference and Exhibition*, 1998: Society of Petroleum Engineers.

[30] V. Menon and D. Wasan, "Particle—fluid interactions with applications to solid-stabilized emulsions Part III. Asphaltene adsorption in the presence of quinaldine and 1, 2-dimethylindole," *Colloids and surfaces*, vol. 23, no. 4, pp. 353-362, 1987.
[31] B. P. Binks, J. Dong, and N. Rebolj, "Equilibrium phase behaviour and emulsion stability in silicone oil+ water+ AOT mixtures," *Physical Chemistry Chemical Physics*, vol. 1, no. 9, pp. 2335-2344, 1999.
[32] S. L. Kokal, "Crude oil emulsions: A state-of-the-art review," *SPE Production & facilities*, vol. 20, no. 01, pp. 5-13, 2005.
[33] P. K. Kilpatrick, "Water-in-crude oil emulsion stabilization: Review and unanswered questions," *Energy & Fuels*, vol. 26, no. 7, pp. 4017-4026, 2012.
[34] G. Urbina-Villalba, "An algorithm for emulsion stability simulations: Account of flocculation, coalescence, surfactant adsorption and the process of Ostwald ripening," *International journal of molecular sciences*, vol. 10, no. 3, pp. 761-804, 2009.
[35] V. Alvarado, X. Wang, and M. Moradi, "Stability proxies for water-in-oil emulsions and implications in aqueous-based enhanced oil recovery," *Energies*, vol. 4, no. 7, pp. 1058-1086, 2011.
[36] L. L. Schramm, "Emulsions: Fundamentals and applications in the Petroleum Industry," *Advances in Chemistry Series*, vol. 321, 1992.
[37] O. K. Kimbler, R. Reed, and I. Silberberg, "Physical characteristics of natural films formed at crude oil-water interfaces," *Society of Petroleum Engineers Journal*, vol. 6, no. 02, pp. 153-165, 1966.
[38] R. Mohammed, A. Bailey, P. Luckham, and S. Taylor, "The effect of demulsifiers on the interfacial rheology and emulsion stability of water-in-crude oil emulsions," *Colloids and Surfaces A: Physicochemical and Engineering Aspects*, vol. 91, pp. 129-139, 1994.
[39] W. Orciuch, A. Moskal, and L. Gradoń, "Evolution of the droplet size distribution during a two-phase flow through a porous media: Population balance studies," *Chemical engineering science*, vol. 68, no. 1, pp. 227-235, 2012.
[40] J. Sjöblom *et al.*, "Our current understanding of water-in-crude oil emulsions.: Recent characterization techniques and high pressure performance," *Advances in Colloid and Interface Science*, vol. 100, pp. 399-473, 2003.
[41] G. Zhou and S. M. Kresta, "Correlation of mean drop size and minimum drop size with the turbulence energy dissipation and the flow in an agitated tank," *Chemical Engineering Science*, vol. 53, no. 11, pp. 2063-2079, 1998.
[42] T. Vermeulen, "Interfacial area in liquid-liquid and gas-liquid agitation," *Chem. Eng. Prog.*, vol. 51, pp. 85F-94F, 1955.
[43] H. T. Chen and S. Middleman, "Drop size distribution in agitated liquid-liquid systems," *AIChE Journal*, vol. 13, no. 5, pp. 989-995, 1967.
[44] F. Sprow, "Distribution of drop sizes produced in turbulent liquid—liquid dispersion," *Chemical Engineering Science*, vol. 22, no. 3, pp. 435-442, 1967.
[45] J. Hinze, "Fundamentals of the hydrodynamic mechanism of splitting in dispersion processes," *AIChE Journal*, vol. 1, no. 3, pp. 289-295, 1955.
[46] C. P. Aichele, M. Flaum, T. Jiang, G. J. Hirasaki, and W. G. Chapman, "Water in oil emulsion droplet size characterization using a pulsed field gradient with diffusion editing (PFG-DE) NMR technique," *Journal of Colloid and interface Science*, vol. 315, no. 2, pp. 607-619, 2007.
[47] J. Sjoblom, *Encyclopedic handbook of emulsion technology*. CRC Press, 2001.
[48] D. Brown and K. Pitt, "Drop size distribution of stirred non-coalescing liquid—liquid system," *Chemical Engineering Science*, vol. 27, no. 3, pp. 577-583, 1972.
[49] R. V. Calabrese, T. Chang, and P. Dang, "Drop breakup in turbulent stirred-tank contactors. Part i: Effect of dispersed-phase viscosity," *AIChE Journal*, vol. 32, no. 4, pp. 657-666, 1986.

[50] T. Lemenand, D. Della Valle, Y. Zellouf, and H. Peerhossaini, "Droplets formation in turbulent mixing of two immiscible fluids in a new type of static mixer," *International Journal of Multiphase Flow*, vol. 29, no. 5, pp. 813-840, 2003.
[51] J. A. Boxall, C. A. Koh, E. D. Sloan, A. K. Sum, and D. T. Wu, "Measurement and calibration of droplet size distributions in water-in-oil emulsions by particle video microscope and a focused beam reflectance method," *Industrial & Engineering Chemistry Research*, vol. 49, no. 3, pp. 1412-1418, 2009.
[52] D. Greaves *et al.*, "Measuring the particle size of a known distribution using the focused beam reflectance measurement technique," *Chemical Engineering Science*, vol. 63, no. 22, pp. 5410-5419, 2008.
[53] M.-T. Lasentec, "Product Group. FBRM® D600 Hardware Manual. Mettler-Toledo AutoChem," *Inc., Redmond, WA*, 2001.
[54] J. A. Boxall, C. A. Koh, E. D. Sloan, A. K. Sum, and D. T. Wu, "Droplet size scaling of water-in-oil emulsions under turbulent flow," *Langmuir*, vol. 28, no. 1, pp. 104-110, 2011.
[55] K. Hollingsworth, A. Sederman, C. Buckley, L. Gladden, and M. Johns, "Fast emulsion droplet sizing using NMR self-diffusion measurements," *Journal of colloid and interface science*, vol. 274, no. 1, pp. 244-250, 2004.
[56] N. van der Tuuk OPEDAL, G. Sørland, J. Sjöblom, and A. T. AS, "Methods for droplet size distribution determination of water-in-oil emulsions using low-field NMR," *Diffusion fundamentals*, vol. 7, pp. 1-29, 2009.
[57] A. Amani, S. Nazar, A. Reza, H. Sabzyan, and G. Azimi, "The measurement of droplet size distribution of water-oil emulsion through NMR method," *Journal of Particle Science & Technology*, vol. 2, no. 1, pp. 31-39, 2016.
[58] R. R. Ernst, "Zurich′ s Contributions to 50 Years Development of Bruker," *Angewandte Chemie International Edition*, vol. 49, no. 45, pp. 8310-8315, 2010.
[59] W. Souza *et al.*, "Effect of water content, temperature and average droplet size on the settling velocity of water-in-oil emulsions," *Brazilian Journal of Chemical Engineering*, vol. 32, no. 2, pp. 455-464, 2015.
[60] Ziess.
[61] C. ASTM, "39, Standard test method for compressive strength of cylindrical concrete specimens," *ASTM International*, 2001.
[62] *Turbiscan™ LAB Stability Analyzer from Formulaction SA*. Available: https://www.labcompare.com/25100-Stability-Analyzers/4864758-Turbiscan-LAB-Stability-Analyzer/
[63] O. Mengual, G. Meunier, I. Cayré, K. Puech, and P. Snabre, "TURBISCAN MA 2000: multiple light scattering measurement for concentrated emulsion and suspension instability analysis," *Talanta*, vol. 50, no. 2, pp. 445-456, 1999.
[64] C. Celia, E. Trapasso, D. Cosco, D. Paolino, and M. Fresta, "Turbiscan Lab® Expert analysis of the stability of ethosomes® and ultradeformable liposomes containing a bilayer fluidizing agent," *Colloids and Surfaces B: Biointerfaces*, vol. 72, no. 1, pp. 155-160, 2009.
[65] B. Xu, W. Kang, X. Wang, and L. Meng, "Influence of water content and temperature on stability of W/O crude oil emulsion," *Petroleum Science and Technology*, vol. 31, no. 10, pp. 1099-1108, 2013.
[66] S. Reddy and H. S. Fogler, "Emulsion stability: determination from turbidity," *Journal of Colloid and Interface Science*, vol. 79, no. 1, pp. 101-104, 1981.
[67] *turbidity meters* Available: http://en.aqualytic.de/products/turbidity-meters
[68] N. Aske, H. Kallevik, and J. Sjöblom, "Water-in-crude oil emulsion stability studied by critical electric field measurements. Correlation to physico-chemical parameters and near-infrared spectroscopy," *Journal of Petroleum Science and Engineering*, vol. 36, no. 1-2, pp. 1-17, 2002.

[69] H. Kallevik, S. B. Hansen, Ø. Sæther, O. M. Kvalheim, and J. Sjöblom, "Crude oil model emulsion characterised by means of near infrared spectroscopy and multivariate techniques," *Journal of dispersion science and technology,* vol. 21, no. 3, pp. 245-262, 2000.
[70] B. Binks and M. Kirkland, "Interfacial structure of solid-stabilised emulsions studied by scanning electron microscopy," *Physical Chemistry Chemical Physics,* vol. 4, no. 15, pp. 3727-3733, 2002.
[71] M. Almeida, R. Charin, M. Nele, and F. Tavares, "Stability studies of high-stable water-in-oil model emulsions," *Journal of Dispersion Science and Technology,* vol. 38, no. 1, pp. 82-88, 2017.
[72] P. Kundu, A. Agrawal, H. Mateen, and I. M. Mishra, "Stability of oil-in-water macro-emulsion with anionic surfactant: Effect of electrolytes and temperature," *Chemical Engineering Science,* vol. 102, pp. 176-185, 2013.
[73] D. J. Pye, "Improved secondary recovery by control of water mobility," *Journal of Petroleum technology,* vol. 16, no. 08, pp. 911-916, 1964.
[74] W. Gogarty, "Mobility control with polymer solutions," *Society of Petroleum Engineers Journal,* vol. 7, no. 02, pp. 161-173, 1967.
[75] N. Rezaei and A. Firoozabadi, "Macro-and Microscale Waterflooding Performances of Crudes which form w/o Emulsions upon Mixing with Brines," *Energy & Fuels,* vol. 28, no. 3, pp. 2092-2103, 2014.
[76] H. Soo and C. Radke, "Flow of dilute, stable liquid and solid dispersions in underground porous media," *AIChE Journal,* vol. 31, no. 11, pp. 1926-1928, 1985.
[77] H. Soo and C. Radke, "A filtration model for the flow of dilute, stable emulsions in porous media—I. Theory," *Chemical Engineering Science,* vol. 41, no. 2, pp. 263-272, 1986.
[78] J. Herzig, D. Leclerc, and P. L. Goff, "Flow of suspensions through porous media—application to deep filtration," *Industrial & Engineering Chemistry,* vol. 62, no. 5, pp. 8-35, 1970.
[79] J. T. G. Overbeek, "Electrochemistry of the double layer," *Irreversible Systems. Colloid Science, 1,* pp. 115-193, 1952.
[80] H. Soo, M. Williams, and C. Radke, "A filtration model for the flow of dilute, stable emulsions in porous media—II. Parameter evaluation and estimation," *Chemical Engineering Science,* vol. 41, no. 2, pp. 273-281, 1986.
[81] G. Falkovich, "Fluid Mechanics: A short course for physicists. 2011," ed: Cambridge University Press.
[82] A. Frohn and N. Roth, *Dynamics of droplets*. Springer Science & Business Media, 2000.
[83] F. M. White, "Fluid mechanics, WCB," *Ed McGraw-Hill Boston,* 1999.
[84] W. H. Hager, "Wilfrid noel bond and the bond number," *Journal of Hydraulic Research,* vol. 50, no. 1, pp. 3-9, 2012.
[85] M. Ding and A. Kantzas, "Capillary number correlations for gas-liquid systems," in *Canadian International Petroleum Conference*, 2004: Petroleum Society of Canada.
[86] G. G. Stokes, *On the effect of the internal friction of fluids on the motion of pendulums*. Pitt Press Cambridge, 1851.
[87] T. Frising, C. Noïk, and C. Dalmazzone, "The liquid/liquid sedimentation process: from droplet coalescence to technologically enhanced water/oil emulsion gravity separators: a review," *Journal of dispersion science and technology,* vol. 27, no. 7, pp. 1035-1057, 2006.
[88] S. A. Gundersen and J. Sjoblom, "Lignosulfonates and Kraft Lignins as O/W Emulsion Stabilizers Studied by Means of Electrical Conductivity," *Encyclopedic Handbook of Emulsion Technology,* p. 361, 2001.
[89] J. Hadamard, "Oeuvres de Jacques hadamard," 1968.
[90] M. Doble, A. K. Kruthiventi, and V. G. Gaikar, *Biotransformations and bioprocesses*. Marcel Dekker New York, NY, USA, 2004.

[91] R. Arntzen and P. A. K. Andresen, "Three-phase wellstream gravity separation," *Encyclopedic Handbook of Emulsion Technology. Sjöblom, J.(Ed.), Marcel Dekker, New York*, pp. 679-694, 2001.
[92] J. Richardson and W. Zaki, "Sedimentation and fluidisation: Part I," *Chemical Engineering Research and Design*, vol. 75, pp. S82-S100, 1997.
[93] S. Jeelani and S. Hartland, "Prediction of dispersion height in liquid-liquid gravity settlers from batch settling data," *Chemical Engineering Research and Design*, vol. 64, pp. 450-60, 1986.
[94] S. Jeelani and S. Hartland, "Dynamic response of gravity settlers to changes in dispersion throughput," *AIChE journal*, vol. 34, no. 2, pp. 335-340, 1988.
[95] S. Jeelani and S. Hartland, "The continuous separation of liquid/liquid dispersions," *Chemical engineering science*, vol. 48, no. 2, pp. 239-254, 1993.
[96] K. Joshi, S. Jeelani, C. Blickenstorfer, I. Naegeli, and E. J. Windhab, "Influence of fatty alcohol antifoam suspensions on foam stability," *Colloids and Surfaces A: Physicochemical and Engineering Aspects*, vol. 263, no. 1-3, pp. 239-249, 2005.
[97] S. A. Jeelani, A. Pandit, and S. Hartland, "Factors affecting the decay of batch liquid-liquid dispersions," *The Canadian Journal of Chemical Engineering*, vol. 68, no. 6, pp. 924-931, 1990.
[98] R. E. Cunha, M. Fortuny, C. Dariva, and A. F. Santos, "Mathematical modeling of the destabilization of crude oil emulsions using population balance equation," *Industrial & Engineering Chemistry Research*, vol. 47, no. 18, pp. 7094-7103, 2008.
[99] A. J. Jaworski and G. Meng, "On-line measurement of separation dynamics in primary gas/oil/water separators: Challenges and technical solutions—A review," *Journal of Petroleum Science and Engineering*, vol. 68, no. 1-2, pp. 47-59, 2009.
[100] N. Khatri, J. Andrade, E. Baydak, and H. Yarranton, "Emulsion layer growth in continuous oil–water separation," *Colloids and Surfaces A: Physicochemical and Engineering Aspects*, vol. 384, no. 1-3, pp. 630-642, 2011.
[101] B. Grimes, "Population balance model for batch gravity separation of crude oil and water emulsions. Part I: model formulation," *Journal of Dispersion Science and Technology*, vol. 33, no. 4, pp. 578-590, 2012.
[102] A. Anisa and A. H. Nour, "Affect of Viscosity and Droplet Diameter on water-in-oil (w/o) Emulsions: An Experimental Study," *J World Academy of Science Engineering and Technology 2010; 38: 692*, vol. 694, 2010.
[103] B. P. Binks and A. Rocher, "Effects of temperature on water-in-oil emulsions stabilised solely by wax microparticles," *Journal of colloid and interface science*, vol. 335, no. 1, pp. 94-104, 2009.
[104] J. Becker, *Crude oil waxes, emulsions, and asphaltenes*. Pennwell Books, 1997.
[105] R. Charoen, A. Jangchud, K. Jangchud, T. Harnsilawat, O. Naivikul, and D. J. McClements, "Influence of biopolymer emulsifier type on formation and stability of rice bran oil-in-water emulsions: whey protein, gum arabic, and modified starch," *Journal of Food Science*, vol. 76, no. 1, 2011.
[106] G. Marti-Mestres and F. Nielloud, "Main surfactants used in the pharmaceutical field," *Pharmaceutical Emulsions and Suspensions*, pp. 1-18, 2000.
[107] J. Asua, *Polymer reaction engineering*. John Wiley & Sons, 2008.
[108] M. Li and C. Garrett, "The relationship between oil droplet size and upper ocean turbulence," *Marine Pollution Bulletin*, vol. 36, no. 12, pp. 961-970, 1998.
[109] D. P. French-McCay, "Oil spill impact modeling: development and validation," *Environmental Toxicology and Chemistry*, vol. 23, no. 10, pp. 2441-2456, 2004.
[110] B. Gopalan and J. Katz, "Turbulent shearing of crude oil mixed with dispersants generates long microthreads and microdroplets," *Physical review letters*, vol. 104, no. 5, p. 054501, 2010.
[111] A. Kolmogorov, "On the breakage of drops in a turbulent flow," in *Dokl. Akad. Navk. SSSR*, 1949, vol. 66, pp. 825-828.

[112] R. Shinnar, "On the behaviour of liquid dispersions in mixing vessels," *Journal of Fluid Mechanics,* vol. 10, no. 2, pp. 259-275, 1961.
[113] F. Groeneweg, F. Van Dieren, and W. Agterof, "Droplet break-up in a stirred water-in-oil emulsion in the presence of emulsifiers," *Colloids and Surfaces A: Physicochemical and Engineering Aspects,* vol. 91, pp. 207-214, 1994.
[114] Z. M. Aman, C. B. Paris, E. F. May, M. L. Johns, and D. Lindo-Atichati, "High-pressure visual experimental studies of oil-in-water dispersion droplet size," *Chemical Engineering Science,* vol. 127, pp. 392-400, 2015.
[115] D. Dan and G. Jing, "Apparent viscosity prediction of non-Newtonian water-in-crude oil emulsions," *Journal of Petroleum Science and Engineering,* vol. 53, no. 1-2, pp. 113-122, 2006.
[116] M. A. Farah, R. C. Oliveira, J. N. Caldas, and K. Rajagopal, "Viscosity of water-in-oil emulsions: Variation with temperature and water volume fraction," *Journal of Petroleum Science and Engineering,* vol. 48, no. 3-4, pp. 169-184, 2005.
[117] E. E. Johnsen and H. P. Rønningsen, "Viscosity of 'live'water-in-crude-oil emulsions: experimental work and validation of correlations," *Journal of Petroleum Science and Engineering,* vol. 38, no. 1-2, pp. 23-36, 2003.
[118] R. Pal, "A novel method to correlate emulsion viscosity data," *Colloids and Surfaces A: Physicochemical and Engineering Aspects,* vol. 137, no. 1-3, pp. 275-286, 1998.
[119] R. Pal, "Evaluation of theoretical viscosity models for concentrated emulsions at low capillary numbers," *Chemical Engineering Journal,* vol. 81, no. 1-3, pp. 15-21, 2001.
[120] A. Einstein, "Calculation of the viscosity-coefficient of a liquid in which a large number of small spheres are suspended in irregular distribution," *Ann. Phys. Leipzig,* vol. 19, pp. 286-306, 1906.
[121] G. I. Taylor, "The viscosity of a fluid containing small drops of another fluid," *Proceedings of the Royal Society of London. Series A,* vol. 138, no. 834, pp. 41-48, 1932.
[122] A. Einstein, *Investigations on the Theory of the Brownian Movement*. Courier Corporation, 1956.
[123] H. Brinkman, "The viscosity of concentrated suspensions and solutions," *The Journal of Chemical Physics,* vol. 20, no. 4, pp. 571-571, 1952.
[124] C. A. Eilers, "Detachable spout," ed: US Patent 2,315,250, 1943.
[125] S. J. Choi and W. Schowalter, "Rheological properties of nondilute suspensions of deformable particles," *The Physics of Fluids,* vol. 18, no. 4, pp. 420-427, 1975.
[126] I. Yaron and B. Gal-Or, "On viscous flow and effective viscosity of concentrated suspensions and emulsions," *Rheologica Acta,* vol. 11, no. 3-4, pp. 241-252, 1972.
[127] N. Phan-Thien and D. Pham, "Differential multiphase models for polydispersed suspensions and particulate solids," *Journal of Non-Newtonian Fluid Mechanics,* vol. 72, no. 2-3, pp. 305-318, 1997.
[128] I. M. Krieger and T. J. Dougherty, "A mechanism for non-Newtonian flow in suspensions of rigid spheres," *Transactions of the Society of Rheology,* vol. 3, no. 1, pp. 137-152, 1959.
[129] W. Richardson and R. Waite, "35—THE FLOW OF STARCH PASTES.(iii) THE EFFECT OF SOAPS AND OTHER ELECTROLYTES ON THE APPARENT VISCOSITY OF HOT STARCH PASTES," *Journal of the Textile Institute Transactions,* vol. 24, no. 11, pp. T383-T416, 1933.
[130] H. P. Ronningsen, "Correlations for predicting viscosity of W/O-emulsions based on North Sea crude oils," in *SPE International Symposium on Oilfield Chemistry*, 1995: Society of Petroleum Engineers.
[131] P. Becher, "Emulsions: theory and practice," 1965.
[132] L. Baldauf, R. Schechter, W. Wade, and A. Graciaa, "The relationship between surfactant phase behavior and the creaming and coalescence of macroemulsions," *Journal of Colloid and Interface Science,* vol. 85, no. 1, pp. 187-197, 1982.

[133] R. E. Antón and J.-L. Salager, "Emulsion instability in the three-phase behavior region of surfactant-alcohoi-oil-brine systems," *Journal of colloid and interface science*, vol. 111, no. 1, pp. 54-59, 1986.
[134] I. B. Ivanov, "Effect of surface mobility on the dynamic behavior of thin liquid films," *Pure and Applied Chemistry*, vol. 52, no. 5, pp. 1241-1262, 1980.
[135] X. Wang and V. Alvarado, "Direct current electrorheological stability determination of water-in-crude oil emulsions," *The Journal of Physical Chemistry B*, vol. 113, no. 42, pp. 13811-13816, 2009.
[136] S. Maaref and S. Ayatollahi, "The effect of brine salinity on water-in-oil emulsion stability through droplet size distribution analysis: A case study," *Journal of Dispersion Science and Technology*, pp. 1-13, 2017.
[137] R. Aveyard, B. Binks, and P. Fletcher, "Interfacial tensions and aggregate structure in pentaethylene glycol monododecyl ether/oil/water microemulsion systems," *Langmuir*, vol. 5, no. 5, pp. 1210-1217, 1989.
[138] M. Jansson, L. Eriksson, and P. Skagerlind, "The effect of tetraalkylammonium ions on the stability of dilute O/W emulsions," *Colloids and surfaces*, vol. 53, no. 1, pp. 157-167, 1991.
[139] K. Shinoda and H. Saito, "The stability of O/W type emulsions as functions of temperature and the HLB of emulsifiers: the emulsification by PIT-method," *Journal of Colloid and Interface Science*, vol. 30, no. 2, pp. 258-263, 1969.
[140] E. DeZabala and C. Radke, "A nonequilibrium description of alkaline waterflooding," *SPE Reservoir Engineering*, vol. 1, no. 01, pp. 29-43, 1986.
[141] M. I. Romero, M. S. Carvalho, and V. Alvarado, "Experiments and network model of flow of oil-water emulsion in porous media," *Physical Review E*, vol. 84, no. 4, p. 046305, 2011.
[142] M. Błaszczyk, P. Pacholski, Ł. Przybysz, and J. Sęk, "Influence of granular bed parameters on emulsion flow and elution process of oil-in-water emulsion," *Technical Sciences/University of Warmia and Mazury in Olsztyn*, 2016.
[143] H. Soo and C. Radke, "Velocity effects in emulsion flow through porous media," *Journal of Colloid and Interface Science*, vol. 102, no. 2, pp. 462-476, 1984.
[144] J. Bryan, J. Wang, and A. Kantzas, "Measurement of emulsion flow in porous media: Improvements in heavy oil recovery," in *Journal of Physics: Conference Series*, 2009, vol. 147, no. 1, p. 012058: IOP Publishing.
[145] X. Fu, R. H. Lane, and D. D. Mamora, "Water-in-Oil emulsions: flow in porous media and EOR potential," in *SPE Canadian Unconventional Resources Conference*, 2012: Society of Petroleum Engineers.
[146] J. L. Bryan, A. T. Mai, and A. Kantzas, "Investigation into the processes responsible for heavy oil recovery by alkali-surfactant flooding," in *SPE Symposium on Improved Oil Recovery*, 2008: Society of Petroleum Engineers.
[147] M. Dong, Q. Liu, and A. Li, "Micromodel study of the displacement mechanisms of enhanced heavy oil recovery by alkaline flooding," in *Proceedings of the International Symposium of the Society of Core Analysts*, 2007, pp. 2007-2047: Citeseer.
[148] C. D. McAuliffe, "Oil-in-water emulsions and their flow properties in porous media," *Journal of petroleum technology*, vol. 25, no. 06, pp. 727-733, 1973.
[149] S. Thomas and S. F. Ali, "Flow of emulsions in porous media, and potential for enhanced oil recovery," *Journal of Petroleum Science and Engineering*, vol. 3, no. 1-2, pp. 121-136, 1989.
[150] A. Mandal and A. Bera, "Modeling of flow of oil-in-water emulsions through porous media," *Petroleum Science*, vol. 12, no. 2, pp. 273-281, 2015.
[151] M. I. Romero, "Flow of emulsions in porous media," in *SPE Annual Technical Conference and Exhibition*, 2009: Society of Petroleum Engineers.

[152] R. Kumar, E. Dao, and K. Mohanty, "Heavy-oil recovery by in-situ emulsion formation," *Spe Journal,* vol. 17, no. 02, pp. 326-334, 2012.
[153] M. Sun, K. Mogensen, M. Bennetzen, and A. Firoozabadi, "Demulsifier in Injected Water for Improved Recovery of Crudes That Form Water/Oil Emulsions," *SPE Reservoir Evaluation & Engineering,* vol. 19, no. 04, pp. 664-672, 2016.
[154] Z. Yazhou, W. Demin, W. Zhipeng, and C. Rui, "The formation and viscoelasticity of pore-throat scale emulsion in porous media," *Petroleum Exploration and Development,* vol. 44, no. 1, pp. 111-118, 2017.
[155] J. P. Gallo-Molina, N. Ratkovich, and Ó. Álvarez, "Multiscale Analysis of Water-in-Oil Emulsions: A Computational Fluid Dynamics Approach," *Industrial & Engineering Chemistry Research,* vol. 56, no. 27, pp. 7757-7767, 2017.
[156] D. Pradilla, W. Vargas, and O. Alvarez, "The application of a multi-scale approach to the manufacture of concentrated and highly concentrated emulsions," *Chemical Engineering Research and Design,* vol. 95, pp. 162-172, 2015.
[157] M. Meyer, M. Mareschal, and M. Hayoun, "Computer modeling of a liquid–liquid interface," *The Journal of chemical physics,* vol. 89, no. 2, pp. 1067-1073, 1988.
[158] I. Kobayashi, S. Mukataka, and M. Nakajima, "CFD simulation and analysis of emulsion droplet formation from straight-through microchannels," *Langmuir,* vol. 20, no. 22, pp. 9868-9877, 2004.
[159] I. Kobayashi, S. Mukataka, and M. Nakajima, "Effect of slot aspect ratio on droplet formation from silicon straight-through microchannels," *Journal of colloid and interface science,* vol. 279, no. 1, pp. 277-280, 2004.
[160] I. Kobayashi, S. Mukataka, and M. Nakajima, "Effects of type and physical properties of oil phase on oil-in-water emulsion droplet formation in straight-through microchannel emulsification, experimental and CFD studies," *Langmuir,* vol. 21, no. 13, pp. 5722-5730, 2005.
[161] P. Linse, "Monte Carlo simulation of liquid–liquid benzene–water interface," *The Journal of chemical physics,* vol. 86, no. 7, pp. 4177-4187, 1987.
[162] H. Zhang, B.-j. Zhang, J. Lu, and S. Liang, "Molecular dynamics simulations on the adsorption and surface phenomena of simple fluid in porous media," *Chemical physics letters,* vol. 366, no. 1-2, pp. 24-27, 2002.
[163] D. McQuarrie, "Statistical Mechanics, Harper Collins, New York(1976)."
[164] B. Wang and P. Cummings, "Non-equilibrium molecular dynamics calculation of the shear viscosity of carbon dioxide/ethane mixtures," *Molecular simulation,* vol. 10, no. 1, pp. 1-11, 1993.
[165] P. Ungerer, V. Lachet, and B. Tavitian, "Applications of molecular simulation in oil and gas production and processing," *Oil & Gas Science and Technology-Revue de l'IFP,* vol. 61, no. 3, pp. 387-403, 2006.
[166] J. Wang and A. L. Ferguson, "Mesoscale simulation of asphaltene aggregation," *The Journal of Physical Chemistry B,* vol. 120, no. 32, pp. 8016-8035, 2016.
[167] A. Wu and Z. Zeng, "Dynamic behaviors of memristor-based recurrent neural networks with time-varying delays," *Neural Networks,* vol. 36, pp. 1-10, 2012.
[168] W. Zheng, C. Sun, and B. Bai, "Molecular Dynamics Study on the Effect of Surface Hydroxyl Groups on Three-Phase Wettability in Oil-Water-Graphite Systems," *Polymers,* vol. 9, no. 8, p. 370, 2017.

2 Dissipative Particle Dynamics and Molecular Dynamic Simulations Assess the Influences of Oil structure and Temperature on Emulsion Stability

Fatemeh Goodarzi, Sohrab Zendehboudi

Faculty of Engineering and Applied Science, Memorial University, St. John's, NL, Canada

ABSTRACT

Water/oil emulsions are one of the important constituents involved in a variety of industries such as pharmaceutical, food, health/beauty care, and oil and gas. Emulsion stability is a crucial aspect of emulsions in the context of transport phenomena and surface science. Interfacial tension (IFT) is a vital property, which is related to the emulsion stability. In this paper, dissipative particle dynamics (DPD) mesoscopic molecular simulations are employed to study the impacts of temperature and oil type on the structural properties and IFT in order to obtain detailed insights on emulsion stability. Flory-Huggins chi parameter (χ) is determined through implementing molecular dynamics (MD) simulations using the solubility parameter calculations as well as the energy of mixing equations using Monte Carlo method as a function of temperature to evaluate the DPD interaction parameter (a_{ij}). The predicted chi parameter is then compared to the experimental data. IFT is evaluated in the presence and absence of an emulsifier for different types of cyclic (Cyclohexane and Benzene) and aliphatic (Octane and Dodecane) oil molecules. The influence of temperature on the IFT is also investigated through integration of DPD and MD approaches. The surfactant effect on the aggregation behaviour of the system is discussed by considering the structural characteristics of the surfactant molecules using the radius of gyration. Comparing the simulation snapshots taken at different simulation time steps, concertation profiles and radius of gyration values, it is observed that in the case of aliphatic hydrocarbons, surfactant molecules will stretch more due to the linear structure of oil molecules. For cyclic hydrocarbons, the radius of gyration is reported to be smaller since less space is available for the interaction of surfactant tail groups with oil molecules. It is also found that the IFT is a function of molecular weight of hydrocarbon. Thus, the highest IFT is for Dodecane(43.62 mN/m) and the smallest IFT is for Benzene (29.68 mN/m), regardless of the structure and polarity of the molecules. By decreasing the interfacial tension, the emulsion coalescence occurs faster and phases start to separate so that the mixture has no longer the characteristics of an emulsion. Constructing the force-field in DPD simulation based on the micro-scale calculations of chi parameter improves the accuracy of simulation where the computational time and cost are reduced. The current study further highlights the importance of beading arrangement and the effect of oil molecule on the interfacial characteristic of hydrocarbon/surfactant/water systems.

Keywords: Water/oil emulsion, Dissipative particle dynamics, Molecular dynamics simulation, Interfacial tension, Cyclic and Aliphatic Hydrocarbon, Radius of Gyration, Emulsifier

2.1 INTRODUCTION

Emulsions are an important element of a wide range of food production processes, oil and gas mixtures, and drugs and beauty products [1]. In multi-component mixtures such as emulsions, suspension or a polymer blend, the interfacial tension (IFT) plays a significant role to describe/characterise the interactions of the particles in the system [2] such that IFT is considered as one of the central thermophysical characteristics of a mixture to investigate the interface behaviours of two immiscible fluids.

IFT is directly proportional to the morphology and rheological behaviours of the components in the mixture. This property can be easily modified by the presence of an amphiphilic substance in the aqueous solution. An amphiphilic compound is a molecule with both hydrophobic and hydrophilic parts in its molecular structure. Amphiphilic compounds are known as surfactants. The surfactant solution can form different phases, depending on the temperature, composition of the mixture, and the presence of salt [3]. Surfactants enable the oil/water system to demonstrate different morphologies as well as stability conditions. Particularly, the properties of surfactant affect the interfacial behaviours of the targeted system, such as the IFT, and thickness and density of the formed layer [4]. These molecules have exhibited various applications in numerous industries ranging from cosmetics, biomedical to petroleum production [5,6]. Oily substances particularly crude oils can be a complex mixture of different hydrocarbon from aliphatic to aromatic hydrocarbons, and surface-active particles such as asphaltene or resin molecules. Due to the amphiphilic structure of surfactant molecules, they showed high potential in various enhanced oil recovery (EOR) methods since they can change the surface activity of molecules present in the mixture [7]. Alkaline/surfactant/polymer (ASP) is one of the EOR techniques used in the petroleum industry to improve the sweep efficiency of the crude oil by changing the IFT [8]. To attain a better understanding regarding the phase and structure of surfactant in an aqueous mixture, a number of researchers employed various experimental and computer simulation methods with focus on the phase behaviours and transport phenomena aspects of the hydrocarbon/surfactant/water systems. There are a variety of experimental approaches to determine the IFT [9] and several researchers presents a large amount of results related to the interfacial tension measurements for water/ hydrocarbon systems and water/ organic solvents in the presence and absence of polymers [10-12]. There are advanced laboratory equipment such as fluorescence, neutron reflection [13] or vibrational sum frequency spectroscopy [14] to analyse the dynamical and structural behaviours of surfactants at the water/oil interface. However, few modeling/simulation techniques are available to model the liquid-liquid interaction at the interface in the mesoscale level. For instance, Meybodi et el. [15] performed a comprehensive study on IFT calculation by developing a correlation in terms of temperature and pressure for 32 types of aliphatic and aromatic hydrocarbon in both liquid and gas phases with water at various process/thermodynamic conditions. The proposed correlation suggested a decrease in IFT with increasing temperature. The estimation capability of the proposed model was acceptable for liquid hydrocarbons; however, the model did not offer an accurate predictive trend for gaseous hydrocarbons to investigate the effect of temperature and pressure. Ataev [11] also conducted an experimental study on determination of the IFT for different hydrocarbons(n-hexane, n-nonane, and n-docecane)/ water systems. Using the sessile drop technique, the IFT values were measured at different temperature conditions. This researcher observed an increase in the IFT with increasing

the temperature, which is in contradict with the trends in the literature. This contradiction was justified by the difference in the behaviour of contacting liquids characteristics, compared to the isolated surface of a liquid. By increasing temperature, the excess interfacial energy will be formed at the interface due to the break of a hydrogen bond between the contacting water and oil molecules or due to solvation of impurities at either phase. Another important aspect mentioned in the research work is the ageing process that is required for the system to attain equilibrium, causing a considerable increase in the decay time. Hence, it will lead to an increase in the IFT values upon an increase in the system temperature.

Experimental methods are expensive and time-consuming. They may also need significant attention to obtain reliable IFT values. Hence, they might not be favorable to predict the magnitudes of IFT especially in cases where accurate results are required immediately [16]. Numerical simulations, on the other hand, provide a complementary approach to experimental methods or even an alternative way to characterize the system [17, 18]. Further investigation of the interfacial behaviours and self-assembly developments are essential. However, such attempts are often restrained by the convenience of experimental practices [19]. Fortunately, various numerical methods including molecular dynamics (MD) [20], Monte Carlo simulation (MC) [21], smooth particle hydrodynamics, and dissipative particle dynamics (DPD) [4] are employed to address the above concerns. Computer simulations have appeared as an influential tool in modelling microstructures of water/surfactant/oil systems in the past few years [12,22, 23]. Atomistic simulations can be employed to study the molecular structures and dynamic behaviours of the system [24-26]. However, there are limitations in time and length scales as well as difficulty in monitoring phase transition processes in mesoscale with this approach [27-29]. DPD introduced by Hoogerbrugge and Koelman [30] and later modified by Espanol and Warren [31] is a broadly approved method in the mesostructure studies of emulsions and suspensions where the statistical mechanics is the fundamental of this strategy [32-34]. The DPD was found to be an ideal technique to model such a coarse-grained mixture [30, 31]. Each DPD particle is counted as a cluster of molecules, experiencing a soft potential interaction with other particles in the system. Therefore, DPD is more accurate compared to MD in terms of computational efficiency [2]. Newton's second law of motion governs the DPD particles motion. DPD system preserves mass and total linear momentum of the system, during which flow kinematics and stress tensor is a part of the solution steps [2]. In the past few years, DPD has been broadly utilized in characterizing suspensions with rigid body particles [30, 35], long-chain molecules such as DNA molecule and polymers [36, 37], and miscible, immiscible or partly miscible liquid-liquid solution interactions [38-40]. The DPD interaction parameter, which is a key parameter to model the conservative forces in the DPD method, is calculated with the Flory-Huggins chi parameter. This value can be obtained using MD simulation [41] or Monte Carlo methods [42]. Rezaei and Modarress [43] applied a mesoscopic DPD simulation method to investigate the IFT of linear alkanes, cycloalkanes, and aromatics with water. Solubility parameter was used to determine a DPD interaction parameter to calculate the IFT values, and the results were compared with the outcome of X-ray scattering analysis. Studies on the IFT analysis for pure hydrocarbon and water systems are required since some cases require this information as the initial input for later configuration and comparisons in their system, however, in most systems, an additive such as a surfactant and/or a polymer is added to the mixture to improve the characteristics of the solution [22]. In many research investigations, various non-ionic and ionic surfactants have been added to the water/hydrocarbon mixtures to modify the interfacial characteristics of the system. For instance, Wang et al. [23, 44, 45] performed a series

of DPD simulations on the structural and interfacial characteristics of water/hydrocarbon systems in the presence of different anionic, cationic, and non-ionic surfactants and also a mixture of these surfactants. The effects of temperature, salinity, and water cut were considered on the vital interfacial and structural characteristics such as IFT and radius of gyration. They analysed a variety of cases with different initial process conditions; however, the type of hydrocarbon was just Octane. Silva and Ruette [41] calculated the IFT values for different types of linear hydrocarbons, glycerol and organic liquids systems and compared them to the data available in the literature. DPD conservative force parameters were obtained using the solubility parameter. It was found that the IFT increases as the number of carbon increases in the linear chain of a hydrocarbon. The data, however, were not collected at the same temperature or pressure. Hence, an inaccuracy/ error was noticed in the proposed trends and estimations. A systematic study on the mesostructure and dynamic behaviours of the surfactant using numerical simulations is an important step toward a comprehensive description of the system, which engages cooperative behaviour such as phase transition or self-assembly [46]. Compared to other thermophysical properties such as viscosity or density, less research has been dedicated to investigation on the dynamic and structural trends of IFT since information on two separate phases is required to describe this key property while other parameters can be described by just one fluid characteristic [15]. The motivation arises from multiple studies on the fundamental behaviours of the immiscible liquid-liquid system such as water/oil emulsion. Hence, it is significant to obtain a precise description of water/oil interface behaviours. In this paper, the primary focus is on the mesostructured study of water/surfactant/oil via DPD simulations. A non-ionic surfactant (hexaethylene glycol monododecyl ether) is chosen to be added to the water/oil mixture. Moreover, we examine the IFT of oil/surfactant/water systems for different hydrocarbon molecules within a broad range of temperatures.

After the introduction section, a brief mathematical description on the DPD approach is provided. Using MD simulation and Monte Carlo method, the Flory Huggins chi parameter is obtained using the cohesive energy density, solubility parameter, and energy of mixing, respectively. The detailed steps toward these calculations using amorphous cell, Forcite and blends Module are described in the next section. The simulation details such as cell configuration and time steps are also given. In the results and discussion section, plots of the radius of gyration, concentration profiles, and IFT behaviours are presented and discussed at different temperatures for the cases of both aliphatic and cyclic hydrocarbons. A comparison was made between the modeling results and experimental data from the literature. In the last section, we summarize the main conclusions of the work and recommendations for future studies where the integrated MD, Monte Carlo, and DPD approach is used.

2.2 THEORY OF COMPUTATIONAL APPROACH

2.2.1 DPD Fundamentals

Dissipative particle dynamics (DPD) is a stochastic and Lagrangian simulation method, which was first developed by Hoogerbrugge and Koelman [2], to study the hydrodynamic performance of complex fluids. DPD is a coarse-grained mesoscopic approach with the aim of describing the components on an increased scale compared to the molecular simulation [47]. Unlike self-

consistent field theory (SCFT), DPD provides information on not only the properties of thermodynamics equilibrium but also dynamics properties and evolution of the molecular structure as a function of time [48]. The advantage of DPD over other atomistic simulation methods such as molecular dynamics (MD) is less simulation time and cost for modelling complex structures due to coarse-graining procedure implemented in the DPD technique, which causes fewer interactions to be considered. Moreover, the choice of larger time-steps is possible in DPD with the same degree of accuracy, compared to MD, due to the soft potentials used in this simulation approach. The lattice Boltzmann method (LBM) is another mesoscopic technique, which can be employed to model the hydrodynamic behaviours of a system. This method, however, has some considerable disadvantages over the DPD method. For example, the liquid description, which is in the form of a lattice symmetry, represents an incorrect physical model of the liquid that causes artefacts for LBM method. Moreover, the lattice method cannot accurately describe the systems under shear, and the systems used to calculate the IFT do not take into account the shear stress on the simulation cell. In the DPD method, soft spherical beads represent a cluster of several single atoms or molecules or a volume of fluid, with underlying the chemistry of molecules. In the case of big molecules like polymers, multiple beads are joined together by a harmonic spring with a constant of k_s [49]. Similar to the MD simulation, the time evolution of a many-body system controlled by classical Newton's equation of motion in DPD approach, is captured to estimate the trajectory of the DPD spherical beads by the following equation [50]:

$$\frac{dr_i}{dt} = v_i \ , \quad \frac{dv_i}{dt} = F_i/m_i \tag{1}$$

where r_i, v_i, and m_i refer to the position vector, velocity vector, and mass of the beads, respectively. The different parts of the total force between *i* and *j* particles is expressed as follows:

$$F_i = \sum_{j \neq i} (F_{ij}^C + F_{ij}^D + F_{ij}^R) + F_{ij}^S \tag{2}$$

in which, F_{ij}^C denotes the conservative force; F_{ij}^D represents the dissipative force; F_{ij}^R refers to the random forces; F_i^S shows the spring force applied on the i^{th} bead by the j^{th} bead; and the remaining term is the spring forces, which is the force as a result of the bonded interactions [51]. The actual physical description of each force type is given below:

$$F_{ij}^C = a_{ij}\omega^C(r_{ij})\hat{r}_{ij} \tag{3}$$

$$F_{ij}^D = -\xi\omega^D(r_{ij})(v_{ij}.\hat{r}_{ij})\hat{r}_{ij} \tag{4}$$

$$F_{ij}^{R} = \sigma\omega^{R}(r_{ij})\xi_{ij}\Delta t^{-(\frac{1}{2})}\hat{r}_{ij} \tag{5}$$

where a_{ij} introduces the maximum repulsion force between beads *i* and *j* which is also called DPD interaction parameter. This parameter illustrates the interaction strength of two interacting particles in the simulation system [43]. $r_{ij} = r_i - r_j, r_{ij} = |r_{ij}|$, $v_{ij} = v_i - v_j$ And $\hat{r}_{ij} =, r_{ij}/|r_{ij}|$ where *r* and *v* refer to the position and velocity vectors of the particles [52], respectively. ξ resembles the dissipation coefficient, which is a randomly fluctuating parameter with stochastic properties [31]; and $\omega^{C}, \omega^{D},$ and ω^{R} are the conservative, dissipative and random forces weight function, respectively. σ refers to the amplitude of the random forces according to $\sigma^2 = 2k_B T\xi$ and Δt is the time step as defined below:

$$\Delta t = 0.04\tau \quad where \ \tau = (\frac{mr_c^2}{k_B T})^{1/2} \tag{6}$$

In Equation (6), k_B is the Boltzmann constant; T refers to the absolute temperature; r_c describes the common effective interaction length or the cut-off radius; and τ is the conversion factor to change time in seconds to time in DPD units. According to the fluctuation-dissipation theorem, the simplified form of the weight functions is given by the following expression [51]:

$$\omega^{C}(r_{ij}) = \omega^{R}(r_{ij}) = [\omega^{D}(r_{ij})]^{\frac{1}{2}} = \begin{cases} 1 - r_{ij}, & r_{ij} \le r_C \\ 0, & r_{ij} > r_C \end{cases} \tag{7}$$

All DPD beads of the same molecule are attached by a loosely bounded spring. The molecule stiffness can be controlled through the spring force [53]. Based on Groot's work, the spring force on particle *i* is found as follows [51]:

$$F_{ij}^{S} = -k_s(r_{ij} - r_0)\hat{r}_{ij} \tag{8}$$

in which, k_s represents the spring constant and r_0 refers to the spring equilibrium distance. The spring constant controls the molecule stiffness; however, the simulation output is a strong function of this variable [12]. There are a variety of values for k_s and r_0 in the literature [53, 54]. The most suggested values in the DPD units are: $k_s = 4, r_0 = 0$ [53, 55, 56]; $k_s = 10, r_0 = 0.86$ [57] ; and $k_s = 100, r_0 = 0.7$ [58].

2.2.2 Parameterisation of Conservative Force

In the DPD approach, the interaction parameter between like and unlike particles in the system should be obtained to model complex fluids.

The accuracy of DPD calculation lies on the correct estimation of the DPD interaction parameter (a_{ij}). An important relationship between Flory-Huggins chi parameter (χ) and a_{ij} was obtained by Groot and Warren in 1997 [51]. Other researchers presented the similar expressions for the DPD interaction parameter as a function of chi parameter [59, 60]. The idea was to express the thermodynamic properties of DPD model and its fluctuation using a soft sphere model as presented below:

$$a_{ij} = a_{ii} + b\chi_{ij} \tag{9}$$

where a_{ii} refers to the DPD interaction parameter for similar particles and b represents a constant with two different values of 3.5 and 1.45 for DPD densities of $\rho = 3$ and 5 in the DPD units, respectively [50].

The value of a_{ii} is determined by the following formula:

$$a_{ii} = [(k^{-1}(T)N_m - 1)/2\alpha\rho]k_BT \tag{10}$$

in which, N_m introduces the coarse-graining degree that corresponds to the number of water molecules in one bead. This is in agreement with experimental values based on water compressibility at a particular temperature [43]. In Equation (10), α is a constant with a value of 0.101 and ρ denotes the density in DPD units. k^{-1} is the inversed dimensionless compressibility of the structure, which is expressed as follows:

$$k^{-1} = \frac{1}{\rho k_B T k_T} = \frac{1}{k_B T}\left(\frac{\partial p}{\partial \rho}\right)_T \tag{11}$$

where $k_T = 1/\rho(\partial\rho/\partial p)_T$ is the common isothermal compressibility, p refers to the pressure, and k_B resembles the Boltzmann constant [43]. Using the Virial theorem, the pressure can be defined based on the forces and the trajectory of the atoms as follows [51]:

$$p = \rho k_B T + \frac{1}{3V}\left\langle \sum_{i}^{N-1} \sum_{j=i+1}^{N} \left(r_i - r_j\right).f_i \right\rangle \tag{12}$$

$$= \rho k_B T + \frac{1}{3V}\langle \sum_i^{N-1} \sum_{j=i+1}^{N} (r_i - r_j).F_{ij}^C \rangle$$

$$p = \rho k_B T + \frac{2\pi}{3}\rho^2 \int r f(r) g(r) dr \quad (13)$$

The first term in the above equations accounts for the kinetic contribution, and the second term defines the potential influence. $g(r)$ is the radial distribution function and V stands for the total volume of the simulation box. The sum in Equation (12) runs over the minimum image pairs, since the periodic boundary condition is applied on the system. Since all the force components, except the conservative non-bonded term, are simplified to be zero, Equation(12) can be rewritten in the following form [61]:

$$p = \frac{k_B T}{r_c^3}\bar{p}, \quad where \quad \bar{p} = \bar{\rho} + \alpha a \bar{\rho}^2 \quad (14)$$

in which, $\bar{p}$ refers to the dimensionless pressure in DPD units.

2.2.3 Flory-Huggins chi parameter (χ_{ij}) calculation

In the polymer chemistry, the interaction between two segments of the polymer is expressed using the Flory-Huggins (FH) chi parameter. This parameter shows the excess of mixing free energy according to the Flory-Huggins model. To set up a relationship between the real phase behaviour of the fluid and DPD model, the Flory-Huggins theory is used to model the DPD liquid free energy. There are several methods to evaluate the chi parameter and DPD interaction parameter in the literature. The FH chi parameter can be obtained using the mixing energy between the DPD beads which, corresponds to segments of a molecule. The mixing energy of two *i* and *j* fragments of a molecule can be calculated by the following formula:

$$E_{mix}^{ij} = 1/2[Z_{ij}\langle E_{ij}(T)\rangle + Z_{ji}\langle E_{ji}(T)\rangle - Z_{ii}\langle E_{ii}(T)\rangle - Z_{jj}\langle E_{jj}(T)\rangle] \quad (15)$$

In Equation (15), Z_{ij}, Z_{ji}, Z_{jj}, and Z_{ii} introduce the coordination numbers for *i* and *j* beads. Employing the Monte Carlo method, $\langle E_{ji}(T)\rangle$, which is the mean pair interaction energy between the beads in the system, can be obtained according to the following equation:

$$\langle E_{ij}(T)\rangle = \frac{\int dE_{ij}P(E_{ij})E_{ij}\exp(-\frac{E_{ij}}{kT})}{\int dE_{ij}P(E_{ij})\exp(-\frac{E_{ij}}{k_BT})} \quad (16)$$

Here, $P(E_{ij})$ represents the pair interaction energy Boltzmann distribution. This term can be computed by the calculation of multiple molecular conformations and orientations among the beads in the simulation cell. The relationship between the mixing energy term and Flory-Huggins chi parameter (χ_{ij}) can be described as follows [62]:

$$\chi_{ij} = \frac{1}{\phi_A\phi_B}\left(\frac{\Delta E_{mix}^{ij}}{k_BT}\right) = \frac{\Delta E_{mix}^{ij}}{RT} \quad (17)$$

where ϕ_A and ϕ_B are the volume fraction of components A and B in the mixture; ΔE_{mix}^{ij} refers to the energy of mixing between the two particles; *R* is the universal gas constant; and *T* is the absolute temperature. Energy of mixing is also a function of cohesive energy term, as expressed by the following equation:

$$\frac{\Delta E_{mix}}{V} = \phi_A(\frac{E_{coh}}{V})_A + \phi_B(\frac{E_{coh}}{V})_B - (\frac{E_{coh}}{V})_{AB} \quad (18)$$

The cohesive energy (E_{coh}) of a system is computed as the difference between the energy of the system and the sum of molecular energies of the particles in the system with the same coordinates, which is determined by the following relationship:

$$E_{coh} = E_{system} - \sum E_{gas} \quad (19)$$

In a physical perspective, the cohesive energy can be defined as the forces keeping the particles together in the liquid phase. In other words, the cohesive energy density indicates the energy of vaporization, which reflects the strength of van der Waals forces holding the particles in the liquid phase. Using cohesive energy values, the solubility parameter can be obtained as the square-root of the cohesive energy density as follows:

$$\delta_i = \sqrt{\frac{E_{coh}}{v_i^0}} \tag{20}$$

where δ_i stands for the solubility parameter term of component *I*; E_{coh} refers to the cohesive energy term; and v_i^0 correponds to the volume of the cell at equilibrium. Another approach to estimate the chi parameter is by means of calculated or experimental solubility parameter values of the components present in the system using the following formula:

$$\chi_{ij} = \frac{V_b}{k_B T}(\delta_i(T) - \delta_j(T))^2 \tag{21}$$

In Equation (21), k_B is the Boltzmann constant; δ_j refers to the solubility parameter of the *i* and *j* components in the mixture; and V_b introduces the average volume of the beads in the DPD simulation.

2.2.4 Determination of Interfacial Tension.

Surface or interfacial tension is commonly obtained by integrating the normal and tangential stress difference across the two segregated phases interface. According to the Irving-Kirkwood equation derived by Lyklema [63], the interfacial tension can be calculated by the following equation:

$$\gamma = \int_0^x (p_n - p_t)dx \tag{22}$$

in which, p_n and p_t refer to the normal and tangential pressure, respectively; and x represents the interface thickness. In the DPD method, the interfacial tension is determined by the following equation in the DPD units:

$$\gamma_{DPD} = \frac{1}{2}\int_0^{L_x}\left[p_{xx}(x) - \frac{1}{2}(p_{yy}(x) + p_{zz}(x))\right]dx \tag{23}$$

where $p_{xx}(x), p_{yy}(x),$ and $p_{zz}(x)$ refer to the ensemble average of the pressure tensor components in *x*, *y* and *z* directions; and L_x represents the box length in *x* direction (the axis normal to the oil/water interface) [61]. The first ½ factor is attributed to the two interfaces in the simulation system [12]. In the DPD calulation, the reduced units are used and length unit is calculated in r_C;

energy unit is KT which is the tempreture of the thermostat; and mass of a DPD bead is the mass unit.

To convert the value of interfacial tension in DPD units to actual physical units (γ_{real}), the following formula can be utilized [64]:

$$\gamma_{real} = \frac{k_B T}{R_c^2} \gamma_{DPD} \tag{24}$$

2.2.5 Radius of Gyration

To gain more information over the structure of surfactant at the water/oil interface, the Radius of Gyration (R_g) is introduced to monitor the degree of stretching. Instead of an end to end distance, the radius of gyrations more meaningful as it provides information on the size of particles in addition to just the end to end distance. A simple schematic of the definition of this two parameter is shown **Figure 1**.

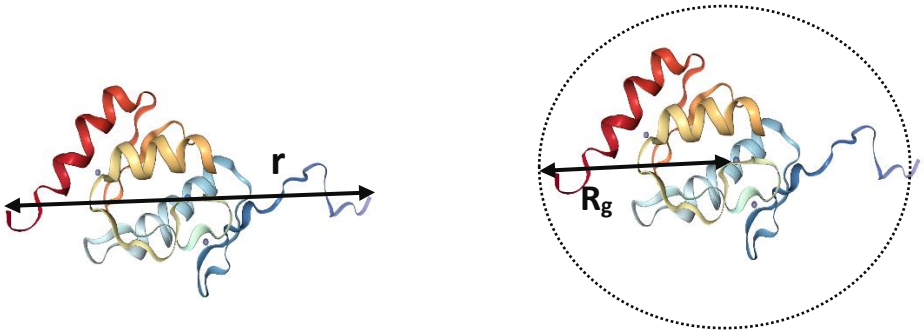

Figure 2-1 Schematic view of (a) end to end distance and (b) radius of gyration

The radius of gyration can be obtained using the following equations:

$$R_g^2 = \frac{1}{N} \sum_{i=1}^{N} (\vec{R}_i - \vec{R}_{cm})^2 \tag{25}$$

$$R_{cm} = \frac{1}{N} \sum_{j=1}^{N} \vec{R}_j$$

$$R_g^2 = \frac{1}{N} \sum_{i=1}^{N} \sum_{j=1}^{N} (\vec{R}_i - \vec{R}_j)^2$$

The radius of gyration of a similar chain is given by$\langle R_g^2 \rangle = \frac{Nb^2}{6} = \langle R_g^2 \rangle / 6$. This is the root mean square of end to end distance, which is bigger than the radius of gyration by a factor of $\sqrt{6}$. It is worth mentioning that the radius of gyration is not the same as the physical radius of a sphere [65].

2.2.6 Coarse-Grained Model

Coase graining (CG) is one of the most important sections of the DPD simulation as it can be employed to estimate the physical characteristics of a system at a considerably reduced computational time. Beading arrangement is very important for an accurate CG simulation. The molecular dynamics of the particles in the system are described by the built force-field in Mesocite module. For different hydrocarbon molecules, a different number of water molecules are joined together using a spring to form one water bead. The bead volume should be as small as possible to attain precise results; however, contrary to aliphatic chains of hydrocarbons, the cyclic compounds cannot be divided further into beads since the cyclic structure should be reserved. The non-bonded interaction among different beads is described by the Lennard-jones potential or Columbus force for the charged beads [66]. In **Figure 2**, the coarse-grained mapping of different aliphatic and cyclic hydrocarbons, surfactant molecules, and water is presented. The surfactant is $C_{12}E_6$, a non-ionic molecule having a hydrophilic group with the formula of $(OC_2H_4)_6OH$ attached to its hydrophobic segment with the formula of $C_{12}H_{25}$. This molecule is composed of 4 beads representing its polar head and four beads forming the nonpolar tail (see Figure 2). All the simulation cases are set up using the Mesocite module in the Material studio package [67]. The same mass, radius, and volume are assigned to all the beads in the system. These properties can be obtained based on the number of water molecules bounded together as one bead. The bead size corresponds to the number of water molecules (N_m), which also describes the degree of coarse-graining. As previously explained, for different hydrocarbon molecules, a different number of water particles will form a bead. In this case, we choose Octane as an oil sample. The molecular volume of Octane is $269.82A^{03}$ and molecular volume of water is $30A^{03}$. Hence, three water molecules need to bound together to form one water bead to follow the equality of mass for each bead. Thus, Nm=3 and the volume of one water bead can be obtained as follows:

$$v_b = N_m v_{water} = 3 \times 30 = 90A^{o3} \quad (26)$$

In Equation (26), v_b refers to the bead volume. The mass of bead can also be determined as follows:

$$m = N_m m_{water} = 3 \times 18 = 54\ amu \quad (27)$$

where *m* stands for the mass of one bead and m_{water} refers to the mass of one water molecule.

To construct the beads representing the different particles in the system, the radius of the bead is also required. Considering a cube with the volume of r_c^3 where r_c refers to the diameter of the bead, the volume of the bead can be obtained by the following equation:

$$r_c^3 = \rho N_m v_{water} \tag{28}$$

$$r_c = (\rho N_m v_{water})^{1/3} = (\rho N_m 30)^{1/3} = (33 \times 90)^{1/3} = 6.46 A^0$$

Here, the bead diameter is calculated considering the coarse-graining degree of Nm=3, and the density of the bead is equal to $\rho = 3$ in DPD units. The DPD density number depends on the compressibility of liquid, which is assumed to be similar to the compressibility of the water [51; 68]. According to Equation (28), the dimeter of the bead is $r_c = 6.46\ A^o$; and the radius of the bead which is half of its dimeter equals $3.23 A^o$. As mentioned earlier, in the DPD simulation technique, the same mass, volume, and radius are assigned to all the beads existing in the system. As an example, for Octane, the mass of the beads is equal to 54 amu with a volume of 90 A^{03} and the corresponding diameter of r_c=6.46 A^o. Since the density and mass of the beads remain constant through the simulation steps, the volume and radius of the simulation cell will be constant as well [66].

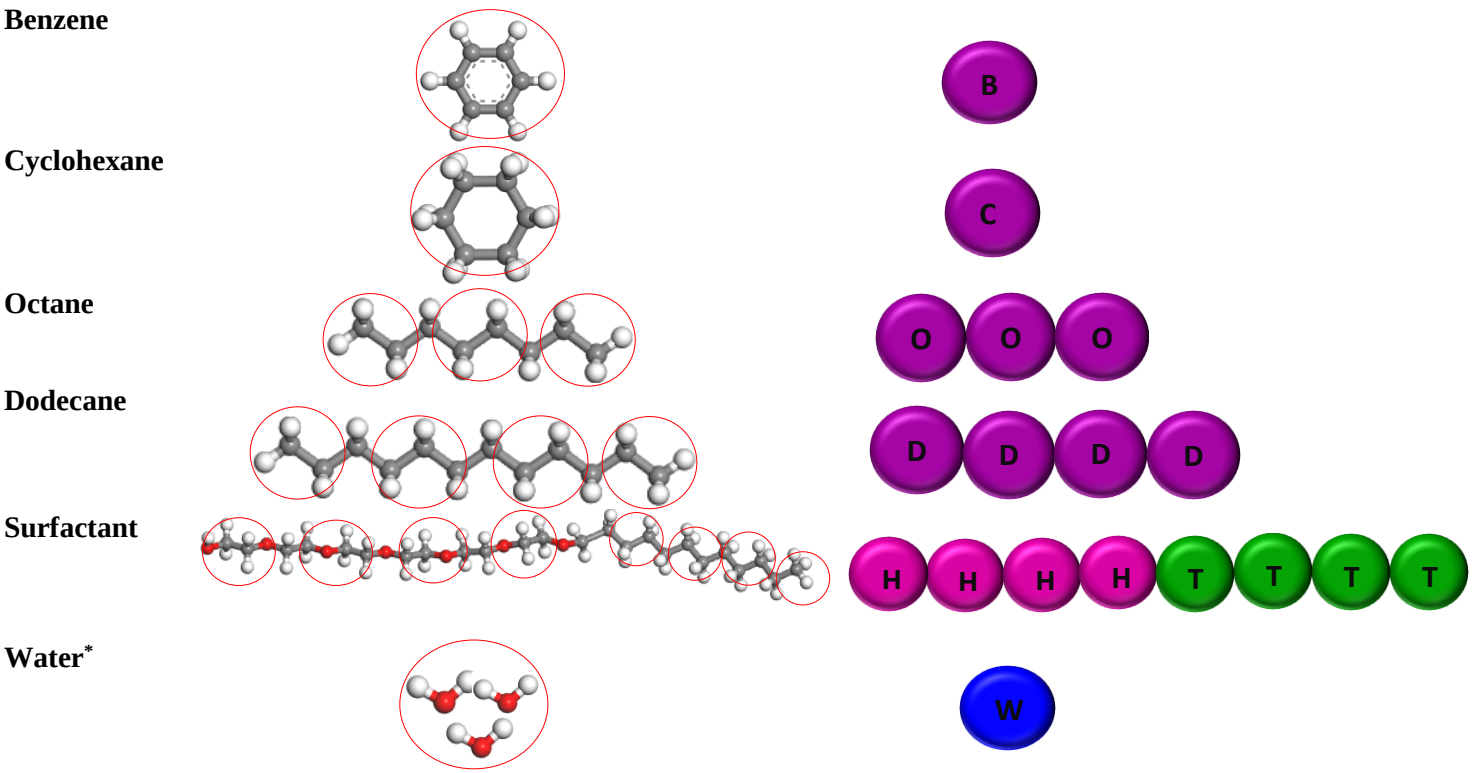

Figure 2-2 DPD particle structure model of oil molecules, water and surfactant. "O" denotes the Octane molecules, "B" refers to the Benzene beads, cyclohexane beads are shown as "CH", Dodecane molecules are referred to as "D", surfactant head and tail are shown with "H" and "T" respectively, and "W" is used to represent water beads in the simulation cell. * Water molecules are

bounded differently based on the molecular volumes of the particles present in the system. In the example shown in the figure, three water molecules represent one bead.

2.2.7 Simulation Methodology

The simulation is intended to provide the interfacial and structural behaviors of oil/water/surfactant systems at the ambient condition. In the DPD method, the calculations are performed in the reduced DPD units. Hence, a reduced temperature of Tr =1, which corresponds to 298.15K, was selected as the reference temperature. The energy scale in the reduced units is K_BT=1, which is equivalent to 0.59191 Kcal/mol in the actual physical unit. The simulation is performed in a cubic box with the dimensions of $100\times100\times100A^o$. The simulation cell contains 11481 beads for the octane/surfactant/water systems, 10584 beads for the dodecane/surfactant/water system, 5723 beads for the cyclohexane/surfactant/water systems, and 6913 beads for the benzene/surfactant/water system. The periodic boundary condition controls the simulation cell. MD simulations are carried out using the Material Studio 2018 Software (Discover/Accelrys, San Diego, California, USA) [67]. The COMPASS force field is employed in the current study for the MD simulation section. After the system is built, the energy minimization is performed to energetically eliminate any undesired spatial arrangements. This, in turn, produces a starting point for further calculations with the reasonably lowest energy level. The system then goes under an NVT ensemble (in which the number of particles, volume, and temperature are fixed). The volume is set at $10^6\ A^{03}$ and the temperature is fixed at 298.15 K ($K_BT = 1$). In the current study, the volume and temperature are controlled using Nose algorithm [69-71]. The random and dissipative force parameters are set to the values of $\sigma = 3, \xi = 4.5$ respectively. At the beginning of the simulation, a random velocity based on Maxwellian distribution is assigned to each atom as the initial configuration of the beads in the cell. The total simulation time is 250 in DPD units (1600 ps) and a time step of 0.01 is applied to integrate the Newtonian equation of motion and to predict the trajectory of all atoms in the system. The Atom-based method is applied to control the van der Waals interactions. A cut-off radius of $3.23A^0$ for the short-term interaction calculations is chosen, which is obtained based on the diameter of the beads in the cell. The force field used in the DPD simulation is a created force field according to the DPD interaction force parameter calculated based on chi parameter. It may be observed without staying too far from our main focus that most simulations run for longer simulation times and smaller time steps. In this work, cases are considered using longer simulation time and the results were found to be completely similar to the cases with shorter total simulation time. The benefit of using shorter simulation time is obvious in terms of computational costs and time. It is important to note that the values reported for the surfactant concentration and water/oil ratio in this paper are based on the volumetric fractions of the beads in the simulation cell. The pressure is the atmospheric pressure and the temperature is 298.15K, unless otherwise indicated. In order to be able to perform the interfacial tension analysis, the simulation cell should be big enough [72]. We choose the cell dimeter to follow this criterion: the x-direction is assumed to be perpendicular to the oil/water interface. Mesoscopic DPD simulation acts as a bridge between the microscale molecular dynamics and continuum mechanics

approach. The chi parameter connects the molecular dynamics to the DPD simulation. An algorithm to demonstrate the simulation/modeling procedure is provided in **Figure 3**.

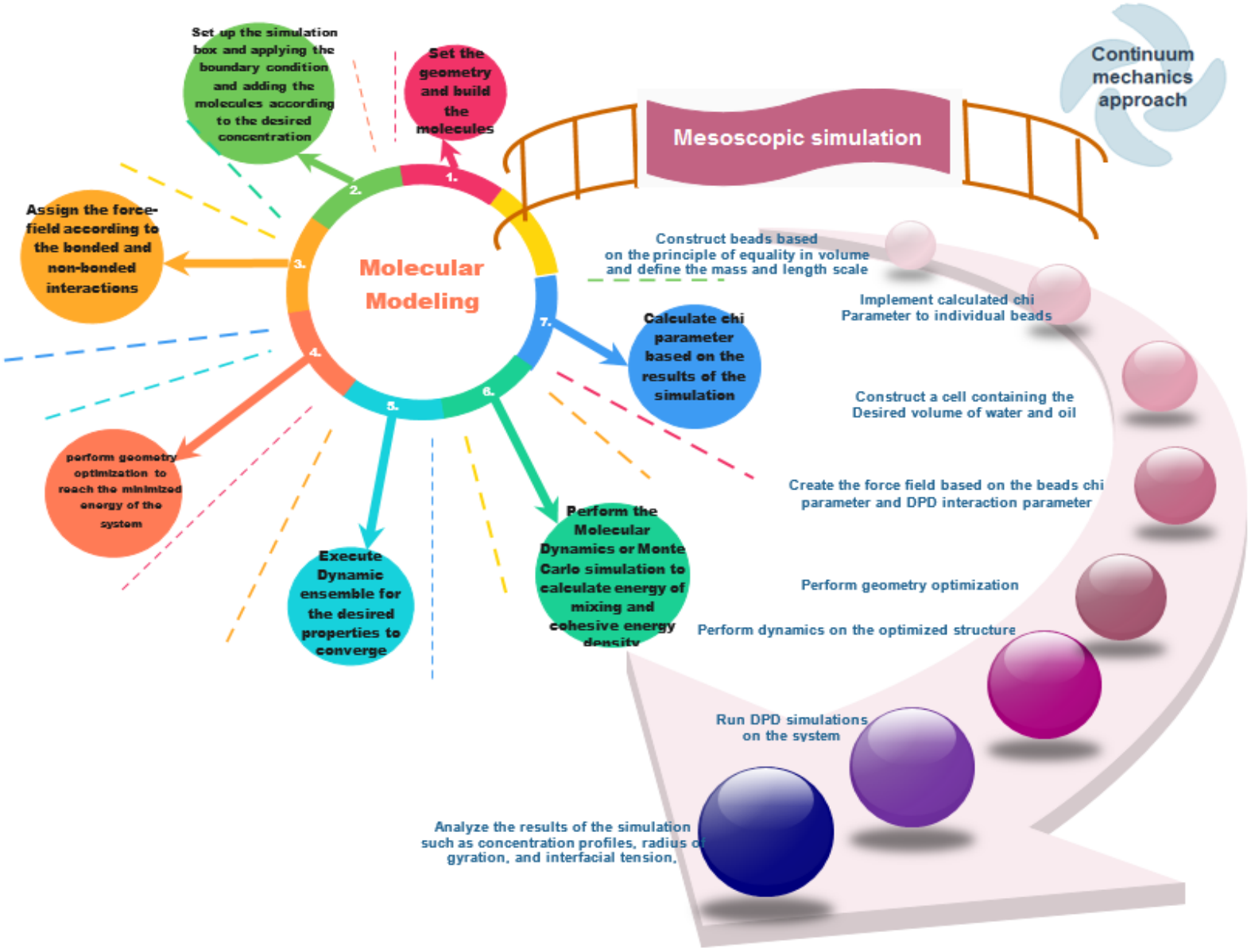

Figure 2-3 An algorithm representing the steps of mesoscopic simulation as a bridge between micro-scale and continuum mechanics approach.

2.3 RESULTS AND DISCUSSION

2.3.1 DPD interaction force parameter Analysis

In this section, we endeavour to investigate the effects of different oil molecule structures and temperatures on the IFT behaviours using the DPD simulation. First, the results of the DPD conservative force parameter calculation using the chi parameter are provided. The solubility parameter of the components present in the system is calculated using the amorphous cell and Forcite module in the Material Studio from the cohesive energy parameter. The method involves preparing the cell for each component with periodic boundary condition and using the experimental densities. In the absence of geometry and equilibrium information, a geometry optimization task and NPT ensemble can be carried out to equilibrate the system. The commercial COMPASS force field is utilized to describe the interatomic interaction, which is well-known for correctly reproducing the experimental densities and solubility parameter. For each structure, the volume and solubility parameters are calculated, and the results are presented in Table 2 for different hydrocarbon molecules and water. The experimental data from the literature are also provided, implying a high accuracy of the simulation results. Liquids with similar solubility parameter will be miscible, and a large difference in this parameter indicates the immiscibility phenomenon. The effect of temperature on the solubility parameter of aliphatic and cyclic hydrocarbons are demonstrated in Figure 4. Based on Figure 4, as the temperature increases, the solubility parameter for all the oil molecule structures decreases; a reduction in the solubility parameter corresponds to a decrease in the cohesive energy density or the internal forces in molecules. Hence, dissolving the molecules into a solvent and overcoming the intermolecular forces will be easier with increasing the temperature. As it is also reported in Table 2, the solubility parameter has the highest value for water, while this parameter holds the smallest magnitude for Octane. The main reason is that water is a polar molecule with the ability to create a hydrogen bond with another water molecules. To dissolve one molecule into another, all the intermolecular and intramolecular forces should be broken. To mix water with another solvent, one should then overcome all the polar and hydrogen bonds. This justifies why the solubility parameter for water amongst all molecules in the system has the maximum value. In oil molecules, since benzene is a cyclic compound with three double bonds, the solubility parameter will be the highest among other oil molecules and octane, which is a linear hydrocarbon with just single nonpolar and London dispersion forces. Therefore, the energy to overcome these forces and interactions will be at the lowest level, compared to other structures. Referring to the methodology section, the Monte Carlo method is also employed to calculate the chi parameter using the energy of mixing. In the Material Studio, the energy of mixing calculation for different base and screen molecules is performed by employing the Blends module. Using the COMPASS force field for the mixing task in the Blends module, values of E_{mix} are estimated, while the atom-based summation method is selected for both electrostatic and van der Waals interaction forces. This module also enables us to figure out the impact of temperature on chi parameter for different molecules. The results of the energy of mixing and corresponding chi parameter are listed in Table 3. The value of DPD interaction force

parameter is also determined according to the given chi parameter from the results of Cohesive energy calculation and energy of mixing for the dodecane/surfactant/water system, as given in Table 4. The results of the DPD interaction force parameter for other systems including octane, benzene and cyclohexane are provided in Appendix. A. Based on Table 4, the a_{ij} values for similar beads are considered to be a_{ii}=25, since the chi parameter for similar particles equals zero. This indicates the complete solubility and zero mixing energy. It should be mentioned that the conservative force for different beads increases form 25 due to the difference in the interactions between the beads. As an example, the DPD interaction between the water molecule and the surfactant head is equal to a_{ij}=30.5, while this value is 57.96 for the water and oil molecules. This difference in the values of the DPD conservative force parameter implies a difference between the type of interactions between the molecules, since both water and surfactant head are polar particles and the oil molecule is a nonpolar chain. Hence, the energy to mix these two molecules and solubility parameter will be higher, leading to an increase in the chi parameter and consequently a_{ij}. Plots on the effect of temperature on both chi parameter and aij term are provided in Figure 5. As mentioned earlier, the DPD conservative force parameter is dependent on chi parameter through a linear function (see Equation (9)). Therefore, both of the terms show a similar trend upon an increase in the temperature. As it is clear from Figure 5, as the temperature increases, the values of chi parameter and conservative force parameter decrease that is in agreement with the literature [45]. This trend reveals the oil molecules and the water molecules will experience less repulsive forces and can dissolve into each other easier, compared to a lower temperature case.

Table 2-1: Calculated solubility parameter for the components in the simulation from the Amorphous cell and Forcite module

Component	Density (gr/cm^3)	Molecular volume(A^{03})	Solubility Parameter$(j.cm^3)^{1/2}$	Solubility Parameter$(j.cm^3)^{1/2}$*
Water	1	30	47.9	47.9
Octane	0.703	269.82	15.4	15.4
Benzene	0.876	148	18.41	18.6
Cyclohexane	0.779	179.4	16.8	16.9
Dodecane	0.749	379.5	16.9	15.9

Table 2-2: Energy of mixing and chi parameter value for different oil molecules and water at T=298.15K

Base	**Screen**	**Emix(J)**	**Chi parameter**

Water	Octane	3.99	6.769231
Water	Dodecane	5.98	10.14154
Water	Cyclohexane	5.26	8.923077
Water	Benzene	4.73	8.012576

Table 2-3: DPD interaction parameters for different beads present in the Dodecane/surfactant/water system at 298.15K

	T	**H**	**O**	**W**
T	25			
H	36.5	25		
O	25	36.66	25	
W	57.95	30.5	57.96	25

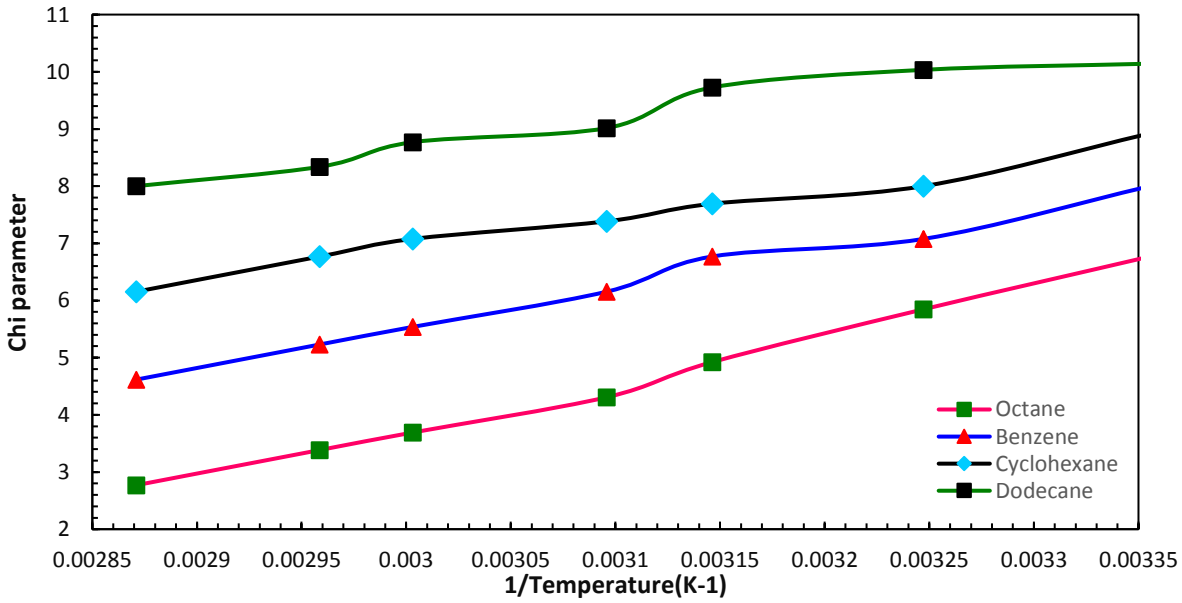

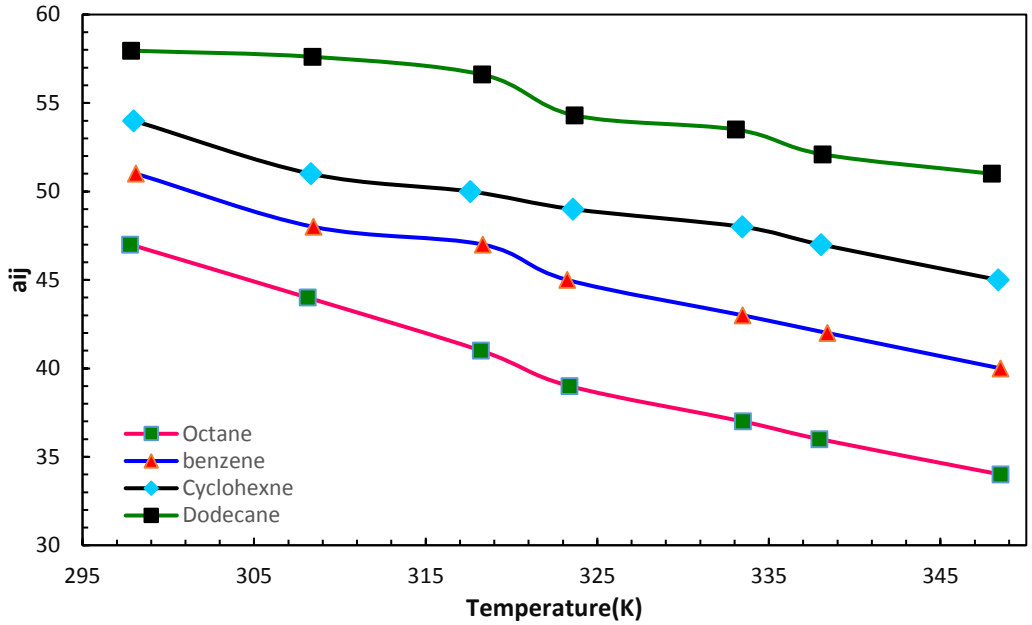

Figure 2-4: (a) Flory-Huggins chi parameter and (b) DPD interaction parameter as a function of temperature for different oil molecules with water

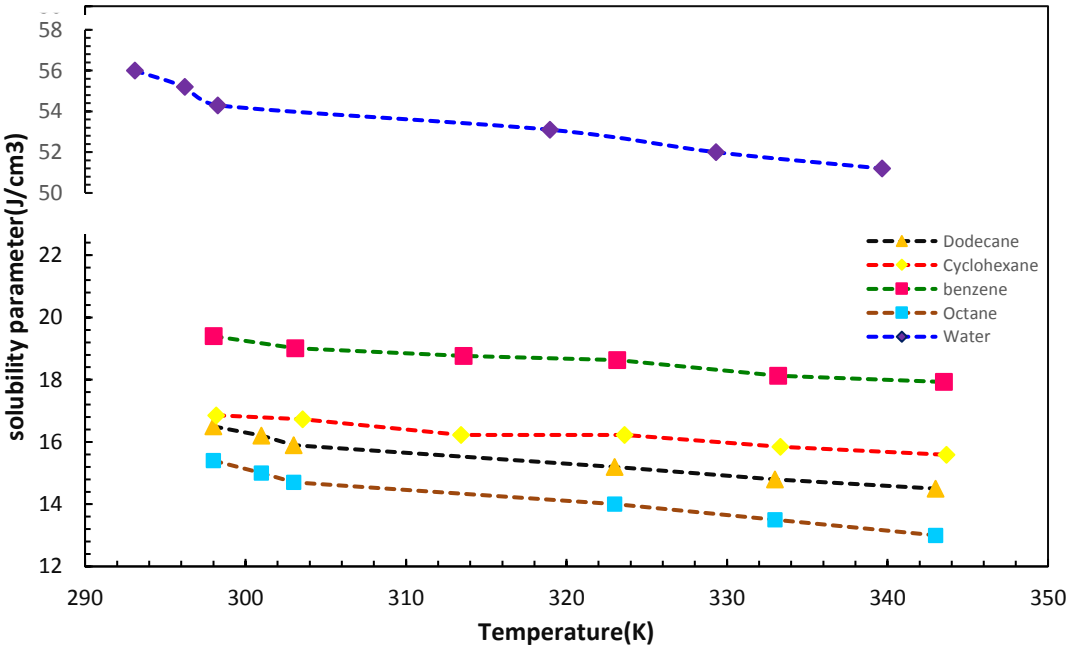

Figure 2-5 Effect of temperature on solubility parameter values of the different types of oil molecules in the DPD simulation

2.3.2 Mesoscopic Studies Analysis

A convenient and reliable method to describe the structural behaviours of oil/surfactant/water systems at the interface is to study the snapshots of the simulation cell. A rough estimation on the orientation of the beads at the interface with a surfactant concentration of Sc=15% and water/oil ratio of WC=1 (volumetric) is provided in **Figure 6**, according to the simulation snapshots taken at the equilibrium state of a dodecane/surfactant/water system. According to the magnified image of the interface, it can be observed that the surfactant molecules are accumulated at the interface so that the hydrophilic group moves toward the water phase and the hydrophobic chain has tendency toward the nonpolar oil phase. This orientation is in accordance with the DPD conservative force calculated in the previous section as well as the nature of the forces between the surfactant head and tail group with the water and oil phases.

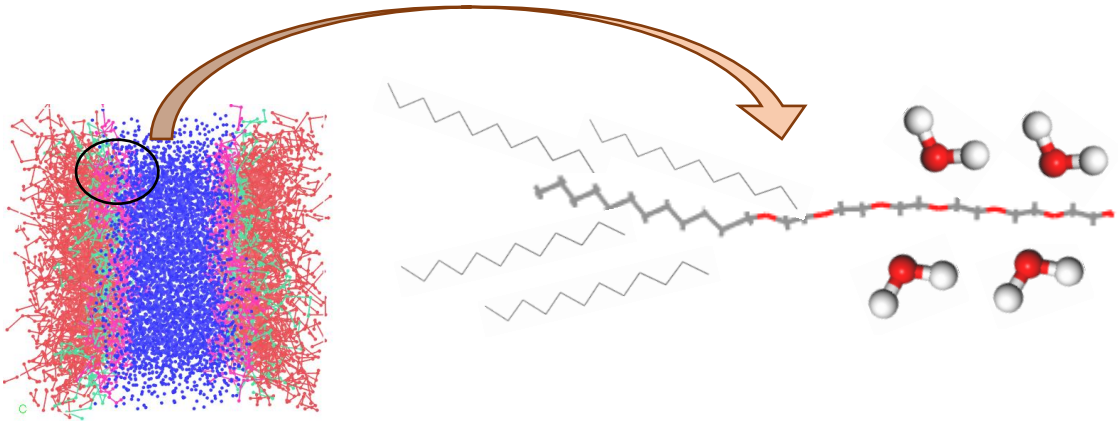

Figure 2-6: Snapshot of side evaluation of water/oil system in the presence of surfactant at Sc=15% and Watercut WC=1 water molecules are represented with blue beads; red beads show oil molecules and pink and green beads refer to the surfactant head and tail respectively

One of the outputs of DPD simulation using the Mesocite module in the Material Studio is the relative concentration profiles as an average of different time steps in the simulation. This characteristic shows the density of the beads in the simulation box in the DPD units. The concertation profiles for different mixtures of oil/surfactant/water at a constant temperature of 298.15 K are depicted in **Figure 7**. The relative concentration of water for all different cases follow the same pattern and value. Thus, the type of hydrocarbon does not affect the concentration of water in the simulation cell. The surfactant curves are however different for each type of hydrocarbon in the system. As it is clear from Figure 7, in the case of cyclic hydrocarbons, the relative concentration of the surfactant molecules is lower, compared to linear hydrocarbons. This behaviour is attributed to the type of interactions between the surfactant tail and the oil molecules in the simulation cell. For the linear hydrocarbons such as octane and dodecane, all the surfactant molecules are centred at the interface, due to the similarity of the surfactant tail and oil molecules. Hence, the surfactant relative concertation shows a higher peak at the interface. That is why the

surfactant molecules will stretch more in aliphatic hydrocarbons systems; however, for cyclic hydrocarbons, the affinity of the oil molecules with the tail groups is not as strong as the linear hydrocarbons. It is concluded that the surfactant molecules will disperse into the oil and water phases and the central concentration at the interface will not be as much as the linear hydrocarbons. The width of the interface is, however, greater for cyclic hydrocarbons system, compared to linear oil molecules.

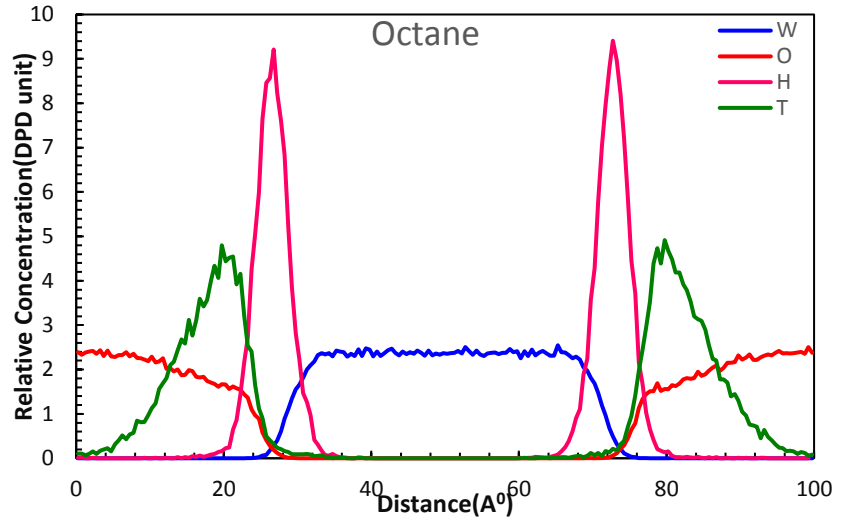

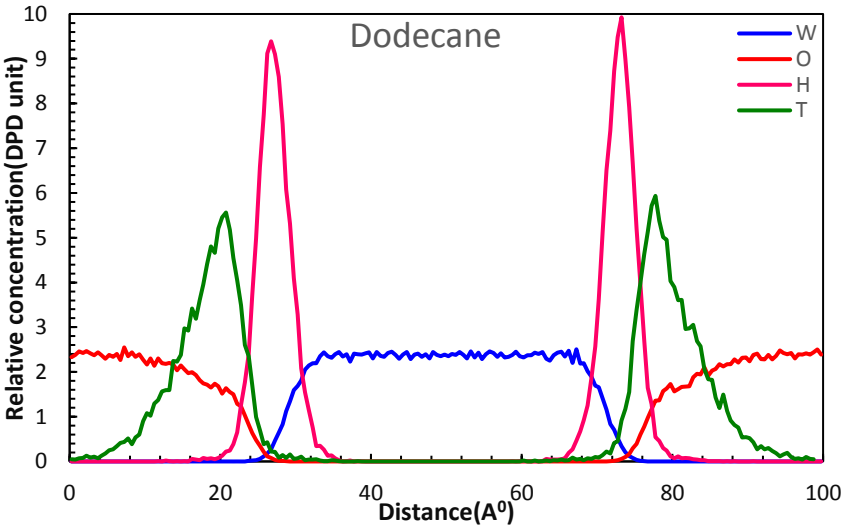

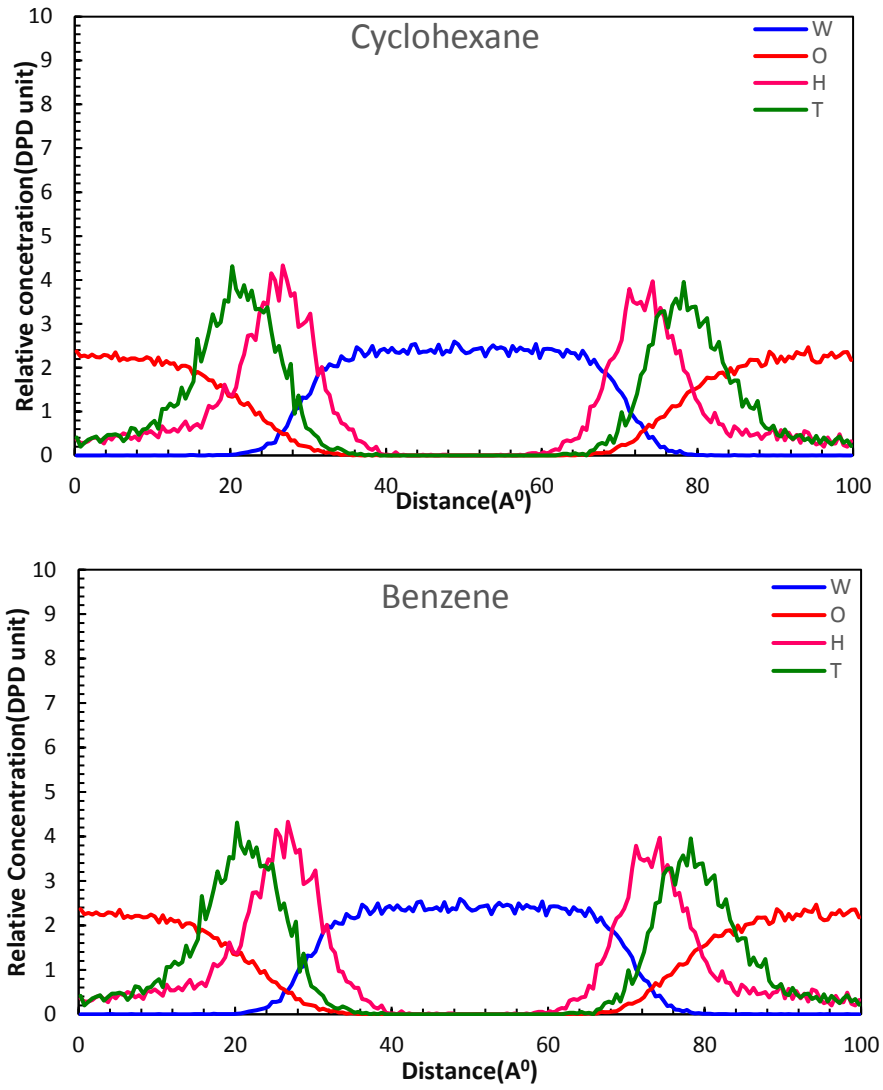

Figure 2-7: Relative concentration values of Hydrocarbon/Surfactant/Water systems at T=298.15K for different Hydrocarbon types where W refers to Water molecules, O represent Hydrocarbon beads, H, and T shows surfactant Head and Tail groups respectively

To obtain adequate knowledge on the structural behaviour of the oil/surfactant/water system, the values of radius of gyration are plotted for different oil structures. This parameter is another output of Mesocite module, which is provided for the beads through the simulation time. The systems are studied at a temperature of 298.15 K under atmospheric condition. According to the simulation results, the *Rg* value increases dramatically at the initiation of simulation and then reach an equilibrium and fluctuates by the time (see **Figure 8**). This trend is the same for all the systems, regardless of the type of beads. The reason for this behaviour is, at first, the surfactant head and tail will stretch toward the water and oil phase, respectively, due to the nature of the molecules in terms of polarity. After this transient increase, the interface is saturated with the surfactant

molecules, and all the beads are oriented based on the similarity in intermolecular forces. Therefore, no noticeable change in the length of surfactant molecules will be observed after this time and the radius of gyration holds a constant value over time. The tail group and cyclic oil molecules are not as compatible as tail and linear oil structures. Thus, the interactions between the tail group and cyclic compounds will be lower and the surfactant molecules will not stretch in a system of cyclic oil/water as much as in a linear oil/water system, leading to a smaller radius of gyration. Comparing the two aliphatic oil compounds, it is observed that octane molecules will cause the surfactant beads to stretch more. In the case of benzene and cyclohexane (as illustrated in Figure 8), the surfactant molecules will stretch more in the presence of cyclohexane. The main reason is that Benzene is a more polar compound, compared to cyclohexane. It means that its interaction with the nonpolar tail of surfactant will be weaker, compared to the cyclohexane. Also, Rg value will be smaller, compared to the cyclohexane system.

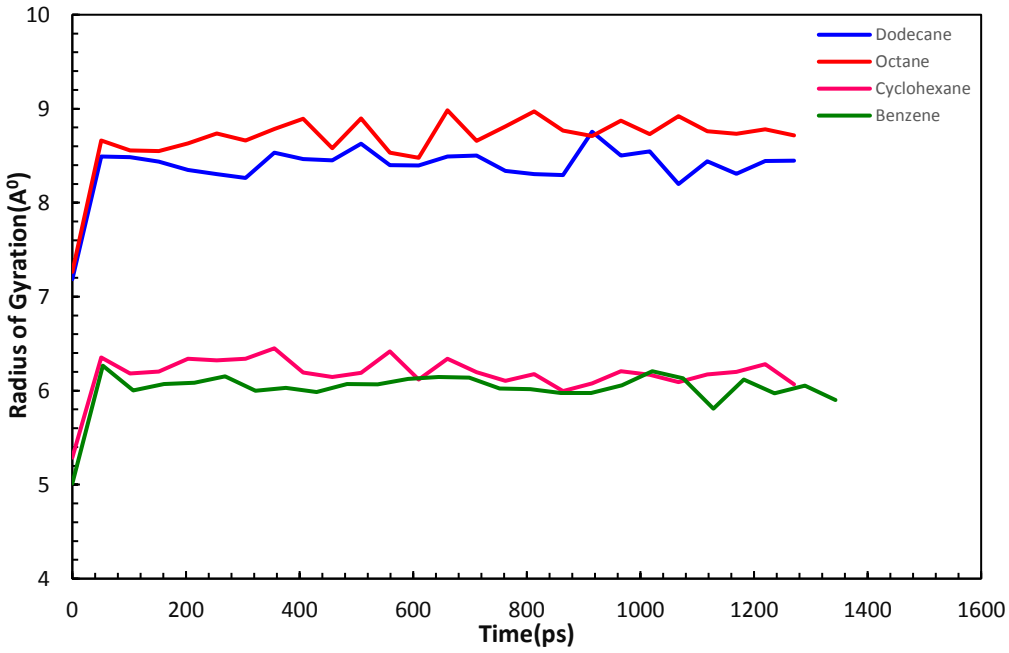

Figure 2-8: Radius of Gyration values for different cyclic and aliphatic hydrocarbon and water systems in the presence of surfactant at T=298.15K

An important output of DPD simulation is the magnitude of interfacial tension (IFT) for various mixtures of oil/surfactant/water at different temperatures. Values of IFT reflect the differences in chemical and structural behaviours of the molecules in the system. A high interfacial tension indicates a low tendency to interact. As described previously, a difference in the solubility parameter reveals immiscibility. Dodecane is the most nonpolar oil molecule and has the highest solubility parameter difference with water. Thus, a mixture of the two phases shows high interfacial energies at the interface. At the same time, Benzene with its cyclic compound and

double bonds exhibits more polarity, implying it is more similar to water with respect to the solubility among other compounds. It is concluded that the IFT created at the interface will be lower. Based on Figure 9, the temperature is a chief factor affecting the IFT of oil/water molecules, regardless of the structure of the oil. In all cases, increasing temperature causes the interfacial tension to decrease. It may be tempting to relate the IFT sensitivity to temperature to the dependence of DPD force parameter a_{ij} to temperature. However, it should be noted that if temperature increases significantly and the long-range interactions are included in the calculation, the IFT variation with temperature may not be related to the temperature-dependent a_{ij}. Generally, by increasing the temperature, the miscibility of compounds increases, resulting in a reduction in the IFT at the interface of two contacting fluids

The DPD results obtained for systems of aliphatic and cyclic oil/ water are compared with the corresponding outputs in the open sources [75] to validate the accuracy of the simulation. The sum of squared error (SSE) is calculated and reported for different cases of oil molecules in the system (see Table 5) according to the following equation:

$$SSE = \sum (IFT_{sim} - IFT_{Exp})^2 \tag{29}$$

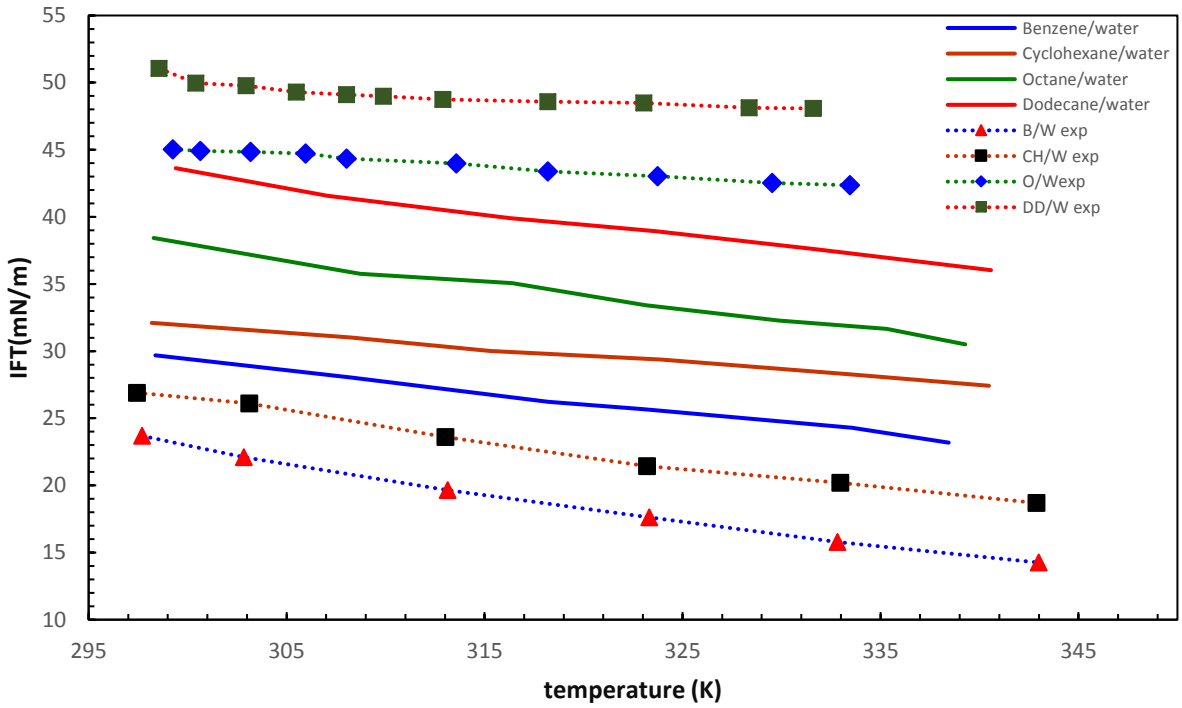

Figure 2-9: Interfacial Tension Variation as a function of Temperature for different systems of oil and water-a comparison of DPD results and experimental values[73; 74]

Table 2-4: Comparison between IFT values from DPD simulation and experimental values at 298.15 K

Hydrocarbon/water	Beading arrangement	IFT_{DPDsim} (mN/m)	IFT_{lit}[75; 76] (mN/m)	SSE
Octane/Water	O[1-3]W[3-1]	37.42	41.02	43.56
Benzene/Water	O[1-1]W[5-1]	29.68	23.68	35.99
Cyclohexane/Water	O[1-1]W[6-1]	32.11	26.91	27.09
Dodecane/Water	O[1-4]W[3-1]	43.62	52.54	49.67

Effect of water content on the interfacial and structural behaviour of the water/surfactant/oil systems is also investigated. According to the previous works [77], the water cut does not affect the relative concentration profiles of water, oil, and surfactant. Hence, we do not discuss it her. It can however change the orientation of the surfactant molecules at the interface. To study the configuration of the surfactant molecules at the interface, the profiles of radius of gyration are illustrated versus time in **Figure 10** for different types of hydrocarbon, while the water-cut varies. As discussed earlier, linear hydrocarbons cause the surfactant molecules to stretch more. Comparing the system of octane/surfactant/water at two different water cut ratios, it can be seen that *Rg* shows higher values for greater water-cuts. At the interface, the surfactant molecules will stretch, and the polar head will be attracted toward the water phase and the nonpolar tail will be

stretched toward the oil beads. In the case of low water-cut, the surfactants will soon interact with the close water molecules at the interface and the degree of stretching is low. However, in the case of high water-cut, more water molecules are available and not only the water molecules at the interface but other water beads far from the interface will attract the hydrophilic segment of surfactant molecules and cause them to stretch more. Therefore, the *Rg* values for higher water cut ratios will be greater. The same justification is valid for cyclohexane/surfactant/water systems as well. As it is clear from Figure 10, more fluctuations are observed for higher water-cut cases for both octane and cyclohexane cases. Fluctuations in the *Rg* values indicate that the surfactant molecules are still stretching, and the interface has not yet been saturated with the surfactant molecules. This effect is more pronounced when higher volumetric concentration of water is available in the system. Thus, it will take more time for surfactant molecules to be aligned at the interface and *Rg* fluctuates more.

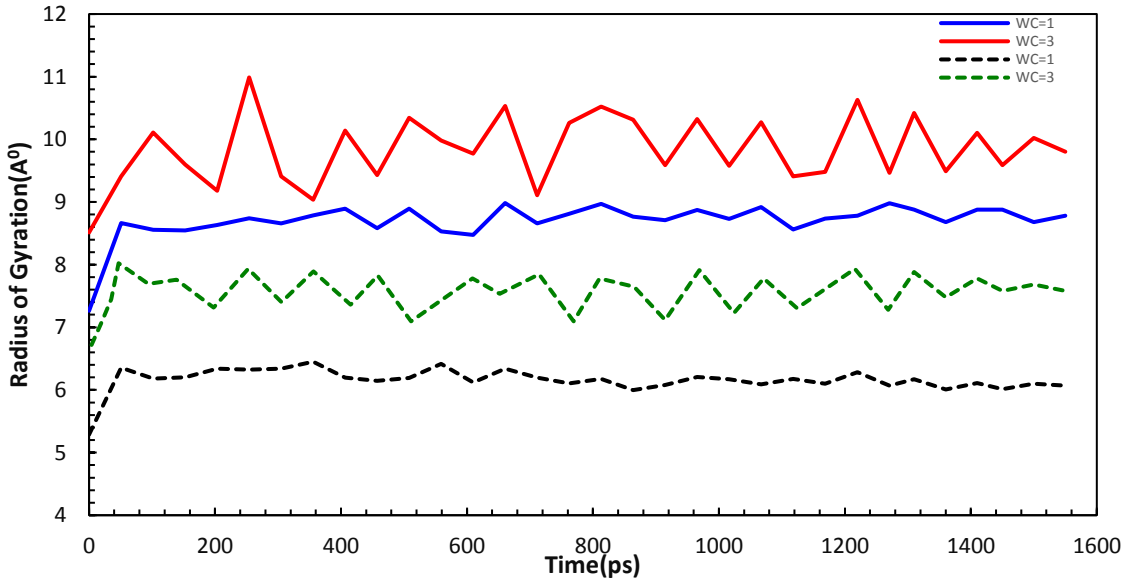

Figure 2-10: Radius of gyration versus simulation time for two systems of octane and cyclohexane as a function of water cut with a surfactant concentration of Sc=15% (volumetric fraction).

To study the impact of water-cut on the interfacial characteristics of the oil/water/surfactant cases, two aliphatic and cyclic hydrocarbons at a surfactant concentration of Sc=15% are considered and three water cut ratios of WC=0.5, 1, and 3 are selected. Plots of IFT versus water-cut are presented in **Figure 11** for both aliphatic and cyclic oil systems. Based on Figure 11, by increasing the water-cut, IFT increases and then decreases. The highest IFT is determined to be at WC=1, where a stable system of oil/surfactant/water causes the interfacial tension to increase. When the WC is low, water droplets are formed in the continuous phase of oil and the surface area available for the surfactant molecules is high, causing the interfacial tension to decrease and the system can

experience equilibrium. The same situation happens when WC reaches above one. In this case, oil droplets are surrounded by the water molecules and available surface area for surfactant molecules increases, leading to a decrease in the IFT.

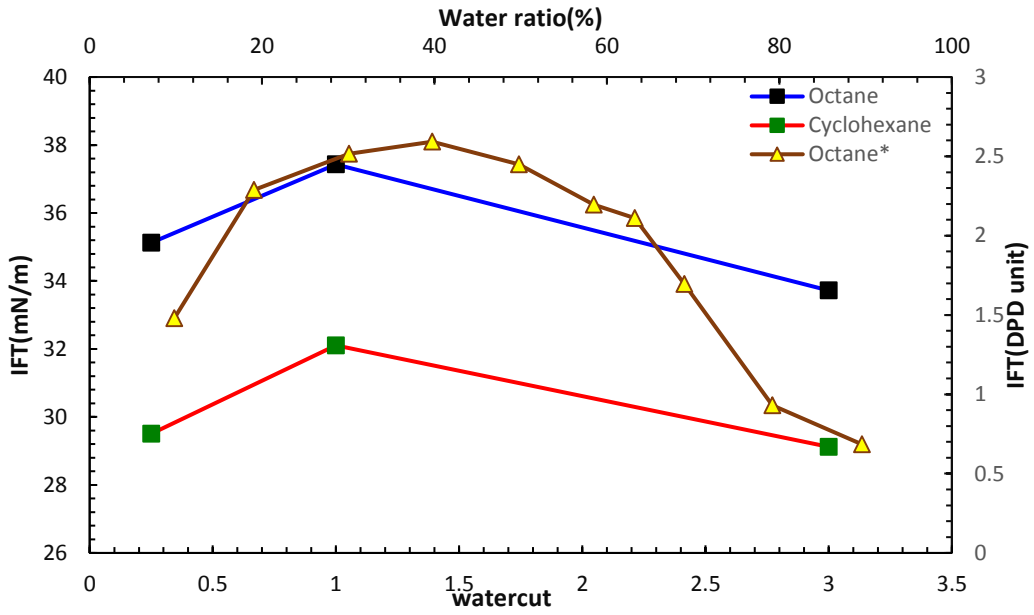

Figure 2-11: Interfacial tension as a function of water cut and/or water/oil ratio in a system of octane/surfactant/water and cyclohexane/surfactant/water for a fixed surfactant concentration of Sc=15%
* Data are extracted from literature[44] for a system of W/O in the presence of a non-ionic surfactant (PEO-PPO-PEO).

An important parameter influencing the IFT of hydrocarbon/water systems is the concentration of the surfactant in the system. The presence of surfactant in the system causes the water and oil molecules to blend easier due to the amphiphilic structure of surfactant. Investigating the structural characteristics of hydrocarbon/surfactant/water systems through analysis of *Rg* at different surfactant concentration, it is obvious that for both types of hydrocarbons (as a representative of linear and cyclic compounds), increasing the surfactant concentration will cause the surfactant molecules to stretch more and align to more extent at the interface (see **Figure 12**). According to Figure 12, when the number of surfactant molecules increases in the simulation cell, more fluctuations are noticed in the *Rg* values, mainly because the interface has not been saturated with surfactant molecules, and the degree of stretching is constantly changing for both octane and cyclohexane systems.

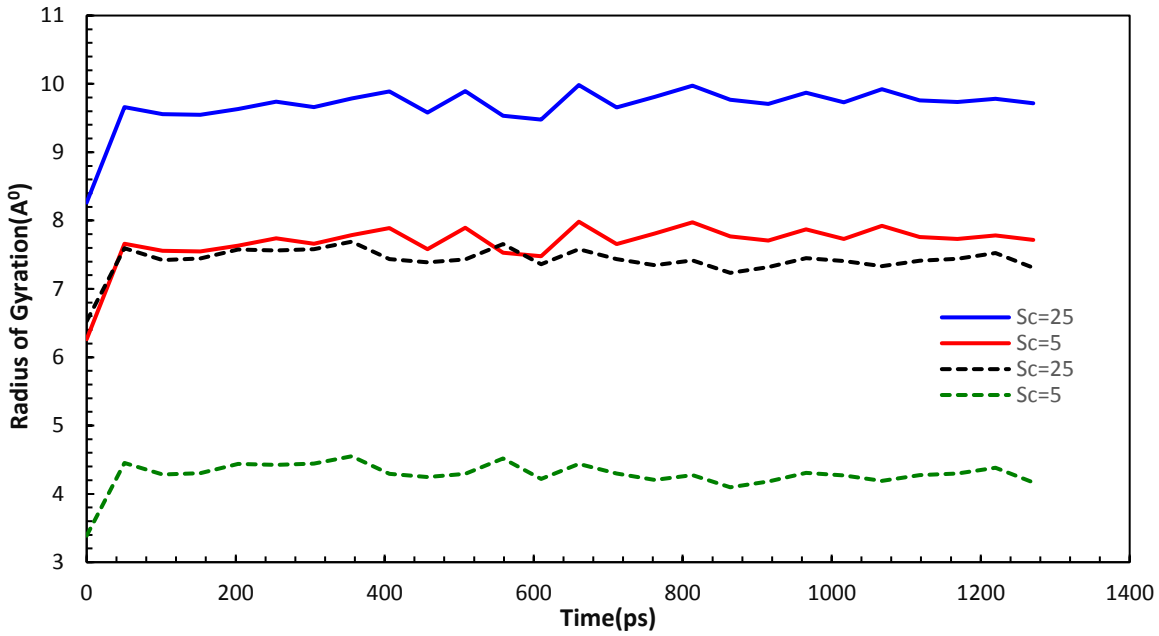

Figure 2-12: Effect of surfactant concentration on Radius of Gyration values for Octane/surfactant/water (solid lines) and Cyclohexane/surfactant/water (dashed lines) systems at T=298.15K and water cut WC=1

The effect of surfactant concentration on the IFT is also demonstrated in **Figure 13**. As it is evident from Figure 13, by increasing the number of surfactant molecules at the interface, the IFT will experience a significant reduction for both cases of octane and benzene hydrocarbon/surfactant/water systems. Adding more surfactant to the simulation cell results in a reduction in the surface energy between oil and water beads at the interface, due to the formation of polar and hydrogen bonds between the water and surfactant and the induced dipole-dipole bonding between the nonpolar oil molecules and the linear segment of surfactant. The reduction continues until the interface is saturated with the surfactant molecules. After the saturation condition, adding surfactant will not reduce the IFT anymore and in some cases an increase in the IFT was reported [75]. The same trend is observed in the literature [4] in the presence of another non-ionic surfactant (CPL) in a benzene/water system.

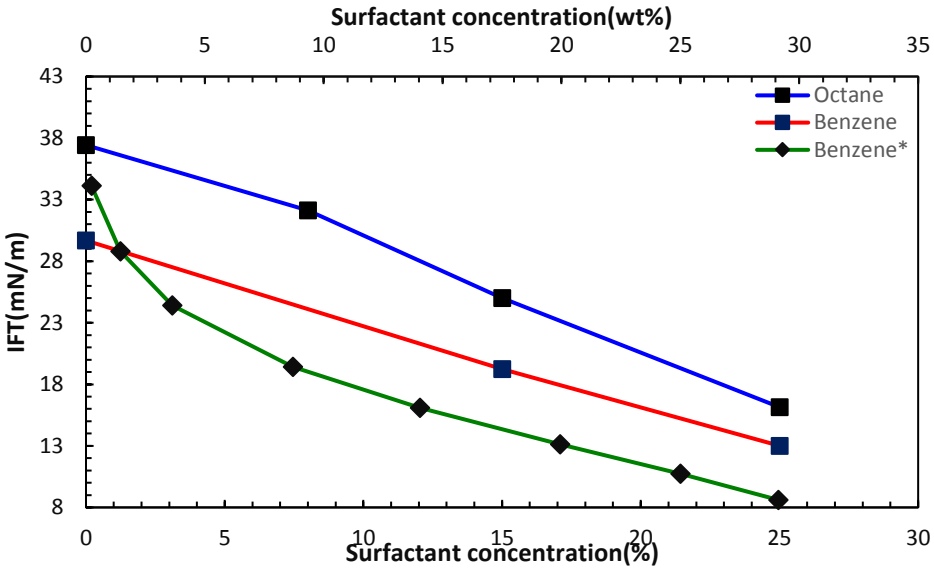

Figure 2-13: IFT versus surfactant concentration for the aliphatic and cyclic hydrocarbon/surfactant/water systems at a Water-cut ratio of WC=1. *Data are extracted from literature [4] for the system of benzene/water in the presence of CPL.

Interfacial and structural characteristics of the water/surfactant/oil systems appear to be important in various science and engineering disciplines. For instance, the orientation of surfactant molecules plays an important role in drug delivery and ducking systems. In food emulsion, the emulsion stability and phase separation are vital factors that influence the quality of products. In the oil and gas industry, the IFT between oil and water phases considerably affects the EOR performance and separation costs and time in both downstream and upstream sections. Hence, comprehensive research studies on the interactions between the molecules of oil, water, and surfactant phases at the interface are essential to provide better design and operation strategies in the corresponding industries.

Further research works on the hydrocarbon/surfactant/water systems are recommended using the integrated strategy of MD and DPD to calculate the interfacial characteristics and conservative force parameters for more complex mixtures of ionic surfactants and polar oil compounds.

2.4 Conclusions

Dissipative particle dynamics (DPD) is a computational algorithm designed to address complex fluid problems in a mesoscale level. The fundamental theory of DPD is a coarse-grained portion of a system can be analysed in a much larger time and length scale that cannot be achieved in microscopic modelling. The structure of molecules in the system affect the beading arrangement and eventually the accuracy of the results. In this research, dissipative particle dynamics and molecular dynamics simulation were performed in systems of aliphatic and cyclic oil/surfactant/water systems to investigate the structural and interfacial characteristics of the system. The results of this work can be summarised as follows:

- The advantages of using coarse-graining methods over other microscopic methods are reducing the particles degree of freedom, ignoring the atomistic configuration in case of modelling complex fluid which causes a substantial decrease in computational cost and time.

-The conservative force parameter values were calculated using chi parameter. This parameter was estimated using molecular dynamics simulation and Monte Carlo method, which created a bridge between microscopic and mesoscopic simulation.

-According to the snapshots taken at equilibrium from the simulation cell and also the relative concentration profiles, it was observed that the surfactant molecules would accumulate at the interface with its head moving toward the water phase and the aliphatic chain orienting to the oil phase. The surfactant concentration found to be a function of the type of oil molecules.

-Investigations on the structural behaviour of surfactant at the interface using the radius of gyration values revealed that the surfactant molecules would stretch more in systems of linear hydrocarbons compared to cyclic compounds since aliphatic chains show high non-polarity compared to cyclic compounds and will attract the surfactant tail groups more.

-Interfacial tension is a very important factor to be considered in various industries such as Enhanced oil recovery or drug delivery systems. In this work, the IFT values were analysed for different cases, and interfacial tension values were calculated to be the highest for dodecane/water system and lowest for Benzene/water systems due to the polarity of the molecules. The results of the simulation found to be in agreement with literature.

-Plots of interfacial tension versus surfactant concentrations show a opposite relation between number of surfactant molecules and IFT value. According to the Rg values and IFT plots, the surfactant will stretch at the interface and forms various types of bond to water and oil phase separately and decrease the interfacial energies and cause equilibrium.

-Water-cut ratio is another inflecting factor on the IFT of the system, at WC=1 the IFT reported to be the highest since the interface formed between oil and water is lowest, by changing the WC to values below one or greater than one, more surface area will be provided for surfactant molecules to aggregate and decrease the interfacial tension.

Further research on the hydrocarbon/surfactant/water systems is recommended using the integrated method to calculate the conservative force parameter for more complex mixtures of ionic surfactants and polar oil compounds.

Nomenclatures

Acronyms

DPD Dissipative particle dynamics

EOR Enhanced oil recovery

HSP Hansen solubility parameter

IFT Interfacial tension

IR Infrared spectroscopy

MD Molecular dynamic

NMR Nuclear magnetic resonance

SCFT Self-consistent field theory

WC water-cut

Variables/Letters

$\langle E \quad (T) \rangle$ Inter and intramolecular force

ΔE_{coh} Cohesive energy;

ΔE_{mix} Energy of the mixing for the mixture,

ΔH^{VAP} Enthalpy of vaporization

F^{C} Conservative force

F^{D} Dissipative force

F^{R} Random forces

F^{S} Spring forces

L_x Length of the box across the x-axis

N_m Coarse graining degree

P_{xx} Pressure tensor across the x-axis

R_g Radius of Gyration

V Partial molar volume,

Z_{ii} Coordination number values

a_{ij} DPD interaction parameter

k_B Boltzmann constant

k_T Isothermal compressibility;

k_s Spring constant

r Position vector of particles

r_0 Spring equilibrium distance.

r_c Cut-off radius or the unit length

v Bead volume

v Velocity vector of particles

v_i^0 Molar volume of the molecule

Δt Time step.

m Mass of the bead

R universal gas constant

R_{cm} Mean position of monomers

T Temperature

$P(E\ )$ Pair interaction energy probability distribution

p Pressure

Greek Letters

$\delta\ (T)$ Temperature dependent solubility parameters

ξ Random number from a zero-mean distribution

ϕ Volume fraction of the phases present in the system,

γ Interfacial tension

χ Flory-Huggins parameter

α Constant equals 0.101

λ Numerical constant to include the effect of temperature

ξ Dissipation coefficient

ρ Density in DPD units

σ Amplitude of the random forces

τ Time-scale

ω Weight function

Subscript

A, B Phases of the system

b Bead

i, j Beads present in the system

REFERENCES

[1] M.V. Lomova, G.B. Sukhorukov, M.N. Antipina, Antioxidant coating of micronsize droplets for prevention of lipid peroxidation in oil-in-water emulsion, ACS applied materials & interfaces 2 (2010) 3669-3676.

[2] D. Pan, N. Phan-Thien, B.C. Khoo, Studies on liquid–liquid interfacial tension with standard dissipative particle dynamics method, Mol. Simul. 41 (2015) 1166-1176.

[3] K. Kubota, N. Kuwahara, H. Sato, Critical behavior of a cationic surfactant in an aqueous salt solution, The Journal of chemical physics 100 (1994) 4543-4547.

[4] K. Shi, C. Lian, Z. Bai, S. Zhao, H. Liu, Dissipative particle dynamics study of the water/benzene/caprolactam system in the absence or presence of non-ionic surfactants, Chem. Eng. Sci. 122 (2015) 185-196.

[5] R.-h. Zhao, L. Zhang, L. Zhang, S. Zhao, J.-y. Yu, Effect of the Hydrophilic− Lipophilic Ability on Dynamic Interfacial Tensions of Alkylbenzene Sulfonates, Energy Fuels 24 (2010) 5048-5052.

[6] M.J. Rosen, Surfactants and interfacial phenomena, Wiley New York, 1959.

[7] J. Barnes, D. van Batenburg, M. Faber, C. Van Rijn, S. Geib, S. Van Kuijk, D. Perez Regalado, T. King, M. Doll, L. Pretzer, Quality Assurance and Control of Surfactants for Field Scale EOR Pilot Projects, Abu Dhabi International Petroleum Exhibition and Conference, Society of Petroleum Engineers, 2015.

[8] Y. Zhu, M. Lei, Studies on surfactant-polymer combination flooding formulations for a high salinity reservoir, SPE EOR conference at oil and gas West Asia, Society of Petroleum Engineers, 2016.

[9] P. Xing, M. Bousmina, D. Rodrigue, M. Kamal, Critical experimental comparison between five techniques for the determination of interfacial tension in polymer blends: model system of polystyrene/polyamide-6, Macromolecules 33 (2000) 8020-8034.

[10] A.A. Rafati, E. Ghasemian, Study of surface tension and surface properties of binary alcohol/n-alkyl acetate mixtures, J. Colloid Interface Sci. 328 (2008) 385-390.
[11] G. Ataev, Anomalous temperature dependence of interfacial tension in water-hydrocarbon mixtures, Russian Journal of Physical Chemistry A 81 (2007) 2094-2095.
[12] Y. Li, Y. Guo, G. Xu, Z. Wang, M. Bao, N. Sun, Dissipative particle dynamics simulation on the properties of the oil/water/surfactant system in the absence and presence of polymer, Molecular Simulation 39 (2013) 299-308.
[13] D. Lyttle, J. Lu, T. Su, R. Thomas, J. Penfold, Structure of a dodecyltrimethylammonium bromide layer at the air/water interface determined by neutron reflection: comparison of the monolayer structure of cationic surfactants with different chain lengths, Langmuir 11 (1995) 1001-1008.
[14] J.C. Conboy, M.C. Messmer, G.L. Richmond, Dependence of alkyl chain conformation of simple ionic surfactants on head group functionality as studied by vibrational sum-frequency spectroscopy, The Journal of Physical Chemistry B 101 (1997) 6724-6733.
[15] M.K. Meybodi, A. Daryasafar, M. Karimi, Determination of hydrocarbon-water interfacial tension using a new empirical correlation, Fluid Phase Equilib. 415 (2016) 42-50.
[16] A.H. Demond, A.S. Lindner, Estimation of interfacial tension between organic liquids and water, Environ. Sci. Technol. 27 (1993) 2318-2331.
[17] J. Liu, Y. Zhao, S. Ren, Molecular dynamics simulation of self-aggregation of asphaltenes at an oil/water interface: formation and destruction of the asphaltene protective film, Energy & Fuels 29 (2015) 1233-1242.
[18] H.H. Al-Kayiem, J.A. Khan, Evaluation of Alkali/Surfactant/Polymer Flooding on Separation and Stabilization of Water/Oil Emulsion by Statistical Modeling, Energy & Fuels 31 (2017) 9290-9301.
[19] X. Song, S. Zhao, S. Fang, Y. Ma, M. Duan, Mesoscopic simulations of adsorption and association of PEO-PPO-PEO triblock copolymers on a hydrophobic surface: From mushroom hemisphere to rectangle brush, Langmuir 32 (2016) 11375-11385.
[20] S. Buell, G.C. Rutledge, K.J.V. Vliet, Predicting polymer nanofiber interactions via molecular simulations, ACS applied materials & interfaces 2 (2010) 1164-1172.
[21] H.-Q. Liang, K.-J. Ji, L.-Y. Zha, W.-B. Hu, Y. Ou, Z.-K. Xu, Polymer membranes with vertically oriented pores constructed by 2D freezing at ambient temperature, ACS applied materials & interfaces 8 (2016) 14174-14181.
[22] M.-y. Xu, Z.-r. Yang, Dissipative particle dynamics study on the mesostructures of n-octadecane/water emulsion with alternating styrene–maleic acid copolymers as emulsifier, Soft Matter 8 (2012) 375-384.
[23] S. Wang, S. Yang, X. Wang, Y. Liu, S. Yang, Q. Dong, Numerical simulations of the effect of ionic surfactant/polymer on oil–water interface using dissipative particle dynamics, Asia-Pacific Journal of Chemical Engineering 11 (2016) 581-593.
[24] F. Pierce, M. Tsige, D. Perahia, G.S. Grest, Liquid− Liquid Interfaces of Semifluorinated Alkane Diblock Copolymers with Water, Alkanes, and Perfluorinated Alkanes, The Journal of Physical Chemistry B 112 (2008) 16012-16020.
[25] M.B.A. Rahman, Q.-Y. Huan, B.A. Tejo, M. Basri, A.B. Salleh, R.N.Z.A. Rahman, Self-assembly formation of palm-based esters nano-emulsion: A molecular dynamics study, Chemical Physics Letters 480 (2009) 220-224.
[26] G. Liu, R. Ma, J. Ren, Z. Li, H. Zhang, Z. Zhang, Y. An, L. Shi, A glucose-responsive complex polymeric micelle enabling repeated on–off release and insulin protection, Soft Matter 9 (2013) 1636-1644.
[27] C. Baig, O. Alexiadis, V.G. Mavrantzas, Advanced Monte Carlo Algorithm for the Atomistic Simulation of Short-and Long-Chain Branched Polymers: Implementation for Model H-Shaped, A3 A A3 Multiarm (Pom-Pom), and Short-Chain Branched Polyethylene Melts, Macromolecules 43 (2009) 986-1002.
[28] K. Hadley, C. McCabe, A structurally relevant coarse-grained model for cholesterol, Biophysical journal 99 (2010) 2896-2905.

[29] X.D. Guo, L.J. Zhang, Z.M. Wu, Y. Qian, Dissipative particle dynamics studies on microstructure of pH-sensitive micelles for sustained drug delivery, Macromolecules 43 (2010) 7839-7844.
[30] P. Hoogerbrugge, J. Koelman, Simulating microscopic hydrodynamic phenomena with dissipative particle dynamics, EPL (Europhysics Letters) 19 (1992) 155.
[31] P. Espanol, P. Warren, Statistical mechanics of dissipative particle dynamics, EPL (Europhysics Letters) 30 (1995) 191.
[32] S.-F. Zhang, L.L. Sun, J.-B. Xu, H. Wu, H. Wen, Aggregate structure in heavy crude oil: using a dissipative particle dynamics based mesoscale platform, Energy & Fuels 24 (2010) 4312-4326.
[33] P. Angelikopoulos, A. Gromov, A. Leen, O. Nerushev, H. Bock, E.E. Campbell, Dispersing individual single-wall carbon nanotubes in aqueous surfactant solutions below the cmc, The Journal of Physical Chemistry C 114 (2009) 2-9.
[34] L. Rekvig, D. Frenkel, Molecular simulations of droplet coalescence in oil/water/surfactant systems, The Journal of chemical physics 127 (2007) 134701.
[35] J.M. Kim, R.J. Phillips, Dissipative particle dynamics simulation of flow around spheres and cylinders at finite Reynolds numbers, Chemical engineering science 59 (2004) 4155-4168.
[36] Y. Kong, C. Manke, W. Madden, A. Schlijper, Simulation of a confined polymer in solution using the dissipative particle dynamics method, International journal of thermophysics 15 (1994) 1093-1101.
[37] X. Fan, N. Phan-Thien, S. Chen, X. Wu, T. Yong Ng, Simulating flow of DNA suspension using dissipative particle dynamics, Physics of Fluids 18 (2006) 063102.
[38] A.T. Clark, M. Lal, J.N. Ruddock, P.B. Warren, Mesoscopic simulation of drops in gravitational and shear fields, Langmuir 16 (2000) 6342-6350.
[39] H. Liu, H.-J. Qian, Y. Zhao, Z.-Y. Lu, Dissipative particle dynamics simulation study on the binary mixture phase separation coupled with polymerization, The Journal of chemical physics 127 (2007) 144903.
[40] H. Goel, P.R. Chandran, K. Mitra, S. Majumdar, P. Ray, Estimation of interfacial tension for immiscible and partially miscible liquid systems by Dissipative Particle Dynamics, Chem. Phys. Lett. 600 (2014) 62-67.
[41] C.D.V. Silva, F. Ruette, Estimation of Interfacial Tension in Mixtures of Linear Hydrocarbons and Immiscible Organic Liquids with Water by Dissipative Particle Dynamics (DPD), International Journal of Fluid Mechanics & Thermal Sciences 4 (2018) 1.
[42] Y. Li, P. Zhang, F.-L. Dong, X.-L. Cao, X.-W. Song, X.-H. Cui, The array and interfacial activity of sodium dodecyl benzene sulfonate and sodium oleate at the oil/water interface, J. Colloid Interface Sci. 290 (2005) 275-280.
[43] H. Rezaei, H. Modarress, Dissipative particle dynamics (DPD) study of hydrocarbon–water interfacial tension (IFT), Chem. Phys. Lett. 620 (2015) 114-122.
[44] S. Wang, J. Zhao, X. Li, S. Yang, X. Wang, Y. Liu, S. Yang, Q. Dong, Numerical simulations on effects of ionic/nonionic surfactant on oil-water interface using dissipative particle dynamics, Asia-Pacific Journal of Chemical Engineering 12 (2017) 268-282.
[45] S. Wang, S. Yang, R. Wang, R. Tian, X. Zhang, Q. Sun, L. Liu, Dissipative particle dynamics study on the temperature dependent interfacial tension in surfactant-oil-water mixtures, Journal of Petroleum Science and Engineering 169 (2018) 81-95.
[46] M. Kranenburg, M. Venturoli, B. Smit, Phase behavior and induced interdigitation in bilayers studied with dissipative particle dynamics, The Journal of Physical Chemistry B 107 (2003) 11491-11501.
[47] J. Koelman, P. Hoogerbrugge, Dynamic simulations of hard-sphere suspensions under steady shear, EPL (Europhysics Letters) 21 (1993) 363.
[48] V.V. Ginzburg, K. Chang, P.K. Jog, A.B. Argenton, L. Rakesh, Modeling the Interfacial Tension in Oil− Water− Nonionic Surfactant Mixtures Using Dissipative Particle Dynamics and Self-Consistent Field Theory, The journal of physical chemistry B 115 (2011) 4654-4661.

[49] T. Spyriouni, C. Vergelati, A molecular modeling study of binary blend compatibility of polyamide 6 and poly (vinyl acetate) with different degrees of hydrolysis: an atomistic and mesoscopic approach, Macromolecules 34 (2001) 5306-5316.
[50] R.D. Groot, T.J. Madden, Dynamic simulation of diblock copolymer microphase separation, The Journal of chemical physics 108 (1998) 8713-8724.
[51] R.D. Groot, P.B. Warren, Dissipative particle dynamics: Bridging the gap between atomistic and mesoscopic simulation, The Journal of chemical physics 107 (1997) 4423-4435.
[52] V. Ortiz, S.O. Nielsen, D.E. Discher, M.L. Klein, R. Lipowsky, J. Shillcock, Dissipative particle dynamics simulations of polymersomes, The Journal of Physical Chemistry B 109 (2005) 17708-17714.
[53] X. Song, P. Shi, M. Duan, S. Fang, Y. Ma, Investigation of demulsification efficiency in water-in-crude oil emulsions using dissipative particle dynamics, Rsc Advances 5 (2015) 62971-62981.
[54] Y. Wang, L. Zhang, T. Sun, S. Zhao, J. Yu, A study of interfacial dilational properties of two different structure demulsifiers at oil–water interfaces, Journal of colloid and interface science 270 (2004) 163-170.
[55] S.L. Kokal, Crude oil emulsions: A state-of-the-art review, SPE Production & facilities 20 (2005) 5-13.
[56] E.n.B. Silva, D. Santos, D.R. Alves, M.S. Barbosa, R.C. Guimarães, B.M. Ferreira, R.A. Guarnieri, E. Franceschi, C.u. Dariva, A.F. Santos, Demulsification of heavy crude oil emulsions using ionic liquids, Energy & Fuels 27 (2013) 6311-6315.
[57] X.D. Guo, J.P. Tan, S.H. Kim, L.J. Zhang, Y. Zhang, J.L. Hedrick, Y.Y. Yang, Y. Qian, Computational studies on self-assembled paclitaxel structures: templates for hierarchical block copolymer assemblies and sustained drug release, Biomaterials 30 (2009) 6556-6563.
[58] Z. Luo, J. Jiang, pH-sensitive drug loading/releasing in amphiphilic copolymer PAE–PEG: Integrating molecular dynamics and dissipative particle dynamics simulations, Journal of controlled release 162 (2012) 185-193.
[59] L. Rekvig, M. Kranenburg, J. Vreede, B. Hafskjold, B. Smit, Investigation of surfactant efficiency using dissipative particle dynamics, Langmuir 19 (2003) 8195-8205.
[60] A.G. Goicochea, M. Romero-Bastida, R. López-Rendón, Dependence of thermodynamic properties of model systems on some dissipative particle dynamics parameters, Molecular Physics 105 (2007) 2375-2381.
[61] A. Maiti, S. McGrother, Bead–bead interaction parameters in dissipative particle dynamics: relation to bead-size, solubility parameter, and surface tension, The Journal of chemical physics 120 (2004) 1594-1601.
[62] Z. Chen, X. Cheng, H. Cui, P. Cheng, H. Wang, Dissipative particle dynamics simulation of the phase behavior and microstructure of CTAB/octane/1-butanol/water microemulsion, Colloids Surf. Physicochem. Eng. Aspects 301 (2007) 437-443.
[63] J. Lyklema, Fundamentals of interface and colloid science: soft colloids, Elsevier2005.
[64] L. Chen, Y. Hu, Q. Liu, Simulation of interfacial tension based on the method of solubility parameter, Comp. Appl. Chem 25 (2008) 697-700.
[65] G.R. Strobl, G.R. Strobl, The physics of polymers, Springer1997.
[66] Y. Ruiz-Morales, O.C. Mullins, Coarse-grained molecular simulations to investigate asphaltenes at the oil–water interface, Energy & Fuels 29 (2015) 1597-1609.
[67] M. Accelrys, Modeling 5.5. Accelrys, Inc.: San Diego (2010).
[68] R.D. Groot, K. Rabone, Mesoscopic simulation of cell membrane damage, morphology change and rupture by nonionic surfactants, Biophys. J. 81 (2001) 725-736.
[69] S. Nosé, A molecular dynamics method for simulations in the canonical ensemble, Molecular physics 52 (1984) 255-268.
[70] S. Nosé, A unified formulation of the constant temperature molecular dynamics methods, The Journal of chemical physics 81 (1984) 511-519.

[71] S. Nosé, M. Klein, Constant pressure molecular dynamics for molecular systems, Molecular Physics 50 (1983) 1055-1076.
[72] X. Sui, Y. Chu, S. Xing, C. Liu, Synthesis of PANI/AgCl, PANI/BaSO4 and PANI/TiO2 nanocomposites in CTAB/hexanol/water reverse micelle, Mater. Lett. 58 (2004) 1255-1259.
[73] D.R. Lide, CRC handbook of chemistry and physics, CRC Boca Raton2012.
[74] R. Perry, D. Green, Perry's Chemical Engineer's Handbook Pdf, (1984).
[75] H. Alasiri, The Behavior of Surfactants in Water/Oil System by Dissipative Particle Dynamics, Rice University, 2016.
[76] E. Mayoral, A.G. Goicochea, Modeling the temperature dependent interfacial tension between organic solvents and water using dissipative particle dynamics, The Journal of chemical physics 138 (2013) 094703.
[77] F. Goodarzi, S. Zendehboudi, A Comprehensive Review on Emulsions and Emulsion Stability in Chemical and Energy Industries, The Canadian Journal of Chemical Engineering 97 (2019) 281-309.

Appendix. A

This appendix reports the magnitudes of conservative force parameter for various molecules in various oil/water/surfactant cases (see Tables A1 to A3).

Table A1: Conservative force parameter table for system of Octane/Surfactant/water

	T	**H**	**O**	**W**
T	25			
H	36.5	25		
O	25	34.5	25	
W	57.95	30.5	47	25

Table A2: Conservative force parameter table for system of Cyclohexane/Surfactant/water

	T	**H**	**O**	**W**
T	25			
H	36.5	25		
O	30	32	25	

W	57.95	30.5	54	25

Table A3: Conservative force parameter table for system of Benzene/Surfactant/water

	T	**H**	**O**	**W**
T	25			
H	36.5	25		
O	28	31	25	
W	57.95	30.5	51.0	25

3 Multiscale modelling on the effect of salinity and non-ionic surfactant on water/oil systems: A molecular dynamics simulation and Dissipative Particle Dynamics study

Fatemeh Goodarzi, Sohrab Zendehboudi

Faculty of Engineering and Applied Science, Memorial University, St. John's, NL, Canada

ABSTRACT

Multiphase systems and their behaviours/characteristics appear to be crucial in a variety of industries such as oil and gas sector, pharmaceutical products, and food industries. In this paper, the mesoscale simulation method is used to predict the interfacial behaviours of the water/oil systems at different temperatures and salt concentrations in the presence of a non-ionic surfactant (hexaethylene glycol monododecyl ether). The dynamic performance of the system can be well reproduced with respect to the results reported in the literature. Dissipative Particle Dynamics (DPD) is employed to model the interfacial properties (e.g., interfacial density and interfacial tension) and structural properties such as the radius of gyration as a function of water/oil ratio, surfactant concentration, temperature, and salinity of oil/surfactant/water mixtures. Molecular Dynamic (MD) simulations are carried out to estimate the Flory-Huggins chi parameter by means of temperature-dependent solubility parameter and cohesive energy calculations using Monte Carlo (MC) method, which is then utilized as an input for the DPD approach. The DPD repulsive interaction parameter (a_{ij}) is also obtained from the dependence of chi parameter to temperature using MD simulations. Both the density profiles and simulation snapshots indicate a well-defined interface between water and oil phases, where the thickness of the layer increases with increasing the surfactant concentration and the peak of density becomes higher accordingly. It is found that the radius of gyration is a weak function of salinity; however, it increases with an increase in the surfactant concentration, revealing that the surfactant molecules become more stretched at the interface. By increasing the water content or water/oil ratio (WC), the interfacial tension increases to reach a maximum value. After the maximum interfacial tension, increasing the water/oil ratio lowers this important parameter. According to the results of the MD simulations, the presence of salt improves the interfacial efficiency of the surfactant by decreasing the interfacial tension, which is in a good agreement with the literature data. Integrating the micro and mesoscale modeling through chi parameter determination improves the accuracy of the calculation. This integration also decreases the calculation time (and costs). This research work offers useful tips for surfactant selection as well as important results and information on the interactions of molecules at water/oil interface, which are central to analyze emulsion stability at different process and thermodynamic conditions.

Keywords: Interfacial behaviors; Surfactant; Salinity; Dissipative particle dynamics; Molecular dynamic simulations

3.1 INTRODUCTION

Determination of interfacial properties, especially Interfacial Tension (IFT), in liquid-liquid and liquid-gas mixtures is of great importance among the scientific communities. In a thermodynamic viewpoint, IFT measures the free energy required for an interface formation between the phases in a specific surface area.[1] Accurate prediction of IFT is challenging due to the difficulty in the identification of numerous unresolved forces at the liquid/liquid interface. A comprehensive knowledge of the principal forces at the interface such as electrostatic, van der Waals interactions, and hydrogen bonds between the molecules are required to successfully determine the interfacial tension values. In spite of detailed calculation, most atomistic simulation tools are still computationally expensive when they are used to simulate the movement and behaviour of atoms individually.[2] The addition of surfactants can modify the interfacial properties of a mixture/system. Surfactant behaviours play a crucial role at the oil/water interface in several applications such as oil recovery, detergency, drug delivery systems, and chemical processes dealing with nanoparticles.[2] A surfactant is a molecule with either an ionic or polar head that is soluble in polar solvents (e.g., water) and with an aliphatic chain of a hydrocarbon as its tail, which is miscible in non-polar mixtures. A surfactant can effectively reduce the interfacial tension of the system.

In this work, we monitor the behaviours of hexaethyleneglycol monododecyl ether ($C_{12}E_6$) at the oil/water interface in the presence of salt. $C_{12}E_6$ comes from alkyl polyethylene glycol ethers family, known as C_mE_n.[3] The chemical formula of these surfactants is $C_mH_{2m+1}(OC_2H_2)_nOH$, while the hydrophilic and non-ionic polar head, $(OC_2H_4)_nOH$ or E_n, is attached to a long nonpolar hydrocarbon tail C_mH_{2m+1} or C_m. C_mE_n is a widely used product for various purposes such as pharmaceutical, cosmetic, and Enhanced Oil Recovery (EOR) techniques.[4,5] Investigation of interfacial tension variations is of great importance to gain insights into the behaviours of multiphase systems and complex fluids such as colloids and/or emulsions. There are some experimental thermodynamic studies on the water/surfactant/oil interface in the open sources including molecular thermodynamic theories of Nagarajan et al. [6,7] However, when the surfactant is a flexible chain, these theories face some restrictions such as identifying the forces and bond length, which limits their application to model the behaviours of various systems at different surfactant concentrations and/or temperatures.[6] The theories are also valid only for mixtures with a low surfactant concentration. Based on a typical measurement tool for IFT determination such as pendant drop tensiometer, the equilibration time increases dramatically when the surfactant concentration is extremely low (for example below 10 ppm in water). Thus, computational techniques become essential to accurately estimate the IFT values for low surfactant concentration systems in a reasonable timeframe where direct experimental measurements become impossible/impractical. Various works have focused on the characterisation of oil/water systems in the presence of surfactant and inorganics salts where the corresponding applications are found

in chemistry, biology, and oil and gas industry.[7] In the past decades, a variety of experimental techniques such as Nuclear Magnetic Resonance (NMR), Infrared Spectroscopy (IR), and conductivity measures were employed to monitor the interfacial behaviours of water/surfactant/oil mixtures. [8-10] For instance, Wiegand et al.[5] reported the IFT values of water and nonpolar fluids using the pendant drop. Cai et al.[11] attempted to determine the IFT of alkane/water systems using two different brines. Experimental measurements can provide in-depth information regarding some features of interfacial interactions such as interfacial tension. However, a proper understanding of phase behaviours or microstructures of the particles in various systems is still missing.[12] The lack of adequate knowledge is attributed to the complexity of multicomponent mixtures and limitations of experimental tools to capture detailed characteristics of such complicated systems with various interfacial behaviours. Thus, it seems essential to seek new methods that offer a detailed description of phenomena taking place in multicomponent mixtures. Analysis of configuration and dynamics of surfacing molecules using numerical models/simulations is central towards a better characterisation of phase transition or self-assembly of the molecules. [13] Dissipative Particle Dynamics (DPD) is an appropriate method to model a coarse-grained system.[14,15] DPD is a mesoscopic modelling technique developed to simulate complex fluids. This model is composed of three distinct types of forces acting among particles, representing the conservative force, responsible for thermodynamic properties of the system, coupled dissipative, and random forces for maintaining a constant temperature.[14] Local and global conservations of momentum are resulted from applying Newton's equation of motion that considers all forces in the system. This is a vital aspect of the DPD technique when hydrodynamics forces are the leading modes in the system.[16] Compared to common dynamic simulations, for example, molecular dynamic simulations, using soft interactions in DPD is taken into account as a major advantage over other simulation methods.[15] A cluster of particles is represented with beads, and soft potential allows for relatively larger time and length scales than what is commonly utilized in other dynamic simulation techniques. [17] DPD provides less detailed information than molecular dynamic simulation. However, it still offers a systematic study of interfacial and structural properties of the targeted systems. In the past decades, various theoretical research works have been performed to characterize the emulsion systems using computer simulations. Rezaei and Modarres[18] employed a DPD mesoscopic simulation to estimate the IFT of different hydrocarbons such as cycloalkanes, aromatics, and aliphatic chains with water. Ginzburg et al.[6] performed DPD and Self-Consistent Field Theory (SCFT) simulation to model the interfacial tension in ternary water/surfactant/oil systems. Three non-ionic surfactant molecules were considered in their simulation ($C_{12}E_8$, $C_{12}E_6$, and $C_{12}E_4$). It was found that addition of surfactant decreases the interfacial tension. However, the results from SCFT method underestimated the values of IFT in the vicinity of Critical Micelle Concentration (CMC). Unlike SCFT, DPD can describe the IFT variation and aggregation of surfactants into spherical micelles near the CMC. Wang et al. investigated the behaviours of water/surfactant/oil systems through multiple DPD simulations considering different ionic/non-ionic surfactant molecules and different combinations of these

molecules.[19-21] Effects of cationic (CTAB), anionic (SDBS), and non-ionic (PEO-PPO-PEO) surfactant molecules were considered at various temperatures, surfactant concentrations, and water/oil ratios. They found that increasing temperature causes the interfacial tension to decrease and the radius of gyration to increase in all cases. It was also observed that the ionic surfactants are more sensitive to temperature than non-ionic ones. It was found that anionic surfactants exhibit a higher resistance to temperature, compared to cationic surfactants due to their stronger hydrogen bonding at the head group. In addition, it was concluded that a mixture of ionic and non-ionic surfactants can reduce the IFT more effectively, compared to a single surfactant type. The variation of the cases considered in their works provides a good comparison among different parameters that influence the structural and interfacial properties of oil/water systems. Remesal et al.[1] performed Molecular Dynamic (MD) simulations to study the impacts of salinity and temperature on the hydrocarbon/brine interfacial tension. A mixture of aromatics and aliphatic hydrocarbons was utilized as the oil phase, and different concentrations of NaCl and $CaCl_2$ were examined. It was concluded that by increasing the salt concentration the values of interfacial tension increase, which is in opposite to some research outputs in the literature.[22] Based on their justification, this trend is due to the electrostatic effect of salt in origin and the salt in the aqueous phase causes difficulty for the water molecules to accumulate at the interface. Increasing the temperature also leads to the reduction of IFT, which is in agreement with previous experimental findings.

It is important to investigate the behaviours of brine/surfactant/oil mixtures at various conditions so that the factors influencing the interfacial and structural properties of the targeted systems are determined. There are a variety of research previously performed on modeling of water/oil systems in EOR processes.[23-36] Giving more information, several mechanistic modeling approaches for chemical/oil/brine/rock systems have been proposed in the literature and the employed models can adequately capture the vital impacts of salinity, temperature, co-solvent on the phase behaviors of surfactant solution.[23-26] Geochemical reactions between crude oil and alkaline agents were also well addressed in the past.[23-29] However, an integrated model that systematically captures the system configuration in a reasonable simulation time and cost is missing. The purpose of this research work is to study the properties of water/surfactant/oil system in the presence of inorganic salt at different water/oil ratio, surfactant and salt concentration, and temperature conditions. DPD and MD simulation methods are implemented to estimate the required parameters such as solubility parameter and Flory-Huggins chi parameter to describe the interficial behaviours of various systems. To the best of our knowledge, there is no such a systematic study in the literature that employs a combination of MD simulation and DPD strategy for investigating the interfacial behaviours and structures of oil/water/surfactant through a detailed sensitivity analysis. The current research investigation aims to comprehensively assess the dynamic behaviors of a water/oil system in the presence of surfactant and salt (with different types) where molecular dynamic simulation and dissipative particle dynamics strategies are employed in a reasonable/ cost effective manner. An extensive knowledge on the interactions of molecules at the interface and the CMC

at various process conditions is attained, which can help to optimize corresponding processes/operations such as EOR in terms of performance and cost.

This paper is organised as follows. After the introduction section, a brief theory of DPD simulations scheme is given. Flory-Huggins chi parameter evaluation using cohesive energy calculations by means of solubility parameter and Blends module, and estimation of mixing energy using Amorphous cell and Forcite module in the Material Studio software are also discussed in Section 2. The cell configuration, conditions of the dynamic simulations, and values of solubility parameter and DPD interaction parameter are provided in the simulation details and methodology section. In the results and discussion section, the calculated values of IFT and the radius of gyration, relative concentration profiles as well as snapshots of cell evolution by time for different cell situations such as water cut, surfactant concentration, salinity, and temperature are included. Finally, the conclusions section lists the remarking results and sheds some lights on possible future works using DPD and MD for various objectives in chemical/process and petroleum engineering.

3.2 THEORY OF COMPUTATIONAL APPROACH

3.2.1 Fundamental equations of DPD theory

Dissipative Particle Dynamics (DPD) is a particle-based computational simulation approach that can be categorised as a branch of coarse-grained Molecular Dynamics (MD). It was first introduced by Hoogerbrugge and Koelman[15] and later revisited by Espanol. [14] Compared to MD, DPD allows the user to choose larger systems and study the cases with longer time periods in a realistic computational framework. [37] This approach relies on the molecular dynamic simulations of a cluster of soft beads interacting with neighbour particles via soft potentials. [38]

DPD has shown to be an effective approach to study the thermodynamic behaviours of polymer blends[39], complex geometries containing fluids with complicated configurations[40], biological molecules[41], and petroleum fluids so that fluid properties under different external effects such as pH[42] or temperature[43] can be estimated. To explore the behaviours of the water/oil systems, we employ the DPD method. The structure of the DPD technique is similar to MD simulations so that the Newton's classical equation of motion is solved to obtain the particles position and momenta using finite time steps.[43] This suitable scheme offers a distinctive numerical algorithm to monitor the dynamic behaviours of coarse-grained systems composed of beads which are defined as a cluster of atoms or molecules.[22] For simplicity, the masses of all beads are chosen to be equal, which is one in reduced DPD units.

Table 1 lists the constitutive forces acting on each bead from the neighbourhood beads to describe the DPD simulation scheme. This interparticle force is a pairwise additive acting between the particle centres and preserving the linear and angular momentums, which satisfy the Newton's third law. [44] The DPD model includes the conservative forces acting between particles *i* and *j* positioned with a distance of *rij* [45] ; namely, (F_{ij}^{C}) is a soft repulsive potential; dissipative forces

(F_{ij}^{D}) represent the frictional forces, which are a function of both position and velocity; and random forces (F_{ij}^{R}) are responsible for maintaining the system temperature. All the force components disappear after this cut-off radius, which is equal to one in DPD reduced unit. The soft-core conservative force allows the system to choose larger time steps in the DPD approach than the common regular ones in MD, which typically involves hard-core potentials such as Lennard-Jones potential. [46] a_{ij} or the DPD interaction parameter controls the intensity of repulsion between two particles, which influences the soft linearly decaying repulsion representing the conservative forces. The dependence of the forces to the distance, calculated by averaging the van der Waals forces spatially, provides the ability to choose large time steps. [47] The strengths of dissipative and random forces are defined in a way to keep the temperature constant. The combined effect of dissipative and random forces is thermostat, which maintains the momentum and properly describes the hydrodynamic behaviours of the system at a large time and length scale. [48]

Table 3-1 Fundamental equations used in the DPD simulations. [11, 14, 15]

Description	Equation	Parameters
Newton's equation of motion	$\frac{dr_i}{dt} = v_i \ , \quad \frac{dv_i}{dt} = f_i/m_i$	r_i, v_i and m_i refers to the position vector, velocity vector and mass of the beads respectively
Force components	$F_i = \sum_{j \neq i} (F_{ij}^{C} + F_{ij}^{D} + F_{ij}^{R}) + F_i^{S}$	F_{ij}^{C} is the conservative force, F_{ij}^{D} represents the dissipative force, F_{ij}^{R} refers to the random forces applied on the i th bead by the j th bead and the remaining term is the spring forces
Conservative force	$F_{ij}^{C} = a_{ij}\omega^{C}(r_{ij})\hat{r}_{ij}$	a_{ij} is the DPD interaction parameter $r_{ij} = r_i - r_j, r_{ij} = \lvert r_{ij} \rvert \ , v_{ij} = v_i - v_j \quad \hat{r}_{ij} =, r_{ij}/\lvert r_{ij} \rvert$, r and v are the position and velocity vectors of the particles ω is the weight function
Dissipative force	$F_{ij}^{D} = -\xi\omega^{D}(r_{ij})(v_{ij}.\hat{r}_{ij})\hat{r}_{ij}$	ξ shows the dissipation coefficient
Random force	$F_{ij}^{R} = \sigma\omega^{R}(r_{ij})\xi_{ij}\Delta t^{-(\frac{1}{2})}\hat{r}_{ij}$	σ refers to the amplitude of the random forces ξ_{ij} zera o-mean Gaussian random variable of unit variance Δt is the time step

Spring force	$F_{ij}^{S} = -k_s(r_{ij} - r_0)\hat{r}_{ij}$	k_s is the spring constant and r_0 refers to the spring equilibrium distance
Weight Functions	$\omega^{C}(r_{ij}) = \omega^{R}(r_{ij}) = [\omega^{D}(r_{ij})]^{\frac{1}{2}}$ $= \begin{cases} 1 - r_{ij}, & r_{ij} \le r_C \\ 0, & r_{ij} > r_C \end{cases}$	r_c depicts the common effective interaction length or the cut-off radius
The amplitude of random force	$\sigma^2 = 2k_B T\xi$	k_B is the Boltzmann constant, T refers to the absolute temperature
Time step	$\Delta t = 0.04\tau$, $\tau = (\frac{mr_c^2}{k_B T})^{1/2}$	

The DPD multi-particle system is described by using the modified velocity Verlet algorithm to integrate Newton's equation of motion [38-40] as follows:

$$r_i(t + \Delta t) = r_i(t) + \Delta t V_i(t) + \frac{1}{2}\Delta t^2 f_i(t) \quad (1)$$

$$\tilde{V}_i(t + \Delta t) = V_i(t) + \lambda \Delta t f_i(t)$$

$$f_i(t + \Delta t) = f_i(r(r + \Delta t), \tilde{V}_i(t + \Delta t))$$

In the above equations, $\tilde{V}_i$ refers to the particle velocity at $t + \Delta t$ [40]. The estimation of position and velocity of the beads by employing this algorithm provides later system evaluations of one's interest[41]. Throughout this paper, reduced units are used instead of actual physical units. R_c is the unit length, K_bT is the unit of energy which is the temperature of the thermostat, and mass of the DPD bead is chosen as the mass unit[42]. Applying this approach to solve the system, the entirely visualised system through mesoscopic snapshots at various time steps during the coarse-grained simulation can be monitored.

3.2.2 Conservative forces parametrization

In the DPD method, the particles represent groups of molecules or atoms, portraying the positions and momentum of a section of fluid. A mesoscale simulation is possible through this coarse-graining method[33].

The conservative force parametera_{ij}, is an important parameter, since it's carrying all the chemical and physical characteristics of the particles present in the system. The dissipative force, principally acts as a friction force amongst the beads. The movements of the particles dissipates energy and opposes

the other particles trajectory. The value of dissipation coefficient (ξ) varies from 2 to 32 and generally is chosen to be 4.5 in DPD units ($\sqrt{\frac{mK_BT}{r_c^2}}$)[43] for accurate results in the literature[41]. Random motion of the molecules governs magnitude the of the random forces present in the model and the corresponding amplitude of the random forces term is taken as σ=3[39] to control the temperature of the thermostat.

When two immiscible liquids such as oil and water mix together they will form an interface. To predict the interfacial properties of the mixture at the interface, a detail description of the forces like van-der-Waals, electrostatic and hydrogen bonding is required[44]. However, in the mesoscopic level, the effect of these forces are lumped into repulsive interaction parameters of a_{ij} and a_{ii} form. This approach is more concerned with the clustering method or averaging the fluid properties compared to detailed atomistic properties. In 1997, Groot and Warren[41] introduced a to determine the inversed dimensionless isothermal compressibility as:

$$k^{-1} = \frac{1}{\rho k_B T k_T} = \frac{1}{k_B T}\left(\frac{\partial p}{\partial \rho}\right)_T \quad (2)$$

In the above equation, $k_T = 1/\rho(\partial\rho/\partial p)_T$ is the usual isothermal compressibility, ρ is the number density of molecule, p indicate the pressure. Based on the expression for k^{-1}, to calculate conservative force parameters for like parameters (a_{ii}) the following equation can be sued:

$$a_{ii} = [(k^{-1}(T)N_m - 1)/2\alpha\rho]k_B T \quad (3)$$

Where N_m represents coarse graining degree which is defined as the number of water molecules in a DPD bead. , α is a constant equals to 0.101, ρ is the density in DPD units, k_B refers to the Boltzmann constant. Based on the values of the constants, $k^{-1} = 16$ for water and $a_{ii} = 25$. As for the a_{ij} coefficient, there are various methods to estimate the value in literature[15]. According to the relation between DPD interaction parameter and Flory-Huggins the interaction parameter (χ)[41], a_{ij} can be obtained using the following formula[37]:

$$a_{ij} = a_{ii} + b\chi_{ij} \quad (4)$$

Where b is a constant and equals to 3.497 when the DPD density $\rho = 3$ and 1.451 when $\rho = 5$ [38].

3.2.3 Flory-Huggins χ parameters analysis

If the heat of mixing follows Hildebrand-Scatchard[45; 46] solution theory, for the pure components or identified components of oil, chi parameter can be calculated using the solubility parameter using experimental measurements or molecular dynamics simulation as below:

$$\chi_{ij} = \frac{V_{ij}}{RT}(\delta_i(T) - \delta_j(T))^2 \quad (5)$$

Where R is the gas constant, V_{ij} is the partial molar volume, which can be assumed to be same as volume of the bead. $\delta_i(T)$ and $\delta_j(T)$ are the temperature dependent solubility parameter of the components present in the system. The value of the solubility parameter can be obtained by enthalpy of vaporization and molar volume by the following equation:

$$\delta_i = \sqrt{\frac{\Delta E_{coh}}{v_i^0}} = \sqrt{\frac{\Delta H^{VAP} - RT}{v_i^0}} \quad (6)$$

Where ΔE_{coh} is the cohesive energy, ΔH^{VAP} is the enthalpy of vaporization and v_i^0 is the molar volume of the molecule. Although eq.* is valid only for non-polar components it is reported to be applicable for polar components as well[47]. for systems including polar components and particles with hydrogen bonding, it is recommended to use Hansen solubility parameter(HSP), but since the outputs are compatible with literature we used[48] the solubility parameter obtained from Hildebrand-Scatchard solution theory.

Molecular mechanics method is usually more accurate since they're solving the Newtonian equation of motion to predict the trajectory of particles at a specific amount of time but at the same time takes a noticeable amount of computational work[15]. Here, we determined the Flory-Huggins chi parameter by calculating the mean pair contact interaction energy between the particles. The mixing energy between i and j DPD particles can be estimated using the following formula[49]:

$$E_{ij}^{mix} = 1/2[Z_{ij}\langle E_{ij}(T)\rangle + Z_{ji}\langle E_{ji}(T)\rangle - Z_{ii}\langle E_{ii}(T)\rangle - Z_{jj}\langle E_{jj}(T)\rangle] \quad (7)$$

Where Z_{ij}, Z_{ji}, Z_{jj} and Z_{ii} are the coordination number values assigned to particle pairs. Monte Carlo method was adopted to estimate the inter and intramolecular forces value for mean pain-interaction energy of two particles ($\langle E_{ji}(T)\rangle$) calculation according to Eq.8:

$$\langle E_{ji}(T)\rangle = \frac{\int dE_{ij} P(E_{ij}) E_{ij} \exp(-\frac{E_{ij}}{kT})}{\int dE_{ij} P(E_{ij}) \exp(-\frac{E_{ij}}{k_B T})} \quad (8)$$

In the above equation, $P(E_{ij})$ stands for the pair interaction energy probability distribution. This pair interaction Boltzmann distribution can be obtained by various molecular orientation and conformation calculations of multiple pairs in the system.

χ_{ij} can also be obtained from the energy of mixing values according to the following equation[15]:

$$\chi_{ij} = \frac{1}{\phi_A \phi_B}\left(\frac{\Delta E_{mix}^{ij}}{k_B T}\right) = \frac{\Delta E_{mix}^{ij}}{RT} \tag{9}$$

3.2.4 Calculation of Interfacial Tension

The interfacial tension is the key criteria to show the interfacial characteristics of the system[23].

$$\gamma = \int_0^x (p_n - p_t)dx \tag{10}$$

Interfacial tension is usually calculated by integrating the normal and tangential stress difference, across the interface separating the phases present in the system. Hence, if the normal to the interfaces are parallel to the x-axis, interfacial tension can be obtained by the following formula using the Virial theorem[50]:

$$\gamma_{DPD} = L_x[\langle P_{xx}\rangle - \frac{1}{2}(\langle P_{zz}\rangle + \langle P_{yy}\rangle)] \tag{11}$$

P refers to the pressure tensor, ⟨ ⟩ indicates the ensemble average of the pressure tensor components and x is the axis normal to the interface. The surface tensor is averaged locally and over the system. To compare the results of the simulation with the actual experimental data the unit of IFT needs to change into the actual physical unit (mN/m) by the following equation:

$$\gamma_{real} = \frac{k_B T}{R_c^2}\gamma_{DPD} \tag{12}$$

Considering the cut-off radius defined previously as R_c =6.64 and the temperature of the system at 293K, Hence the conversion factor will be calculated as:

$$\frac{k_B T}{R_c^2} = \frac{1.38 * 10^{-23} * 298.15}{(6.46 * 10^{-10})^2} = 9.86\ mN/m \tag{13}$$

3.2.5 Radius of Gyration

The orientation and structure of polymer molecules at the oil/water interface can be described by evaluating the degree of curliness, which can be calculated by end-to-end distance[51]. Instead of end-to-end distance, the radius of Gyration (R_g) of big molecules is more expressive instinctively as it provides an estimation of polymer coil size[52] as well as being able to experimentally

obtained. In polymer physics, the radius of gyration is describing the polymer chain dimensions[53]. This property is defined at a given time for a specific molecule as:

$$R_g^2 = \frac{1}{N}\sum_{i=1}^{N}(\vec{R}_i - \vec{R}_{cm})^2 \tag{14}$$

$$R_{cm} = \frac{1}{N}\sum_{j=1}^{N}\vec{R}_j$$

$$R_g^2 = \frac{1}{N}\sum_{i=1}^{N}\sum_{j=1}^{N}(\vec{R}_i - \vec{R}_j)^2$$

Where R_{cm} is the mean position of monomers and $\vec{R}_i$ denotes the vector for a whole polymer molecule. It's worthy to mention that rathe dius of gyration of a sphere shaped molecule is not sathe me as its actual physical radius[52].

3.3 METHODOLOGY: MOLECULAR MODEL AND SIMULATION

3.3.1 Molecular Dynamics simulation details

In this section detail procedure for calculating the chi parameter using the molecular dynamics simulation is described using two different methods. These values will later be implemented as the input for DPD simulation to calculate the conservative force DPD interaction parameter and to define the force fields accordingly.

3.3.2 The energy of mixing, chi parameter calculations and Blends module

A blend methodology/approach is employed to estimate the chi parameter, based on the energy of mixing. This method calculates the miscibility of binary mixtures. To predict the χ_{ij} parameter, the input for this module is only the molecular structure of the components, which are *i* and *j* beads, and the force-field. In our research, we use the blends module in the Material Studio, Accelrys, to determine the Flory-Huggins chi parameter.

3.3.3 Cohesive energy density, solubility parameter, Amorphous cell and Forcite module

The solubility parameter is a temperature dependent factor, which is utilized to obtain the solubility behaviour of the mixture, based on cohesive energy density. Employing the Material Studio package, important parameters such as the solubility parameters, cohesive energy density, and Flory-Huggins chi parameter of any type of molecules are forecasted. In this method, the amorphous cell and Forcite modules are used to construct a cell containing an amorphous blend of two

components. Following this approach, we perform MD simulations to obtain the cohesive energy density values and corresponding solubility parameters. To prepare the cell for the actual calculation and make sure that the system is at the correct temperature, the particles should attain the equilibrium condition. Hence, an NVT ensemble (representing a dynamic process to equilibrate the system, while the number of moles, volume, and temperature are constant) using velocity scale thermostat is conducted.

3.3.4 Dissipative Particle Dynamics details

The DPD simulation is a mesoscopic coarse-graining method, which relies on the coarseness of the grains. It should be noted that the number of water molecules directly affects the computational accuracy of the interfacial tension calculation. An inaccurate model can cause large deviations from the experimental data. [64] In this simulation, three water molecules need to be grouped in one bead. The oil molecule is divided into four beads to satisfy the principle of volume equality in the beads. The surfactant tail is constructed by four beads, and four beads are attached by a harmonic spring to form the surfactant head. The spring constant is set to $k = 4$ and the equilibrium distance is assumed to be at $r_c = 1$. For simplicity, we adopt water bead, oil bead, and surfactant head and tail with the shortened notations of W, O, H, and T, respectively. The coarse-graining format for the beads present in the system is shown in Figure 1. As it is clear from Figure 1, three water molecules are bounded to create one W bead. Dodecane oil molecules are broken into 4 O beads; the surfactant molecules ($C_{12}E_6$) are in the format of 4 surfactant head group and 4 surfactant tail group or H4T4; and two beads connected together by a spring represent the NaCl molecules.

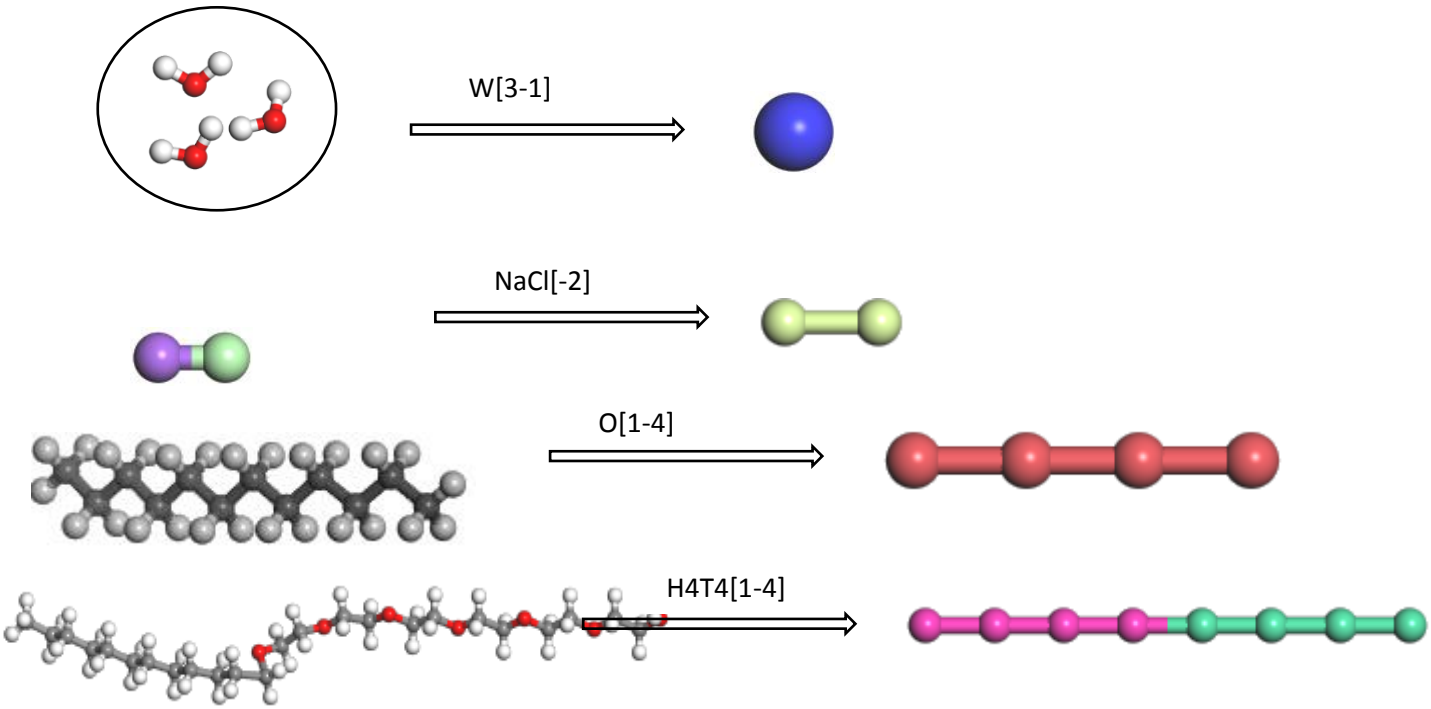

Figure 3-1 Coarse-graining scheme for the beads present in the system

All the calculation have been performed using the Mesocite module in the material Studio package [55]. The same volume, radius and mass are assigned to all the beads in the system. The number of water molecules (N_m) in each bead dictates the size of the beads where N_m shows the coarse-graining degree[56]. In our case, three water molecules were bound to form one bead, hence N_m=3. The molar mass of water is 18 gr/mol[57]; therefore:

$$V_{Water} = molar\ mass * \frac{1}{Density} * \frac{1}{Avogadro\ number} = \frac{18gr}{mol} * \frac{1}{\frac{1gr}{cm^3}} * \frac{1}{6.022 * 10^{23}\frac{molecule}{mole}} = 30\ A^{o3} \quad (15)$$

Hence the volume of one water bead when N_m=3 will be:

$$v_b = N_m v_{water} = 3 * 30 = 90 A^{o3} \quad (16)$$

Where v_b depicts the bead volume. The mass unit can be calculated based on the coarse-graining degree as follows[58]:

$$m = N_m m_{water} = 3 * 18 = 54\ amu \quad (17)$$

In Eq.17 m refers to the mass of the bead and m_{water} is the water molecule mass. To specify the bead structure in Material Studio we need to have the bead radius as well. To define the diameter of a bead consists of N_m water molecules, if ρ shows the number of beads per r_c^3 where r_c refers to the diameter of the bead which is used as the length scale in DPD calculation, the following equation can be used[41]:

$$r_c^3 = \rho N_m v_{water} \quad (18)$$

$$r_c = (\rho N_m v_{water})^{1/3} = (\rho N_m 30)^{1/3} = 3.107(\rho N_m)^{1/3}$$

$$\tau = 14.1 N_m^{5/3} \quad (19)$$

In the above equation, the degree of coarse-graining equals to N_m=3 and ρ which is defined as the bead density or the number of beads is $\rho = 3$ which is the properties of a liquid with the compressibility similar to of water[41; 56]. According to Eq*, $r_c = 6.64\ A^o$, and radius of the bead will be 3.32 A^o. The conversion factor used to change the DPD units to actual physical units is also given in Eq.13.As it mentioned before, in DPD simulation, the same mass, volume and radius is assigned to all the beads in the system and these values remain constant throughout the simulation steps[58]. The simulation cell contains around 10^4 beads. The calculation is performed

in a cubic simulation box with dimensions of 100*100*100 A^o and the temperature is set to 293 K ($K_BT = 1$) while the periodic boundary condition is applied in all the directions and the cell is big enough to perform the interfacial tension calculation[59] . The total time steps in the simulation is 50000 while the time steps set to 0.01 and the initial configuration of the system is random. What is worth taking a moment to flag is that the similar simulation was performed for longer total a time and smaller time steps and the results were found to be similar to the same case with the proposed shorter total time which substantially decreased the total calculation time. It is necessary to mention that both the surfactant and salt concertation in the simulation is the volume fraction of these beads in the cube. To calculate the interfacial tension values, the x-direction is set to be perpendicular to the water/oil interface. A schematic flow chart is presented in **Figure.2** which indicate the multiple steps to calculate the interfacial tension and other properties such as radius of gyration ation or concentration profiles from the DPD simulation.

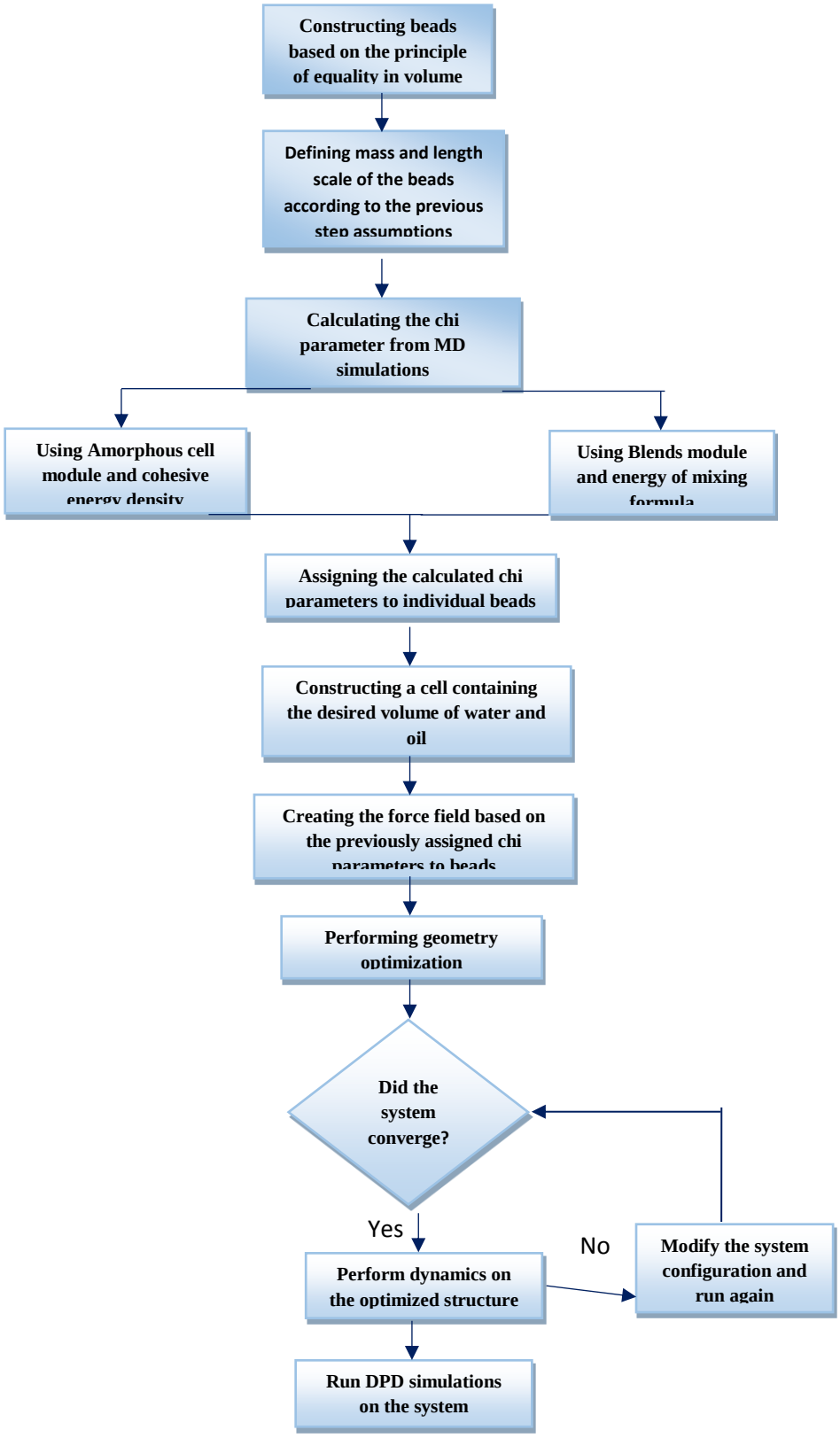

Figure 3-2 Schematic flowchart of DPD simulation

3.4 LIMITATIONS OF MD AND DPD

This section further highlights the drawbacks of the simulation approaches employed in this research work.

The limitations of Molecular Dynamic (MD) simulation are listed below:[15,16]

- Molecular dynamics strategy is proper for modeling/simulation at micro-scale levels.
- Classical mechanics is generally utilized in the MD simulation, while this approach exhibits poor performance to describe dynamic behaviors of very light particles.
- To attain numerical stability, the MD simulation runs need short time-steps.
- Variation in molecular structure of some cases/components might take nanoseconds, microseconds, milliseconds or longer, depending on the type and chemical structure of the substance.
- There is still a challenge with the timescale of MD simulations so that long time-scale is not feasible in most real cases.
- There are approximations with the force fields. Thus, selection of a suitable and precise force field remains a challenge.
- Some particular molecular bonds, which are important in chemical processes/phenomena, might not break or form over MD runs for simulating typical functions.

There are the following drawbacks with the Dissipative Particle Dynamics (DPD):[15-18]

- The DPD technique is suitable to simulate dynamic behaviors at meso-scales. Thus, DPD approach is not able to capture the molecular interactions at nanoscale and microscale levels, which are a key aspect at or close to boundaries.
- There are no clear physical definitions for some variables/parameters involved in the DPD approach.
- DPD units should be mapped to physical units according to the output characteristics.
- The system properties and constitutive equation should be known while implementing DPD.
- Further proper parameters and algorithms in the DPD method should be formulated in order to handle various complex problems including multiphase flow, complicated transport phenomena, and biological membrane where a variety of morphologies, geometries, and flow regimes might be involved.
- High computational costs are needed for most real applications. This encourages researchers to develop more effective and faster algorithms/procedures.

In addition to the above drawbacks, a comparison between the predictions and real data for some parameters such as radius of gyration in both MD and DPD approaches is not possible as those parameters cannot be measured or determined using laboratory tools.[15-18]

3.5 RESULTS AND DISCUSSION

In this section, the results of molecular dynamics and Monte Carlo methods to calculate the chi parameter are presented. The values of solubility parameter and energy of mixing are then calculated and reported. The effect of temperature on both of these variables is investigated and the results are presented through several plots. The DPD interaction parameter is the most

important output which is needed to obtain the interfacial properties. The effects of different variables such as surfactant and salt concentration, water cut, and temperature are also studied on both structural and interfacial characteristics of the system, which are represented through various figures in this section.

3.5.1 DPD conservative force parameter calculation

Our attempt is to investigate the effects of surfactant concentration, salinity, and temperature on the concentration profiles, the radius of gyration, and the interfacial tension. The main intention is to combine the physics at the atomistic level and to expand it to the mesoscopic scale using chi parameter calculations. This integration will decrease the computational time and offer a larger time and length scale. After performing a geometry optimization on the defined structure of the molecules in the system, a mixing task is conducted. The results of this phase of research investigation are presented in **Table 3**. Compatible molecules such as oil and surfactant tail appear to have a chi parameter close to zero, which indicates miscibility. The influence of temperature on chi parameter is another output of this module as depicted in **Figure 3**. As it is clear, by increasing temperature, the magnitude of chi parameter lowers, implying an increase in the miscibility of the molecules.

Table 3-2 Calculated values of energy of mixing and corresponding chi parameter for the molecules present in the system at T=298.15 K and atmospheric pressure.

Base	Screen	Emix	Chi parameter
Water	Oil	5.983	10.14154
Water	Surfactant Head	0.999	1.693
Water	Surfactant Tail	5.981	10.138
Surfactant Tail	Surfactant Head	2.0967	3.5538
Oil	Surfactant Tail	0	0
Oil	Surfactant Head	2.0967	3.5538

The results of the conservative force parameter calculations using the Blends module are reported in Table 3. According to Table 3, the results of the simulation are close to the data in the literature, implying a very good agreement between the literature data and predictions. This method provides a procedure to estimate the chi parameter through capturing the miscibility behaviour of mixtures. The thermodynamic behaviours of the system can be predicted directly from the beads chemical characteristics. Hence, by defining the molecular structure and the force-field type, the energy of mixing and corresponding chi parameter are calculated. **Figure 4** presents the distribution of the

solubility parameter of the molecules in the mixture as a function of temperature. According to Figure 4, the solubility parameter is not a strong function of temperature. Only for the case of water, the variation of solubility parameter is slightly noticeable. This is due to hydrogen-bond, which causes the cohesive energy density to be larger, compared to other molecules. The same trend is observed in the literature. [21]

Table 3-3 Cohesive energy density and solubility parameter of the components in the simulation

Component	**Density(gr/cm^3)**	**Molecular volume (A^{o3})**	**Echo**	**Solubility Parameter**
Water	1	30	3.144e+9	56
Oil	0.749	379.5	3.065e+8	16.9
Surfactant head	1.1132	82	1.008e+9	34.7
Surfactant Tail	0.85	93	2.859e+8	16.5

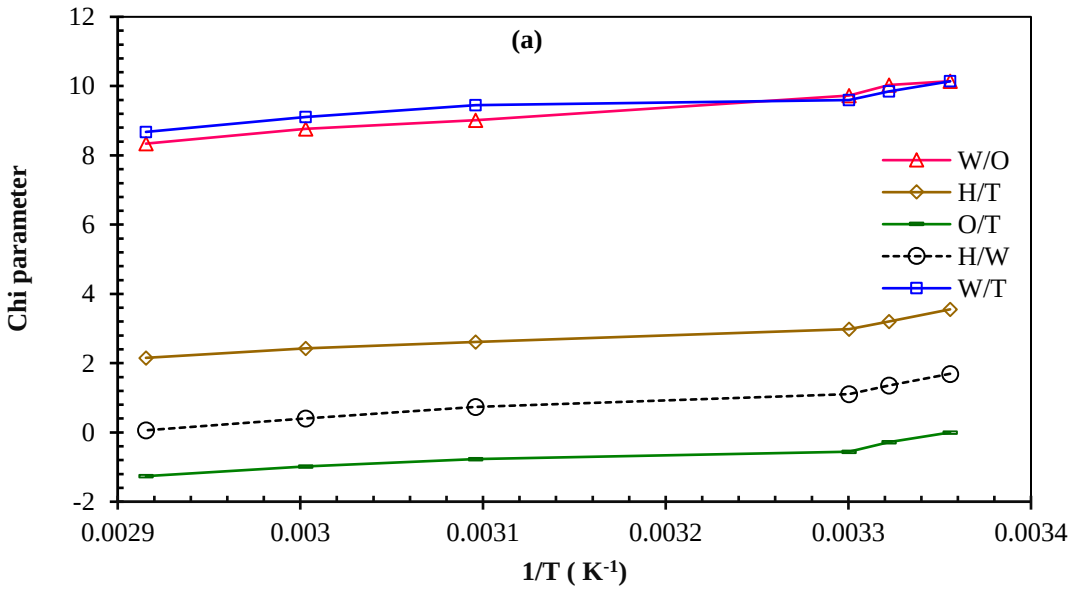

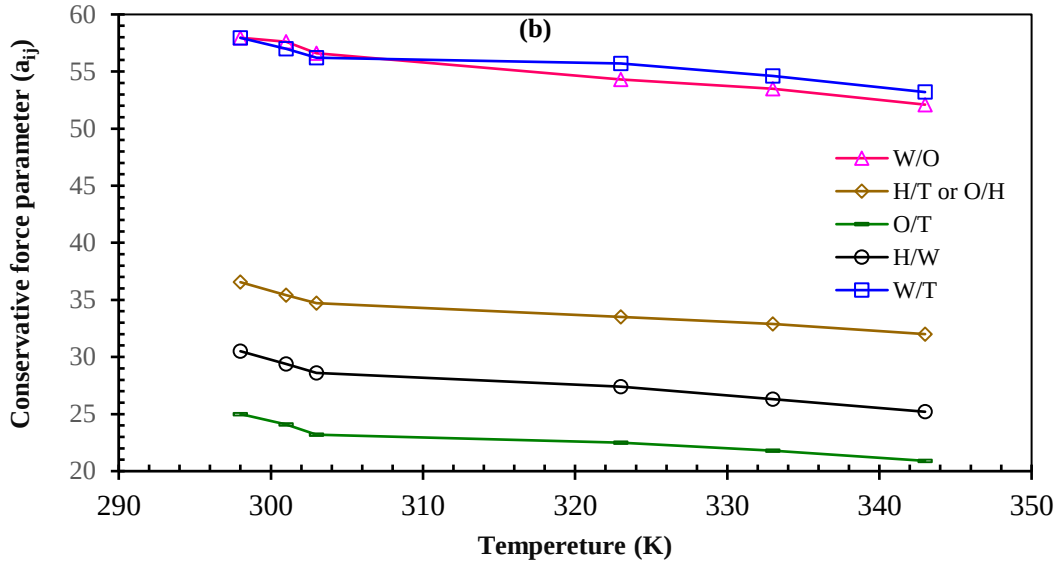

Figure 3-3 Effect of temperature on (a) dimensionless Flory-Huggins chi parameter of different components and (b) DPD interaction parameter.

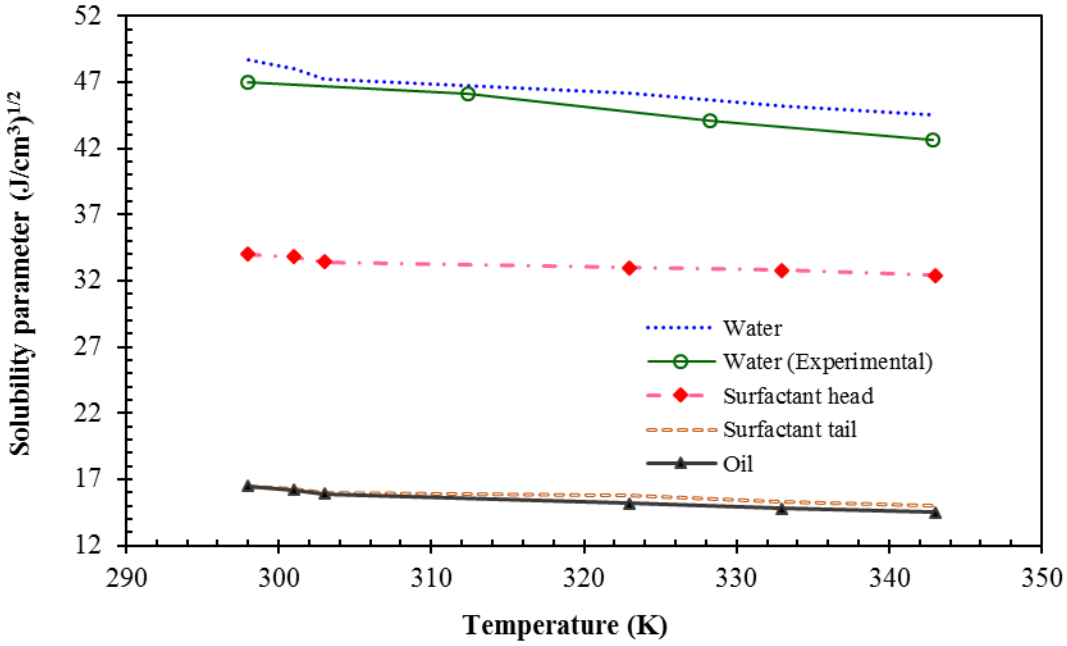

Figure 3-4 Solubility parameter for molecules present in the system as a function of temperature

The results of DPD simulations are usually determined based on two criteria. The coarse-graining method of molecules and the DPD beads interaction are a function of the coarse-graining mode. There are multiple methods in the literature to calculate the conservative force parameter (a_{ij}).

Groot and Warren[52], and Maiti and McGrother[64] proposed that *i-i* molecules experience the same type of interaction as *j-j* molecules, meaning that $a_{ii} = a_{jj}$. It was mentioned before that $a_{ii} = 25$. It was reported that this value gives reliable results for the oil/water systems IFT.[70] Hence, the same value is assigned to the interaction parameter of all the particles in the system in our model. As discussed before, the DPD conservative force parameter, (a_{ij}), is a function of Flory-Huggins chi parameter (χ_{ij}). a_{ii} represents the interactions between two similar beads (a_{ii}=25), implying no interactions between the beads. This parameter increases when the nature and structure of molecules are different. For example, a_{ij}=25 for the oil bead with the surfactant tail, since both of them are nonpolar aliphatic chains of hydrocarbons. However, a_{ij}=57.95 for the water beads with surfactant tail, since water is a polar molecule. To include the effect of salt on the interfacial behaviours of water/surfactant/oil, there are various methods to demonstrate the presence of salt in the system. Some researchers include the effect of salt by changing the DPD interaction parameter of water and no actual salt beads are considered in the system. [21] In this work, an individual bead is assigned to the NaCl molecule and a separate DPD interaction parameter is calculated for it such that it is possible to investigate and monitor the influence of salt on the interfacial and structural properties of the system.

The values of DPD interaction parameter based on the conservative force approach for the bead pairs in the simulations are obtained through calculating the energy of mixing and cohesive energy density according to Equation (7) and Equation (11). The corresponding results are shown in **Table 4**.

Table 3-4 DPD interaction parameters for different beads present in the system

	T	**H**	**O**	**W**	**NaCl**
T	25				
H	36.5	25			
O	25	36.66	25		
W	57.95	30.5	57.96	25	
NaCl	60	32	60.4	25.5	25

3.5.2 Spatial structure of water/surfactant/oil system

One way to describe the surfactant structure at the oil/water interface is to study the snapshots directly taken from the structure at different timesteps during the simulation. Snapshots of the water/surfactant/oil cell for different surfactant and salt concentration and varying water/oil ratio are shown in **Figure.5**. According to the DPD interaction parameter and the corresponding chi parameter calculated in the previous section, beads with similar chi parameter or aij values are more miscible. Based on Table.2 oil and surfactant heads group are almost miscible. Hence surfactant head beads will stretch toward the oil phase. Same goes with surfactant head group and water molecules. Water is a polar molecule and will attract the surfactant glad group via dipole-dipole bonding. The NaCl molecules also disperse into the water phase through electrostatic forces. The oil/surfactant/water system goes to the same structure in the presence and absence of salt. It can be clearly observed than by the time; surfactant molecules adsorbed at the interface while their tail group oriented toward the oil phase and head group attached to the water phase and NaCl beads disperse in the water. By comparing the final structure of the system (1) and (3), the number of surfactant molecules and the interface thickness has clearly increased by surfactant concentration. According to the magnified images at the surface, in case of WC=0.25, the surface will curve toward the oil phase which case the water molecules to be captured, and water-in-oil emulsion will be formed, when WC=3, the interface will curve toward the water phase, causing the oil molecules to be surrounded will water molecules and oil-in-water emulsion will be the result of this configuration. This result is in accordance with previous work by Li et al.[61] on the effect of water cut on the type of emulsion formed. Another point worth to mention is that, by comparing the final structures of case (a) and (C), when the surfactant concentration is low the head and tail groups scatter at the interface randomly. When the surfactant concentration increases to 15% at case (A), the rearrangement of surfactant molecules is now more compact and ordered at the interface.

By simulation initiation, the surfactant head and tail groups starts to orient based on their bonding preference, as they are accumulating at the interface, the surface area is being saturated with surfactant molecules and by the time, this interface will bend to expand and create more space and area for surfactant molecules to be adsorbed at the interface, that's why the interface at the final configuration is more curved compare to the initial structure.

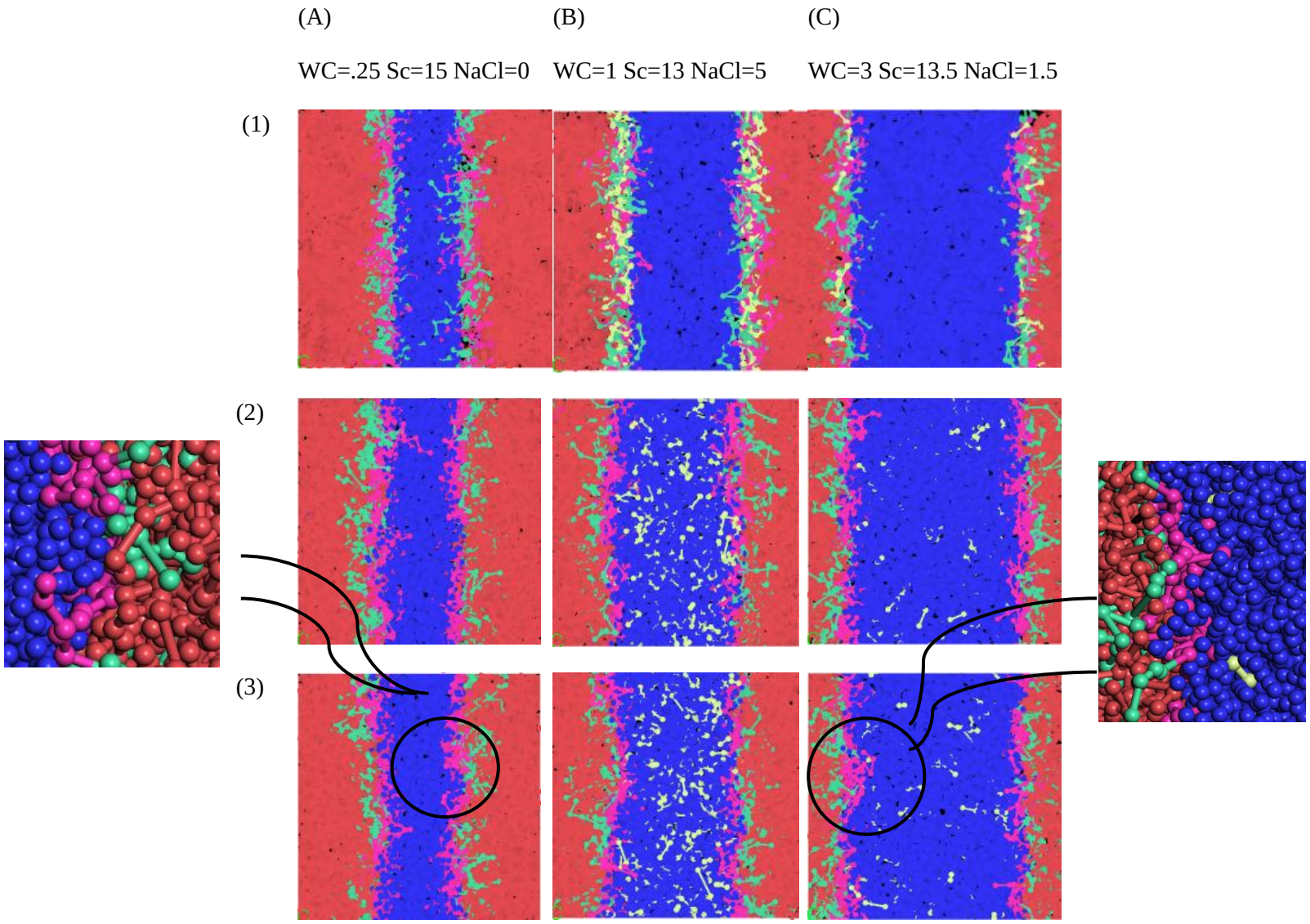

Figure 3-5 Snapshots of the water/surfactant/oil system simulation at different WC, Sc and salinity of (a) WC=.25 Sc=10 NaCl=0, (b) WC=1 Sc=13 NaCl=5, (c) WC=3 Sc=13.5 NaCl=1.5 at three different time steps of (1) Initial configuration, (2) half of simulation time and (3) final structure. Water beads are shown in blue, oil beads in red, surfactant head in pink, surfactant tail in green and salt beads in yellow.

3.5.3 Effect of surfactant concentration on interfacial and structural properties

A key aspect of surfactants is their ability to lower the interfacial tension in water/oil mixtures. The interfacial characteristics of oil/water systems are crucial in various industrial applications such as chemical EOR proceses[69] and pharmaceutical industry.[72] To examine the overall efficiency of surfactants, their abilities to reduce the interfacial tension and the absorption tendency of the head and tail groups are investigated. To study the characteristic of surfactant, the relative concentration profiles for different beads existing in the system are obtained according to the snapshots of the simulation, as demonstrated in **Figure 6** for different surfactant concentrations. This property indicates the distribution of different beads present in the system, which can be calculated by averaging the number of beads per volume across the length of the simulation box. In the relative concentration profiles, it is obsered that water and oil phases have their own distinct relative concentration, indicating that the system is large enough to describe each phase characteristics, separately. Based on the concentration profiles in Figure 6, a well-defined interface can be detected between the oil and water phases. According to Figure 6, the concentration profiles for surfactant molecules grow higher with increasing the surfactant concentration, implying that the concentration of surfactant molecules increases at the interfaces and the beads are more packed at the interface. Simultaneously, the width of the peak for surfactant beads increases as well. It can be concluded that the interface thickness increases as more surfactant is being added to the system.

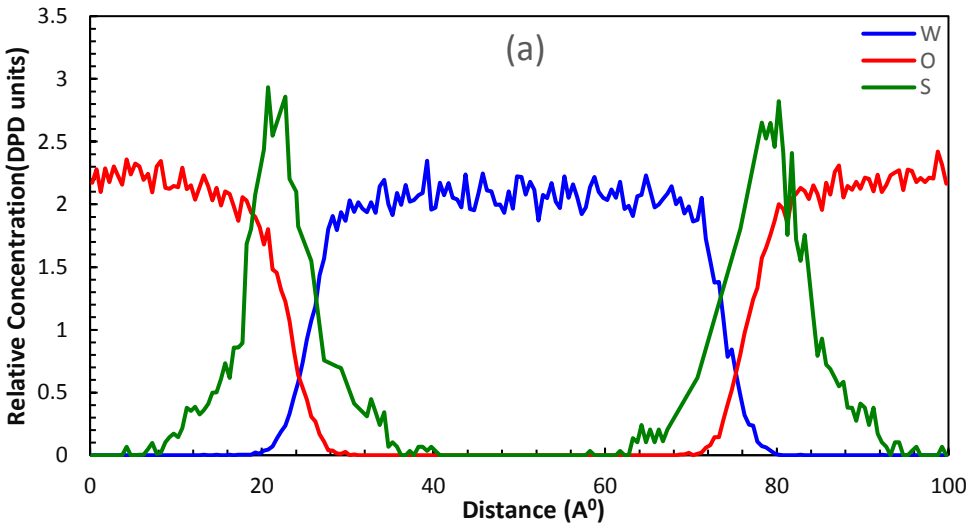

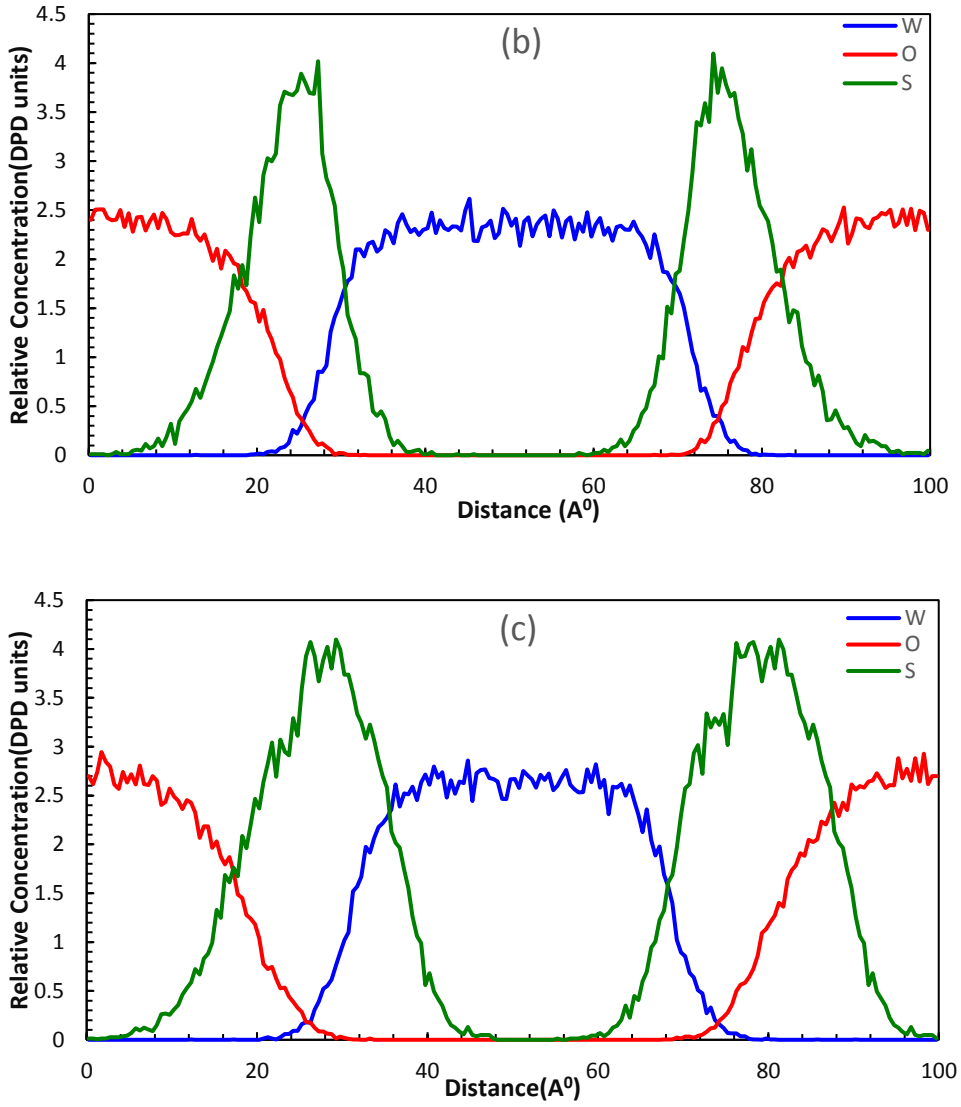

Figure 3-6 Relative concentration profiles at water content WC=1normal to the interface for different surfactant concentration (a) Sc=5%, (b) Sc=15% and (c) Sc=25%

To gain more insights into the structural behaviour of the beads under the surfactant concentration change, the values of the Radius of Gyration is investigated during the simulation time. As it mentioned before, this parameter describes the degree of stretching. As it is evident from **Figure 7,** the values of Rg increase and then reach an equilibrium and fluctuates around a certain value by the time. High values of Rg indicates that the surfactant molecules are oriented in the perpendicular direction to the interface. Fluctuation can be noticed more when the surfactant concertation is low mainly because the interface has not yet been saturated with surfactant molecules and the overall increase demonstrate that the surfactant chains are become straighter, however, less fluctuation can be noticed at high surfactant concentration, mainly because the interface is saturated with surfactant molecules now and the hydrophobic segment of surfactant turn into oil and hydrophilic

head attracted to water phase, that's why the Rg values is almost invariable. The magnified image on the orientation of molecules at the interface shows how the salt molecules dissolve and attracted to the water phase and the stretching of head and tail groups of surfactants toward water and oil phase respectively.

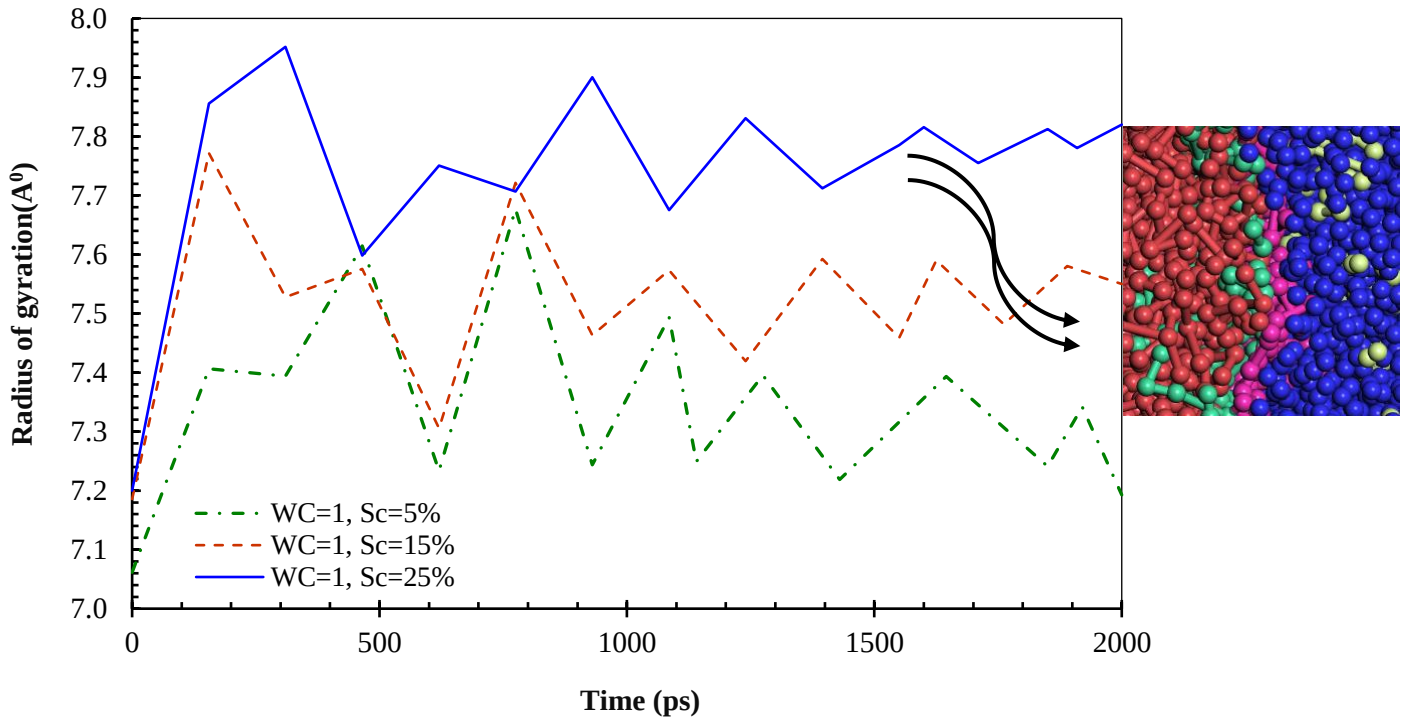

Figure 3-7 Effect of surfactant concentration on Radius of Gyration at water content WC=1 and different surfactant concentration

The surfactant concertation has a significant effect on the stability of water/oil mixtures. The effect of surfactant concentration for different water/oil ratios is provided in **Figure 8**. As it is evident from the figure, interfacial tension decreases strongly by addition of a surfactant and will approximately become zero when the oil/water interface is fully saturated with the surfactant molecules. When the number of surfactant molecules in the mixture increases, more molecules will aggregate at the interface. The polar head of the surfactant molecule will be adsorbed by the water molecules by dipole-dipole interaction, and the non-polar tail of the surfactant will be attracted toward the oil phase by covalent bonding. This configuration causes the interfacial tension of the interface to decrease, and when the density of the surfactant molecules increases at the system, the interfacial tension value will drop more. This trend continues until the interface is saturated with surfactant molecules and after his point increasing the concentration of surfactant is not changing the IFT anymore, and the add surfactant molecules will disperse into oil or water phase.

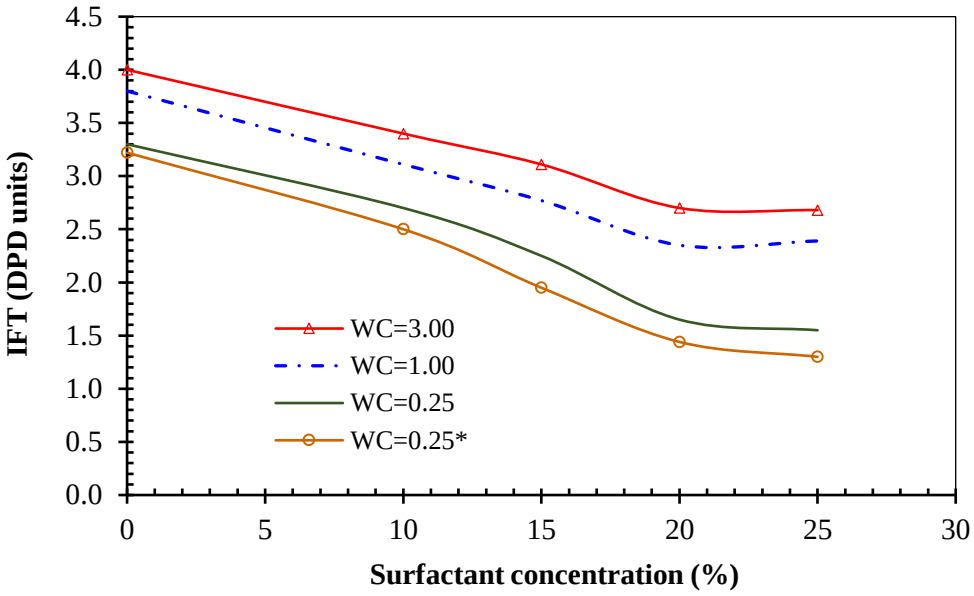

Figure 3-8 Effect of Surfactant concentration on Interfacial Tension values

3.5.4 Effect of salinity on surfactant adsorption behaviour

In this section, the influence of inorganic salt concentration on the absorption behaviours of the surfactant at the oil/water interface is analysed. **Figure 9** shows the relative concentration profiles versus the salinity at a specific water content and surfactant concentration. As it is evident from Figure 9, the NaCl molecules will disperse through the water phase by forming ion-dipole bonding. It is also confirmed from the calculated conservative force parameter (a_{ij}) for the water and NaCl beads that shows the compatibility of the two molecules. By increasing the NaCl concentration in the system, the salt profile exhibits higher peaks. It is observed that increasing NaCl bead concentration results in an increase in the absorption capability of the surfactant molecules at the interface. This is evident according to a higher peak of the surfactant concentration profile which, illustrates more surfactant packing at the interface.

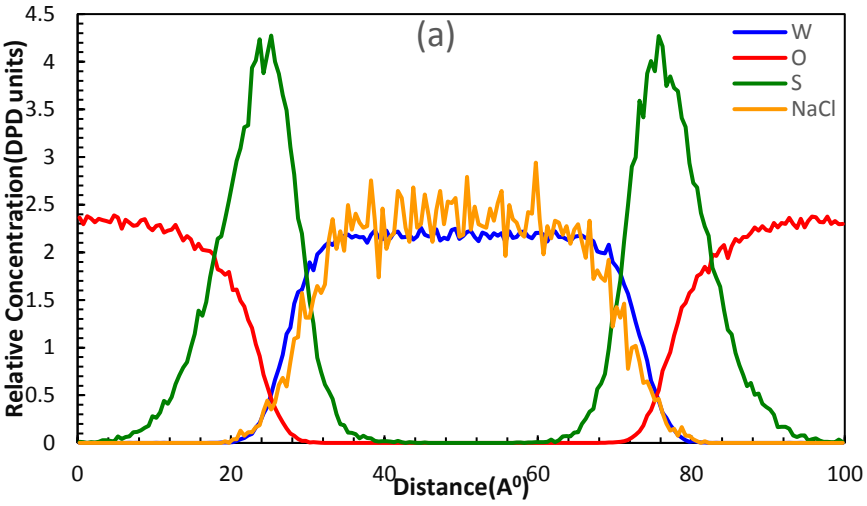
(a)
W
O
S
NaCl
Relative Concentration(DPD units)
Distance(A⁰)
0
0.5
1
1.5
2
2.5
3
3.5
4
4.5
0
20
40
60
80
100

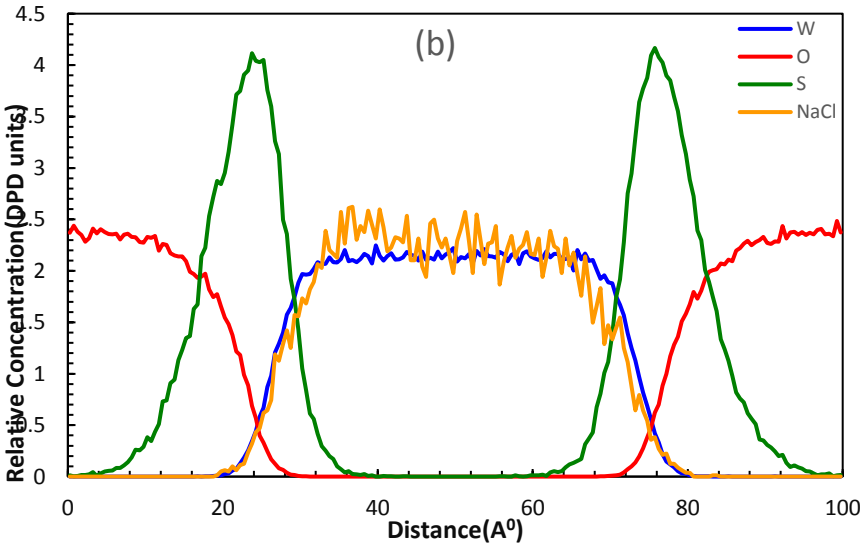
(b)
W
O
S
NaCl
Relative Concentration(DPD units)
Distance(A⁰)
0
0.5
1
1.5
2
2.5
3
3.5
4
4.5
0
20
40
60
80
100

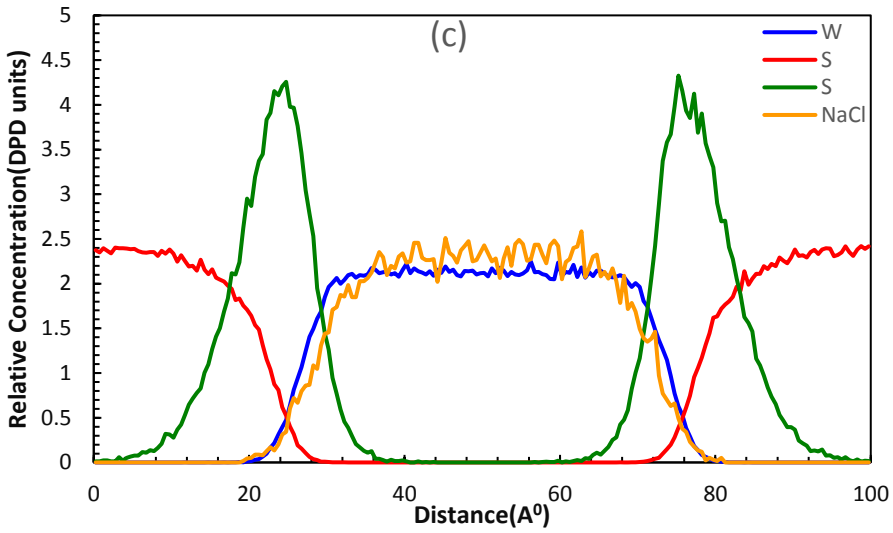

Figure 3-9 Effect of salinity on concentration profiles at water cut=1, Surfactant concertation=10% and (a) NaCl=2%, (b) NaCl=3%, and (c) NaCl=5 along the x-axis normal to the water/oil interface

To investigate the effect of salt in the system, the values of interfacial tension are determined at different surfactant concentrations, water-cuts, and salt concentrations, as presented in **Figure 10**. As it is clear, the interfacial tension decreases significantly by adding a small amount of the salt to the system. The interfacial tension reduction is dependent on the number of surfactant molecules absorbed at the water/oil interface. By increasing the salt concentration in the system, the electrostatic repulsion between the surfactant head molecules will decrease. The electric double layer around the surfactant head beads will be also compressed due to the presence of the electrolyte in the system, which causes the surfactant molecules to pack closer at the interface. Hence, the interfacial tension will be lowered further as more surfactant molecules are absorbed at the interface. However, after adding more salt, the IFT remains unchanged. This behaviour can be attributed to the interactions between NaCl molecules and polar surfactant head groups. The mutual repulsion between the surfactant polar head beads is partially shielded because of the ions released in the system. The absorption capability of the surfactant will be increased/ improved at the interface; however, once the surfactant concentration reaches a maximum value at the interface (e.g., CMC), adding more salt does not affect the density of surfactant molecules at the interface. Hence, the IFT remains almost constant.

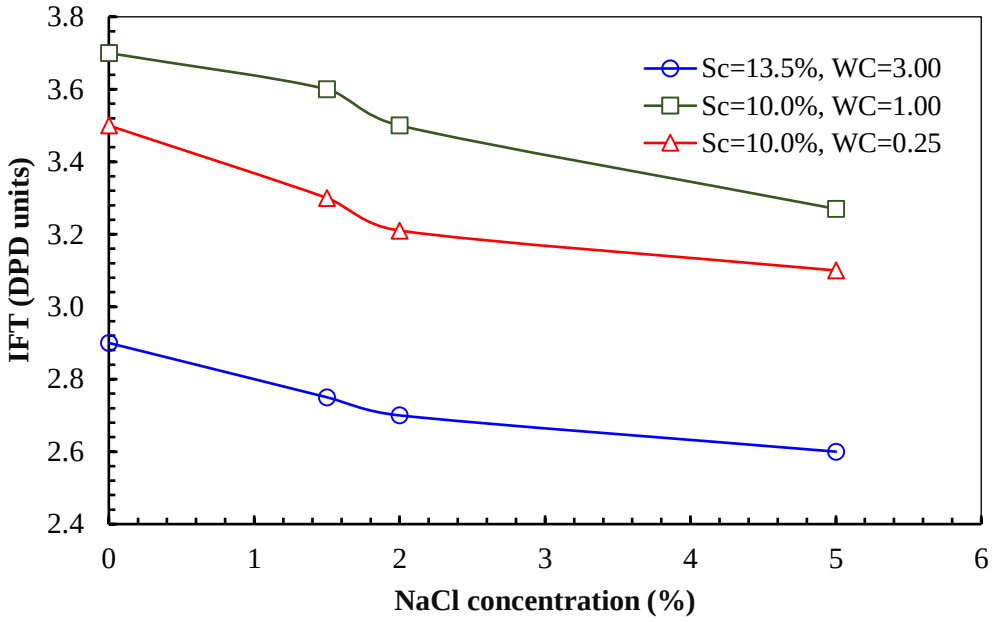

Figure 3-10 Effect of Salinity on IFT at different surfactant concentration and water/oil ratio in the system

To describe the impact of salinity on the structure of surfactant molecules at the water/oil interface, the variation of gyration radius of the surfactant molecules with time is shown in **Figure 11** for two cases [water cut (WC)=1 and a surfactant concentration (Sc) of 13.5% & WC=0.25 and Sc=10%]. The R_g parameter for different salt concentrations experiences an initial spike and fluctuates by the time. Based on Figure 11, the presence of salt (and increasing its concentration) lowers the repulsion between surfactant head groups and causes the surfactant molecules to accumulate easier at the interface. When there is a high salinity in the system, the water molecules form a negative and positive partial charge on their oxygen and hydrogen head, respectively. Once the salt is dissolved in water, the salt will be attached to the water molecules through an ion-dipole bond. According to **Figure 12**, the water molecules are occupied with the ions in the system. The higher the salinity of the system, the more water molecules are occupied with them. This phenomenon causes a reduction in the degree of stretching for the surfactant molecules as fewer water molecules are available to interact with the surfactant head groups. This is the main reason that the *Rg* experiences a decrease trend when the salinity in the system increases.

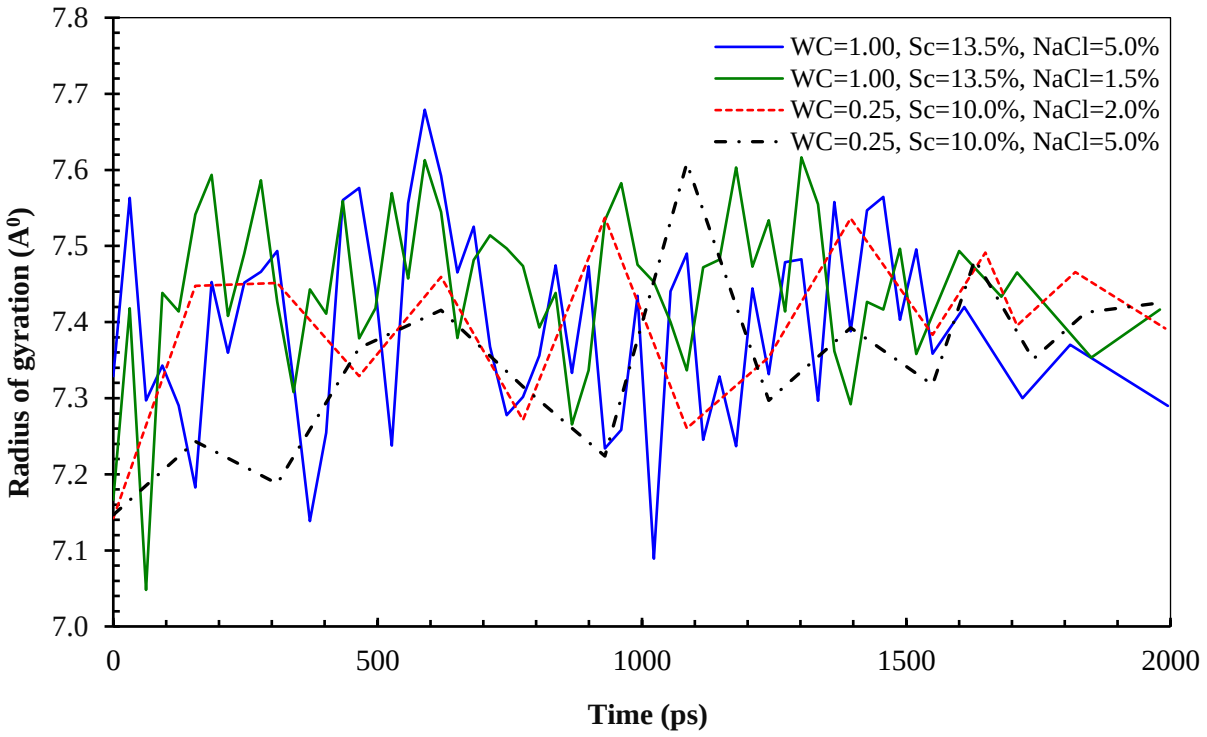

Figure 3-4 Effect of salinity on Radius of Gyration at T=298.15K

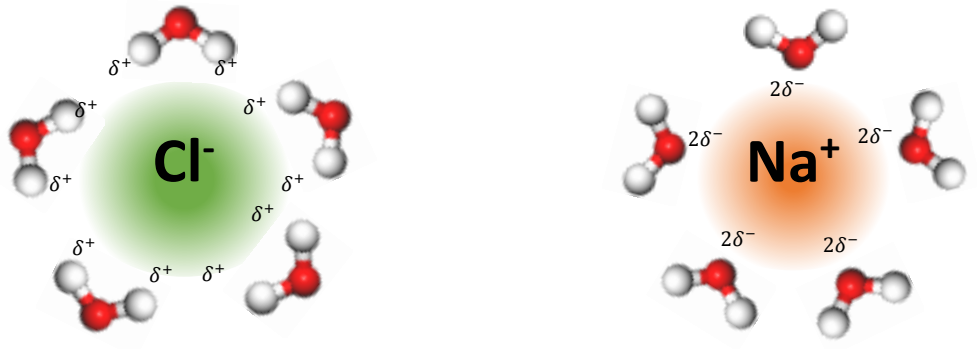

Figure 3-12 Schematic figure on the behaviour and configuration of dissolved salt ions in water (modified after[63])

To investigate the effect of salt type, the interfacial tension values for different concentrations of $CaCl_2$ are also calculated at a temperature of T=298.15K and a surfactant concentration of Sc=15%. The results for both NaCl and $CaCl_2$ are shown in **Figure 13**. As it is clear from Figure 13, by increasing the $CaCl_2$ concentration, the magnitude of the interfacial tension of the system will be lowered as expected. This behaviour/trend is the same for NaCl and $CaCl_2$ cases while studying the effect of salt. In fact, the presence of ions in the system decreases the electrostatic repulsion between the surfactant molecules and cause them to pack easier at the interface, leading to a decrease in the interfacial tension. This effect is more pronounced for $CaCl_2$ molecules as the

number of dissociated ions in the system is higher, compared to the NaCl case. Thus, a greater reduction in the system interfacial tension due to the presence of $CaCl_2$ is noticed. It is worth noting that if the concentration of the salt exceeds a certain value depending on the temperature and surfactant concentration conditions, the interfacial tension will start to increases by adding more salt molecules to the system, since the excess ions will create a barrier between the oil and water phases, causing a reverse behaviour in terms of IFT versus salt content.[75,76]

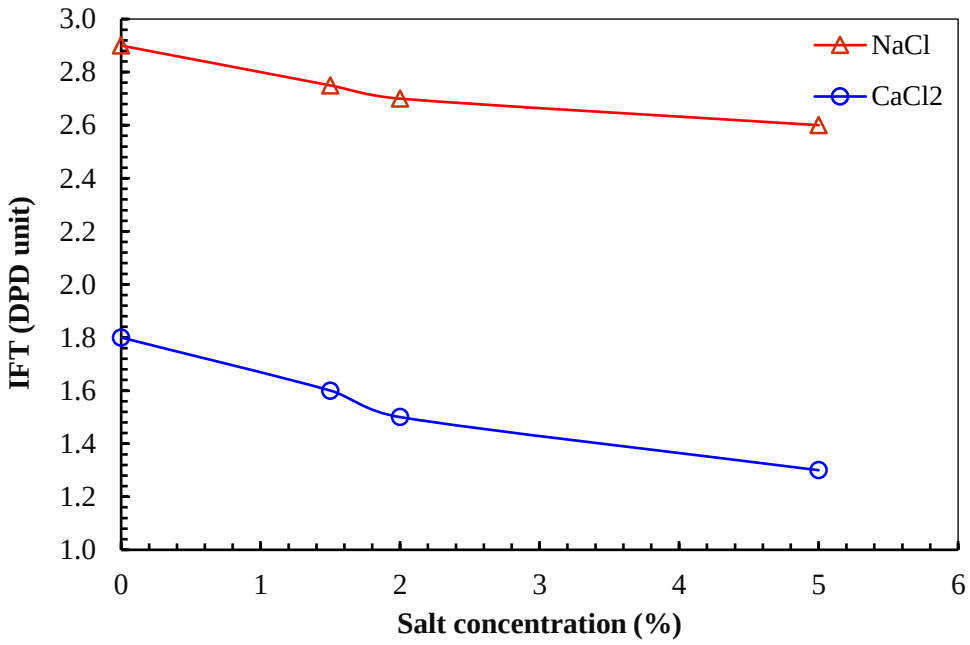

Figure 3-5 Effect of NaCl and $CaCl_2$ on IFT at different concentrations in the presence of surfactant (Sc=15%) at T=298.15K and atmospheric pressure.

3.5.5 Effect of water content on the interfacial and structural behaviour of the system

To analyse the effect of water content on concentration profiles of the beads present on the system, three cases are considered at different water/oil ratio and a specific surfactant concentration of Sc=13.5% and Salinity of NaCl=1.5%. As it is evident form the results shown in **Figure 14**, concentration profiles do not seem to be a strong function of the water content of the simulation cell. The packing of surfactant molecules at the interface remains unchanged with an increase in water/oil ratio.

According to the phase volume theory, the type of emulsifier, oil and water phase characteristics, preparation mechanism and phase volume fraction, control the type of emulsion formed in the system[23]. As it was observed before, when the water content is 0.25, water-in-oil emulsion was formed in the system, while at WC=4, oil droplets were formed in the aqueous solution and oil-in-water emulsion was detected. At low water/oil ratio, water droplets will form with the help of surfactant while the oil is the continuous phase and the rest of surfactant molecules are dispersed

into the oil phase freely as there is not enough interface for the surfactant molecules to be adsorbed. When the water content increase in the system, an interface will be formed between the oil and water phase. In this transition zone, no droplets were found in the system. Hence the interfacial tension starts to increase. By the continuous increase in water concentration, this time oil droplet will aggregate in the form of droplets, and interfacial tension drops again. **Figure 15** shows the effect of water content on interfacial tension values. As it is evident form the figure, the interfacial tension increases and then decrease with water content increase in the system. Based on the configuration of the surfactant molecules at the interface, one can conclude that interfacial tension is dependent on the morphology of the system.

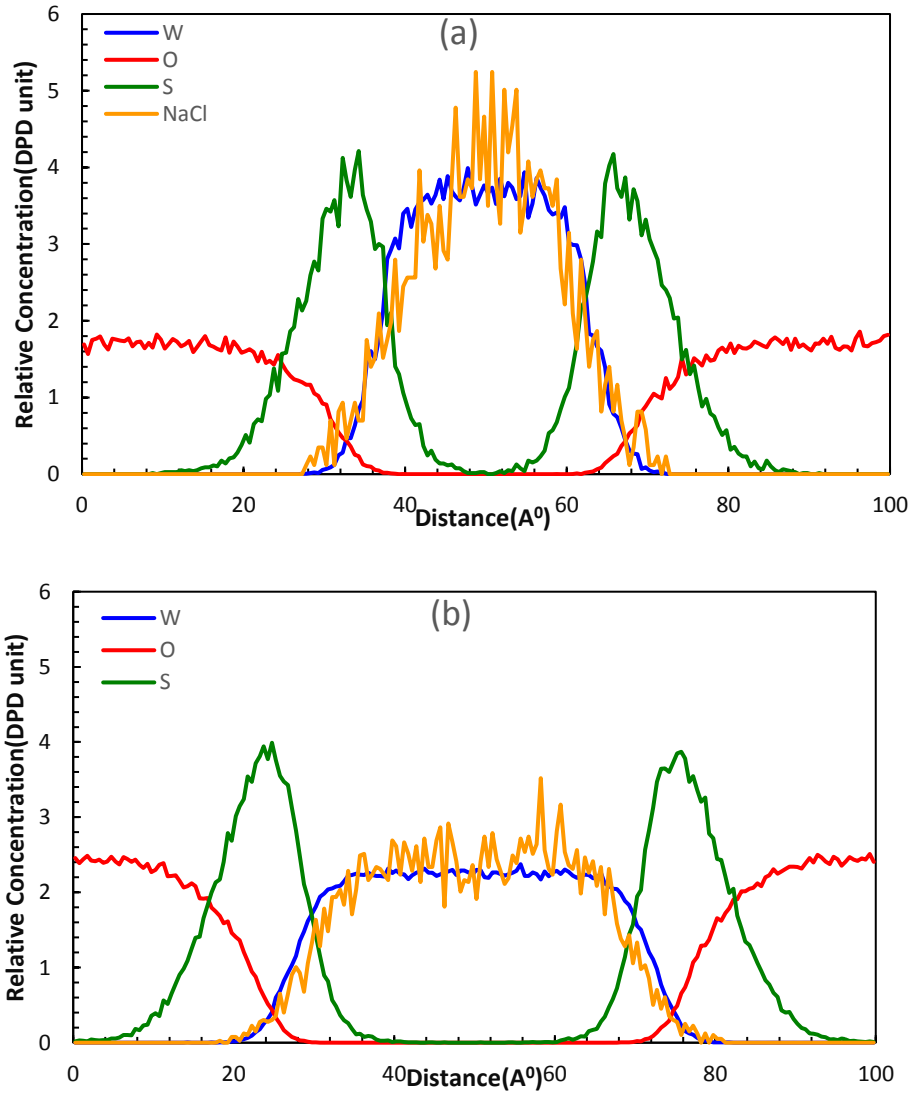

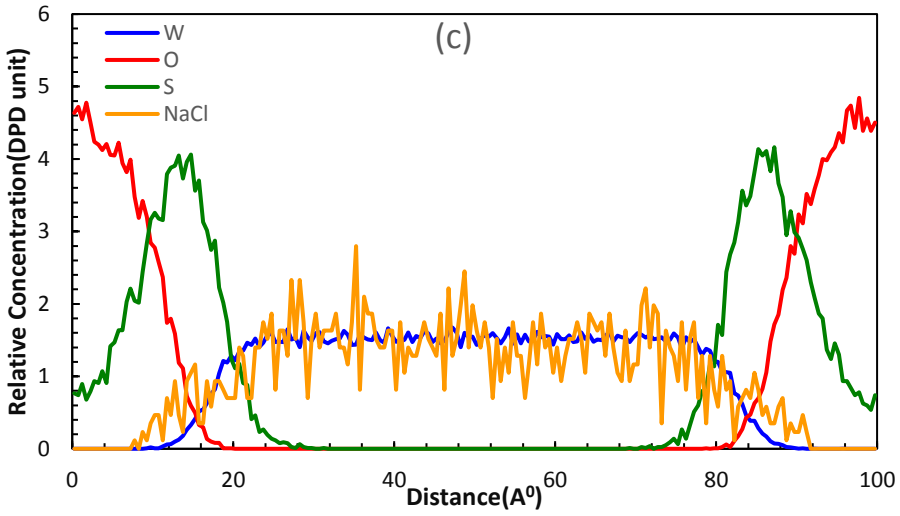

Figure 3-6 effect of Water Content on concentration profiles for Sc=13.5% and NaCl=1.5 and (a) WC=0.25 (b) WC=1 (c) WC=3

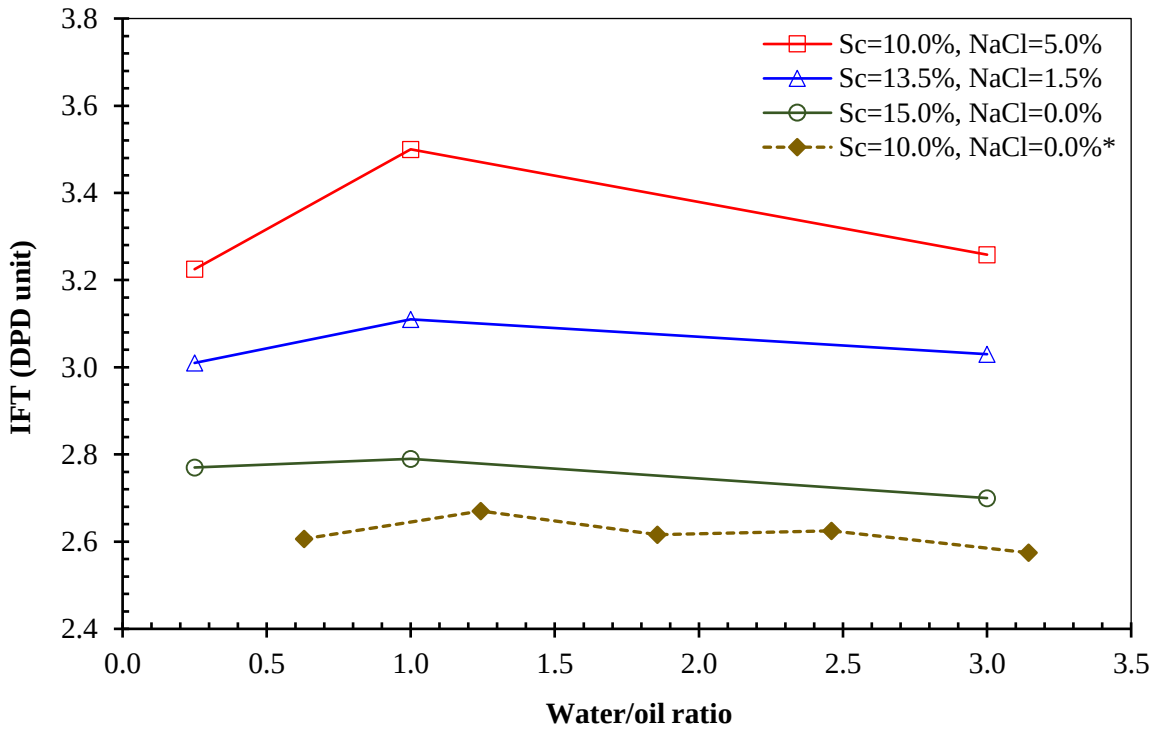

Figure 3-7 Interfacial tension versus water content at different surfactant concentrations [*Literature data are extracted from the reference [73]] at T=298.15 K and atmospheric pressure.

To investigate the effect of water content on the structural behaviour of surfactant at the interface the value of the radius of gyration is plotted versus simulation time for three different water/oil ratio at Surfactant concertation of Sc=13.5% and salinity of NaCl=1.4 %. An increase in the value

of Rg indicates that the molecules are more stretched and aligned to more extent in the perpendicular direction to the water/oil interface. As it is clear from **Figure 16**, Rg shows bigger numbers when the water/oil ratio is higher. The fluctuation in the trend is obvious since the surfactant molecules have not yet been saturated at the interface. The straight line, however, is observed after simulation initiation for water cut=0.25. This trend can be justified by knowing the fact that presence of salt causes the surfactant molecules to pack easier and since the salinity is low in the system, and the volume of water is less than other cases the interface will be saturated sooner with the surfactant molecules. Hence no big fluctuations would be observed in Rg values. This reason behind this behaviour is that, in case of high water content in the cell, after all the dissolved salt ions are surrounded by partially polar water molecules, there is still some space for surfactant head groups to stretch toward water molecules, hence the Rg fluctuates as a sign that surfactant molecules are still packing at the interface, while when the water content is less, after they interact with ions present in the system through ion-dipole bonds, the number of water molecules available at the interface is less and equilibrium reaches faster.

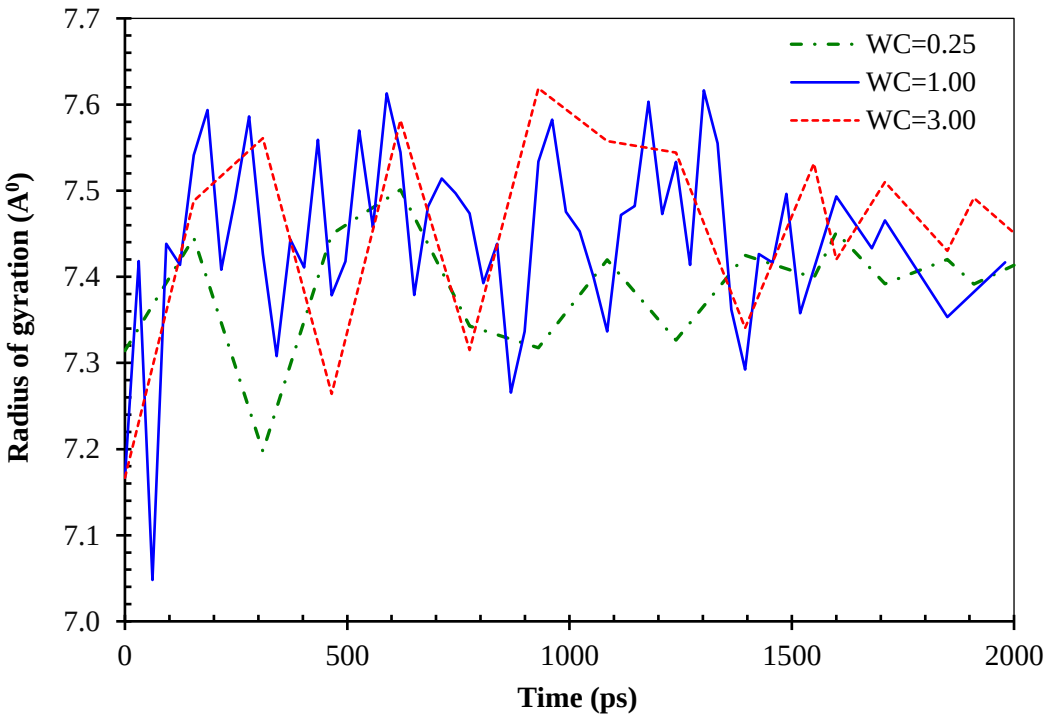

Figure 3-8 Effect of WC on radius of Gyration at Sc=13.5% NaCl=1.5%

3.5.6 Effect of temperature on interfacial and structural properties of the system

In this section, we analyze the effect of temperature on the structural and interfacial behaviours of the water/surfactant/oil systems in the presence of salt. The surfactant molecules are easy to absorb at the water/oil interface, due to tendency of the head and tail groups to the water and oil phases respectively, leading to the formation of an interfacial film. The characteristics of the interfacial

film are influenced by the properties of the surfactant and oil. Temperature appears to be a dominant factor affecting the surfactant characteristics at the water/oil interface. **Figure 17** represents the relative concentration profiles of the beads in the system at three different temperatures. According to Figure 17, by increasing temperature, the relative concentration of the water, oil, and NaCl beads remains constant; however, the relative concentration of the surfactant molecules is influenced by the temperature. It is obvious from Figure 17 that the concentration of the surfactant molecules at the interface increases and the interfacial film thickness decreases with increasing temperature. The main reason for the behaviour is that most of the surfactant molecules are accumulated and oriented at the interface based on the peak height in the surfactant concentrations.

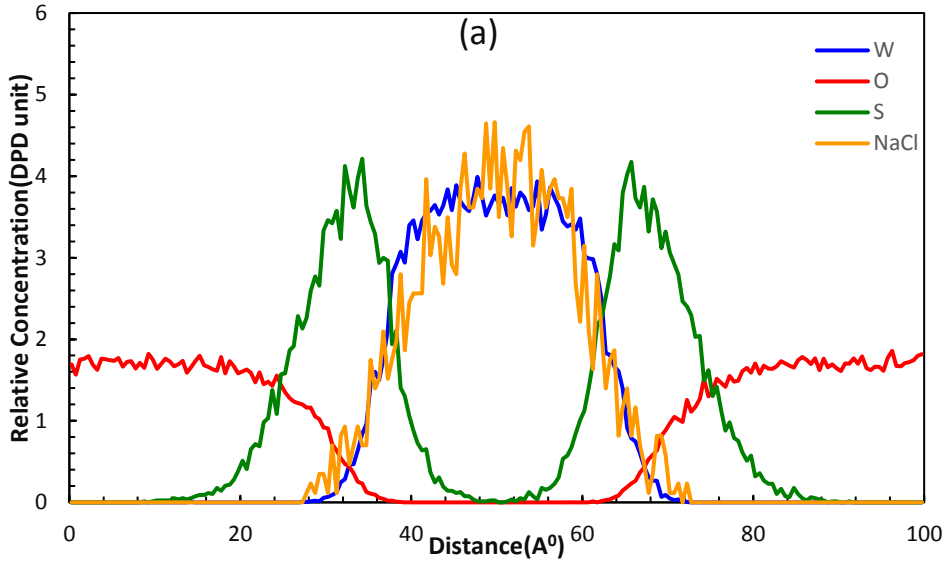

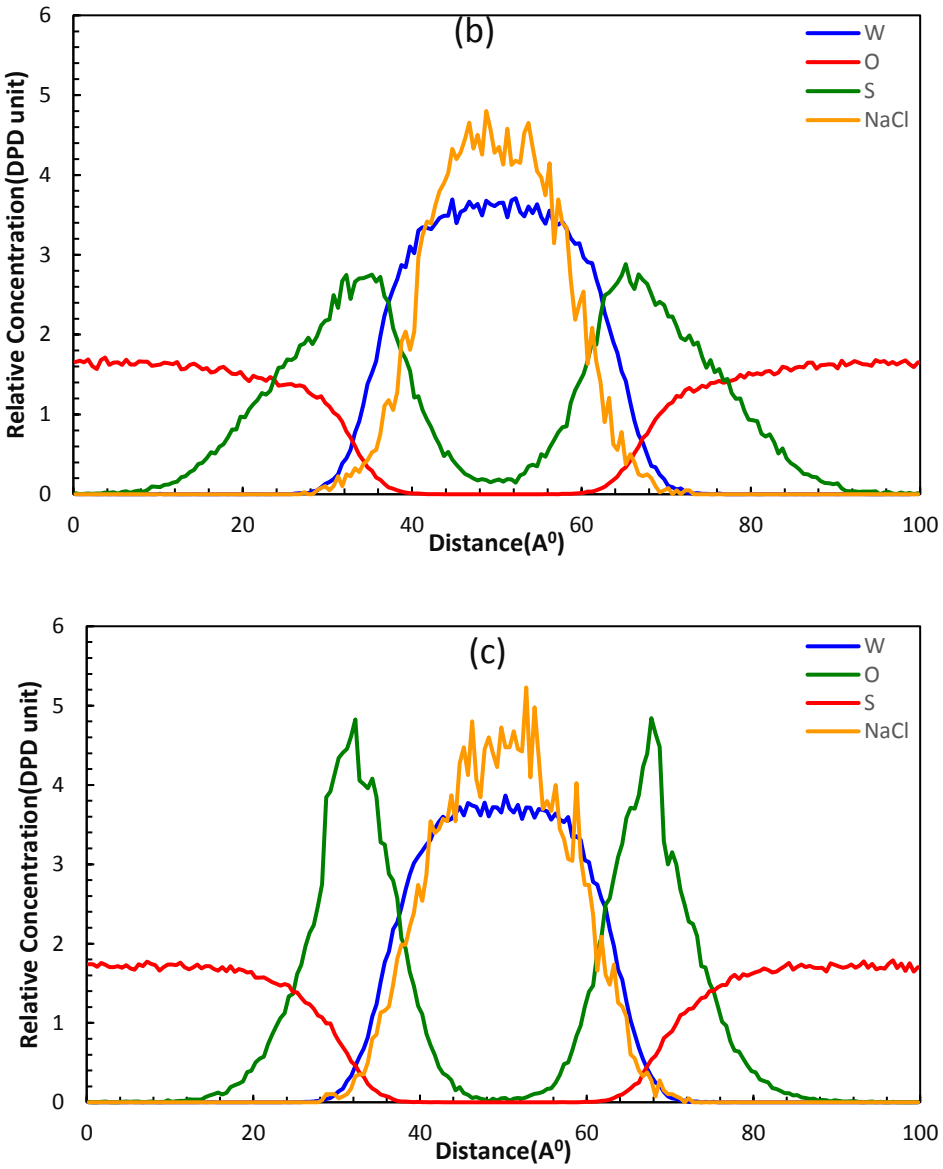

Figure 3-9 Concentration profiles of water/surfactant/oil system with presence of salt at WC=0.25, Sc=13.5, NaCl=1.5 at different temperatures of (a) T=298K, (b) T=323K, and (c) T=343K

The instantaneous values of gyration radius at various temperatures are compared in **Figure 19**. It is observed that the R_g values are increased with increasing temperature. In fact, when the temperature increases, the interface does not need to bend for creating an excess area for the surfactant molecules to be absorbed at. There are two reasons for this phenomenon. Firstly, by increasing the temperature, the hydrogen bond strength and the electrostatic interactions between the water and the polar head group increase. [77] Secondly, increasing temperature leads to maintaining the van der Waals repulsive forces between the oil and surfactant tail to weaken. As a result, the surfactant modules will extend at the interface, and the radius of gyration will increase over time accordingly.

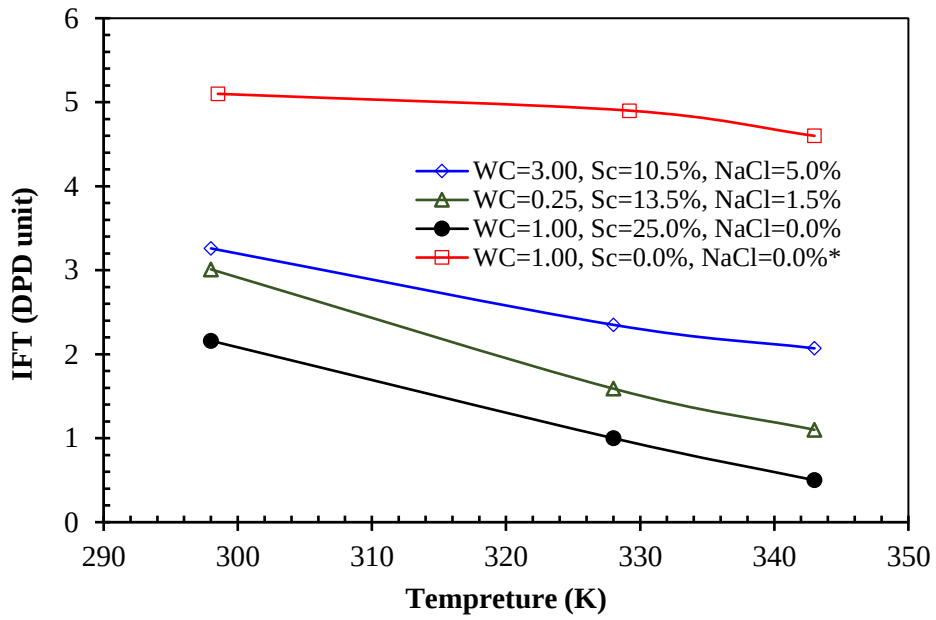

Figure 3-10 Effect of Temperature on Interfacial tension variation at different water-cut, surfactant concentration and salinity values

Figure 18 shows the variations of the interfacial tension with temperature where different water-cuts, surfactant concentrations, and salinities are tested. It is found that by increasing the temperature, the interfacial tension is reduced. This behaviour can be attributed to the enhancement of surfactant activity and an increased absorption at the interface due to an increase in the temperature, leading to a decrease in the interfacial tension. As it is evident, the slop of the line for a higher surfactant concentration is greater. Providing a justification, at a low surfactant concentration, the number of surfactant beads at the interface is low. Thus, the temperature effect cannot be monitored well, compared to the high surfactant concentration sample, where there is a large number of surfactant molecules at the interface and the effect of temperature is more pronounced. The same trend was observed experimentally by Alasiri[65] in the absence of surfactant.

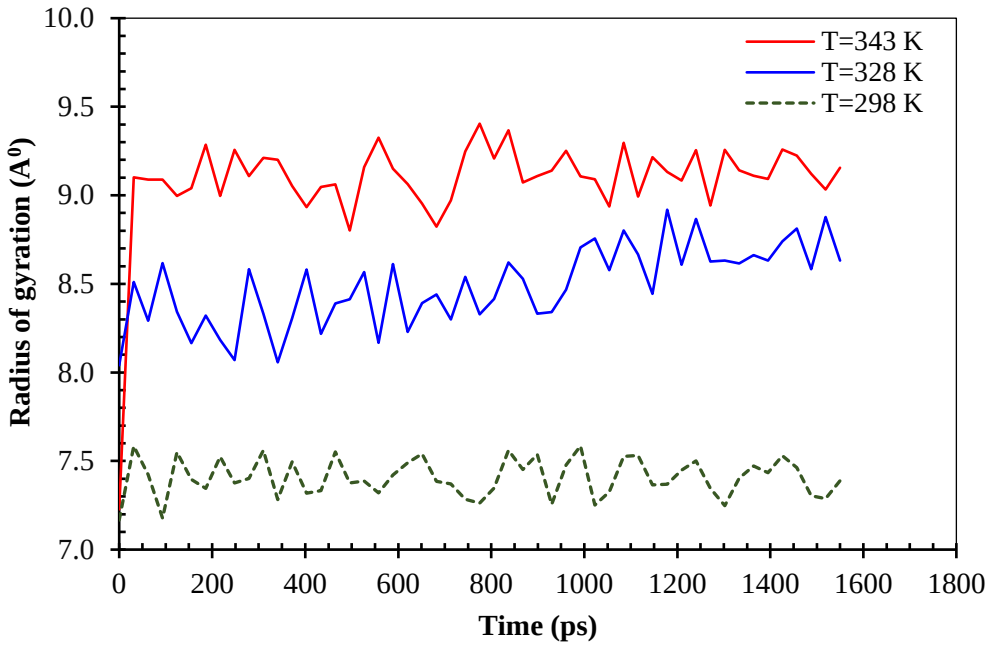

Figure 3-11 Effect of temperature on Radius of Gyration values at three different temperature values of 298K, 328K, and 343K

There are several petroleum reservoirs with the favourable condition for various EOR methods; however high temperature and salinity are the main challenges.[78] The temperature and salinity considerably influence the surfactant performance, absorption behaviours, and interfacial characteristic of the system. [21] The presence of salt and the released ions enhances the absorption of surfactant molecules at the interface through decreasing the repulsion between the polar heads of surfactant molecules, resulting in a reduction in the interfacial tension. An increase in the temperature causes a reduction in the DPD interaction parameter (a_{ij}), which leads to the surfactant molecules to pack easier at the interface. The reduction in the repulsion between the surfactant molecules within the system causes it to reach equilibrium and stability faster.

The computer simulation tools have gained popularity to study the behaviours of various systems/processes due to their ability to efficiently solve the complex interactions in different chemical and physical structures, while most of the analytical mathematical approaches rely on some assumptions to give an approximate solution. Moreover, using computational techniques, it is feasible to control the process conditions and thermodynamic and physicochemical parameters of the system, while it is almost impossible in the experimental works. Dissipative particle Dynamics (DPD) method is one of the most popular/powerful techniques, which has been recently utilized to model the thermodynamic and interfacial behaviours of complex fluids/mixtures at the coarse-grained level. Employing the DPD method, we can investigate the complicated behaviours of emulsions and their stability, which can have broad applications in various areas such as drug delivery systems, polymer production and processing, and oil production and transportation.

3.6 CONCLUSION

In this research investigation, we conduct a series of theoretical simulation runs through employing the Dissipative Particle Dynamics (DPD) to study the interfacial and structural properties of the brine/surfactant/oil mixtures. The DPD interaction parameter is calculated by two different approaches namely, molecular dynamic simulation and Monte Carlo approaches. The dissipative particle dynamics and molecular dynamic simulations offer effective strategies to forecast the interfacial and structural behaviours of hydrocarbon/surfactant/brine systems. The main outputs of the research work are summarized as follows:

- Based on the snapshots taken at different timesteps, the tail groups of the surfactant are immersed in the oil phase, while the head groups are penetrated into the water region. The gyration radius (R_g) is employed to characterize the structural properties of the beads in the system. By increasing the surfactant concertation, the magnitude of R_g increases, which indicates the stretching of the surfactant beads and their penetration into the oil and water phases. Increasing the temperature also helps the orientation and configuration of the surfactant molecules at the interface, leading to an increase in R_g.
- The head group of the surfactant is a polar molecule, which is in the form of hydrated ion in water. By adding salt to the system, the interfacial tension initially experiences a significant decrease as the released ions shield the repulsion between the surfactant head groups at the interface. However, once the surfactant molecules are saturated at the interface, further increase in the salt concentration does not vary the interfacial tension anymore.
- It was found that an increase in the temperature lowers the extent of interfacial tension. Based on the radius of gyration, the surfactant molecules at the interface are more stretched at higher temperatures, which is in agreement with the previous experimental and simulation works.
- By increasing the water/oil ratio (WC), the interfacial area will increase and cause a reduction in the surfactant concentration at the interface. Thus, the interfacial tension will increase with increasing the water/oil ratio by around WC=1. At this condition, both oil and water phases are present in the system as two separate phases. Therefore, IFT holds the highest value. With a continuous increase in the water content, less interface will be available for the surfactant molecules. Hence, their concentration will increase at the interface, leading to a decrease in the value of interfacial tension.
- Aqueous solutions of non-ionic surfactants appear to produce stable mixtures. However, they are not sensitive to the electrolytes so that their activity would be limited at the interface. It is recommended to study the key interfacial and structural behaviours of ionic surfactants in the future works. Incorporation of polymer in water/surfactant/oil systems is also recommended to better characterise alkaline surfactant polymer flooding operations.

ACKNOWLEDGMENTS

The authors would like to thank InnovateNL, Memorial University, Natural Sciences and Engineering Research Council of Canada (NSERC), and Equinor Canada for the financial support of this work.

REFERENCES

(1) Remesal, E. R.; Suárez, J. A.; Márquez, A. M.; Sanz, J. F.; Rincón, C.; Guitián, J., Molecular dynamics simulations of the role of salinity and temperature on the hydrocarbon/water interfacial tension. *Theor. Chem. Acc.* **2017,** *136* (6), 66.
(2) Paria, S.; Khilar, K. C., A review on experimental studies of surfactant adsorption at the hydrophilic solid–water interface. *Adv. Colloid Interface Sci.* **2004,** *110* (3), 75-95.
(3) Laughlin, R., Equilibrium vesicles: fact or fiction? *Colloids Surf. Physicochem. Eng. Aspects* **1997,** *128* (1-3), 27-38.
(4) Shi, L.; Tummala, N. R.; Striolo, A., C12E6 and SDS surfactants simulated at the vacuum− water interface. *Langmuir* **2010,** *26* (8), 5462-5474.
(5) Wiegand, G.; Franck, E., Interfacial tension between water and non-polar fluids up to 473 K and 2800 bar. *Berichte der Bunsengesellschaft für physikalische Chemie* **1994,** *98* (6), 809-817.
(6) Ginzburg, V. V.; Chang, K.; Jog, P. K.; Argenton, A. B.; Rakesh, L., Modeling the Interfacial Tension in Oil− Water− Nonionic Surfactant Mixtures Using Dissipative Particle Dynamics and Self-Consistent Field Theory. *The journal of physical chemistry B* **2011,** *115* (16), 4654-4661.
(7) Aske, N., Characterisation of crude oil components, asphaltene aggregation and emulsion stability by means of near infrared spectroscopy and multivariate analysis. *Norwegian University of Science and Technology* **2002**.
(8) Puig, L.; Sanchez-Diaz, J.; Villacampa, M.; Mendizabal, E.; Puig, J.; Aguiar, A.; Katime, I., Microstructured polyacrylamide hydrogels prepared via inverse microemulsion polymerization. *J. Colloid Interface Sci.* **2001,** *235* (2), 278-282.
(9) Fanun, M.; Wachtel, E.; Antalek, B.; Aserin, A.; Garti, N., A study of the microstructure of four-component sucrose ester microemulsions by SAXS and NMR. *Colloids Surf. Physicochem. Eng. Aspects* **2001,** *180* (1-2), 173-186.
(10) Sui, X.; Chu, Y.; Xing, S.; Liu, C., Synthesis of PANI/AgCl, PANI/BaSO4 and PANI/TiO2 nanocomposites in CTAB/hexanol/water reverse micelle. *Mater. Lett.* **2004,** *58* (7-8), 1255-1259.
(11) Cai, B.-Y.; Yang, J.-T.; Guo, T.-M., Interfacial tension of hydrocarbon+ water/brine systems under high pressure. *J. Chem. Eng. Data* **1996,** *41* (3), 493-496.
(12) Chen, Z.; Cheng, X.; Cui, H.; Cheng, P.; Wang, H., Dissipative particle dynamics simulation of the phase behavior and microstructure of CTAB/octane/1-butanol/water microemulsion. *Colloids Surf. Physicochem. Eng. Aspects* **2007,** *301* (1-3), 437-443.
(13) Kranenburg, M.; Venturoli, M.; Smit, B., Phase behavior and induced interdigitation in bilayers studied with dissipative particle dynamics. *The Journal of Physical Chemistry B* **2003,** *107* (41), 11491-11501.
(14) Espanol, P.; Warren, P., Statistical mechanics of dissipative particle dynamics. *EPL (Europhysics Letters)* **1995,** *30* (4), 191.

(15) Hoogerbrugge, P.; Koelman, J., Simulating microscopic hydrodynamic phenomena with dissipative particle dynamics. *EPL (Europhysics Letters)* **1992,** *19* (3), 155.
(16) Frenkel, D.; Smit, B., Understanding Molecular Simulation: From Algorithms to Applications (New York: Academic). **2002**.
(17) Fermeglia, M.; Pricl, S., Multiscale modeling for polymer systems of industrial interest. *Prog. Org. Coat.* **2007,** *58* (2-3), 187-199.
(18) Rezaei, H.; Modarress, H., Dissipative particle dynamics (DPD) study of hydrocarbon–water interfacial tension (IFT). *Chemical Physics Letters* **2015,** *620*, 114-122.
(19) Wang, S.; Zhao, J.; Li, X.; Yang, S.; Wang, X.; Liu, Y.; Yang, S.; Dong, Q., Numerical simulations on effects of ionic/nonionic surfactant on oil-water interface using dissipative particle dynamics. *Asia-Pacific Journal of Chemical Engineering* **2017,** *12* (2), 268-282.
(20) Wang, S.; Yang, S.; Wang, X.; Liu, Y.; Yang, S.; Dong, Q., Numerical simulations of the effect of ionic surfactant/polymer on oil–water interface using dissipative particle dynamics. *Asia-Pacific Journal of Chemical Engineering* **2016,** *11* (4), 581-593.
(21) Wang, S.; Yang, S.; Wang, R.; Tian, R.; Zhang, X.; Sun, Q.; Liu, L., Dissipative particle dynamics study on the temperature dependent interfacial tension in surfactant-oil-water mixtures. *Journal of Petroleum Science and Engineering* **2018,** *169*, 81-95.
(22) Soto-Ángeles, A. G.; del Rosario Rodríguez-Hidalgo, M.; Soto-Figueroa, C.; Vicente, L., Complementary experimental-simulational study of surfactant micellar phase in the extraction process of metallic ions: Effects of temperature and salt concentration. *Chem. Phys.* **2018,** *501*, 15-25.
(23) Dang, C.; Nghiem, L.; Nguyen, N.; Yang, C.; Chen, Z.; Bae, W., Modeling and optimization of alkaline-surfactant-polymer flooding and hybrid enhanced oil recovery processes. *Journal of Petroleum Science and Engineering* **2018,** *169*, 578-601.
(24) Mohammadi, H.; Delshad, M.; Pope, G. A., Mechanistic modeling of alkaline/surfactant/polymer floods. *SPE Reservoir Evaluation & Engineering* **2009,** *12* (04), 518-527.
(25) Khorsandi, S.; Qiao, C.; Johns, R.T., Robust geochemical simulation of alkali/surfactant/ polymer flooding with an equation of state. In: Paper SPE-182656 Presented at the SPE Reservoir Simulation Conference, Montgomery, TX, USA, 20–22 February **2017**.
(26) Korrani, A.K.N., Sepehrnoori, K., Delshad, M., A mechanistic integrated geochemical and chemical-flooding tool for alkaline/surfactant/polymer floods. *SPE J.* **2016**, 21 (01), 32–54.
(27) Chen, Z., Huan, G., Ma, Y., Computational methods for multiphase flows in porous media. Society for Industrial and Applied Mathematics **2006**, p.531.
(28) Goodarzi, F.; Zendehboudi, S., A comprehensive review on emulsions and emulsion stability in chemical and energy industries. *The Canadian Journal of Chemical Engineering* **2019**, 97 (1), 281-309.
(29) Zendehboudi, S.; Ahmadi, M.A.; Rajabzadeh, A.R.; Mahinpey, N.; Chatzis, I., Experimental study on adsorption of a new surfactant onto carbonate reservoir samples—application to EOR. *The Canadian Journal of Chemical Engineering* **2013**, 91 (8), 1439-1449
(30) Olayiwola, S. O. ; Dejam, M., A comprehensive review on interaction of nanoparticles with low salinity water and surfactant for enhanced oil recovery in sandstone and carbonate reservoirs. *Fuel* **2019**, 241, 1045-1057.
(31) Olayiwola, S. O.; Dejam, M., Mathematical modelling of surface tension of nanoparticles in electrolyte solutions. *Chemical Engineering Science* **2019**, 197, 345-356.
(32) Olayiwola, S. O.; Dejam, M., Surface tension of nanoparticles in electrolyte solutions, 71st Annual Meeting of the APS (American Physical Society) Division of Fluid Dynamics, Atlanta, Georgia, USA, 18-20 November **2018**.

(33) Saboorian-Jooybari, H.; Dejam, M.; Chen, Z., Half-century of heavy oil polymer flooding from laboratory core floods to pilot tests and field applications, Paper SPE 174402, 2015 SPE Canada Heavy Oil Technical Conference, Calgary, Alberta, Canada, 9-11 June **2015**.
(34) Mashayekhizadeh, V.; Kord, S.; Dejam, M., EOR potential within Iran. *Special Topics & Reviews in Porous Media - An International Journal* **2014**, 5(4), 325-354.
(35) Amirian, E.; Dejam, M.; Chen, Z., Performance forecasting for polymer flooding in heavy oil reservoirs. *Fuel* **2018,** *216*, 83-100.
(36) Saboorian-Jooybari, H.; Dejam, M.; Chen, Z., Heavy oil polymer flooding from laboratory core floods to pilot tests and field applications: Half-century studies. *Journal of Petroleum Science and Engineering* **2016,** *142*, 85-100.
(37) Yeh, P. D.; Alexeev, A., Mesoscale modelling of environmentally responsive hydrogels: emerging applications. *Chem. Commun.* **2015,** *51* (50), 10083-10095.
(38) Liang, X.; Wu, J.; Yang, X.; Tu, Z.; Wang, Y., Investigation of oil-in-water emulsion stability with relevant interfacial characteristics simulated by dissipative particle dynamics. *Colloids Surf. Physicochem. Eng. Aspects* **2018,** *546*, 107-114.
(39) Groot, R. D., Electrostatic interactions in dissipative particle dynamics—simulation of polyelectrolytes and anionic surfactants. *The Journal of chemical physics* **2003,** *118* (24), 11265-11277.
(40) Goicochea, A. G., Adsorption and disjoining pressure isotherms of confined polymers using dissipative particle dynamics. *Langmuir* **2007,** *23* (23), 11656-11663.
(41) Murtola, T.; Bunker, A.; Vattulainen, I.; Deserno, M.; Karttunen, M., Multiscale modeling of emergent materials: biological and soft matter. *PCCP* **2009,** *11* (12), 1869-1892.
(42) Alarcón, F.; Pérez, E.; Goicochea, A. G., Dissipative particle dynamics simulations of weak polyelectrolyte adsorption on charged and neutral surfaces as a function of the degree of ionization. *Soft Matter* **2013,** *9* (14), 3777-3788.
(43) Mayoral, E.; Goicochea, A. G., Modeling the temperature dependent interfacial tension between organic solvents and water using dissipative particle dynamics. *The Journal of chemical physics* **2013,** *138* (9), 094703.
(44) Silva, C. D. V.; Ruette, F., Estimation of Interfacial Tension in Mixtures of Linear Hydrocarbons and Immiscible Organic Liquids with Water by Dissipative Particle Dynamics (DPD). *International Journal of Fluid Mechanics & Thermal Sciences* **2018,** *4* (1), 1.
(45) Goicochea, A. G.; Altamirano, M. B.; Hernández, J.; Pérez, E., The role of the dissipative and random forces in the calculation of the pressure of simple fluids with dissipative particle dynamics. *Comput. Phys. Commun.* **2015,** *188*, 76-81.
(46) Yong, X., Modeling the Assembly of Polymer-Grafted Nanoparticles at Oil–Water Interfaces. *Langmuir* **2015,** *31* (42), 11458-11469.
(47) Forrest, B. M.; Suter, U. W., Accelerated equilibration of polymer melts by time-coarse-graining. *The Journal of chemical physics* **1995,** *102* (18), 7256-7266.
(48) Rekvig, L.; Kranenburg, M.; Vreede, J.; Hafskjold, B.; Smit, B., Investigation of surfactant efficiency using dissipative particle dynamics. *Langmuir* **2003,** *19* (20), 8195-8205.
(49) Groot, R. D.; Madden, T. J., Dynamic simulation of diblock copolymer microphase separation. *The Journal of chemical physics* **1998,** *108* (20), 8713-8724.
(50) Groot, R. D.; Madden, T. J.; Tildesley, D. J., On the role of hydrodynamic interactions in block copolymer microphase separation. *The Journal of chemical physics* **1999,** *110* (19), 9739-9749.
(51) Verlet, L., Computer" experiments" on classical fluids. I. Thermodynamical properties of Lennard-Jones molecules. *Phys. Rev.* **1967,** *159* (1), 98.
(52) Groot, R. D.; Warren, P. B., Dissipative particle dynamics: Bridging the gap between atomistic and mesoscopic simulation. *The Journal of chemical physics* **1997,** *107* (11), 4423-4435.

(53) Xu, M.-y.; Yang, Z.-r., Dissipative particle dynamics study on the mesostructures of n-octadecane/water emulsion with alternating styrene–maleic acid copolymers as emulsifier. *Soft Matter* **2012,** *8* (2), 375-384.
(54) Goel, H.; Chandran, P. R.; Mitra, K.; Majumdar, S.; Ray, P., Estimation of interfacial tension for immiscible and partially miscible liquid systems by Dissipative Particle Dynamics. *Chemical Physics Letters* **2014,** *600*, 62-67.
(55) Scatchard, G., Equilibria in Non-electrolyte Solutions in Relation to the Vapor Pressures and Densities of the Components. *Chem. Rev.* **1931,** *8* (2), 321-333.
(56) Hildebrand, J.; Wood, S., The derivation of equations for regular solutions. *The Journal of Chemical Physics* **1933,** *1* (12), 817-822.
(57) Blanks, R. F.; Prausnitz, J., Thermodynamics of polymer solubility in polar and nonpolar systems. *Industrial & Engineering Chemistry Fundamentals* **1964,** *3* (1), 1-8.
(58) Ryjkina, E.; Kuhn, H.; Rehage, H.; Müller, F.; Peggau, J., Molecular Dynamic Computer Simulations of Phase Behavior of Non-Ionic Surfactants. *Angew. Chem. Int. Ed.* **2002,** *41* (6), 983-986.
(59) Field, M. J.; Bash, P. A.; Karplus, M., A combined quantum mechanical and molecular mechanical potential for molecular dynamics simulations. *J. Comput. Chem.* **1990,** *11* (6), 700-733.
(60) Dong, F.-L.; Li, Y.; Zhang, P., Mesoscopic simulation study on the orientation of surfactants adsorbed at the liquid/liquid interface. *Chem. Phys. Lett.* **2004,** *399* (1-3), 215-219.
(61) Strobl, G. R.; Strobl, G. R., *The physics of polymers*. Springer: 1997; Vol. 2.
(62) Rudin, A.; Choi, P., *The elements of polymer science and engineering*. Academic Press: 2012.
(63) Fixman, M., Radius of gyration of polymer chains. *The Journal of Chemical Physics* **1962,** *36* (2), 306-310.
(64) Maiti, A.; McGrother, S., Bead–bead interaction parameters in dissipative particle dynamics: relation to bead-size, solubility parameter, and surface tension. *The Journal of chemical physics* **2004,** *120* (3), 1594-1601.
(65) Accelrys, M., Modeling 5.5. Accelrys. *Inc.: San Diego* **2010**.
(66) Groot, R. D.; Rabone, K., Mesoscopic simulation of cell membrane damage, morphology change and rupture by nonionic surfactants. *Biophysical journal* **2001,** *81* (2), 725-736.
(67) Hansen, C. M., *Hansen solubility parameters: a user's handbook*. CRC press: 2002.
(68) Ruiz-Morales, Y.; Mullins, O. C., Coarse-grained molecular simulations to investigate asphaltenes at the oil–water interface. *Energy & Fuels* **2015,** *29* (3), 1597-1609.
(69) Li, Y.; Guo, Y.; Xu, G.; Wang, Z.; Bao, M.; Sun, N., Dissipative particle dynamics simulation on the properties of the oil/water/surfactant system in the absence and presence of polymer. *Molecular Simulation* **2013,** *39* (4), 299-308.
(70) Rezaei, H.; Amjad-Iranagh, S.; Modarress, H., Self-Accumulation of Uncharged Polyaromatic Surfactants at Crude Oil–Water Interface: A Mesoscopic DPD Study. *Energy Fuels* **2016,** *30* (8), 6626-6639.
(71) Li, Y.; Guo, Y.; Bao, M.; Gao, X., Investigation of interfacial and structural properties of CTAB at the oil/water interface using dissipative particle dynamics simulations. *J. Colloid Interface Sci.* **2011,** *361* (2), 573-580.
(72) Shi, K.; Lian, C.; Bai, Z.; Zhao, S.; Liu, H., Dissipative particle dynamics study of the water/benzene/caprolactam system in the absence or presence of non-ionic surfactants. *Chemical Engineering Science* **2015,** *122*, 185-196.
(73) Rezaei, H.; Modarress, H., Dissipative Particle Dynamics Study of Interfacial Properties and the Effects of Nonionic Surfactants on Hydrocarbon/Water Microemulsions. *J. Dispersion Sci. Technol.* **2016,** *37* (7), 969-979.

(74) Song, X.; Zhao, S.; Fang, S.; Ma, Y.; Duan, M., Mesoscopic simulations of adsorption and association of PEO-PPO-PEO triblock copolymers on a hydrophobic surface: From mushroom hemisphere to rectangle brush. *Langmuir* **2016,** *32* (44), 11375-11385.
(75) Alasiri, H. The Behavior of Surfactants in Water/Oil System by Dissipative Particle Dynamics. Rice University, 2016.
(76) Kumar, B. Effect of salinity on the interfacial tension of model and crude oil systems. University of Calgary, 2012.
(77) Xu, J.; Zhang, Y.; Chen, H.; Wang, P.; Xie, Z.; Yao, Y.; Yan, Y.; Zhang, J., Effect of surfactant headgroups on the oil/water interface: An interfacial tension measurement and simulation study. *J. Mol. Struct.* **2013,** *1052*, 50-56.
(78) Sepehr, F.; Paddison, S. J., Dissipative Particle Dynamics interaction parameters from ab initio calculations. *Chem. Phys. Lett.* **2016,** *645*, 20-26.

CONCLUSION

In this research, a series of micro and meso-scale simulation were performed to describe the behaviour of oil/surfactant/water systems. Molecular dynamics simulation and Monte Carlo method were employed to calculate the chi parameter which later implemented in dissipative particle dynamics calculation to obtain the interfacial and structural characteristics of the system. The following are the outcomes of the work:

-Using dissipative particles dynamics reduced the computational time and cost required to model complex fluid structures through lumping a segment of matter into beads. The beading arrangements influence the accuracy of the results.

-The solubility parameter and energy of mixing computed using cohesive energy formula and Monte Carlo method. The effect of temperature on both these parameter showed a decrease as temperature rises, indicating higher miscibility of particles at higher temperatures.

-Investigations on the type of oil molecules present in the system showed aliphatic hydrocarbons tend to form a more stable emulsion compared to cyclic hydrocarbons, according to the IFT values measured at the interface.

- Interfacial tension values were estimated at different surfactant concentration. As more surfactant molecules were added to the system, the IFT values decreased, the radius of gyration showed higher values and the interface saturated faster since there are more surfactant molecules in the mixture and at the interface.

-the addition of salt to the system, improved the adsorption of surfactant molecules at the interface, according to a surge in surfactant concentration profiles peak taken from relative concentration plots. Hence the IFT values decrease as more ions dissociated in the mixture.

- Water-cut ratio determined to be a controlling factor over the type of emulsion formed, for water-cut ratios higher than 1, oil droplets will form in water and in the case of water-cut ratios less than one, oil in water emulsion will be formed in the system.

- Radius of gyration values shows the degree of surfactant stretching at the interface. This value increased when surfactant molecules are more oriented normal to the interface. Increasing the temperature cause the hydrophilic group of surfactant to stretch toward the water phase and the non-polar hydrophobic chain of surfactant to penetrate through the oil phase more in comparison to a lower temperature, hence the values of interfacial tension decrease by a rise in temperature which is in consistent with the trend reported in literature.

The studies conducted here throws some light on the efficiency of dissipative particle dynamics and employed an integrated method through connecting micro and mesoscale simulation by chi parameter calculation to accurately investigate the interfacial and structural characteristics of the

coarse-grain system. Further research on the application of dissipative particle dynamics on simulation of complex structures of polymers or ionic surfactant for EOR purposes or drug delivery systems is recommended.